DOE/ID/12062--T1

DE83 002581

CONTRACT NO. DE-FC07-79ID12062

THE GEOLOGY AND SURFACE GEOCHEMISTRY OF THE ROOSEVELT SPRINGS KNOWN GEOTHERMAL RESOURCE AREA, UTAH

Prepared for:

United States Department of Energy

NOTICE

PORTIONS OF THIS REPORT ARE ILLEGIBLE. It has been reproduced from the best available copy to permit the broadest possible availability.

Prepared by:

Dr. J. S. Lovell
Dr. W. T. Meyer
Barringer Resources Inc.
1626 Cole Boulevard, Suite 120
Golden, Colorado 80401

and

Dr. D. J. Atkinson
Hydrothermal Energy Corporation
2519 Horseshoe Canyon Road
Los Angeles, California 90046

DISCLAIMER

This report was prepared as an account of work sponsored by an agency of the United States Government. Neither the United States Government nor any agency thereof, nor any of their employees, makes any warranty, express or implied, or assumes any legal liability or responsibility for the accuracy, completeness, or usefulness of any information, apparatus, product, or process disclosed, or represents that its use would not infringe privately owned rights. Reference herein to any specific commercial product, process, or service by trade name, trademark, manufacturer, or otherwise, does not necessarily constitute or imply its endorsement, recommendation, or favoring by the United States Government or any agency thereof. The views and opinions of authors expressed herein do not necessarily state or reflect those of the United States Government or any agency thereof.

MASTER

DISTRIBUTION OF THIS DOCUMENT IS UNLIMITED

DISCLAIMER

This report was prepared as an account of work sponsored by an agency of the United States Government. Neither the United States Government nor any agency Thereof, nor any of their employees, makes any warranty, express or implied, or assumes any legal liability or responsibility for the accuracy, completeness, or usefulness of any information, apparatus, product, or process disclosed, or represents that its use would not infringe privately owned rights. Reference herein to any specific commercial product, process, or service by trade name, trademark, manufacturer, or otherwise does not necessarily constitute or imply its endorsement, recommendation, or favoring by the United States Government or any agency thereof. The views and opinions of authors expressed herein do not necessarily state or reflect those of the United States Government or any agency thereof.

DISCLAIMER

Portions of this document may be illegible in electronic image products. Images are produced from the best available original document.

TABLE OF CONTENTS
ROOSEVELT SPRINGS GEOTHERMAL AREA

LIST OF FIGURES

LIST OF TABLES

LIST OF PLATES

(in pocket at rear of report)

APPENDICES

ABSTRACT

Available data on the Roosevelt area were synthesized to determine the spatial arrangement of the rocks, and the patterns of mass and energy flow within them. The resulting model lead to a new interpretation of the geothermal system, and provided "ground truth" for evaluating the application of soil geochemistry to exploration for concealed geothermal fields. Preliminary geochemical studies comparing the surface microlayer to conventional soil sampling methods indicated both practical and chemical advantages for the surface microlayer technique, which was particularly evident in the case of As, Sb and Cs. Subsequent multi-element analyses of surface microlayer samples collected over an area of 100 square miles were processed to produce single element contour maps for 41 chemical parameters. Computer manipulation of the multi-element data using R-mode factor analysis provided the optimum method of interpretation of the surface microlayer data. A trace element association of As, Sb and Cs in the surface microlayer provided the best indication of the leakage of geothermal solutions to the surface, while regional mercury trends may reflect the presence of a mercury vapour anomaly above a concealed heat source.

INTRODUCTION

Under the terms of Cooperative Agreement No. DE-FC07-79ID 12062 with the Department of Energy, Barringer Research Inc. (BRI) undertook to investigate the application of soil geochemistry to exploration for concealed geothermal fields using the Roosevelt Hot Springs in Utah as a test area. The project was carried out in four phases, with Phase I being the development of detailed three dimensional models for the hydrological and geothermal regimes in the Roosevelt Hot Springs area based on existing geological, geophysical and soil geochemical data. This portion of the study was carried out by Hydrothermal Energy Corporation, with the results forming the first segment of this report.

In Phase II, the practical application of soil microlayer chemistry as a low-cost exploration method for detecting "blind" geothermal reservoirs was tested by comparison with conventional soil sampling techniques on selected profiles at Roosevelt Springs. A wide range of elements was determined on these samples using a combination of analytical methods including multi-element inductively coupled plasma emission spectroscopy. The results of this orientation survey, carried out by Barringer Research Inc., were used to identify the elements that would be most effective for detecting concealed geothermal activity, and established that the surface microlayer as the preferred sampling medium for the next phase of the project.

Phase III involved the collection of surface microlayer on a grid system covering a total of 100 square miles, with subsequent multi-element analysis of the resulting samples. All analytical data were recorded in computer compatible form and merged with the digitized sample locations to produce contour maps for each component.

The final report and interpretation makes use of factor analysis to assist in data integration, and compares the surface microlayer geochemical results with the known subsurface structure and hydrogeology of the field.

GEOLOGIC SETTING OF THE STUDY AREA

REGIONAL GEOLOGIC SETTING

INTRODUCTION

The Roosevelt Hot Springs KGRA lies near the intersection of several geologic zones of major significance (Figure 1). These are: 1) the transition zone between the Basin and Range province and the Colorado Plateau; 2) the Intermountain Seismic Belt; 3) the Pioche Mineral Belt; 4) a zone of late Tertiary-Quaternary volcanism; and 5) the geothermal belt of Lund-Thermo-Roosevelt-Cove Fort.

THE BASIN AND RANGE/COLORADO PLATEAU TRANSITION

The boundary between these two provinces lies east of Roosevelt (Figure 1A). The Basin and Range province is characterized by major block faulting and tilting dating from early Tertiary to the present time. Typical of these large Basin and Range fault blocks are the Mineral Range and the Escalante graben, between which Roosevelt is located.

In the Colorado Plateau to the east on the other hand, while normal faults are common, vertical offsets are very much smaller and the rocks are generally flat-lying, except in local monoclinal warps.

The boundary between these two physiographic provinces in this part of Utah is relatively abrupt, and lies along a discontinuous series of faults along the west side of the Pavant Range, the Gunnison Plateau and the Wasatch Range.

The development of the two physiographic provinces is part of the Cenozoic evolution of the region. But this contrast between mobility to the west and stability to the east has a much longer history: the boundary also corresponds approximately to the transition in the Paleozoic and Mesozoic between geosynclinal-orogenic belts to the west and the more stable and relatively undeformed platform to the east. Even the Precambrian rocks show a contrast between high-grade metamorphic and granitic terrains to the east, and relatively low-grade metamorphics to the west.

The boundary thus had its beginnings in Precambrian times.

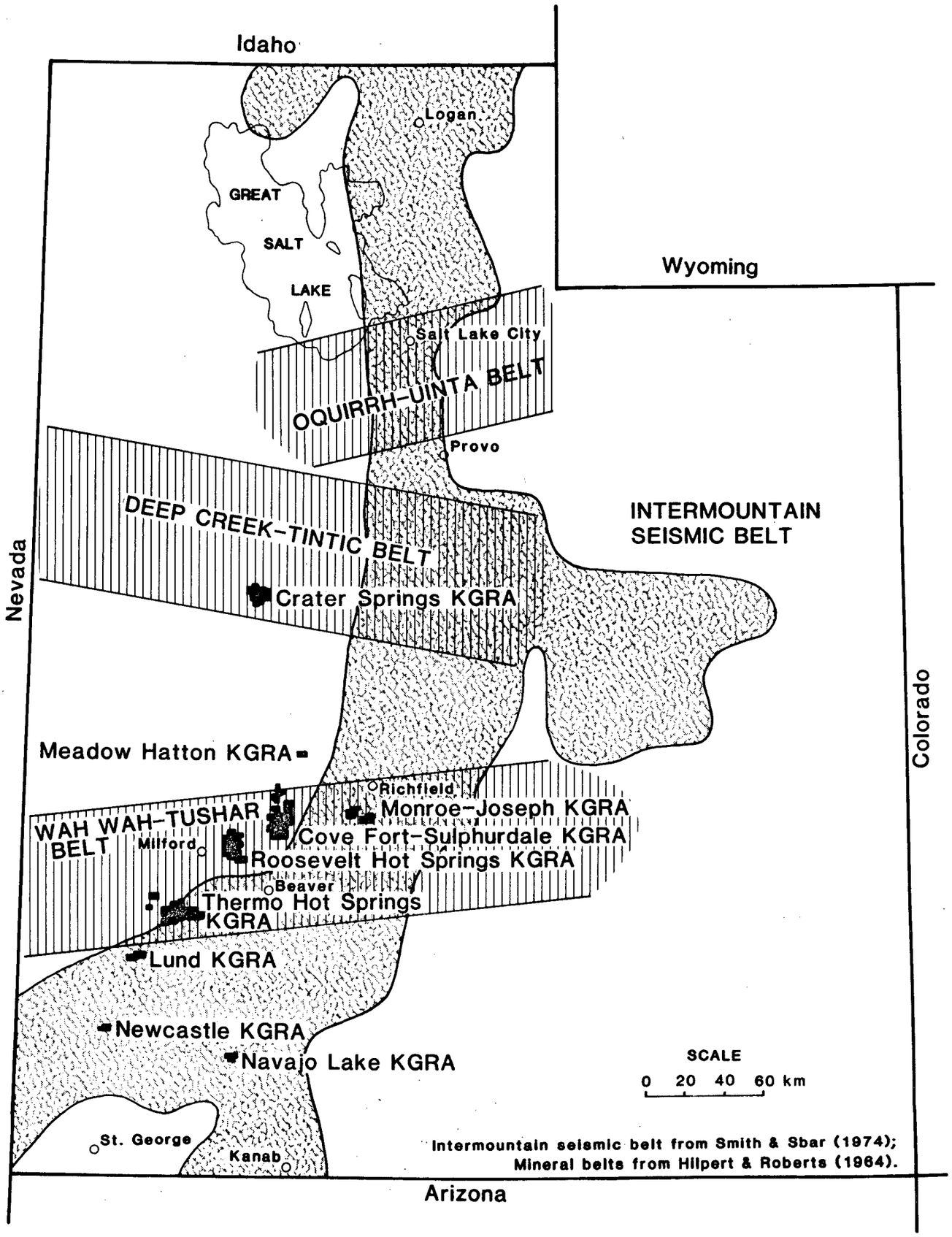

Figure 1

DISTRIBUTION OF TECTONIC ZONES & KGRA's IN UTAH

FIGURE 1A:

PHYSIOGRAPHIC SUBDIVISIONS OF UTAH

FROM STOKES, 1977

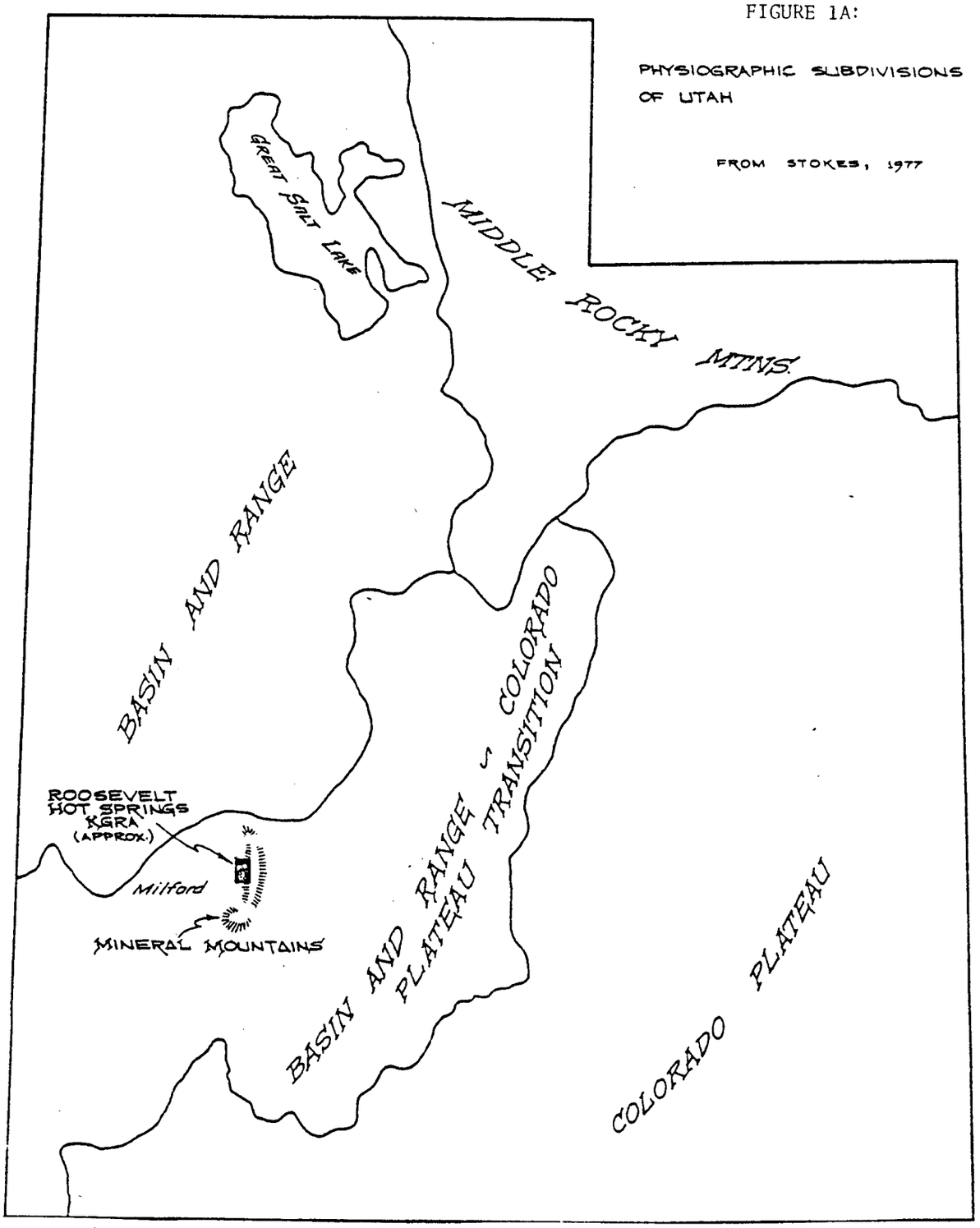

THE INTERMOUNTAIN SEISMIC BELT

The Intermountain Seismic Belt lies along this province boundary in this part of Utah (Smith and Sbar, 1974; Sbar et al., 1972). This currently active seismic zone trends northward along the boundary between the Basin and Range and Colorado Plateau provinces, up into Idaho. In the area just southeast of Roosevelt, however, the trend changes abruptly to west-southwest and the belt passes obliquely across southeast Utah into Nevada (Figure 2). The setting of the Intermountain Seismic Belt is more clearly seen in Figure 3. The seismicity involves shallow focii, generally less than 15 km deep. Earthquake swarms are sometimes located along the zones of geothermal features (Smith and Sbar, 1974).

Based on the geophysical data, and the observations and discussions of Sbar et al., (1972), Smith and Sbar (1974), and Keller, Smith and Braile (1975), the contrast in tectonic style and history between the Basin and Range and Colorado Plateau provinces appears to indicate different crustral structures for the two provinces (Archambeau et al., 1969; Roy et al., 1968; Blackwell, 1969; Julian, 1970; Prodehl, 1970; Roy et al., 1971).

The Colorado Plateau shows lower heat flow and a thicker crust (about 40 to 50 km). The Basin and Range area here has a higher heat flow, averaging 2 HFU, and a thinner crust (around 25 to 30 km). In addition, the upper mantle has a lower P-wave velocity than below the Colorado Plateau. This contrast extends to about 100 km depth.

In order to clarify details of the crustal structure in the boundary zone in this area, Keller, Smith and Braile (1975) made a seismic refraction survey of the zone and found a thin crust (around 25 km), a low-velocity layer in the crust at a depth of 8 to 15 km, and a low P_n velocity of about 7.5 km/sec from refraction at the boundary between crust and upper mantle. They concluded that a mantle upwarp of low-velocity material is present along the transition zone, and extends over 50 km east and over 30 km west of the boundary. The transition in crustal structure lies east of the province boundary based on seismic refraction work (Keller, Smith and Braile, 1975; Ryall and Stuart, 1963; Braile et al., 1974). Shuey et al., (1973) showed that a change in crustal magnetization also occurs 50 km east of the province boundary.

FIGURE 2: THE INTERMOUNTAIN SEISMIC BELT

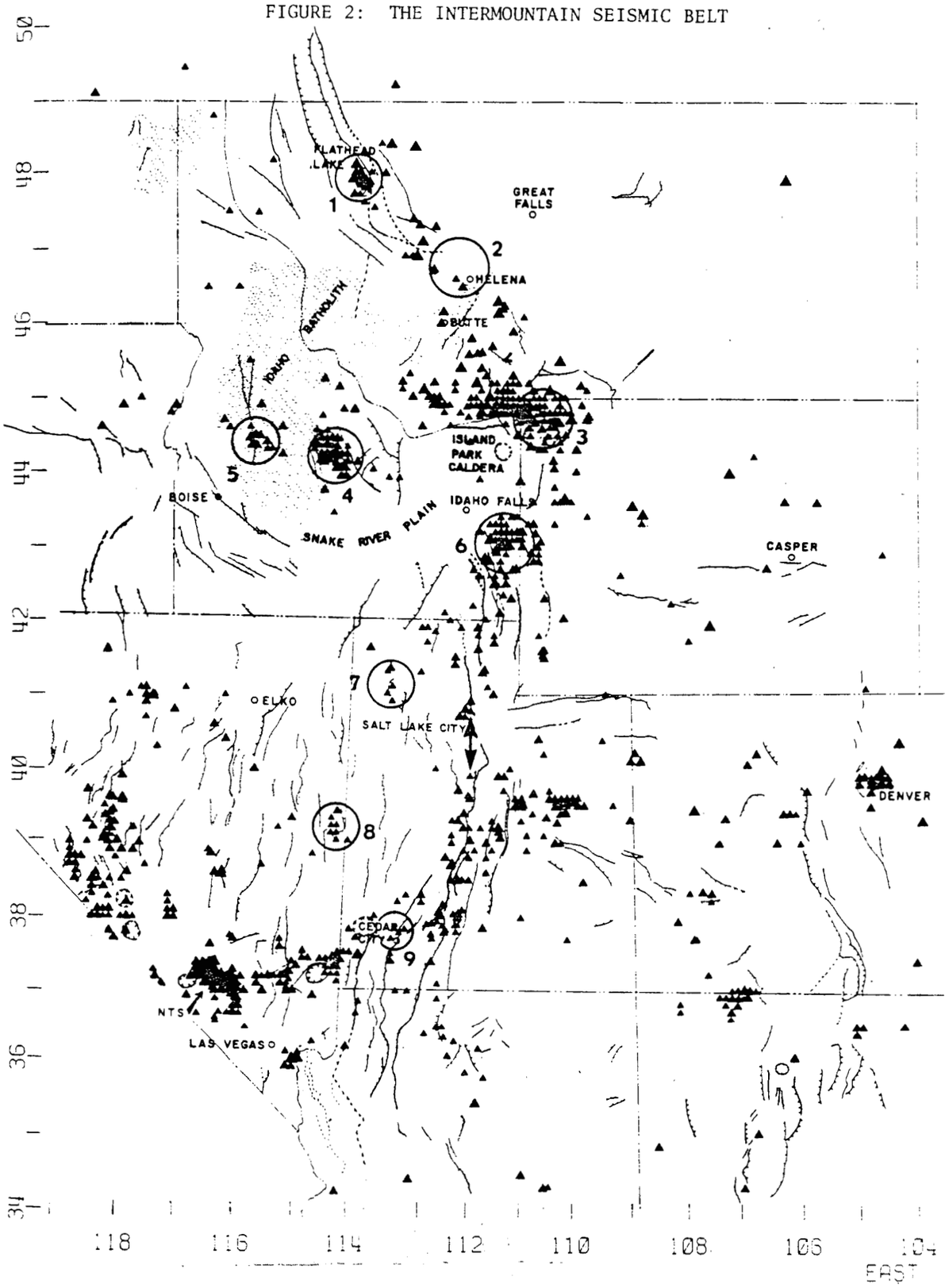

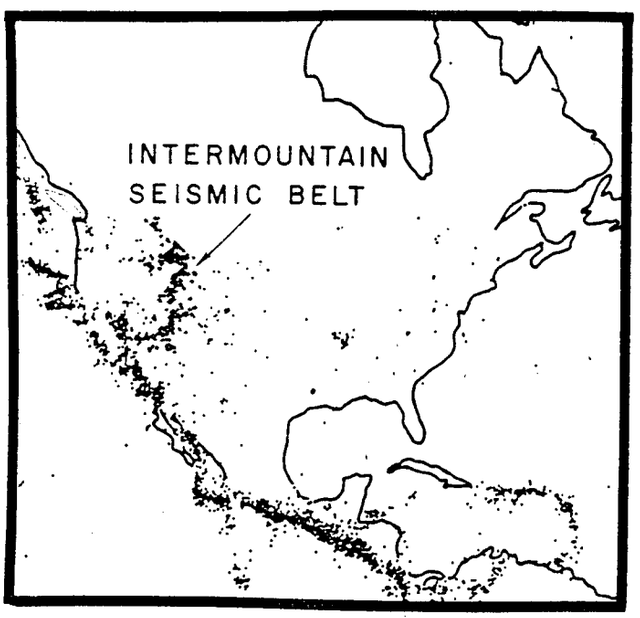

FIGURE 3: CRUSTAL SETTING OF THE
INTERMOUNTAIN SEISMIC BELT

These geologic and geophysical data can be integrated into a model in which the Intermountain Seismic Belt reflects motion along a boundary between subplates of the North American plate. East of Roosevelt the zone of movement trends N-S along the boundary between the Great Basin portion of the Basin and Range province and the Colorado Plateau. In southwest Utah the seismic trend shifts abruptly to WSW across the southern boundary of the Great Basin plate. To the north, an east-trending seismic belt separates the Western Rocky Mountains from the Great Basin and the Snake River Plain. This pattern (Figure 2) outlines the boundaries of the Northern Rocky Mountain and Great Basin subplates, which are moving west relative to the stable part of the North American plate. This overall motion was considered by Smith and Sbar (1974) as related to a mantle plume that tracked northeastward beneath the Snake River Plain and is now below Yellowstone. In the south and west parts of the Great Basin, deformation presently involves NW-SE extension related to relative movement between the North American and Pacific plates.

The Roosevelt area is thus located close to the intersection of two subplate boundaries, the east margin and south margin of the Great Basin subplate.

THE PIOCHE MINERAL BELT

Another major belt that crosses the Roosevelt region is the Wah-Wah-Tushar mineral belt, which trends east and west. Such E-W belts of mineralization, Cenozoic igneous activity, and faulting have been described by several geologists, beginning as early as Butler et al., in 1920. Geophysical anomalies, particularly gravity and magnetic features, coincide with these E-W belts.

The Pioche belt of eastern Nevada (Roberts, 1964), and the Wah-Wah-Tushar belt of south central Utah (Hilpert and Roberts, 1964), were combined by Shawe and Stewart (1976) into the Pioche mineral belt (Figure 4). Roosevelt lies close to its central axis.

The belt (Rowley et al., 1978), which trends slightly north of east from Nevada across much of Utah, is over 50 km wide and is characterized by mineralization including Au, Ag, Pb, Zn, W, U, F, Mn, Cu, Mo, and Ba (Cohenour, 1963: Walker and Osterwald, 1963; USGS Utah Geological and Mineral Survey, 1964; Lindsey et al., 1973 and 1975; Van Alstine, 1976). Many of the mineralized areas

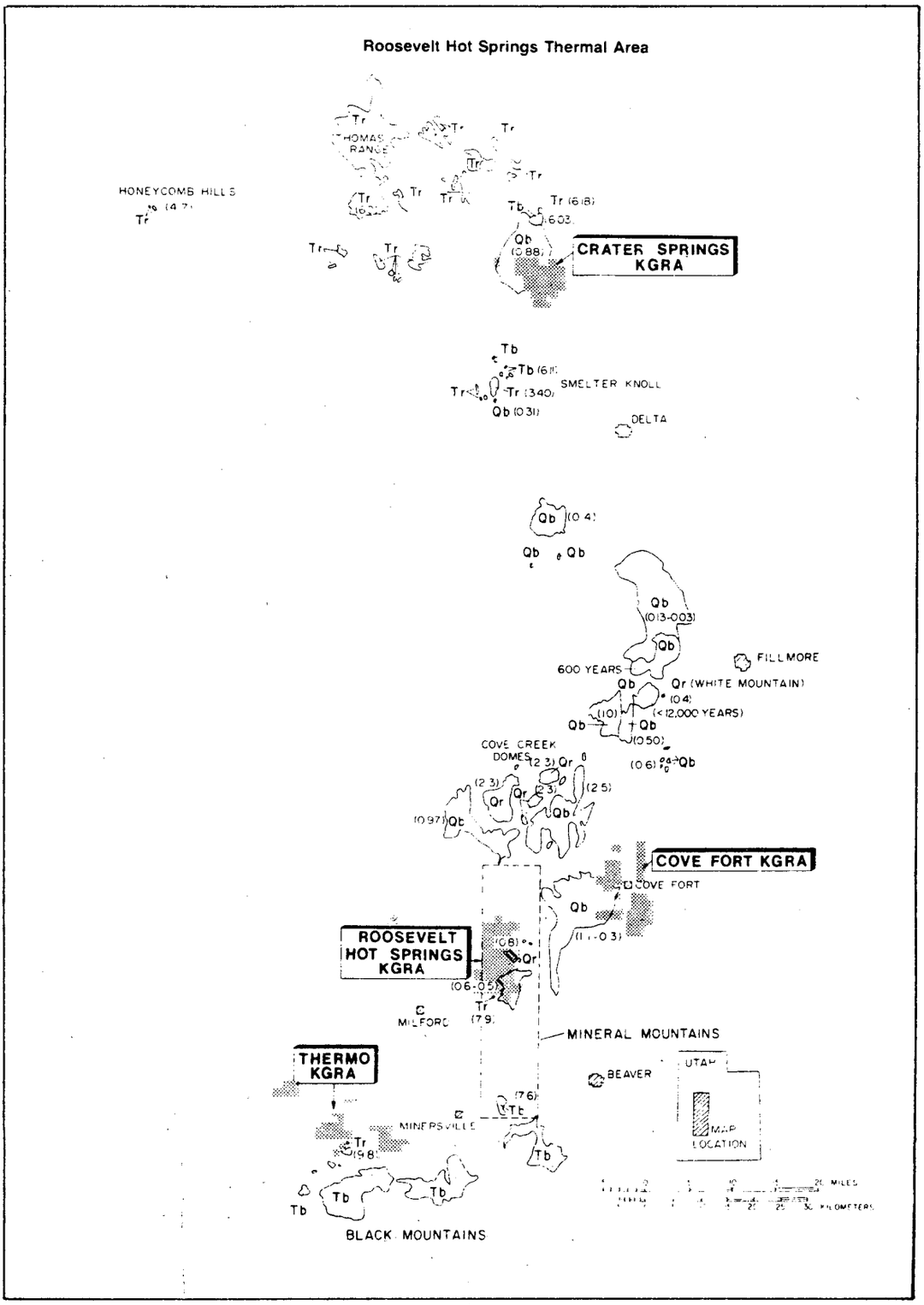

Figure 4

DISTRIBUTION, TYPE AND AGE OF YOUNG VOLCANIC ROCKS

lie near alkalic rhyolite centers, ranging in age from Middle Miocene to Pleistocene. This is especially true of the younger F, W, S, U, and Be mineralization (Rowley, 1978). Most of the mineralization is mid to late Tertiary in age, though the belt may have been in existence earlier.

The Pioche belt is a zone of structural and topographic highs, encompassing the highest mountains in southern Utah, and bringing relatively large areas of older rocks to surface. East-west faults and major lineaments can be traced across the area in satellite imagery and on the ground. Faults of similar trend may play an important role in structural control at Roosevelt itself, as discussed later in this report.

The Blue Ribbon lineament (Rowley, 1978) is one such major lineament that can be traced along the southern part of the Pioche belt, through Thermo, and across into Nevada. It probably continues across the aeromagnetic quiet zone and becomes the Warm Springs lineament.

The belt of mineralization corresponds to a broad, very elongate aeromagnetic high (Stewart et al., 1977). Many smaller highs and lows within it correspond to volcanic centers and shallow plutons, mostly of Cenozoic age (Hilpert and Roberts, 1964; Zeitz et al., 1976). By far the most prominent of these granitic plutons is the Mineral Mountains quartz monzonite, which with its metamorphic roof forms the reservoir rock of the Roosevelt geothermal field.

The volcanics of the Pioche belt are basalts, andesites and rhyolites. There are a number of major volcanic centers, ranging in age from Eocene or Oligocene to present. Four dated alkali rhyolites along the Blue Ribbon lineament show progressively younger ages to the east (Anderson and Rowley, 1975; Rowley et al., 1977).

LATE CENOZOIC VOLCANISM

Late Cenozoic volcanics along the east edge of the Great Basin, including the Roosevelt area, show a bimodal association of basalt, or basaltic andesite, with rhyolite. The Mineral Mountains immediately east of Roosevelt exhibit a series of well preserved and very young rhyolite domes and flows, with some ashes. Some of these rocks are only 0.5 m.y. old. Extensive Quaternary basalt flows derived from a volcanic center in the Cove Fort area lap up against the northeast edge of the Mineral Mountains; these are

generally 1.1 to 0.3 m.y. old but there is evidence of some extremely recent activity. There are other basaltic vents in the northeast Mineral Mountains. Ward et al., (1978) showed the distribution of late Cenozoic volcanic rocks near Roosevelt, and their estimated ages (Figure 4).

THE GEOTHERMAL BELT OF LUND-THERMO-ROOSEVELT-COVE FORT

A series of major and minor geothermal areas lie in a zone northeast and southwest of Roosevelt, which at present is the only one of them moving toward commercial production.

SUMMARY

From this outline of geologic and geophysical data relevant to the regional setting of Roosevelt, it is clear that this Known Geothermal Resource Area and the neighboring KGRAs of Thermo and Cove Fort lie within the Pioche mineral belt near the Great Basin-Colorado Plateau boundary. The area is characterized by a thin crust and high heat flow. A mantle upwarp is probably present, along the eastern margin of the Great Basin. Major, and seismically very active, subplate boundaries lie nearby to the east and south. Extensive rhyolitic and basaltic volcanism in the immediate area is as recent as 0.5 to 0.3 m.y.

GEOLOGY OF THE MILFORD VALLEY

INTRODUCTION

The present physiography and geology of the area in which Roosevelt is situated is dominated by the effects of late Cenozoic block faulting and volcanism. The most recent phases of tectonism are discussed later in this report, but before doing that the earlier geology and history will be summarized as a background for understanding the present evolution of the geothermal system.

THE CRYSTALLINE BASEMENT

The oldest rocks in the area are the regionally metamorphosed Precambrian sediments and volcanics, which form a basement of crystalline schists and gneisses. They crop out at the present surface only in the Roosevelt area, an immediate pointer that the geothermal area as a whole constitutes a major structural high, with downfaulted blocks on four sides.

THE SEDIMENTARY SEQUENCE

Above the basement lies a sedimentary sequence of miogeosynclinal rocks beginning with Eocambrian-Cambrian clastics and continuing through the well-sorted sandstones, shales and limestones of the lower and upper Paleozoic, into the Triassic and Jurassic.

Detailed accounts of the stratigraphy have been given by Woodward (1968, 1973), Hintze (1973), Welsh (1973a, 1973b), Stokes (1973), and Peterson (1974).

During the Jurassic the eugeosynclinal area further west had already begun its major deformation, but in the region encompassing Roosevelt, it was during most of the Cretaceous that the sedimentary pile was involved in successive phases of orogeny, the Sevier orogeny. Large-scale eastward overthrusting followed the classic orogenic pattern here, with decollements developing, particularly at the base of the Eocambrian-Cambrian Prospect Mountain quartzite, which, in different areas, is now seen overriding rocks ranging in age from Cambrian to Mississippian (Armstrong, 1968a, 1968b; Nolan, 1943).

The interpretation of Sevier thrusts as gravity gliding plates moving away from areas of uplift has been propounded by Eardley (1968, 1969) and refuted by Woodward (1970). The classical interpretation, rather than gravity gliding, is favored by the structural evidence.

The deformed rocks of the Sevier orogenic belt in the Roosevelt area show Nand NW-plunging folds as well as the large-scale eastward overthrusting already described. They are overlain uncomformably by late Cretaceous conglomerates. Laramide uplift and block faulting followed the Sevier orogeny, the Cenozoic history was dominated by block fault movements, and extensive volcanism dating from late Eocene or early Oligocene to the present (Erickson, 1973).

VOLCANIC ROCKS

In the Roosevelt area (Figure 4) mid-Tertiary volcanics (andesites and basalts dated around 20 m.y. old), occur in the Black Mountains southwest of Minersville. Rhyolites about 10 m.y. old occur just north of these areas in isolated knobs just south of the Thermo KGRA. Rhyolites around 8 m.y. old occur just south of Roosevelt KGRA in Corral Canyon, and basalts about the same age occur just east of Minersville. Basalts and rhyolites about 2 m.y. old occur in the Cove Creek Domes north of Roosevelt. The Cove Fort basalts just to the northeast span the range 1.1 to 0.3 m.y.; during part of the same time span, the Roosevelt rhyolite domes and flows were forming (0.8 to 0.5 m.y. ago).

There is thus a very obvious bimodal association of basaltic and rhyolitic volcanism during recent evolution of this area.

IGNEOUS ROCKS

The Mineral Mountains granitic pluton itself is Tertiary in age. Park (1968) gave it an age of about 15 m.y.; Armstrong (1970) put it around 9 m.y.; Ward et al., (1978) reported K-Ar ages ranging from 10.0 to 12.6 m.y. and noted progressively younger ages to the south. All of these dates may simply result from resetting and the pluton is probably older. Lipman et al., (1978) reported about 35 m.y. based on Rb-Sr (see also Bowers, 1978 and Nielson et al., 1978), and Sibbett and Nielson (1980) consider it to be 20 to 29 m.y. old.

Exposures of the granite are very extensive and make this the largest area of exposed plutonic rocks in Utah.

STRUCTURAL BLOCKS

The most obvious structural elements of the Roosevelt area are the horst of the Mineral Mountains and the Escalante graben of the Milford valley. Roosevelt lies close to the fault zone between them.

The Mineral Mountains horst (Figure 5) is broken into three parts, separated by faults that cross the range. The northern part was mapped in detail by Leise (1957). The rocks are Cambrian in age: the Prospect Mountain quartzite, the Pioche shale and a series of dark grey limestones. A major thrust sheet was mapped here, with klippen of Prospect Mountain quartzite forming the caps of the hills. Unconformably above the Cambrian are outcrops of a conglomerate identified as the Cretaceous Indianola formation, but the correlation is based only on lithologic comparison of this 112' sequence with the Indianola in the Canyon Range (Christiansen, 1951).

The southern part of the Mineral Range, south of the Pass Road from Milford to Beaver, is made up of Precambrian metamorphic rocks overlain by a sequence of Paleozoic and Mesozoic sedimentary rocks, and Tertiary volcanics. The sedimentary sequence includes Paleozoic dolomites and limestones, overlain by the Topache formation (Mississippian limestones); the Permian Coconino sandstone and Kaibab limestone; and a thin, possibly Cretaceous, conglomerate (Earll, 1957). The volcanics are andesite to latite in composition, and dominate the southeast part of the Mineral Range.

The main, central section of the Mineral Range extends between the County Line fault to the north, and the faults of Pass Canyon to the south. This central block has extensive outcrop areas of gneiss and schist on the west side of the range in the Roosevelt area, but is mainly composed of the Tertiary granitic intrusion of the Mineral Mountains pluton. Cutting this are the very young rhyolite domes and flows of the area east of Roosevelt.

The known geothermal field of Roosevelt is in the area where the Precambrian metamorphic rocks are cut by the Tertiary pluton.

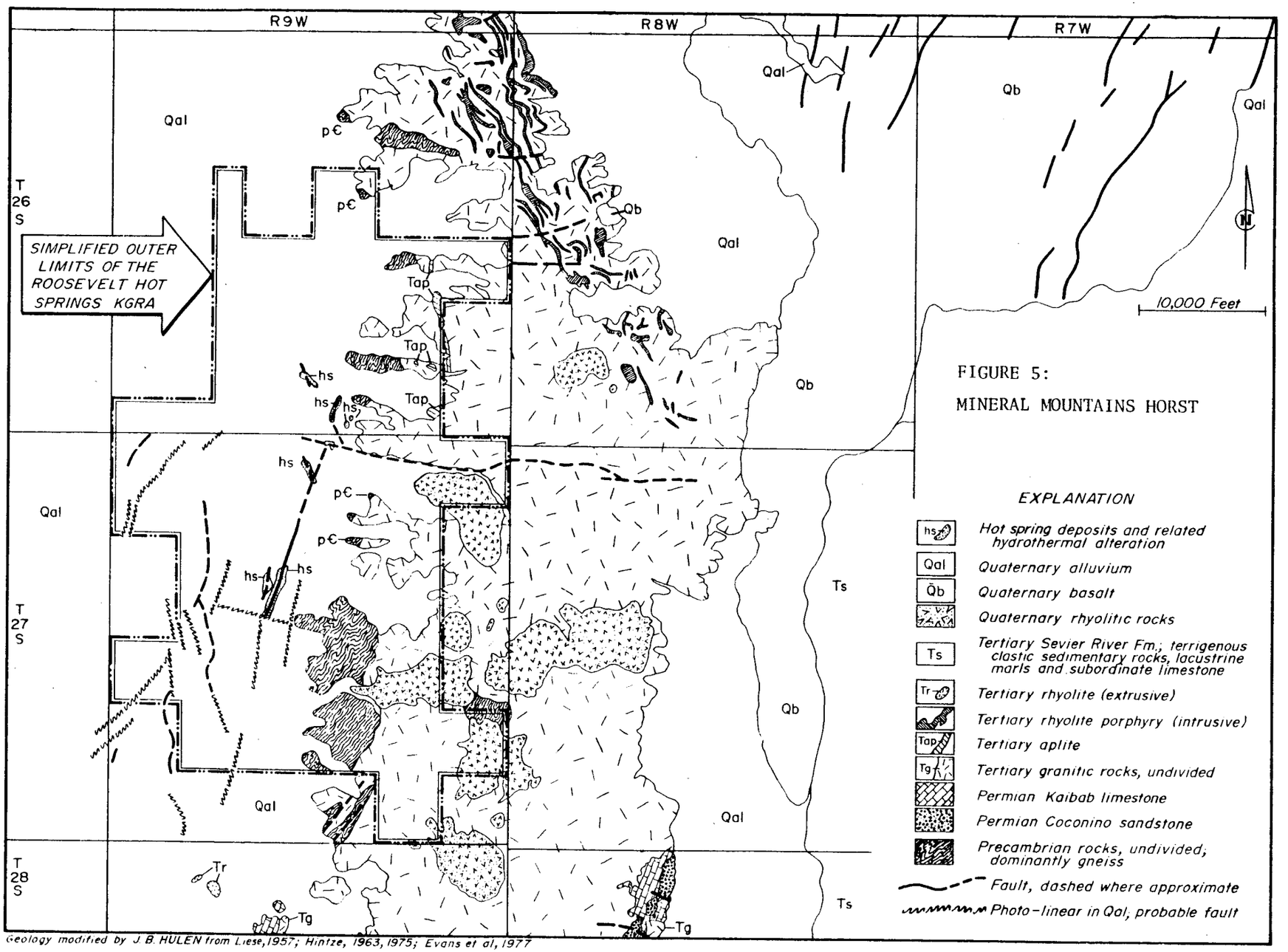

FIGURE 5:

MINERAL MOUNTAINS HORST

Geology modified by J.B. HULEN from Liese, 1957; Hintze, 1963, 1975; Evans et al, 1977

The geology of the area of the field has been mapped by Earll (1957), Peterson (1975), Evans (1977), Nielson et al., (1978) and Sibbett and Nielson (1980). The map by the latter authors (their Plate I) is the most up-to-date and detailed version.

On the opposite, west side of the Escalante graben are, from north to south, the San Francisco Mountains; the Beaver Lake Mountains; the Rocky Range; and the Star Range (Figure 6).

The San Francisco Mountains block (East, 1966; Butler, 1913) contains an extensive overthrust slice, with the Cambrian Prospect Mountain quartzite forming its sole, lying above Cambrian and Ordovician carbonates. The thrusting also involves Mississippian and Pennsylvanian limestones. Early Tertiary conglomerates overlie these rocks uncomformably, and mid-Tertiary volcanic flows and pyroclastics cover most of the eastern part of the block.

The Beaver Lake Mountains have been described by Barosh (1960) and Welsh (1973). Sevier thrusting carries Cambrian (and late Precambrian) quartzites and carbonates over Devonian dolomites (Simonson) and Mississippian limestones (Monte Cristo). The Paleozoic sequence includes Cambrian Prospect Mountain quartzite and Pioche shale; Ordovician Pogonip formation, Eureka quartzite, and Fish Haven dolomite; Silurian dolomite (Laketown and Sevy); Devonian Simonson dolomite and Cove Fort quartzite; and the Mississippian Monte Cristo limestone. Over large regions the sequence is cut by Tertiary granitic rocks.

A few miles to the southeast is the Rocky Range (Whelan, 1973; Whelan and Hintze, 1973; Welsh, 1973). Tertiary granitic rocks occupy a large part of the range, and Tertiary volcanics cover large areas to the northeast and northwest. The sedimentary sequence is steeply dipping, with N and NW strikes, and includes the Permian Talisman quartzite, Toroweap and Kaibab-Plympton formations; and the Triassic Moenkopi.

A few miles further south is the Star Range (Baer, 1962; Abou-Zied, 1968, 1973; Baer, 1973). Tertiary granite cuts the eastern part of the Range. The sedimentary sequence includes the Devonian Sevy and Guilmette dolomites and Pilot shale; Mississippian Redwall limestone; Pennsylvanian-Permian limestone; Permian Talisman quartzite, Toroweap carbonates and gypsum; and Kaibab-Plympton limestones; Triassic Moenkopi, Shinarump and Chinle formations; and Jurassic Navajo sandstone. Bedding dips at moderate to steep angles to the southeast.

FIGURE 6:

ESCALANTE GRABEN

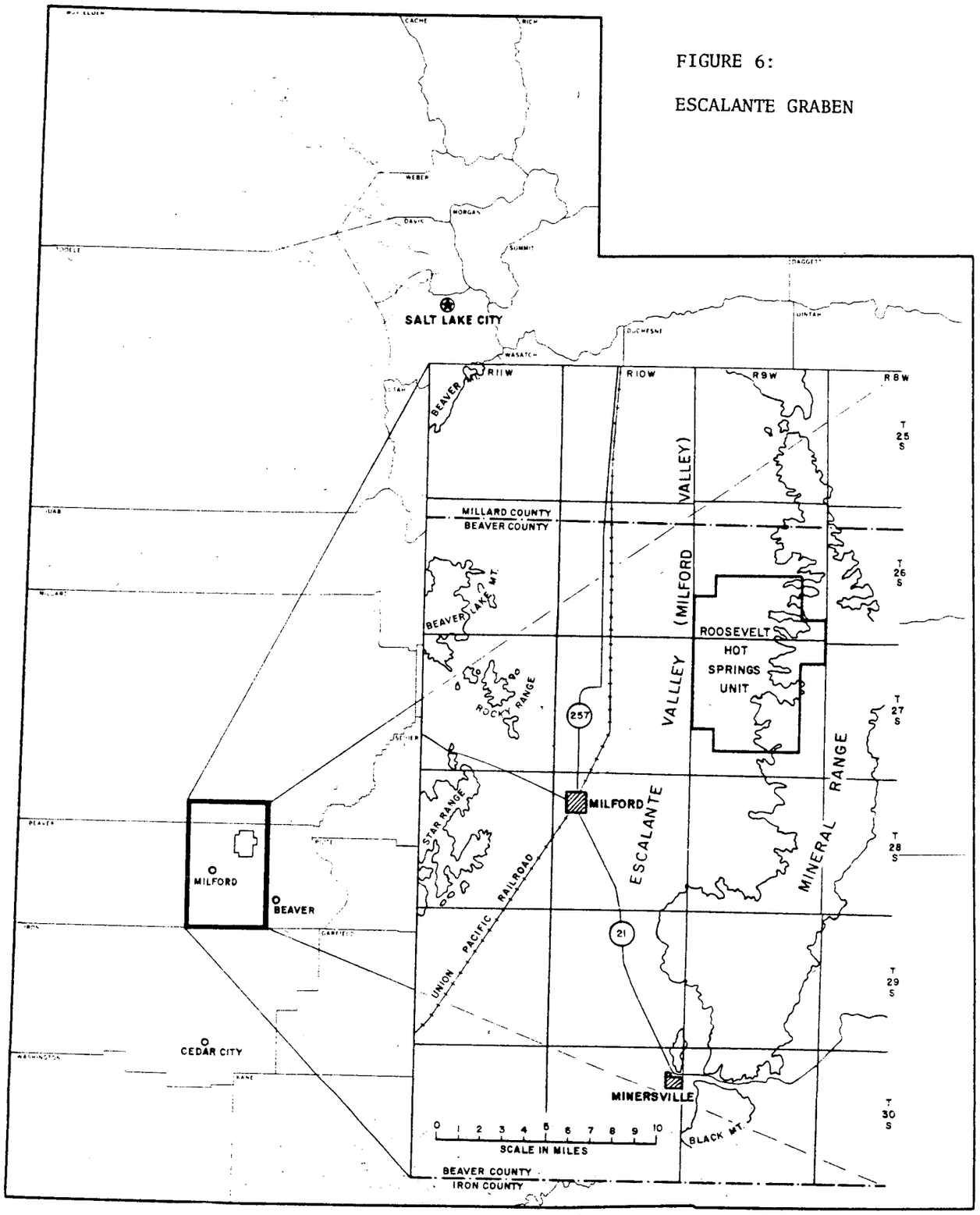

ROOSEVELT HOT SPRINGS UNIT
LOCATION MAP
BEAVER COUNTY, UTAH

THE STUDY AREA

GEOLOGY AND STRUCTURE OF THE STUDY AREA

INTRODUCTION

The area of sampling in this geochemical study was chosen to span a broad zone on each side of the known geothermal area, encompassing the eastern half of the Milford Valley and the western part of the Mineral Range.

On the east it includes a major part of the central Mineral Mountains and the KGRA itself. To the west it covers a wide strip of the Escalante graben of Milford Valley.

THE MINERAL RANGE

The bulk of the Roosevelt section of the Mineral Range is made up of granitic rocks of the Tertiary pluton. Precambrian metamorphic rocks crop out at the ends of ridges east of the geothermal field, and also for two or three miles to the south. The present land surface is evidently close to the roof of the pluton, and productive geothermal wells intersect both the Precambrian metamorphics of the roof, and the Tertiary plutonic rocks that intrude them.

Figure 7 is taken from Sibbett and Nielson (1980) and is a cross-section along the line A-A' on the geologic map (Plate 1).

FAULTING IN THE MINERAL RANGE

Cutting the Mineral Range in this area there are several sets of steep to vertical faults. One set that is particularly prominent trends about 30^{o} west of north. Some of these faults are vertical; others dip west at high angles.

Another prominent set of faults trends northward or, less commonly, slightly east of north. The Opal Mound fault is perhaps part of this set. It may be better to divide this group of faults into two sets, with the N-trending set representing extension, and the other set a shear direction.

A third set of faults in the Mineral Mountains trends between west and west-northwest. The Negro Mag Wash fault is the best known of these, but there are other important WNW-trending fault zones, as

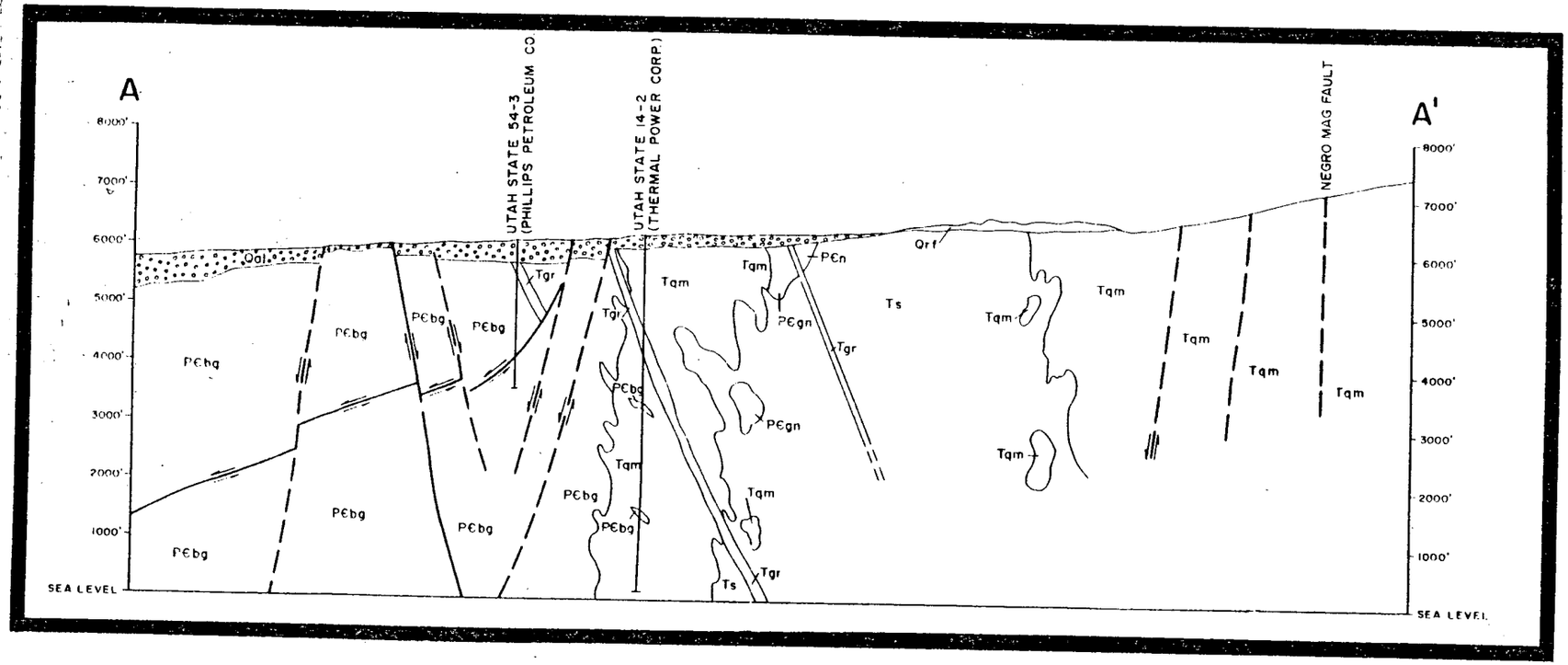

FIGURE 7: CROSS-SECTION A-A: MILFORD VALLEY GRABEN, THE GEOTHERMAL FIELD, AND THE MINERAL RANGE.

in Salt Cove half a mile north of Negro Mag Wash, in the cove two miles north of Salt Cove, and in a zone crossing the range south of Pinnacle Pass.

Further south, similar WNW-trending fault zones have not been mapped within the range, but can be extrapolated into it from faults in the alluvial area to the west, as is discussed in the next section, on photo-interpretation of the Milford Valley.

Faults of the fourth set, that dip at low angles to the west, have been interpreted as low-angle normal, or denudation faults (Nielson et al., 1978, Sibbert and Nielson, 1980). In places, brecciated zones up to forty feet thick are seen in these fault zones. Offsets of lithologic units by a fault in the area between Wildhorse Canyon and Ranch Canyon are considered to demonstrate that relative displacement on the fault is consistent with this interpretation. However, it is difficult to demonstrate this conclusively, as the fault cuts across the roof of the pluton and across a variety of roof pendants, thus making correlation of markers across the fault rather uncertain.

An alternative interpretation is that the fault is the upper, low-angle part of an upthrust, that is, a steep fault that involves reverse rather than normal dip slip, and curves upward to progressively lower angles of dip as lower overburden pressure near surface changes the balance between vertical and horizontal principal stresses.

To the north, in the area of Big Cedar and Little Cedar Cove a fault of the same trend is much steeper; and the same is seen to the south. This may support the interpretation of these faults as part of a system of upthrusts, with steeper dips corresponding to lower structural levels at the time the faults were formed. However, the evidence is inadequate to do more than suggest this alternative view.

Nielson et al., (1978) concluded that of the four sets, the low-angle faults were the oldest; that the NNW-trending faults developed from movement on the first set; that the WNW-trending set developed next; and that the N to NNE-trending set formed last.

FAULTING IN THE MILFORD VALLEY AND THE GEOTHERMAL FIELD

The present-day fault activity, and some details of the structure of the valley (the Escalante graben) can be inferred from the traces of recent movement seen on the ground and in air photographs, and from the extensive geophysical data that have been developed in the last few years.

Many of the faults mapped in the range are clearly seen on the air photographs. On the other hand, many of the air photo linears in the area of the range show no demonstrable displacement when examined on the ground, and Sibbett and Nielson accordingly do not show them on their map as faults.

Interpretation of air photographs, as part of this study, has produced the map of faults and fractures shown in Figure 8.

The linears mapped on Figure 8 are related both to fault zones with detectable displacement and to zones of fractures on which there may have been no significant movement. Both are equally important with respect to this study, as both may offer equally effective upward pathways for geochemical transport.

The linears mapped in the valley are of particular interest as they tend to mark zones on which very recent motion has disturbed the present land surface. The shallow alluvial cover is obviously not capable of sustaining and transmitting significant stresses. The pattern mapped on the surface is only the pattern of response of the shallow cover to motions occurring at depth in more consolidated material. It is thus not surprising that the zones of linears tend to be discontinuous, and sometimes contain sections in which short linear features lie at a small angle to the overall trend, en echelon. They are, nevertheless, excellent guides to zones of present or very recent movement, and to the available pathways for fluid migration. Their relationship to the location and interpretation of geochemical anomalies found in this work, is thus critically important.

The map of faults (Figure 8) appears, at first sight, somewhat confusing, and it is accordingly dissected in terms of several major fault sets, which are treated separately, one after the other, in the following sections.

R10W

R9W

R8W

T
26
S

Pacific

Union

SCF

NMW

OMF

T
27
S

T
28
S

Figure 8

FAULT & FRACTURE
ZONES

SCF Salt Cove Fault

NMW Negro Mag Wash Fault

OMF Opal Mound Fault

Boundary of Study Area

WNW-Trending Faults

The Negro Map Wash fault is the best known example of the WNW-trending faults (WNW-4, Figure 9). It appears to split after about a mile west of its intersection with the Opal Mound fault, with one branch continuing the WNW-trend and the other branch trending more nearly westwards. Traces of WNW-4 are lost about five miles west of the Opal Mound fault, but the main branch is apparently seen again a few miles further to the northwest. A parallel zone about a mile to the north of the Negro Mag Wash fault (WNW-4) is here referred to as the Salt Cove fault zone, WNW-3. It can be traced westward about ten miles across the valley and at its west end appears to join the extension of the main branch of the Negro Mag Wash fault just mentioned.

In the western part of its course, the Salt Cove fault breaks up into three zones arranged en echelon at an angle, in a pattern that suggests the zone may be a steep to vertical right-handed strike-slip fault.

Similar features are seen along the Negro Map Wash fault thought they are not so marked. That fault is also probably a right-handed strike-slip fault. Where it is seen in the range, Sibbett and Nielson show it as down-dropped on the north side. Crebs and Cook (1976) on the other hand concluded that the fault had a down-to-the-south displacement of about 60' in their N-S gravity profile about 1,000' west of its intersection with the Opal Mound fault. These geometric relations do not consider lateral offset, and would still be consistent with the interpretation that the most significant movement on the fault has been strike slip. A supporting argument can be made that the Negro Mag Wash fault offsets the northward continuation of the Opal Mound fault to the east.

Another prominent member of the WNW set of linears lies two miles further north, emerging from the range in the mid-part of section 23 (26S/9W). This zone (WNW-1 and WNW-2) can be followed west-northwest for six miles across the valley, with a branch extending NW from where the fault intersects the edge of the range.

South of the Negro Mag Wash fault about five to six miles, there are two other prominent WNW faults, one along the incised part of Ranch Canyon (WNW-6), and the other half a mile to a mile north of this (WNW-5). The Ranch Canyon linear WNW-6 can be traced 5½

R10W

R9W

R8W

T
26
S

T
27
S

T
28
S

Pacific

Union

WNW-1

WNW-2

WNW-3

WNW-4

WNW-5

WNW-6

WNW-7

WNW-8

WNW-9

Figure 9

WNW-TRENDING FAULTS

Boundary of Study Area

miles WNW-ward, where it is cut off by a N-trending fault scarp of a different system involving westward down-dropping. WNW-5 trends more nearly northwest for about six miles and then meets an E-W linear that cuts across the same N-trending fault scarp.

Relative offset on the two faults WNW-5 and 6 again seems to involve right-handed movement. This can be inferred from their effect on N-trending faults near lower Ranch Canyon Road, two miles west of the Mineral Range. This point is discussed in more detail later. It is notable that Crebs and Cook (1976) also concluded that faults of this WNW orientation were right-handed on the basis of their offsets of gravity features in the area of the geothermal field.

There are a few other shorter, less consistent, traces of the WNW set of faults. One is the broad zone (WNW-7) about four miles south of WNW-6. Another is a zone WNW-8 that would intersect the Opal Mound fault in the northern part of the Opal Mound itself, north of the line between sections 9 and 16 (27S/9W). WNW-9 is a short zone just south of WNW-8.

N-Trending Faults

Fault scarps of this set (Figure 10) are quite prominent, and were in part mapped by Peterson (1975), Nielson et al., (1978), and Sibbett and Nielson (1980). They often show visible evidence of vertical movement, almost always with the west or valley side being down-dropped.

They consist of discontinuous traces, straight or curving, that form irregular patterns that branch and intersect. They clearly represent collapse structures in very shallow unconsolidated surface materials resulting from upward propagation of displacement in more consolidated material at slightly greater depths. These are apparently major N-trending down-to-the-basin faults that are currently active in the continuing evolution of this part of the Escalante graben. (On the other side of the graben to the west, beyond the area of this study, one can map similar N-trending faults, forming a symetrical set; on these, the east side is down-dropped).

Figure 10 shows the N-trending fault system. There are two main zones. One passes a mile or two west of the geothermal field, and the other lies four miles further west.

R10W

R9W

R8W

T 26 S

T 27 S

T 28 S

Pacific

Union

N-1

N-2

N-3

N-4

N-3

N-2

Figure 10

N-TRENDING FAULTS

Boundary of Study Area

The two zones cannot be traced continuously over the length of the study area. N-1 and N-2 appear to correspond, but there is a large gap between them. N-3 is more continuous except between WNW-4 and WNW-5.

These discontinuities may partly be explained by local erosion of the scarps. But there is probably another factor. The crystalline basement and the Tertiary sequence above it have been sliced into separate blocks by the major through-going WNW-trending strike-slip faults.

In the different blocks between these faults, present day down-to-the-basin movement is probably occurring on different members of the family of N-trending faults in each block: hence the lack of continuity in recent scarps along any one of the N-trending faults.

N-3 is the westernmost member of this system within the study area. It lies about 1½ miles east of the railroad, in the southern third of the area. Followed northwards, it is cut by WNW-5 and then becomes hard to trace, but can be picked up again about four miles to the north. Southwards, it curves to a southwest trend as it passes out of the mapped area, before resuming its southward course and passing east of Milford. The line of fault scarps of N-3 is straight and almost continuous, with the surface relatively down-dropped to the west. Short sets of ENE linears show tiny right-handed offsets of the N-trending zone.

From the intersection of N-3 with WNW-5, a branch curves somewhat east of north, aligned with another set of faults that trend NNE (NNE-6). The trace disappears between the Negro Mag Wash and Salt Cove faults (WNW-4 and WNW-3), but it is again seen as NNE-8, a series of fault scarps with west side down. NNE-8 finally intersects with N-1 in the northeastern part of the area.

The second major N-trending zone (N-2) lies three to four miles further east. In the southern half of the area there are two lines of scarps that are much more irregular and broken than N-3; they seem to from two parallel sets about half a mile apart, representing a very irregular response of the shallow alluvial cover to movements on two N-trending faults at greater depth. Above both fault lines, which can be traced more than ten miles, the west side appears to be down-dropped, but within the zone between them there are locally some scarps down to the east where the cover has broken into smaller horsts and grabens.

The southern part of N-2 crosses one of the gravity profiles of Crebs and Cook, (1976) (profile B) and they interpret it as a major fault, west side down, with a dip slip of 1500', using a density contrast of 0.5 gm/cc (Figure 11).

Although the two zones of N-2 are somewhat discontinuous and curvilinear, it seems clear they are offset both by WNW-5 and WNW-6. In each case the north side is displaced relatively eastward. This seems to confirm the hypothesis that the WNW set of faults are right-handed strike-slip faults, and to show that some of the movement on them post-dates formation of the N-trending faults.

N-2 cannot be traced as far north as Negro Mag Wash, but seems to reappear again after a 6½ mile gap, as N-1. Here there are two parallel zones that are fairly linear and persistent, three-quarters of a mile apart. Just north of the boundary of the map there are two other short parallel linears a little east and west.

If these two faults comprising N-1 can be correlated with the two faults of N-2, then right-handed offset by the WNW fault system is again implied.

The fault zone N-2, at its southern end, shows the same curve from a southward to a southwest trend that was noted in describing N-3. This change in trend corresponds with the gravity pattern portrayed by Carter and Cook (1978) just southwest of the index number 4 on their figure 8 (p. 54) which is reproduced here as Figure 12. A triangular fault block with unusually shallow basement is indicated by the gravity data, which also gives major expression to the fault zone of WNW-5 and WNW-6.

In the north part of the area, between N-3 and N-1, there is another segment of N-trending fault traces, this one without obvious vertical displacement of the surface. It is labeled N-4 and is about 3 miles long. The zone changes trend when followed southward, and ends at its intersection with WNW-3 and WNW-4.

In summary, N-3 and N-2/N-1 correspond to major down-to-the-basin normal faults, based on seismic, magnetic and gravity data, and other structural evidence (Figure 12A).

We thus arrive at a picture of the basement cut into a series of blocks by WNW-trending faults, (especially WNW-4, -5 and -6), which are right-handed strike-slip faults. These cut and displace

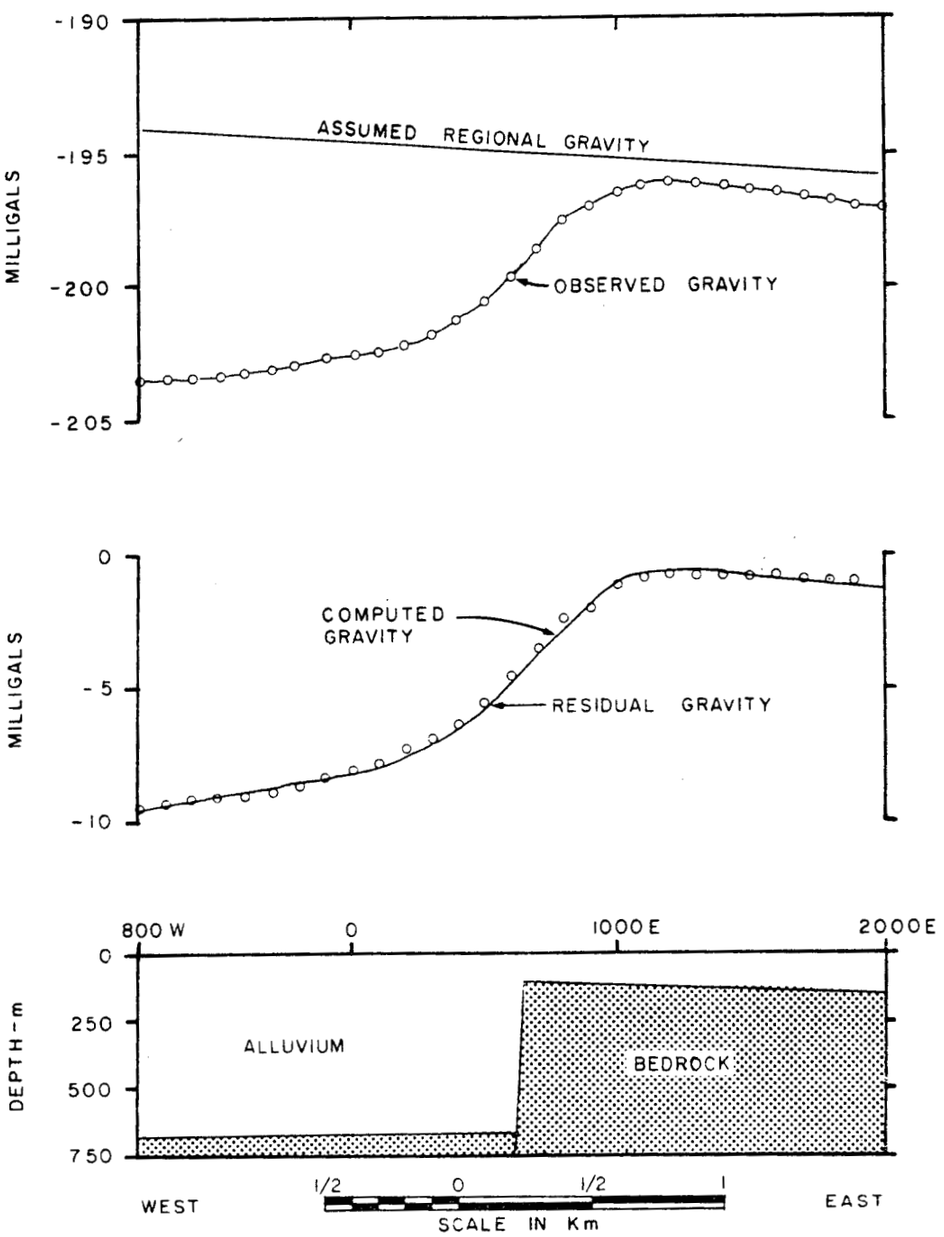

Figure 11: Interpretive two-dimensional model for gravity profile B. Assumed density contrast is 0.5 gm/cc.

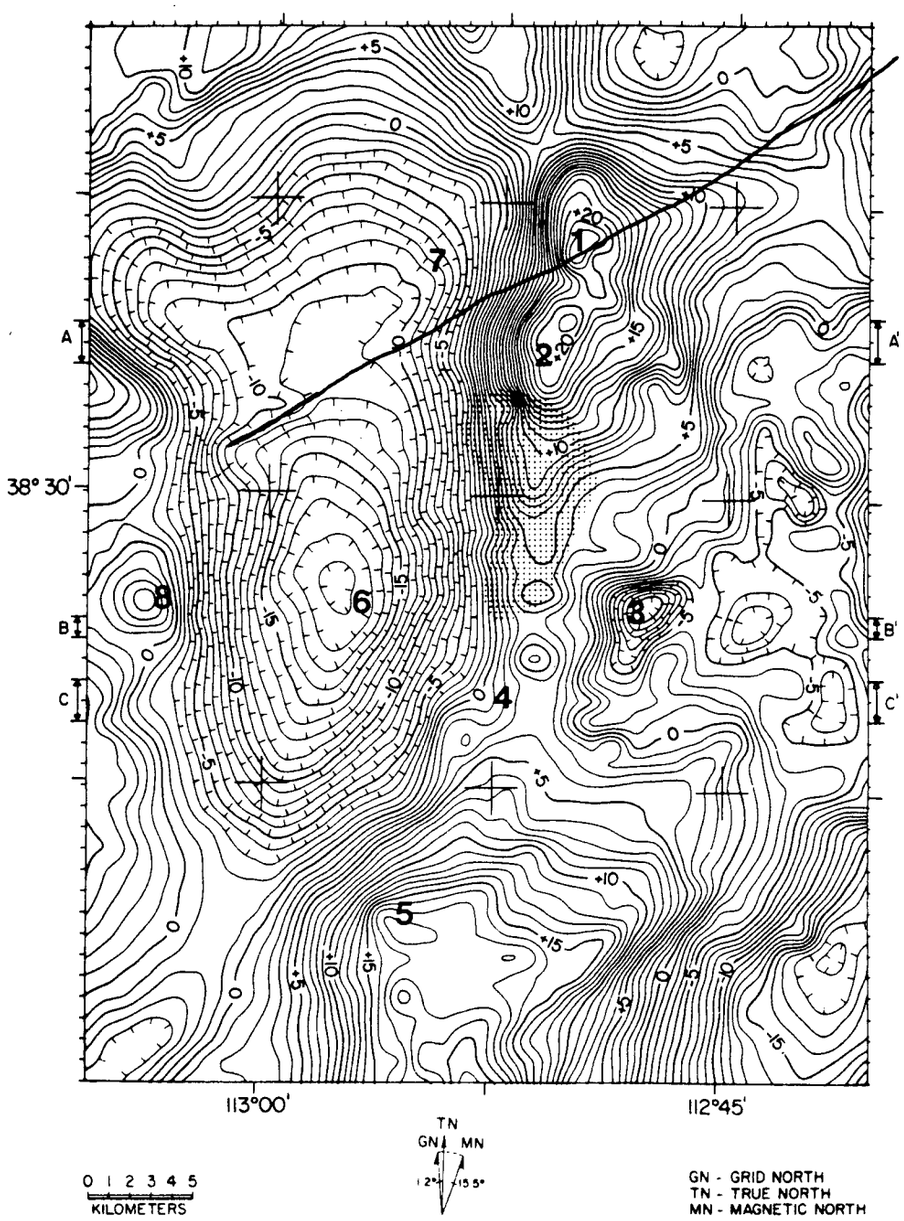

Figure 12: Residual gravity anomaly map with best-fit projected regional removed; contour interval = 1 mgal.

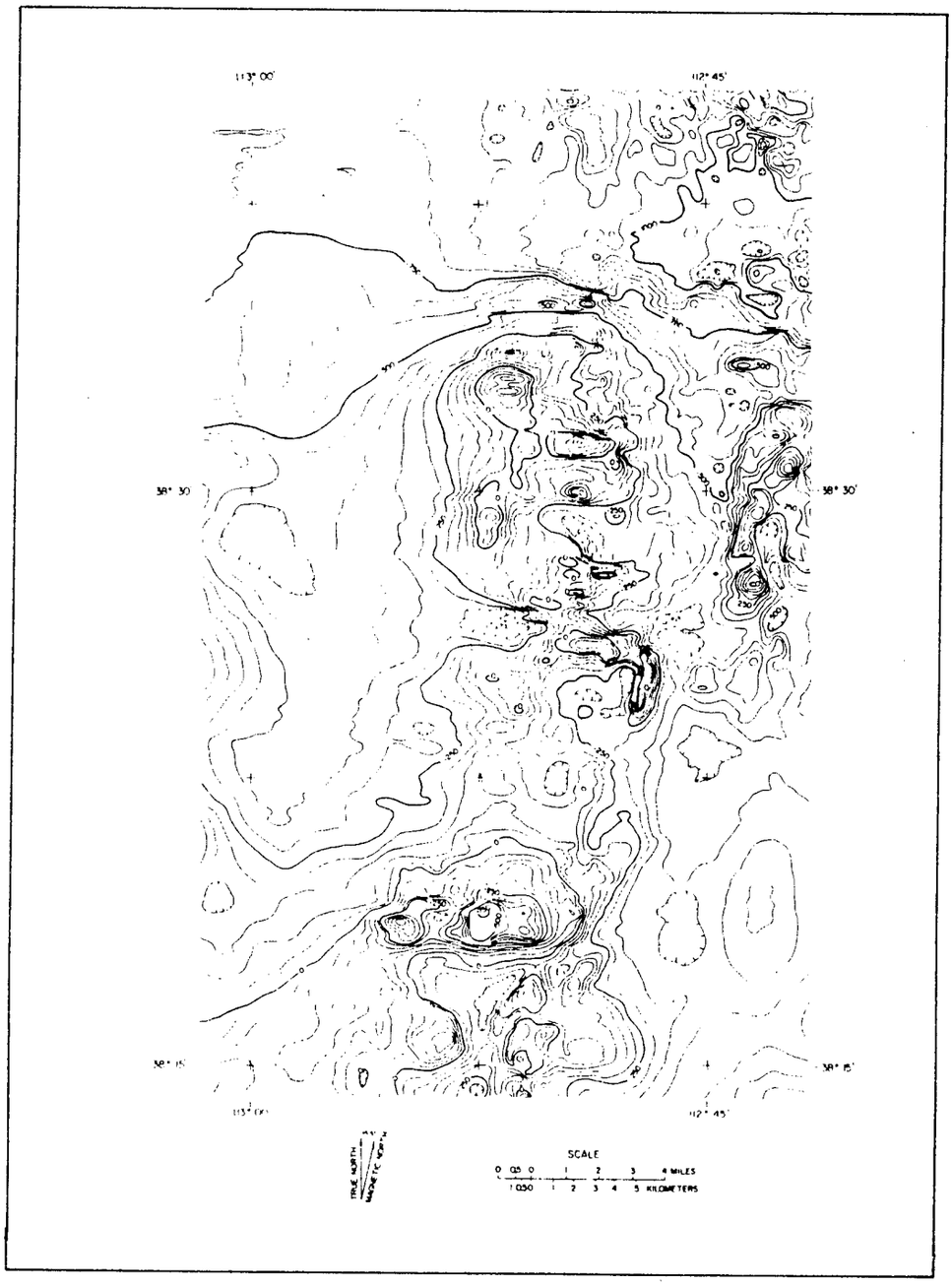

Figure 12a

TOTAL MAGNETIC FIELD INTENSITY: RESIDUAL ANOMALY MAP

the set of N-trending down-to-the-basin normal faults that control the gross geometry of this part of the Escalante graben.

NNE-Trending Faults

Obliquely extending from the west edge of the fault map (Figure 13) there is a narrow triangular area, forming the northwest portion of the map, which is dominated by NNE-trending faults. The belt runs slightly west of Milford and can be traced on Landsat imagery a long distance to the south, two or three miles beyond Thermo, where it ends against the ENE-trending frontal fault of the Black Mountain block.

North of Milford, the same fault zone continues to an area about 2½ miles west of the northern tip of the Mineral Range: there it is truncated by a WNW linear that is very clearly displaced in the imagery. The NNE-trending zone is about a mile wide, and can be traced more than thirty-four miles on the imagery, without break or deviation.

The east edge of this zone (NNE-1) can be clearly seen on the air photographs, and can be traced as far as the Negro Mag Wash fault but no further. However, it appears that WNW-1 and WNW-2 end abruptly where NNE-1 would pass if its trace were projected. Of all the WNW faults, only the Negro Mag Wash fault can be traced across this NNE-trending zone.

West of NNE-1 there are a large number of short linears parallel to it within the map area; NNE-2, -3 and -4 have been specifically labeled.

East of it, there are far fewer, though some are seen near Ranch Canyon (NNE-5) and two other zones lie a few miles west of the Opal Mound and Negro Mag Wash fault intersection (NNE-6 and -7).

NNE-8 is probably the extension of NNE-6, as mentioned earlier in the discussion on N-trending faults, seeming to connect N-3 and N-1, and to act as one of the down-to-the-basin fault zones. Most members of this system of NNE-trending faults, however, seem likely to be steep or vertical strike-slip faults, rather than normal faults, based on linearity, undeviating direction, and persistence over more than thirty-four miles. However there is no direct evidence of the dip of the NNE-trending faults, nor is there evidence of the sense of displacements on them.

R10W

R9W

R8W

T 26 S

T 27 S

T 28 S

NNE-1

NNE-2

NNE-3

NNE-4

NNE-5

NNE-6

NNE-7

NNE-8

Pacific

Union

Figure 13

NNE-TRENDING FAULTS

Boundary of Study Area

One major NNE-trending zone lies immediately south of the area of the fault map. It is seen very plainly in satellite imagery as a broad zone extending NNE-ward from the westernmost point of the southern Mineral Mountains to the area between Ranch Canyon and Corral Canyon. On the ground it is seen to be a zone of less sparse vegetation. On air photos a series of parallel fault traces can be identified within it. It lies west of the series of rocky knobs that emerge from the alluvium in the broad embayment of Milford Valley through which The Pass Road makes its way.

ENE-Trending Faults

A conspicuous linear feature trending ENE can be seen on the satellite imagery to cross the northern part of the study area. It can be traced into the area from the southern part of the Pavant Range, across the northern margin of the Cove Fort basalt field and into the northern Mineral Mountains just north of Pinnacle Pass. It then continues across the Milford Valley to the southern part of the Rocky Range. As it crosses the valley, it appears as a series of two darkened zones, arranged en echelon. At the east edge of the NNE-trending linear, NNE-1 it becomes difficult to follow any further.

On the air photos these features are not picked up well (Figure 14). At Pinnacle Pass, a series of air photo linears trending ENE can be traced for about five miles (ENE-1) and at the Pass itself these were mapped by Sibbett and Nielson (1980).

Parallel to this zone, and three miles north, is ENE-2 which is traceable for six miles. Another two miles to the north, a third linear (ENE-3) extends five miles.

These zones are important to the structural interpretation, not only because the satellite linear appears to be traceable for at least many tens of miles, but because it corresponds in the Milford Valley to a major feature in the gravity picture developed by Carter and Cook, 1978 (see Figure 12).

Faulting of this orientation can be inferred to produce several effects on the gravity pattern. It appears to offset the main north-trending fault zone on the east side of the graben, between the index numbers 1 and 2 of Figure 12, with relative eastward offset of the north side of the fault. Such right-handed motion is consistent with the pattern of the two en echelon segments

R10W

R9W

R8W

T 26 S

T 27 S

T 28 S

Pacific

Union

ENE-1

ENE-2

ENE-4

ENE-5

ENE-6

Figure 14

ENE-TRENDING FAULTS

Boundary of Study Area

relative to the overall trend of the satellite linear. From a point on the gravity map just south of index number 1, the zone can be inferred to pass WSW, cutting the graben into two markedly different parts, with simple basin geometry to the south centered around the index number 6, but with a much more complex geometry to the northwest.

Other areas on the gravity map show evidence of faults of the same orientation, for example trending southwest from index number 4. Furthermore, the frontal fault of the Black Mountains block south of Thermo has this same trend. The magnetics (Figure 12 A) show the en echelon zone.

Faults of this ENE system, though they are not well represented by linears visible in the air photographs, are sufficiently important structurally that they are likely to provide major pathways for upward geochemical transport and thus to be of significance in the geochemical interpretation.

ENE-4 intersects the Opal Mound fault south of Negro Mag Wash, and ENE-5 extends between N-3 and N-2 in the Ranch Canyon area. The fact that tiny offsets of the scarps of N-3 are right-handed confirms the concept that these ENE-trending faults are right-handed strike-slip faults, and are probably close to vertical.

SUMMARY

There are four major sets of faults in the northern part of the Milford Valley. The simplest are the N-trending normal faults which show down-dropping on their western side and control the geometry on the Escalante basin, as indicated by the gravity picture. They probably dip west at around 60^{o}. This set is cut and in places displaced by the major WNW-trending set, which are probably vertical right-handed strike-slip faults.

The NNE-trending fault zone cutting across the northwest portion of the area perhaps post-dates the WNW system, since it appears to truncate them and remain undeviated by them. It probably represents a steep zone of strike-slip motion, though there is little evidence to confirm this hypothesis except that the zone is characterized by seismic activity with focal depths greater than 10 km, Ward et al., 1978).

The ENE-trending faults appear to be major right-handed strike-slip

faults. The en echelon zone appears to have major structural effects, reflected in the gravity and the magnetic patterns.

The Opal Mound Fault

Interestingly enough, the Opal Mound fault remains something of an enigma, as its strike lies between that of the N-trending and the NNE-trending sets. Its strike is perpendicular to the WNW-trending faults. Gravity data and present physiography indicate current vertical motion on it, east side down; but this could merely be the most recent motion. Its dip is not really known. It has not been identified with certainty in the wells east of it, and is shown in cross-sections with a 60^{o} eastward dip only because of the east-side-down displacement seen along its surface trace. It could be vertical or dip west.

The best producing wells, 54-3 and 3-1, are too shallow to reach the Opal Mound fault if it does dip east at 60^{o}. They were drilled to 2,882' and 2,728' respectively, while the Opal Mound fault would be expected at about 3,300' to 3,400' in these wells. (They could, however, intersect an unnamed NNW-trending fault mapped by Nielson et al., 1978).

In well 13-10 the Opal Mound fault would be expected at about 2,100'. Production comes from various intervals between 1718' and TD at 5,351'. Thus the bottom 3,200' of this well would be in the footwall of the Opal Mound fault, given the model of a 60^{o} dip to the east. The dip would have to be closer to 80^{o} if the well is entirely in the hanging wall of the fault.

Well 72-16 would have intersected the fault at about 1,500', but TD was only 1,254'.

Thus the evidence does not demonstrate that there is a clear-cut relation between production and intersections with the Opal Mound fault, nor that the direction or angle of dip can really be determined from the well data.

NNW-Trending Faults

The Mineral Range exhibits a system of NNW-trending faults that are particularly common southeast of the field (Nielson et al., 1978; Sibbett and Nielson, 1980). A group of these appears to trend right into the southeast part of the field from the ridges

of Precambrian metamorphics, and it has been suggested that these faults make a major contribution to the fracture permeability of the reservoir.

Faults of this kind have not been mapped in the present study of air photos of the Milford Valley. They would appear to be presently inactive, in the sense that no movement on them has left its traces on the ground surface in the valley.

SPATIAL ARRANGEMENT OF THE ROCK MASSES

The previous section dealt with the structural framework of the Roosevelt region and with the major fault and fracture zones that might provide the easiest pathways for upward geochemical transport to the surface.

In this section, the region in and around the geothermal field itself is examined in more specific detail. The relevant available data on the form and distribution of the different rock masses below the surface are reviewed, as a kind of geometric dissection in three dimensions.

In the mountains immediately east of the field, the ridges and spurs coming down to the valley are made up of metamorphic rocks intruded by Teritary granitic rocks.

The contact between the two is complex, as the metamorphic rocks form roof pendants in the Tertiary pluton, and numerous Tertiary dikes cut the metamorphic rocks. Additionally, the contact is in some places faulted.

The inevitable irregularity of such a contact means one cannot easily determine the sense of displacement along faults that cut it. Nor can one extrapolate very easily underneath the alluvial cover in the area of the geothermal field.

The rocks intruded by the Tertiary pluton are of three types: 1) a sequence of banded gneisses of Precambrian age; 2) hornblende gneisses that are probably Precambrian; and 3) granodiorites of unknown age which, to the southeast, cut Cambrian carbonates and may be Jurassic in age (Sibbett and Nielson, 1980).

The banded gneiss sequence consists of light colored, well foliated genisses and schists that are somewhat variable in composition. There is some development of migmatite textures. Isoclinal and ptygmatic folds are common. The hornblende gneiss is a foliated quartz monzonite which intrudes the banded gneisses. The biotite granodiorite or biotite-hornblende granodiorite is a dark colored biotite granodorite or biotite-hornblende granodiorite that is only weakly foliated.

The Tertiary igneous rocks of the pluton in the area of the geothermal field consist of syenites and leucocratic granite, biotite granite, and some quartz monzonite, and are cut by dikes of aphanitic diabase, dark colored fine-grained granite, and microdiorite. Ward et al., (1978) considered the pluton might be as young as 10 m.y. in age on the basis K-Ar data. However, the Precambrian metamorphic rocks have given a similar date (10.5 m.y.) based on K-Ar data, and Sibbett and Nielson (1980) concluded that the Tertiary pluton may be assumed to be 20-29 m.y. in age, with some more recent thermal event resetting the date.

Production in successful wells has been entirely dependent on fracture permeability in the granitic and metamorphic rocks discussed above.

One might expect that the various metamorphic and igneous rocks would be characterized by different fracture densities, and that some rock-types might thus prove to be better reservoir rocks. However, data on production intervals in the field seems to show no correlation with rock-type, and no observer has commented on such a relationship. Instead, the key feature seems to be the intersection of major fracture and fault zones.

Over the geothermal field, between the Opal Mound fault and the Mineral Range, the alluvial cover ranges up to about 700' thick. Crebs and Cook (1976) published a series of gravity profiles, two of which lie along E-W lines across the main portion of the field. Depths to basement were interpreted using a density contrast of 0.5 gm/cc. The profiles show that at the Opal Mound fault, the basement is deeper on the E side. They estimated the vertical offset at about 165' on both profile 4,000 N, through the middle of section 3(27S/9w), and profile 2200 N, which runs approximately through the middle of section 10.

Such relative movement down to the east of the Opal Mound fault conforms with what is seen at the surface, where Peterson (1975) observed that the ground was apparently downdropped at least 20' to the east in the area of the Opal Mound (section 16). She added that surface displacement at the north end of the fault is probably about 15' down to the east.

West of the Opal Mound fault, Crebs and Cook indicated a horst trending slightly east of north, with the Opal Mound fault forming the eastern boundary of this upfaulted block. Depths to basement

over this horst are in places less than 75' according to their profile 2,200 N near the Opal Mound, and are 117' at hole DH 1 on profile 4,000 N, some 6,000' further north.

Confirmation of the thinness of the alluvial cover in the area of the geothermal field comes from other well data such as at well 3-1 (285'), 14-2 (about 260'), 13-10 (about 270'), 72-16 (about 480' but faulted), and 52-21 (about 590').

West of the Opal Mound, the alluvium gradually thickens to the west. Depth to basement in the center of the Milford Valley has been estimated by different authors in the range 1.8 km (5,900') by Crebs and Cook (1976), 1.5 km (4,900') by Carter and Cook (1978), 1.8 km (5,900') by Tripp et al., (1978), and greater than 1.8 km by Gertson and Smith (1979).

It seems possible that the depth to bedrock in the center of the basin may be considerably greater than 6,000'. Gertson and Smith (1979) in their interpretation of a seismic refraction profile across the Milford Valley concluded that the overall density contrast of the valley fill was much smaller than that used in the calculations by Crebs and Cook (1976) and Carter and Cook (1978).

Their interpretation of the structure of the Milford Valley was a three-layer model, in which the surface layer, ranging in thickness from around 300' to around 2,000', corresponds to the Quaternary alluvium. They concluded this upper layer has its maximum development slightly east of the center of the valley.

The second layer below it was interpreted as a thick section of Tertiary rocks, with no obvious correlation to any sequence of rocks seen in outcrop at the edges of the valley. They discarded the idea that this second layer could consist of Paleozoic or Mesozoic sedimentary rocks, on the basis of gravity data. They assigned a density contrast of 0.2 gm/cc but comment that if the fifth-order residual they used contained local anomalies, then either the density contrast must in fact be larger, or the valley fill must be thicker in order to fit the observed gravity data. This second layer ranges in thickness from over 4,000', at its maximum, to zero at the edge of the valley where it wedges out below the younger alluvium.

The maximum development of the second layer lies somewhat to the west of the center of the valley (Figure 15, from Gertson and Smith, 1979).

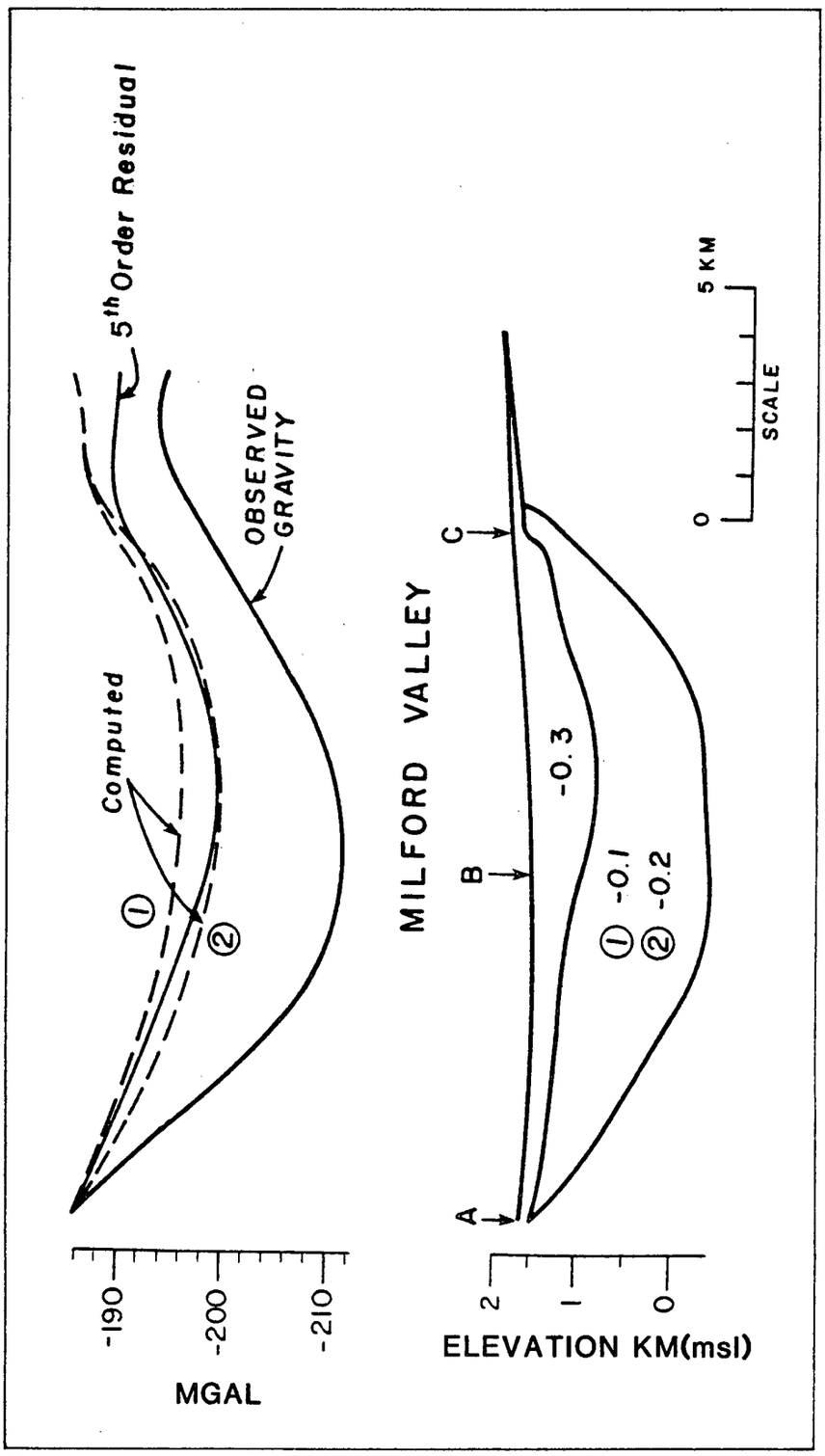

Figure 15

CROSS-SECTION OF MILFORD VALLEY, FROM SEISMIC & GRAVITY DATA

To summarize and simplify the details discussed above, we arrive at the following generalization:

If we could strip the overlying rocks away from the Precambrian metamorphics and the Tertiary pluton, and look directly at the shape of the basement surface, we would see spurs of the Mineral Range coming down to around 6,100' above sea level at the eastern edge of the Milford Valley. In the geothermal field immediately to the west, the basement level drops to around 300' to 700' below the surface. At the Opal Mound fault, the basement surface is upfaulted to a depth of only 75' to 125' before again falling gradually to the west (with some abrupt steps down-to-the-valley on two or three N-trending faults), before reaching a maximum depth considerably in excess of 6,000' west of the center of the valley.

On this basement surface, in this part of the Milford Valley, there is a thick wedge of Tertiary sedimentary rocks that almost fills the basin, but wedges out before reaching the margins.

Finally, over this Tertiary wedge, the surface layer of Quaternary alluvium lies as a blanket over the valley, its thickness varying from 300' to 700' in the geothermal field (where it lies directly on the crystalline rocks) to about 100' just west of the Opal Mound fault, and then gradually increasing to as much as 2,000' in the east central part of the Milford Valley, before thinning again toward the west side of the valley.

This, in essence, is the three-dimensional geometry of the rock masses which we need to consider in conjunction with the pattern of fractures and faults discussed earlier, in looking at the surface geochemical patterns.

In the next section, the history and results of the exploration drilling of the field are summarized in preparation for the detailed discussion of the reservoir later in the report.

RESULTS OF DEEP DRILLING AT ROOSEVELT

The first drilling in the Roosevelt area was in late 1967, in the area of the Opal Mound. Dr. Eugene Davie and Mr. A.L. McDonald drilled to 80' and found boiling water; they plugged and abandoned the hole. A second hole was drilled a few hundred feet further east to 165'; the water in the hole flashed to steam. This hole

was also plugged, but was then redrilled the following spring to a depth of 165' where the well became hard to control, flowing steam and hot water. It was finally plugged and abandoned.

Phillips Petroleum Company began a series of production tests in the spring of 1975, and additional wells were later drilled by Getty and by the ATO group composed of Amax, Thermal Power, and O'Brien Resources.

The well locations are shown on Figure 16. The commercially successful wells are Phillips' 3-1 (the commercial discovery well) 54-3, 13-10, 25-15, and 12-35; and ATO's 14-2 and 72-16.

The non-producing wells are Phillips' 82-33, 9-1, and 24-36; and Getty's 52-21.

In summary, the results and details of deep drilling are as follows, with the commercially successful wells described first, in the order in which they were drilled.

PPC 3-1 (55-3): TD 2728'; 7" casing at 2210'. Production interval 2210'-2728: tested at over 1.2 million lb/hr hot water. Location: SW¼ NE¼, Section 3, T. 27S, R. 9W. Drilled April-May, 1975.

PPC 54-3: TD 2882'; 9-5/8" casing at 1804'. Production interval 1804'-2882': reported to flow in excess of 1 million lb/hr hot water, over 500°F, and over 500 BTU/lb: rated "best well". Location: SW¼ NE¼, Section 3, T.27S., R.9W. Drilled July-August 1975.

PPC 12-35: TD 7324': 9-5/8" casing at 1814'. 7" liner to 4500'. Reported infiltration of cool surface water: thermal aquifer above 440°F now lined off: impossible to test satisfactorily. Location: NW¼ NW¼, Section 35, T.26S., R.9W. From NW corner, 330' S., 990' E. Drilled August-October, 1975.

PPC 13-10: TD 5351'; 9-5/8" casing at 1715'. Production interval ? 1718'-5351'; tested above 1 million lb/hr hot water at 75-125 psig. Location: Section 10, T.27S., R.9W. From NW corner, 1822' S., 200' E. Drilled October-November, 1975.

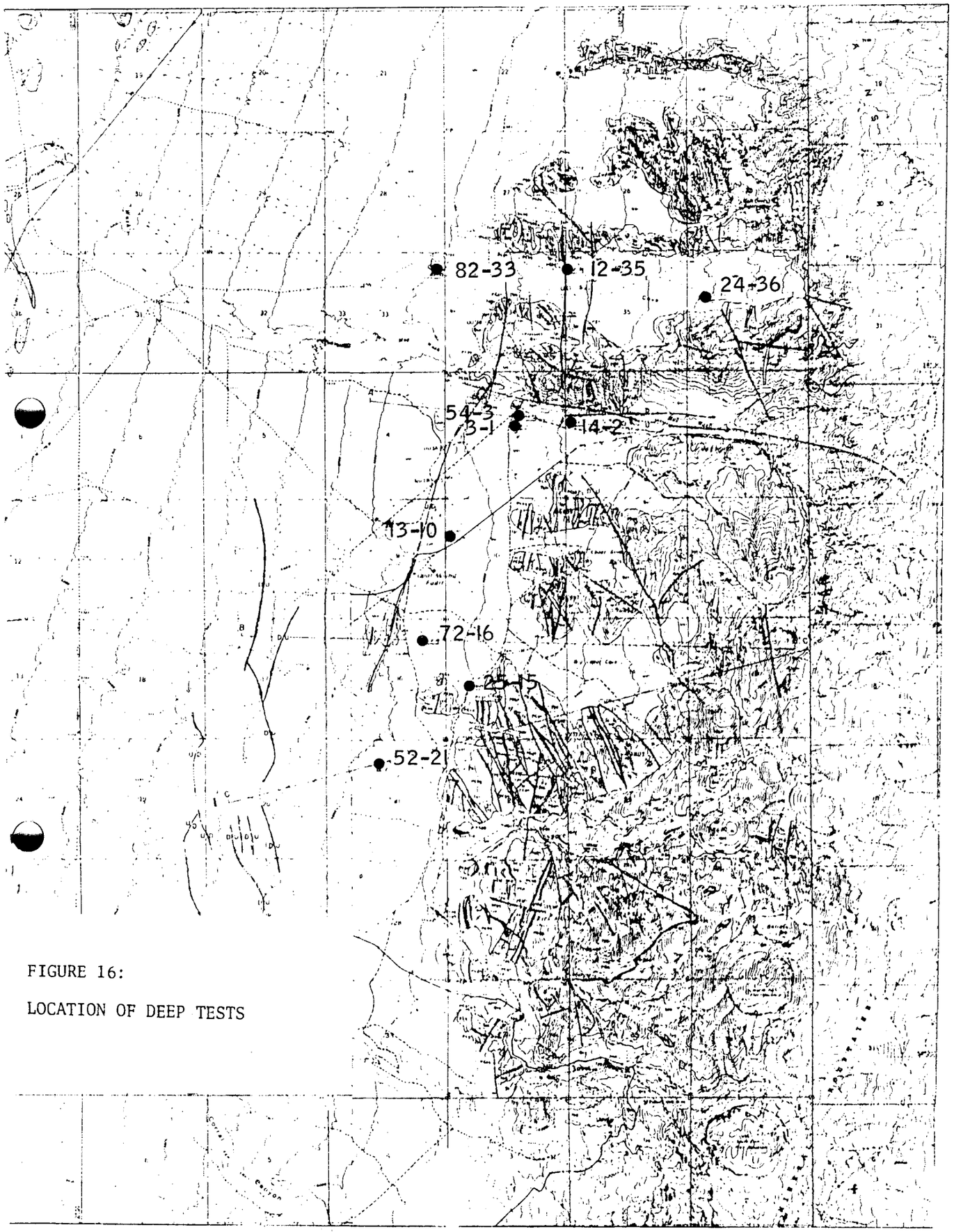

FIGURE 16:

LOCATION OF DEEP TESTS

PPC 25-15: TD 7500'; 9-5/8" casing at 2500±. Original TD planned to be 6000': no flow data. Report of cooling by inflow of near-surface water. Less satisfactory than wells to north. Location: Section 15, T.27S., R.9W. From W¼ corner, 330'S., 330'E. Drilled August-November, 1976.

ATO 14-2: TD 6108': 9-5/8" casing at 1805'. Flow tested at 447,500 lb/hr. 355 psia. Maximum temperature 514°F. Net enthalpy 485 Btu/lb around 4000'. Location SW¼, NW¼, Section 2, T.27S., R. 9W. Drilled September-November, 1976.

ATO 72-16: TD 1254': 9-5/8" casing at 1098'. Flow reported at 1.3 million lb/hr. 432° F. 355 psia. Maximum temperature 470°F. Hot water entries at 312', 500', 625' and 1244'. Location: Section 16, T. 27S., R. 9W. from NE corner, 990'S, 990'W. Drilled November-December, 1976.

Data for the non-producing wells are as follows:

Phillips 9-1: TD 6885'. Bottom hole temperature 446°F; low permeability. Very small flow. Location: NW¼ NE¼, Section 9, T. 27S., R. 9W. Drilled March-April, 1975.

Phillips 82-33: TD 6028'. Permit to deepen requested. 13-5/8" casing to 575'. Temperature between 300° and 350°F. Possible injection well. Location Section 33, T.26S., R.9W. From NE corner 1284'S., 77' W. Drilled November-December, 1975.

ATO 24-36: TD 6107'. Location: SW¼NW¼, Section 36, T.26S., R.9W. Drilled November-December, 1977.

Getty 52-21: TD 7478'. Temperature 402.4°F at TD. No flow. Location: NE¼ NW¼, Section 21, T.27S., R.9W. Drilled February-May, 1978.

There have been no further deep tests since Getty's drilling of 52-21, except for a well about five miles WNW of the field that was drilled to over 12,501 in March-July 1979. This is McCulloch's Acord #1-26, in the SW¼, Section 26, T.26S., R.10W. Full results have not been released, but economic reservoir temperatures were reached.

MASS AND ENERGY FLOW SYSTEMS

TEMPERATURE GRADIENT AND HEAT FLOW PATTERNS

By 1977 shallow temperature gradients had been measured in at least 39 holes, and the results were described by Sill and Bodell (1977). More recently, Wilson and Chapman (1980) have described and discussed data from 53 holes, 39 of them slim temperature gradient tests, and four of them the deep tests 72-16, 14-2, 9-1 and 52-21.

Sill and Bodell published a series of three thermal gradient contour maps based on data from different depth intervals: 30-60 m, 60-100 m, and below 100m. In the shallowest of these, for the interval between 30 and 60 m they showed two maxima, one (960°C/km) in the southern part of the field in the area of wells 72-16 and 25-15, and a second maximum (944°C/km) north of the Negro Mag Wash fault about 3000 feet southwest of well 82-33 near the Salt Spring south of Salt Cove.

In the series of measurements approximately on the east-west line through wells 72-16 and 25-15, there is a symmetry on each side of the area of maximum values, with gradients decreasing equally both to east and west. The pattern gives no indication of a difference between the productive area of the field of the Opal Mound fault, and the apparently barren area to the west. In fact to the east, at the boundary of the Mineral Range, the contours are shown as indicating a continuing fall in gradient, whereas for several miles to the west the values continue to remain high, slightly over 200°C/km.

In the northern part of the field a lobe to the northwest is present in the shape of the contours, though the details show that the lobe had to be drawn somewhat arbitrarily due to lack of data points. One reading to the west, just north of Negro Mag Wash fault gives 393°C/km, suggesting another interpretation of the shape of the lobe that would involve a more westward or WNW-ward trend to the axis of the lobe, rather than the NW direction which is given. (Later data supported this rather different interpretation of the pattern, as discussed below).

The plot for the intermediate depth interval from 60 to 100 m again shows two maxima, the southern one in the same location as

in the 30 to 60 m interval, near well 72-16 and 25-15. The northern one is displaced about 1,100 feet from the equivalent 30 - 60 m maximum. In this intermediate level of 60 to 100 m, the maxima are 575°C/km and 482°C/km, slightly over half the values observed in the interval 30 to 60m. The number of data points at this depth is much smaller, and contouring here shows a lobe in the area southwest of the field.

The final map of the three, presenting data in those wells that were drilled below 100 m, shows a curving ridge of higher values that follows the Opal Mound fault, extending from slightly south of well 72-16 up to the west of wells 54-3 and 3-1, through 82-33 and on to the northwest (though here again there is only a single data point in that area to constrain the pattern that is inferred from the data).

Sill and Bodell noted the coincidence of their patterns of maximum temperature gradients with the patterns from the first separation dipole-dipole work of Ward and Sill (1976, Figure 1). The resistivity pattern in the area west and northwest of the intersection of the Opal Mound and Negro Mag Wash faults may in fact have influenced the contouring of the temperature gradient data in that area. It is interesting to note that one reading on the dipole-dipole traverse 5950N just north of the Negro Mag Wash fault is the lowest value in the whole survey, 1 ohm-meter, though this is an isolated value among a series ranging from around 20 to 40 ohm-meters.

Wilson and Chapman, benefiting from the advantage of 14 additional data points, show in their map of surface conductive heat flow (Figure 17) a much more westward trend in the elongation of the lobe northwest of the field. Their map shows a very striking contrast between areas north and south of the Negro Mag Wash fault. While some of this could be subjective because of the small number of data points west of the field, the pattern is consistent with a plume of near-surface hot water moving WNW on the north side of Negro Mag Wash, with much less indication of such near-surface flow south of Negro Mag Wash. However, it could also indicate near-surface leakage from the Negro Mag Wash and Salt Cove fault zones <u>west</u> of the Opal Mound fault.

The average temperature gradient for Basin and Range conditions in Utah is about 35 to 40°C/km; in the Roosevelt region observed gradients range from around one third of that value to as much as 3331°C/km in the near surface part of well 72-16.

Figure 17

SURFACE CONDUCTIVE HEAT FLOW FOR ROOSEVELT HOT SPRINGS KGRA

For this present study, it is important to interpret the pattern of temperature gradients and heat flow in terms of conditions at depth. Wilson and Chapman make a different interpretation than the one preferred here. They admit that their procedure involves computing conductive heat leaking from an obviously convection dominated system. They do consider that the small lobe that projects eastward along the Negro Mag Wash fault is related to a "near surface feature and does not necessarily represent the reservoir geometry." And they comment on the strong fault control of the heat flow pattern. However in projecting downwards from the surface in order to assess the size and shape of the reservoir, they conclude that the northwest plume area, and the eastern spur just mentioned, are features still present 400 m below surface (Figure 18).

The available data on the reservoir are not sufficient to prove or disprove the concepts shown in the figure for the reservoir shape, with its elongate reservoir extension to the northwest and west north of the Negro Mag Wash fault. However, the method of calculation does not seem to be applicable to the situation at Roosevelt, for the following reasons.

Wilson and Chapman comment on the difficulty of separating conductive and convective regimes. At this point there is perhaps a problem with semantics. In a well it is easy to break the temperature-depth curve into isothermal sections which clearly represent convective circulation, and sloping gradients that represent conductive cooling. Looking at the heat flow map of Roosevelt, the question is: what aspects of the map express an upward conductive heat flow that would enable one to map out and delineate the field at depth, and what aspects are distortions of that picture produced by vertical upflow of geothermal fluids, and lateral motion in the shallow subsurface of hot plumes of geothermal brine?

This is critically important because in interpreting geochemical features at the surface, it is important to distinguish between elements in the heat flow pattern that are related to conduction and express the lateral variation in temperature at reservoir depth, from elements in the pattern that are related instead to shallow plumes. It is easy to see how geochemical signatures at the surface can be produced as a result of the massive upward movement of fluids, and the existence of lateral flows of brine at relatively shallow depths. It is less easy to see how a signature

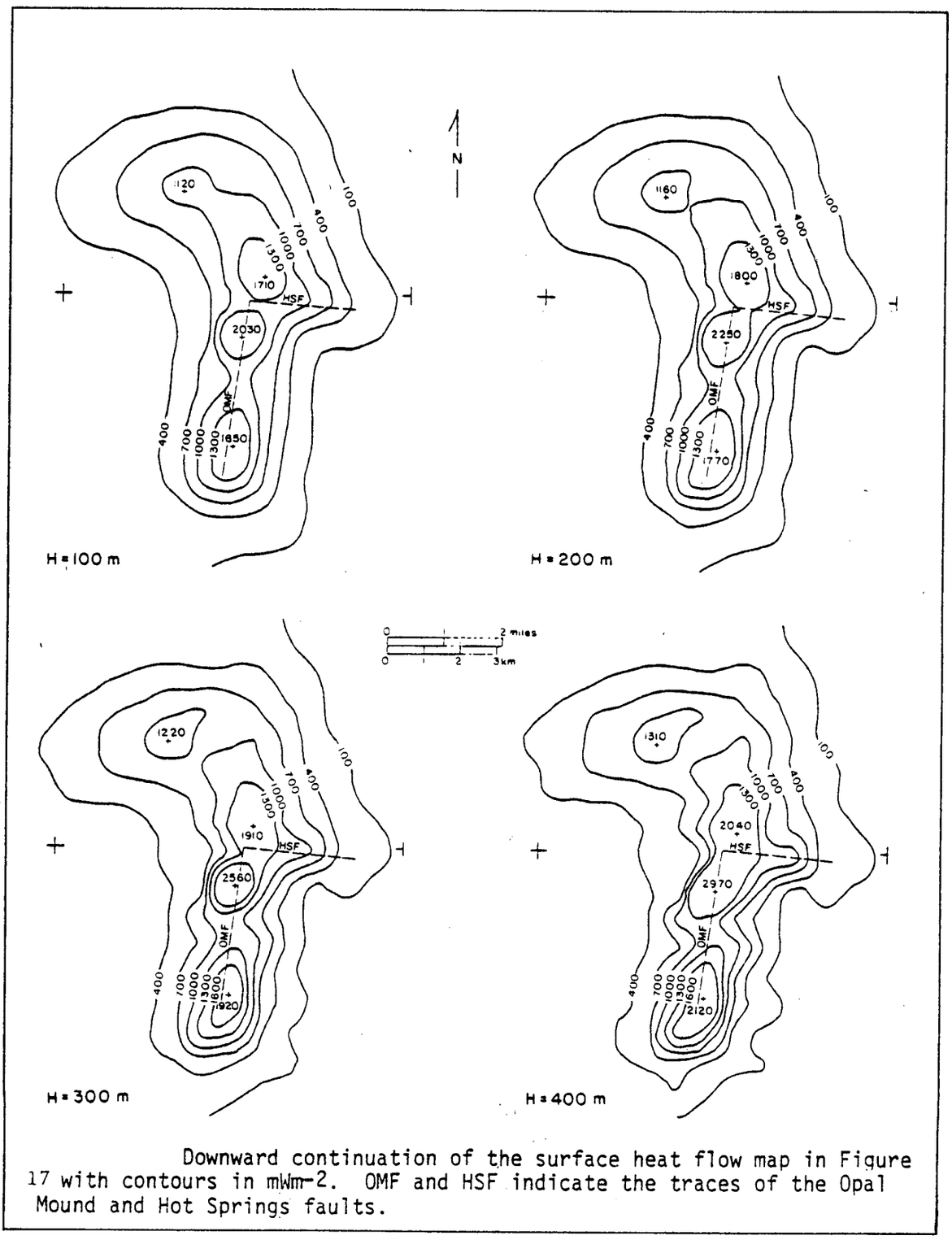

Downward continuation of the surface heat flow map in Figure 17 with contours in mWm-2. OMF and HSF indicate the traces of the Opal Mound and Hot Springs faults.

Figure 18

confined to the area vertically above the deep reservoir itself could be picked up on surface, without being smeared out by the near surface plumes.

It seems clear that the temperature gradients in the shallow holes in fact portray the lateral variation of temperature at relatively shallow depths, and are profoundly influenced by near-surface lateral flows of hot fluids fed to shallow levels up the Opal Mound fault and the Negro Mag Wash fault (and possibly a few other minor vertical conduits).

However, Wilson and Chapman argue along the following lines. They agree on the difficulty of distinguishing between convection and conductive regimes, and propose to resolve it by separating the zones above and below the water table. Above the water table, they consider that non-linearity in temperature/depth curves, which produces the key problem in downward extrapolation from the surface, could be caused by: 1) changing rock composition and/or porosity; 2) water vapor movement from evapotranspiration; 3) lateral heat conduction; 4) increasing water saturation as the water table is approached from above; and 5) temperature-dependent thermal conductivity. Discussing UU 75-1A, they observe that the rock in the hole is uniform, which rules out item 1. Item 2 they compute to be negligible, and item 3 to be sufficiently small to be ignored. Of the remaining possibilities, 4 and 5, they determine that the only significant effect is that of increasing water saturation with depth.

Below the water table, non-linear temperature/depth profiles can be caused by: 1) change in thermal conductivity as a function of composition, temperature, and porosity; 2) convective lateral heat transfer; 3) vertically flowing water; and 4) heat production from exothermic clay alteration reactions. Again considering UU-75-1A, item 1 is eliminated as being negligible. To evaluate the relative importance of the other three mechanisms, they agreed that it would be necessary to solve simultaneous equations for the conservation of momentum and mass flow, conservation of energy, and Darcy's Law. Instead, they use an approximation which they admit "neglects any contribution from free convection, turbulence, and lateral heat transfer. Since no hydrologic information was available to analyze the magnitude of the contribution from convective lateral heat transfer, it will be ignored here. However, this contribution could be substantial in the region above the reservoir."

They determine that, ignoring lateral heat transfer, vertical water flow is the dominant mechanism causing curvature in temperature profiles below the water table. They go on to say that their "consistent assignment of gradients at 30 m does not define the thermal nature within the deep geothermal system, but it is valuable in outlining near surface geometry and the extent of the system." This is the key point. Their method "can be applied to regions above a hypothesized reservoir where conductive heat transfer dominates." Thus the method is valid for determining conditions in the near-surface zone of upwelling and lateral motion of shallow discharge, but it does not provide a picture of the deep reservoir itself.

The picture that seems to be most valid on the basis of the data presently available is one of maximum heat flow along a line parallel to the Opal Mound fault, with gradients falling symetrically to the east and west, and with a southern termination corresponding to the zone between wells 72-16 and 52-21. In the north the zone north of the Negro Mag Wash fault appears to be leaking, even west of the Opal Mound fault, and producing a noticeable plume of near-surface hot brine flowing WNW along the main direction of ground water flow.

It is interesting to note that west of the southern part of the field the temperature gradients fall for about a mile and a half and then begin to rise again on the west side of the fault scarps of N-2. Just beyond these fault scarps gradient holes GPC-14, GPC-15 and TPC-10 show heat flow values of 336, 282, and 374 mWm^{-2}. At a distance of three quarters to one and a half miles west of N-2 the gradients are higher again: in GPC-6, PPC-WW2, and TPC-4 they are 430, 438 and 430 mWm^{-2}.

These measured gradients appear to indicate that further leakage of hot brine may be occurring at depth in this zone. Wilson and Chapman comment on the possibility of water leakage from an impermeable upthrown block in this area. In a later section, confirmatory evidence from well chemistry is discussed.

THE SHALLOW GROUNDWATER FLOW SYSTEM

The shallow groundwater system in the alluvial valley-fill of this part of the Escalante graben has been well described by Mower and Cordova (1973, 1974).

Irrigation wells in very large numbers exist in the fifty square miles south of the town of Milford, where agricultural development has been extensive, and overpumping has produced large declines in the level of the water table, as much as thirty feet in some wells.

Away from that area, well control is sparse, but it has still been possible to develop a picture of the shape of the potentiometric surface (Figure 19) from which the directions of ground water flow, generally perpendicular to the contours, can be read.

In the area of the KGRA, contours were omitted for lack of data, but they would clearly run north-northeast, with a progressive steepening of the slope of the water table as the edge of the range is approached. The movement of near-surface groundwater in the area of this study would thus be towards the west-northwest; velocities of water movement would probably be on the order of feet per day.

Within the alluvium of the main part of the valley, three main productive aquifers have been recognized and developed, with a combined thickness that reaches a maximum of over 800; about twenty miles south of Milford.

In the section of the valley west of the geothermal field, the aggregate reservoir thickness seen in the wells is between 100' and 300'.

Northwest of the field, this thickness is reduced over a wide area to less than 100', a change that could correspond to a possible flow path of mixed geothermal and non-thermal water; alteration, collapse of porosity, or mineral deposition over a long period of time may have reduced aquifer capacity.

Mower and Cordova (1973) estimated that approximately 14 million acre-feet are in storage in the valley, less than half of which may be recoverable. Annual recharge in 1970 and 1971 amounted to an average of 58,000 acre-feet while discharge averaged 81,000

FIGURE 19: POTENTIOMRTRIC-
SURFACE CONTOURS MAP

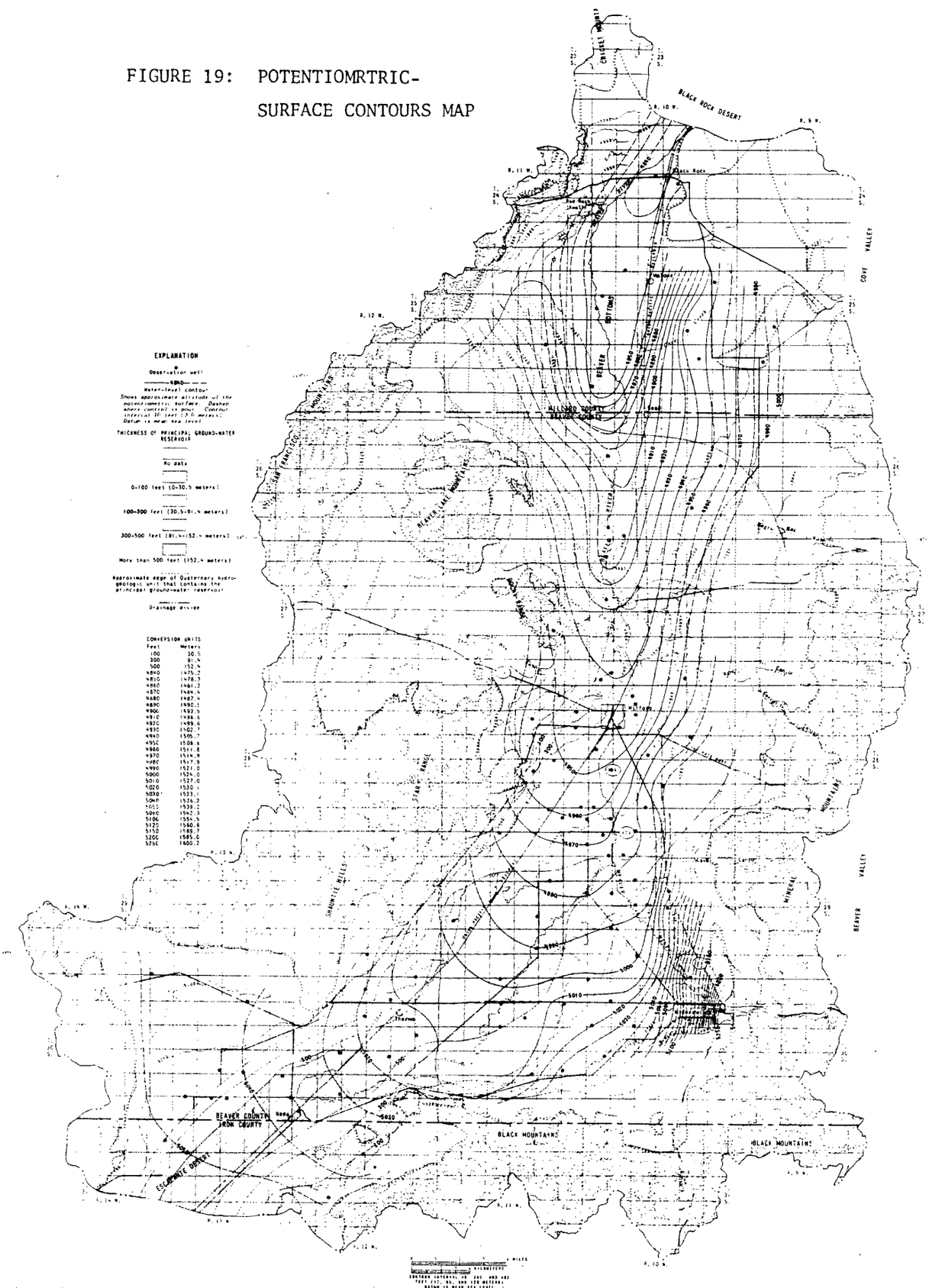

MAP OF THE MILFORD AREA, UTAH, SHOWING APPROXIMATE THICKNESS OF THE PRINCIPAL GROUND-WATER RESERVOIR AND POTENTIOMETRIC-SURFACE CONTOURS, MARCH 1972

acre-feet, of which 56,100 acre-feet was pumped from the irrigation wells.

In the main reservoir zones, Mower and Cordova (1973) estimated the transmissivity as ranging from about 1000 to slightly more than 40,000 ft^2/day, the higher values being found in the central part of the valley where the section is characterized by thick, well-sorted coarse sands and gravels. The storage coefficient is estimated to range from about 0.001 near the central part of the valley to 0.2 on the edge of the valley. Smith (1980), in developing a model to test the hypothesis of interbasin flow from the Beaver Valley into the Milford Valley, chose to use values for hydraulic conductivity in the range 0.1 to 10 ft/day for the Milford Valley alluvium. For the Tertiary valley fill below the Quaternary alluvium, Smith used the range 10^{-6} to 10^{-3} ft/day.

Water table depths in the Milford Valley west of the geothermal field are generally a few tens of feet, increasing to perhaps as much as 200' to 300' near the edge of the mountain range.

Composition of the shallow groundwater in the period 1970-1972 averaged 569 mg/l TDS in the wells, and 530 mg/l in the springs. The geothermal brines by contrast generally have 6,000 to 7,000 mg/l TDS.

To summarize the shallow, non-thermal groundwater system: a simplified picture adequate for the purpose of this work involves WNW-ward movement of cold shallow groundwater within the alluvial valley-fill across the area of the geothermal field and its surroundings, down into the center of the valley where the flow turns northward to an exit at the north end. The water table is from 100' to 300' below ground surface in the area under study. The groundwater contains less than 600 mg/l TDS.

Into this cold WNW-ward flow of groundwater, the geothermal fluids rise: hot liquid brines, steam, CO_2, H_2S, and other gases. The pattern of mixing between the rising geothermal fluids and the shallow groundwater is expressed in the pattern of chemistry and temperature of the near-surface waters, which are discussed in the next section.

CHEMISTRY OF THE SHALLOW GROUNDWATER

In order to place in perspective the chemical data on the reservoir fluids presented later, the available analyses of non-thermal surface groundwaters in the Milford Valley, taken from wells and springs, have been plotted in Figure 20A and B. The data are biased by the large number of observations in wells in the irrigated farming district immediately south of Milford.

However, most of the areas of the valley are represented in the data. There is an obvious and striking contrast between the geothermal brines, which plot in a very small field in the upper right section of Figure 20 A, and the shallow groundwaters. The former average 6,000 to 7,000 ppm TDS; the latter average less than 600 ppm TDS.

In Figure 20A and B, well samples 4, 5, 6, and 7 stand out as atypical, with relatively high Na, K and Cl values, closer in composition to the geothermal brines than to the shallow groundwaters of the valley. Total dissolved solids are: 4,600 ppm (4); 2,940 ppm (5); 1,840 ppm (6); and 647 ppm (7). Locations of these four wells are shown in Figure 21. The pattern suggests that the analyses may be demonstrating an admixture of geothermal brines into the normal valley groundwater.

While wells 4 and 5 are 1½ to 2 miles west of Reed, and thus located northwest of the field, wells 6 and 7 are due west of the main section of the Opal Mound fault. As the hydraulic gradient produces a flow to the WNW from the Roosevelt area, the presence of a component of thermal water in wells 6 and 7 would only be consistent with westward leakage of geothermal brines along the whole stretch of the Opal Mound fault, and not just north of the Negro Mag Wash, which would be another piece of evidence that tends to contradict the idea that the Opal Mound fault acts as an impermeable seal, and constitutes a total barrier preventing geothermal fluids from passing directly westwards from the main part of the field.

However, an alternative explanation is, of course, that another zone of leakage exists between the field and wells 6 and 7, beneath the alluvium of the Milford Valley west of the field. The heat flow pattern there suggests that this may in fact be occurring, as discussed in the previous section of this report.

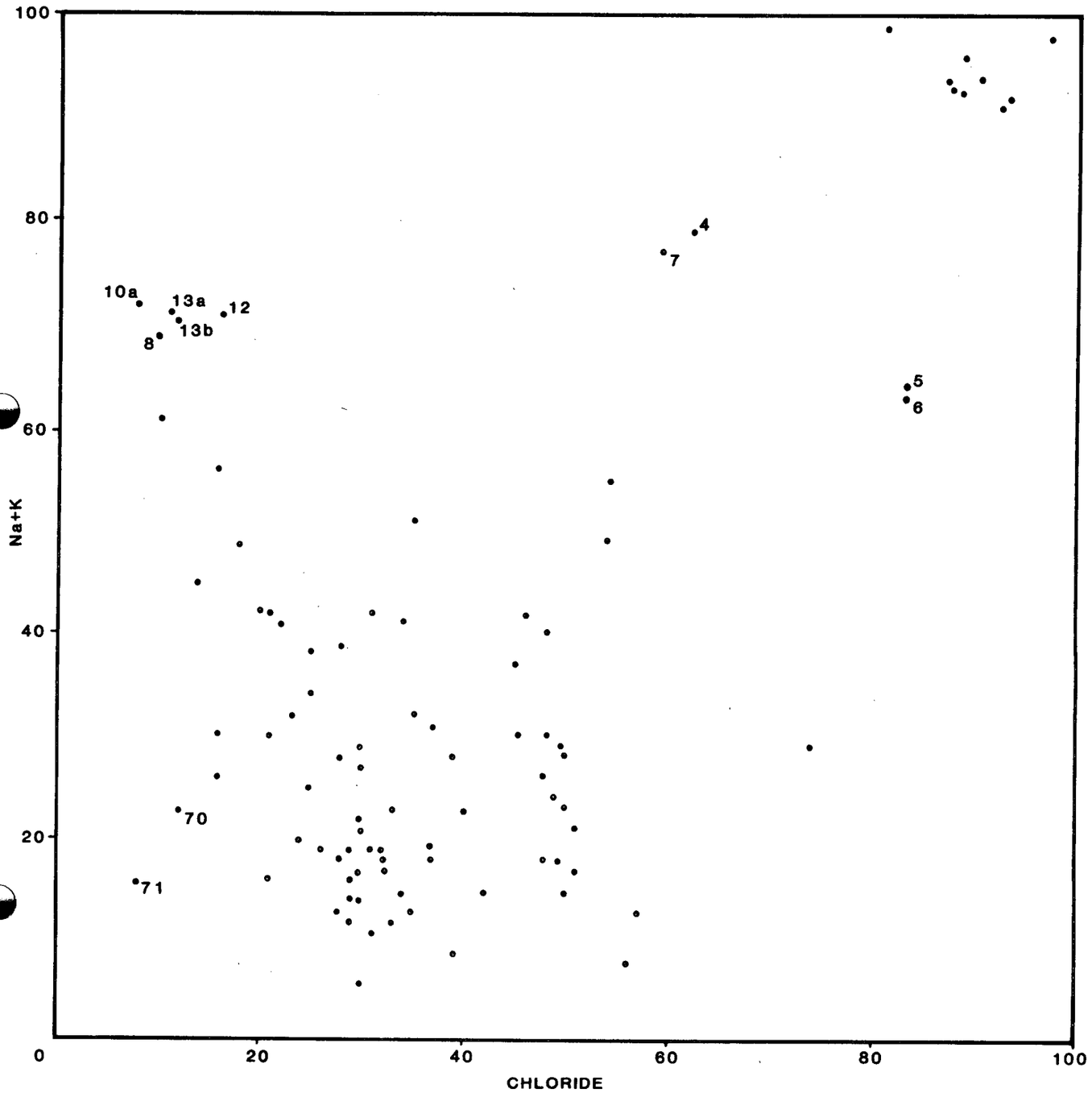

Figure 20a

MILFORD VALLEY WELLS & SPRINGS

MAJOR ANIONS & CHLORIDE

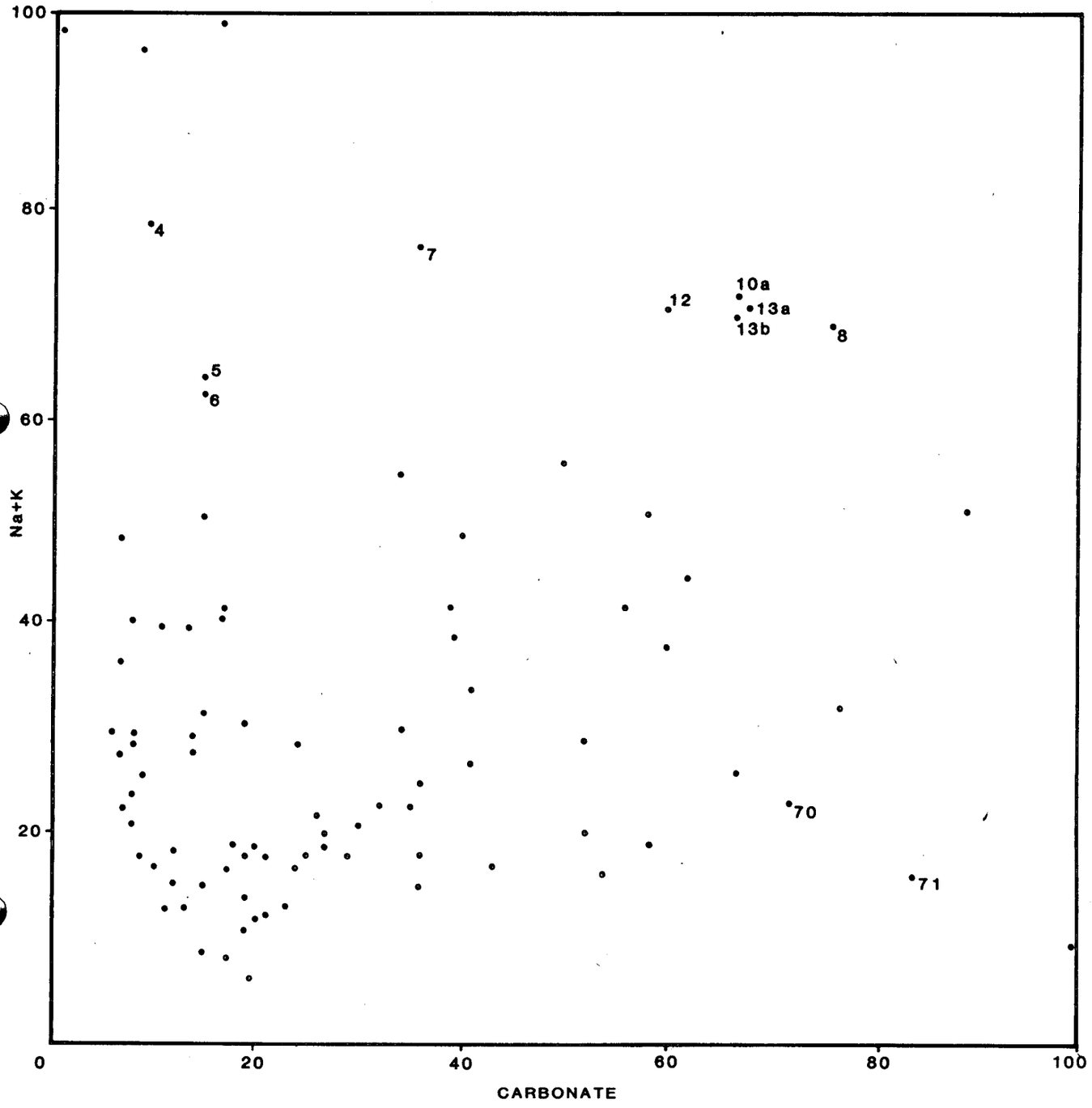

Figure 20b

MILFORD VALLEY WELLS & SPRINGS

MAJOR ANIONS & BICARBONATE

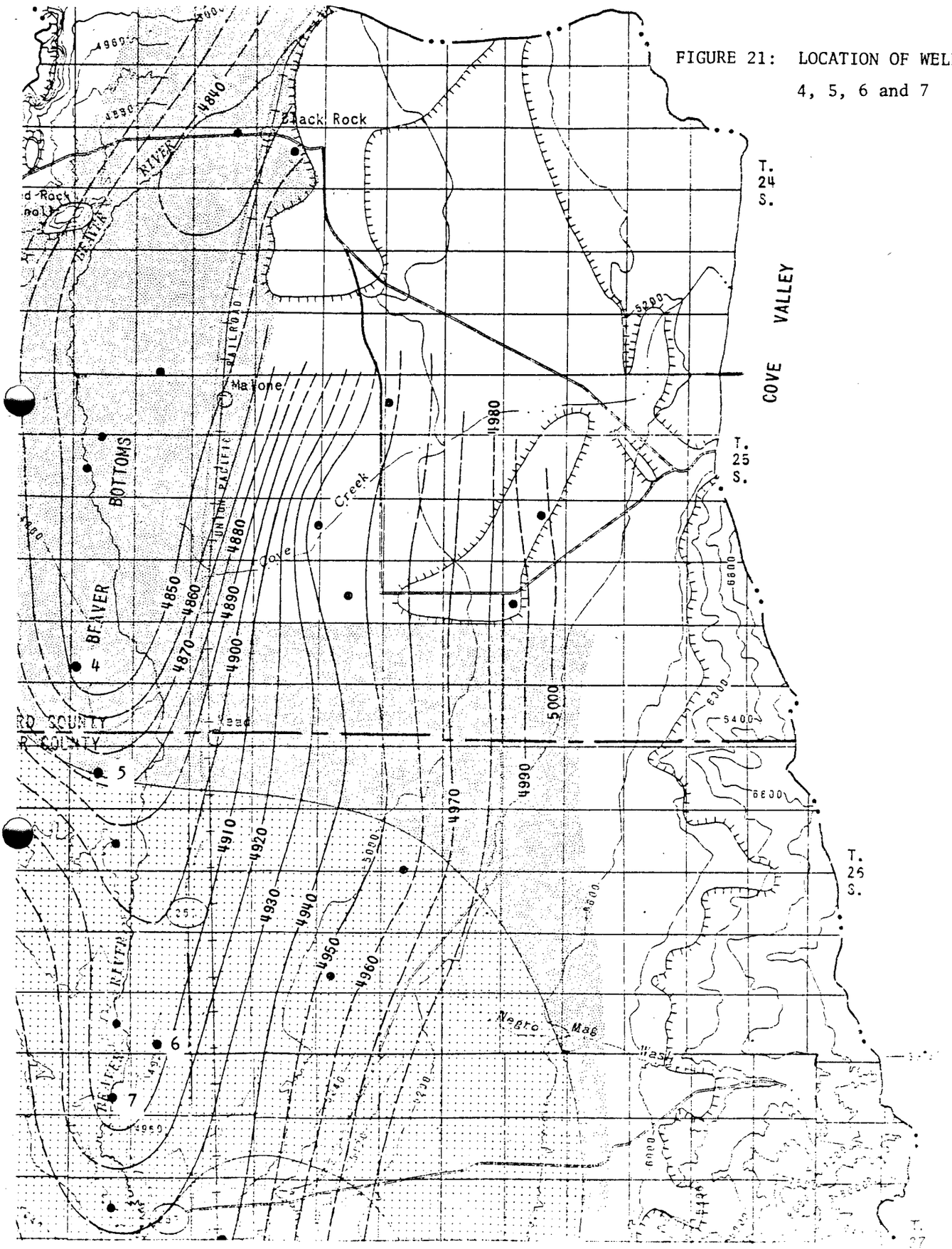

FIGURE 21: LOCATION OF WELLS 4, 5, 6 and 7

It is unfortunate that so little data has been published on the chemistry of groundwaters immediately around the geothermal field, because it is important for the present geochemical study to know as accurately as possible which parts of the area are underlain by groundwater containing some component of leaking geothermal brines, and which are not.

The waters in the main area of irrigation wells typify the valley fill groundwater (see the main cluster of points in the bottom left quarters of Figures 20 A and B). They are calcium - magnesium sulfates and bicarbonates, generally with less than 1,000 ppm TDS.

Spring samples 70 and 71 represent the recharge of calcium bicarbonate waters from the mountains.

However, much of the recharge to the shallow aquifers in the farming area around Milford is by infiltration from irrigated fields, so the concentration of dissolved solids is tending to increase there with time, and therefore to increase toward the north end of the irrigated area down the hydraulic gradients. At the same time, chemical reactions are producing changes in composition. Wells 8, 10, 12, and 13 are all within a mile or so of Milford, at the north end of the irrigated district. They illustrate this effect, being displaced on the plot away from the cluster of samples from the main irrigated area. They are displaced in the direction of the Na and K corner of the plot.

The trend representing this process is thus toward increase in sodium and potassium but involves a reduction in chloride, not an increase.

The trend for wells 4, 5, 6 and 7 is quite different. It involves increase in sodium and potassium, but also an increase in chloride.

Hence, the conclusion drawn here that the wells 4, 5, 6 and 7 show evidence of mixing with geothermal brines, and that their composition is not a function of non-thermal geochemical processes in the valley fill.

This conclusion has two implications. It implies that geothermal reservoir conditions may exist west of the Opal Mound fault, in the valley.

It also implies that the area southwest of the intersection of the Negro Mag Wash and Opal Mound faults may be one of westward flow of geothermal brines in the shallow subsurface, similar to the more obvious plume of brine long recognized to exist north of the Negro Mag Wash.

THE ROOSEVELT FIELD

EXTENT OF THE RESERVOIR

The location and extent of the reservoir at Roosevelt has generally been defined on the basis of the temperature gradient pattern and the results of the deep tests described earlier in this report. The pattern of variation in temperature gradients has outlined an area of high heat flow (Figure 17) centered roughly along a four or five mile section of the Opal Mound fault, though the heat flow anomaly is aligned somewhat more north and south than the trace of the fault, and there is a pronounced lobe extending north and west of the intersection of the Opal Mound and Negro Mag Wash faults.

BOUNDARIES OF THE RESERVOIR

The Opal Mound fault has usually been regarded as the western boundary of the field, on the basis of Phillips' well 9-1, which proved to be hot but dry, and two other strat tests of Phillips, one 1700' and the other 2300' deep. The horst between the Opal Mound fault and well 9-1 is thought to be a strip of hot dry rock sealed from the main reservoir to the east by the Opal Mound fault itself.

However, the Opal Mound fault has clearly provided a major pathway to the surface for geothermal fluids, and because the zone to the west of it has been tested only by the single well 9-1, the conclusion that the zone is hot but dry is perhaps unjustified. (It is tempting to draw that conclusion, however, as a basis for comparing the geochemical signature above a zone of hot dry rock with that above a reservoir.)

The southern boundary of the field is usually taken to correspond to two fault zones between the productive Phillips well 25-15 and Getty's 52-21 about a mile to the southwest. This boundary corresponds with two faults that were inferred on the basis of resistivity, gravity, and photo-interpretation (faults 2 and 4 of Ward and Sill, 1976, Figure 4). It also corresponds to the noticeable change in trend of magnetic features in the magnetic anomaly map of Carter & Cook (1978).

The eastern boundary of the field is a rather more arbitrary zone in the foothills of the Mineral Range in which the temperature gradients gradually become less to the east. The boundary is therefore economic, more than physical. There is no indication of an abrupt break, though the fall in temperature gradients does become more rapid once one passes somewhat east of well 14-2. There is a lobe of high temperature gradients along the eastern extension of the Negro Mag Wash fault, clearly related to the flow of hot fluids near surface on that fault.

The northern boundary of the field is the most difficult to define. The northernmost potentially productive well is 12-35, where infiltration of cool surface water was reported, but temperatures in excess of 440°F apparently exist. The high temperature gradients continue to be observed for perhaps a mile north of 12-35, but there have been no further tests in that area. A mile west of 12-35, Phillips' well 82-33 proved disappointing with temperatures between 300°F and 350°F.

In some of the temperature gradient data in this northern area, there are temperature reversals at depth, and the heat flow pattern to the north and west of the intersection of the Opal Mound and Negro Mag Wash faults has generally been interpreted as related to a plume of relatively near-surface hot water, "overflowing from the field and being carried northwest" by the general movement in the near-surface groundwater regime.

However, the heat flow pattern (Figure 17) is not entirely consistent with that interpretation but suggests rather that geothermal fluids may be rising along the Negro Mag Wash fault in a zone that extends west for at least four miles from its intersection with the Opal Mound fault. The temperature gradient pattern is in fact consistent with the idea that geothermal fluids are rising from depth in the WNW-trending zone of both the Negro Mag Wash and Salt Cove faults. But defining the reservoir in terms of the surface pattern of temperature gradients is probably misleading in any case. The temperature gradient pattern is clearly very much an expression of upward movement of geothermal fluids into the near-surface zone along the Opal Mound and Negro Mag Wash faults. The heat-flow anomaly is, in fact, centered about the intersection of these two faults.

A more accurate picture of the location and areal extent of the geothermal reservoir might have been visible if the pattern of

conductive gradients had not been so distorted in the upper few thousand feet by the effect of major upward transport of hot fluids along the two major fault zones.

Trying to define the field another way, in terms of results of production tests, one sees more clearly how little the field is in fact known. Looking again at the four boundaries of the field, one sees that, to the west, the disappointing results of 9-1 discouraged any further drilling west of the Opal Mound fault, although Peterson noted that linear ridges west of the Opal Mound fault may represent relics of earlier, now sealed faults that were formerly part of the geothermal leakage system reaching the surface. Also, just south of the Negro Mag Wash, the Opal Mound fault has a branch trending northwest, along which large areas of silicified alluvium give clear evidence of earlier leakages to surface in the area west of the Opal Mound fault.

To the south, the boundary has been defined solely by the single unsuccessful well, 52-21. The eastern boundary is known only to show gradual increase in depth to commercial temperatures, from a gradient test and a single test well, 24-36. The northern boundary is even less well known, with inconclusive data from 12-35 and no further drilling north of that.

Much more is known about the main area that has been drilled, and the next section discusses the three-dimensional geometry of the caprock and the reservoir.

DETAILED GEOMETRY OF THE CAPROCK AND THE RESERVOIR

To interpret the pattern of distribution of geochemical anomalies at the surface above the known geothermal field, requires at least a generalized picture of the three-dimensional geometry of the rock masses, i.e. the depth and form of the cap, and of the upper surface of the reservoir itself.

Part of the cap is clearly visible at and near the surface along the Opal Mound and Negro Mag Wash faults, but these zones of self-sealed rocks are obviously upward projecting extensions from the main portion of the cap produced by precipitation from hot waters flowing up along the faults and escaping at the surface.

Below the surface we have data from several wells, and can estimate conditions in some of the other proprietary wells from the casing programs.

For well 14-2, Bamford, Christensen and Capuano (1980) have summarized data on the caprocks. They interpret the zone of self-sealing to run from around 800', or a little higher, down to 1800'; the base of the cap is thus around 1800' below surface.

In well 54-3, casing was set at 1,804', suggesting that the base of the cap may be around 1,800' in that hole also. In 3-1 casing was set at 2,210' which may imply that the bottom of the cap there is slightly deeper, but still around 2,000'.

In 72-16, Bamford et al., (1980) considered the cap extends from close to surface to 650' or deeper. The logs suggest the bottom of the hole, below 1,245', may provide the major part of the production. The base of the cap may therefore be close to 1,200' in this part of the reservoir.

It hardly needs to be emphasized that the cap is not a totally distinctive, continuous layer of complete alteration and self-sealing in the granitic and metamorphic rocks, but is instead an irregular and discontinuous zone characterized by varying degrees of alteration and fracture filling, with irregular upper and lower surfaces; its geometric details are related both to presently active and to formerly active major and minor fluid pathways responsible for the formation of the cap in the past and at the present time.

If we extrapolate from the data in the wells, using the assumption that the cap is related broadly to the form of the isothermal surfaces as we see them today (which involves assuming that the cap is mainly related to the form of the present geothermal reservoir) then we can formulate a picture in which the upper surface of the cap lies somewhere between the surface and a depth of 1,000' in the area close to the Opal Mound fault, and falls to greater depths towards the east and west. The base of the cap (i.e. the top of the reservoir) is generally 2,000' deep in the area where the Opal Mound and Negro Mag Wash faults intersect. It is somewhat shallower a little further south (about 1,200' at 72-16), but becomes progressively deeper to the east, to the west, and to the south. If well 52-21 is viewed as lying entirely within the zone of self-sealing that constitutes the cap, then the base of the cap rapidly deepens to the south of well 72-16 to more than 7,500'.

North of the Negro Mag Wash fault, in the area of wells 82-33 and 12-35, data on the depth to the top of the reservoir are not available. In 12-35, a thermal aquifer in excess of 440°F is reported to be lined off, presumably in the zone between 1,814' and 4,500'. The top of the reservoir here may thus be somewhere in this range below 1,800'.

The base of the reservoir has not been reached in any of the production wells.

RESERVOIR CONDITIONS

The geothermal reservoir at Roosevelt is hot-water dominated. The reservoir fluid is very close to a pure sodium chloride brine in composition, with between 6,000 and 7,000 ppm TDS. Silica ranges up to about 380 ppm: pH is between 6 and 8 in surface samples.

Subsurface temperatures reach well over 500°F, and successful wells produce over 1 million lb/hr of fluids. Pressure is slightly over 2,000 psi.

Geothermometry gives estimated temperatures similar to those observed in the wells with values up to 563°F from the Na-K-Ca geothermometer. Equilibration at reservoir temperature is thus indicated by the chemistry. The reservoir volume appears to be large relative to the present minor rate of discharge at the surface, and the reservoir fluids evidently have a relatively long residence time.

The reservoir rocks are the granitic intrusives of the Tertiary Mineral Mountains pluton and the metamorphic gneisses and schists which it intruded. Intergranular porosity of the reservoir rocks is essentially zero, and the reservoir depends purely on fracture permeability.

Strong convective movement seems to be occurring within the reservoir, taking advantage of the throughgoing fractures: chemical analyses show very little variation from one well to another.

FLUID CHEMISTRY

Table 1 gives chemical data from production wells 54-3, 3-1, 14-2, and 72-16; from the "dry" wells 9-1 and 52-21; from the springs of Roosevelt Hot Springs, and from the small seep about 1,300' northwest of the springs.

Figures 22A and B are plots of these analyses, showing how similar in composition the waters from the producing wells are to one another, and to the discharge that formerly occurred at Roosevelt Hot Springs.

The chemical composition of the seep indicates that some mixing with a small proportion of cold surface groundwater has probably occurred.

The waters in wells 52-21 and 9-1 also appear to be mixtures of reservoir fluids with a small percentage of groundwater, perhaps a little less than 10%. Such an interpretation would, if it is correct, refute the concept that the horst west of the Opal Mound fault is completely sealed and prevents reservoir fluids from passing westward into the area of well 9-1; and that the southern boundary of the field is a similar zone of total sealing between wells 72-16 and 54-21. Wells 9-1 and 52-21 may be in communication with the reservoir. The lower temperatures and slightly diluted compositions found in 9-1 (BHT 446^{o}F) and 52-21 (BHT 402.5^{o}F) would be compatible with this concept of mixing, for example if the hot water component of the mixture in 52-21 were around 480^{o}F.

The alternative explanation, of course, is that the hot waters sampled in wells 9-1 and 52-21 belong to separate, isolated flow systems, and have equilibrated at the lower temperatures observed in the area of these two wells. But Na-K-Ca geothermometry, however, gives 504^{o}F for well 9-1. (For 52-21 it gives about 425^{o} to 440^{o}F).

MINOR ELEMENT CHEMISTRY

To supplement the data on compositional variation in the major elements in the geothermal fluids, Table 2 is a listing of available data on minor element composition of the reservoir fluids. These data are significant in terms of the patterns of element distribution seen in the hydrothermal alteration zones, in the hot spring deposits, and in the soils and the surface microlayer.

	54-3		3-1	14-2		72-16			9-1			52-21			ROOSEVELT H.S.		SEEP		
	a	b		a	b	a	b	c	a	b	c	a	b	c	a	b	a	b	c
Na	2000	2000	2437	2150	2200	1800	2000	2072	2210	2000	1780	1845	1900	1900	2080	2500	1840	4200	1800
K	400	410	448	390	410	380	400	403	425	374	440	237	218	216	472	488	274	378	280
Ca	7.0	10.1	8.0	9.2	6.9	12.4	12.2	31	83	41	69.1	106	114	107	19	22	122	133	107
Mg	0.1	0.24	0.01	0.6	0.08	0.29	0.29	0.26	--	0.74	1.0	5.2	3.9	4.0	3.3	0	25	17	23.6
Cl	3600	3400	4090	3650	3650	2110	3260	3532	3800	2140	2860	2810.8	2885.1	2881.6	3810	4240	3210	3800	3200
HCO_3	200	200	180	185	185	181	181	181	--	--	485	602.9	550.0	615.0	158	156	298	536	300
SO_4	55	54	59	78	60	33	32	48	122	67	120	78	86	85	65	73	120	142	70
SiO_2										364	362	190							
TDS	6700	6442	7067	--	--	6074	6444	6752	--	6520	--	5940	5727	5677	7040	7800	6063	7506	5948
pH	6.2	6.7-7	6.3	5.9	6.2	7.83	7.53	5.0	--	5.9	7.3	6.4	7.3	7.3	--	7.9	6.5	8.2	6.43
T(^oF)	--	260	205	14	9	--	--	92	--	--	70	--	--	--	.83	55	25	17	28
Geothermometer																			
Na-K-Ca		295	293	292	256	293	289	288	274	262	--	227	219	219	293	284	235	246	239

TABLE 1: Summary of Chemical Analyses, Geothermal Brines

TABLE 2: **Minor Element Composition of Reservoir Fluid**

Element	ppm
Ba	0.26
Cu	0.2
As	3. - 3.6
Li	15 - 28
B	23 - 38
F	2.8 - 6
Br	5
Pb	0.18
Zn	0.2
Mn	0.2
Rb	3.9
Be	0.004
Cs	5
Sr	1.5
Ce	3

Source: Bamford et al. (1980)

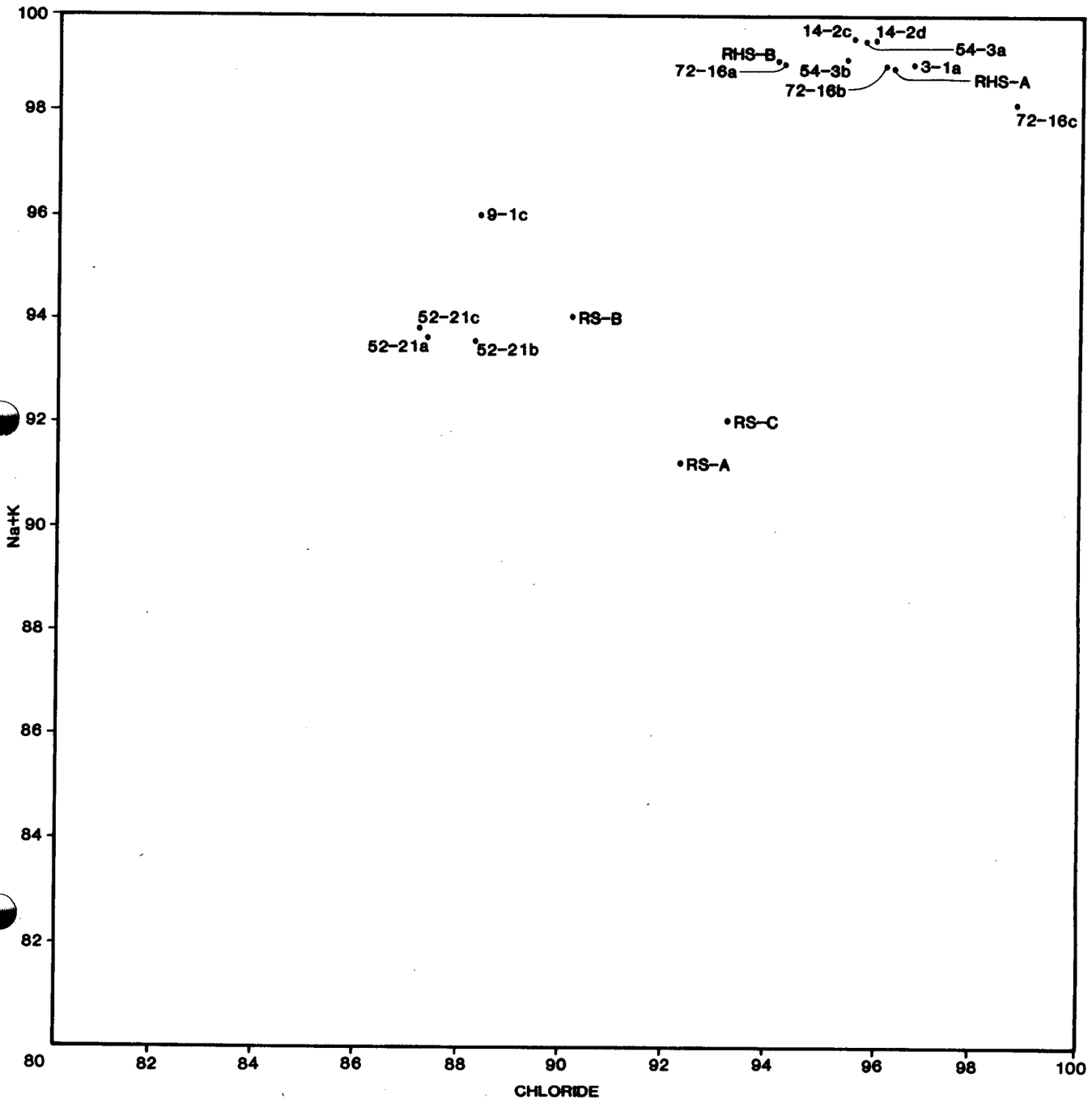

Figure 22a

GEOCHEMISTRY OF RESERVOIR FLUIDS & PLUME

MAJOR ANIONS & CHLORIDE

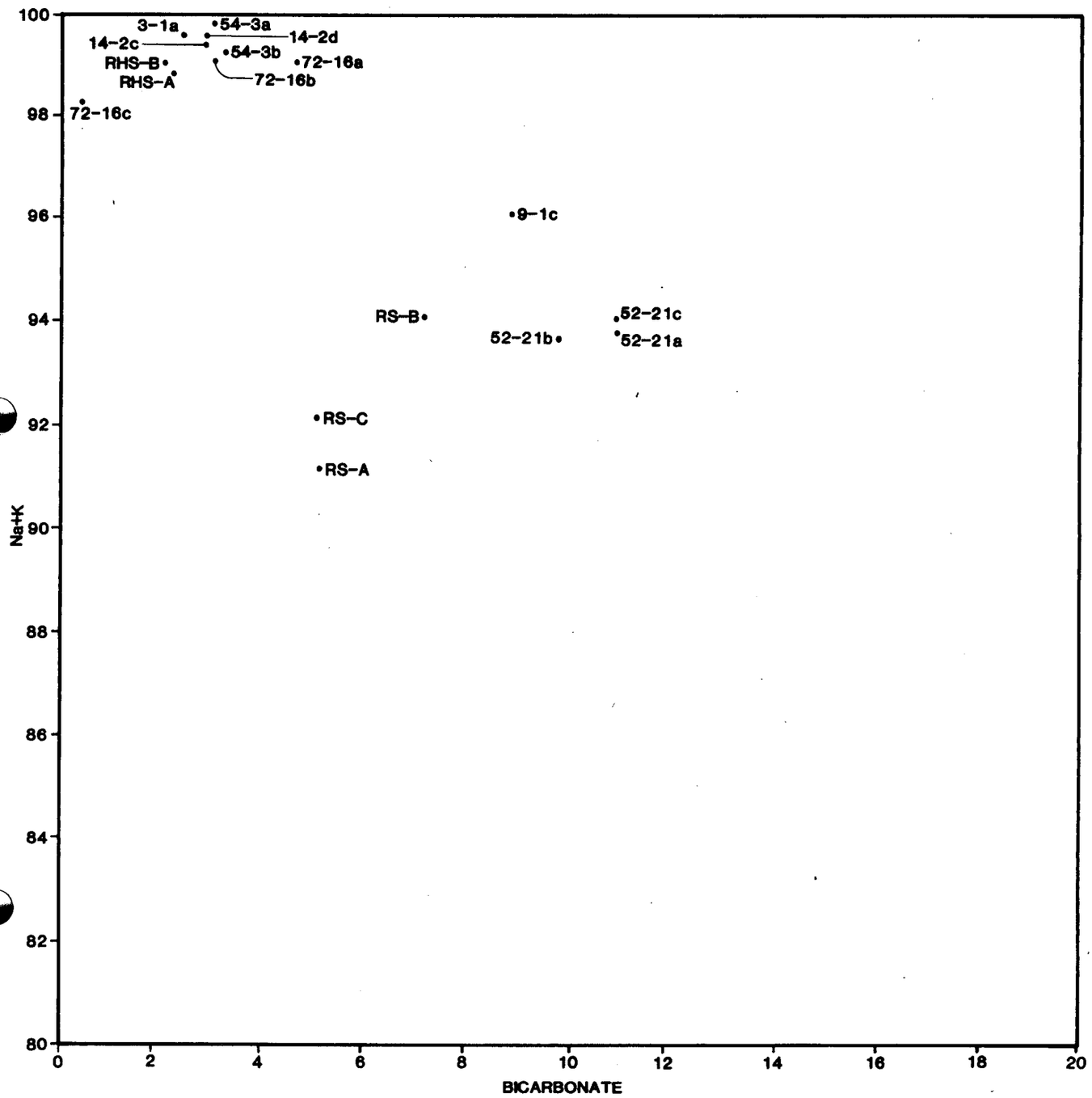

Figure 22b

GEOCHEMISTRY OF RESERVOIR FLUIDS & PLUME

MAJOR ANIONS & BICARBONATE

One notable point is the high boron content. Along with the structural setting and other features, the evidence suggests that the Roosevelt reservoir as it is presently known may be a differentiated, high-level reservoir that is connected with and evolved from a deeper geothermal system. This is an important and encouraging point in terms of the geothermal potential of the areas surrounding Roosevelt.

ORIGIN OF THE RESERVOIR FLUID

The origin of the reservoir fluid has been discussed by Bowman (1979) and Rohrs and Bowman (1980), whose work on hydrogen and oxygen isotopes (Figure 23) indicated that the reservoir fluid is derived almost entirely from surface water of local meteoric origin: rainfall and snow melt in the Mineral Range could provide most if not all of the recharge. The possibility of some small contribution from the Tushar Mountains (the next range east of the Mineral Mountains), by interbasin flow across the Beaver Valley and under the Mineral Mountains, was found unlikely in Smith's (1980) simulation using reasonable patterns of hydraulic conductivities and gradients.

Work on isotopes has also confirmed the picture of minimal pervasion of the massive reservoir rocks by the reservoir fluid, and permeability that is confined almost totally to the fracture systems.

THE RESERVOIR FLOW SYSTEM

The reservoir system is most easily examined by looking first at the reservoir and then at the system of leaking fluids and gases which rise to the surface from it.

Detailed data on the reservoir are unfortunately fragmentary, because of the proprietary interests of the operators. Phillips is in the especially difficult position of developing the field while some of the other lease holders in the KGRA have not signed the unit agreement for field development; yet its staff has been extremely cooperative and helpful in the work described in this report.

The reservoir fluids are sodium chloride brines with about 6,000 to 7,000 mg/l TDS. That the liquid mass in storage in the reservoir is large relative to the amount of discharge is indicated by

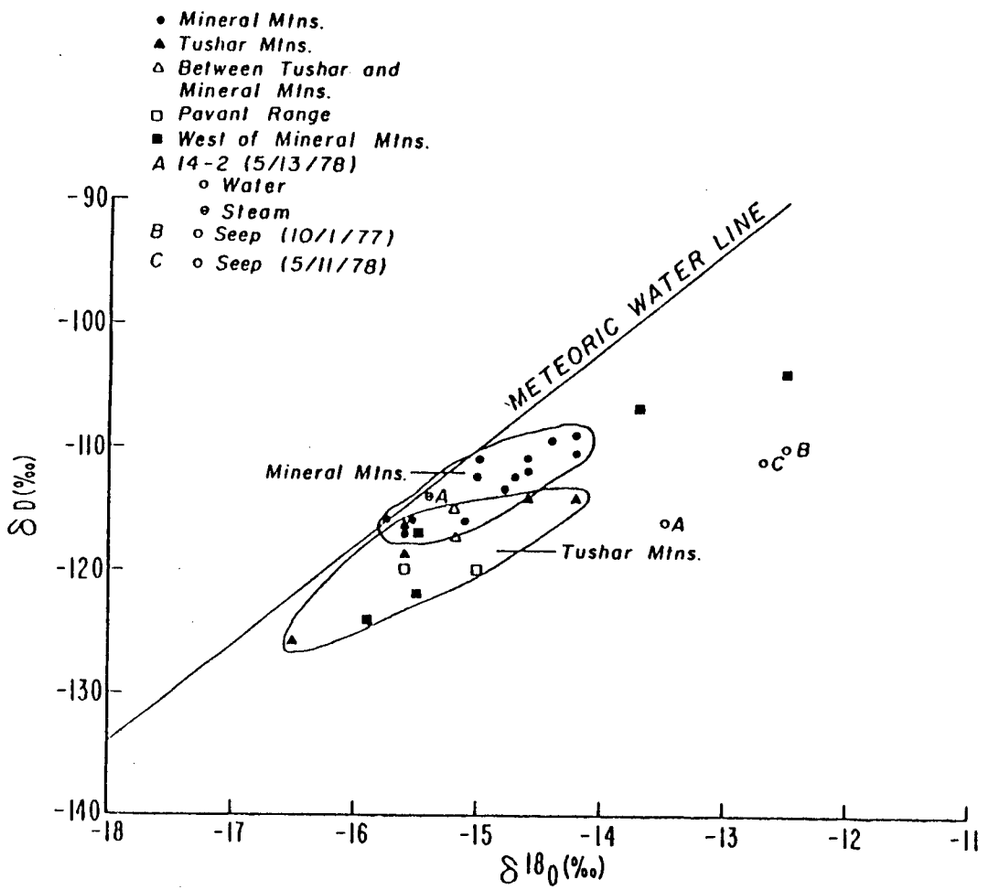

Figure 23: A plot of δD versus $\delta^{18}O$ for cold spring and thermal waters from the vicinity of the Roosevelt Hot Springs thermal area.

the carbon isotope data, though this picture could be distorted by thermal effects remobilizing ^{13}C from the surrounding rocks. However, a long residence time for water in the reservoir is also suggested by the low tritium values (less than 1 TU) which indicates an age greater than twenty years. (Data for local cold spring water in the Mineral Mountains shows 50 to 70 TU).

Another piece of evidence pointing in the same direction is the very close agreement between observed reservoir temperatures and those calculated using various geothermometers. The reservoir waters have reached equilibrium with the granitic country rocks at reservoir temperatures. The ^{18}O shift relative to meteoric waters also shows equilibrium conditions, and a long residence time at high temperature.

TEMPERATURE DISTRIBUTION AND CONVECTIVE CIRCULATION

Details of temperature distribution within the reservoir are not well known. Apparently the production wells show isothermal conditions below the point at which the reservoir is penetrated, and it has been assumed that strong convective circulation is occurring within the reservoir. If so, and if we assume the Opal Mound fault is at least a partial barrier to flow to the west, then we might envision the main upward convective movement to be focused along the Opal Mound and Negro Mag Wash faults, rising to the shallowest parts of the reservoir. The downward moving paths would generally be to the east in this area, carrying the brines to greater depth, towards the poorly defined east margins of the field.

This picture is consistent with the fact that the well closest to the intersection of the Opal Mound and the Negro Mag Wash faults (54-3) is rated as the "best well," showing a temperature well in excess of 500°F and with enthalpy of more than 500 Btu/lb. In 14-2 the temperature is 514°F.

There are no temperature data for 3-1 and 13-10. 72-16 had a maximum temperature of 470°F. Temperature in 25-15 is not known, but 52-21 showed a maximum temperature of 402°F at TD (7478'). West of the Opal Mound fault, well 9-1 showed a maximum temperature of 446°F at almost 7,000'. In 82-33, northwest of the field, temperatures reached 300° to 350°F; TD is 6,028'.

There have been extensive long-term flow tests, the most recent being a flow test of 54-3 in the winter of 1980-81. It is not known what interference between the wells has been demonstrated. Indications of convective movement, and the relative similarity in composition of fluids from different parts of the field, have encouraged the idea that there is relative good mixing within the reservoir.

Open factures, and zones of intense fracturing appear to be the important keys to production. In 14-2, for example, hot water entries have been inferred in short intervals between 800' and 1,400', 1,600' to 1,800', 2,850' to 2,925', and 5,400' to 5,800' (Glenn and Hulen, 1979). These correspond well to the hot water entries discussed by Bamford et al., (1980). In 72-16, similar zones of hot water entry occur around 312', 514', 628', and possibly the most important zone, at 1,245'. In the unproductive well, 52-21, no hot water entries were detected by chemical means.

PATHWAYS TO THE SURFACE

The cap of the reservoir has already been described. It has clearly been breached for long periods of time by the Opal Mound fault, the Negro Mag Wash fault, and other faults, which have provided pathways to surface for the hot brines that precipitated the siliceous sinter of the opal deposits, and cemented the surrounding alluvium. The history of the faults seems likely to be one of alternating sealing, and then fresh access to the surface as a result of renewed movement along the fault. They still provide channelways for liquid leakage and for gaseous emanations.

GEOCHEMICAL PROCESSES

GEOCHEMICAL PATTERNS IN THE SURFACE ZONE

HOT SPRING DEPOSITS

The hot spring deposits of the Roosevelt area (Figure 24) have been mapped and described by several authors. The most conspicuous deposits, and those which probably have the oldest history, are the siliceous sinter aprons of the Opal Mound itself, along the Opal Mound fault.

The second largest area is around the intersection of the Opal Mound fault with the Negro Mag Wash fault: opaline siliceous sinter occurs around Roosevelt Hot Springs, and there are numerous large areas of alluvium that show cementing or coating with opaline chalcedonic sinter, silica, hematite, calcite, and manganese oxides.

There is another large patch of cemented alluvium near well 82-33 in the northeast portion of section 33 (26S/9W).

It is significant that large areas of cemented alluvium lie west of the trace of the Opal Mound fault, generally along faults that branch from it or along NW or WNW-trending faults. The patch of cemented alluvium at the eastern margin of section 4 (27S/9W), for example, is clearly along a NW-trending fault that intersects the Opal Mound fault where it crosses the eastern boundary of that section.

Other patches of alluvium that are cemented by hematite and manganese oxides occur along the Negro Mag fault west of its intersection with the Opal Mound fault.

A large area of cemented alluvium occurring in the northeast corner of section 33 (26S/9W) is located along the WNW-trending Salt Cove fault.

It is thus evident that the zone west of the Opal Mound fault was at one time an area where reservoir fluids reached the surface, whether or not it is now a zone of hot dry rock sealed from the reservoir by the Opal Mound fault.

The hot spring deposits consist of laminated opaline sinter formed on broad flat aprons, locally with steep laminations along narrow

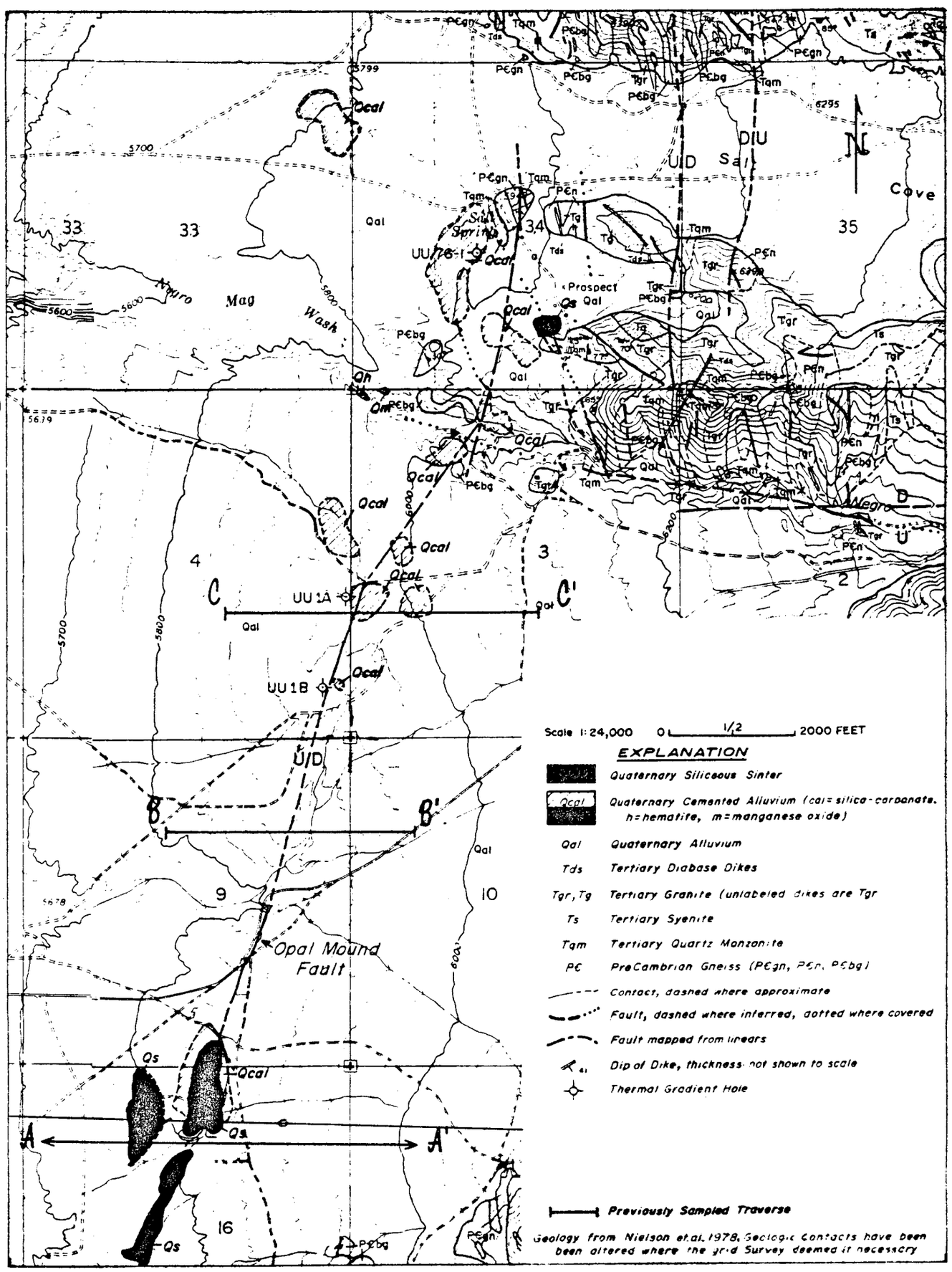

Figure 24

GEOLOGY & ALTERATION MAP ROOSEVELT HOT SPRINGS KGRA

zones of upward flow. In some places the sinter is porous. It is generally composed of opal, cristobalite, and microcrystalline quartz, with alunite and some sulphur and traces of realgar.

Attempts have been made to estimate, on the basis of paleomagnetic and other data, how long the hot spring deposits have been forming (Brown, 1977a, 1977b; Bryant and Parry, 1977). The beginning of sinter deposition has been estimated at various figures between 35,000 and 350,000 years ago.

The hydrothermal system is evidently older than the sinter however, for the alluvium on which the Opal Mound sits contains eroded fragments of hydrothermally altered rocks. In shallow drill holes in alluvium that exhibits siliceous and carbonate cementing and iron and manganese oxide staining, Hulen (1978) pointed out that some of the fragments of metamorphic and granitic rock showed alteration that had clearly occurred before their incorporation in the alluvial deposit. The fragments show alteration very like the hydrothermal alteration observed in similar crystalline rocks above the reservoir; but in the alluvium they co-exist with eroded fragments of unaltered pumice and perlite, thus dating the alteration as prior to deposition.

PRESENT-DAY GAS DISCHARGE

Areas of hot ground have been noted, for example, by Petersen (1975), near each of the areas of hot spring deposits. Encrustation of native sulphur have also been observed in these areas and along the surface trace of the Negro Mag Wash fault, which is clearly a major zone of de-gassing, with steam, CO_2, H_2S, and ongoing sulphur deposition.

The presence of helium in anomalous amounts in soil gas samples was described by Hinkle et al., (1978). They made two E-W traverses across the field and the area west of it. Interestingly, some of the areas of highest values occurred in the area west of the Opal Mound fault.

The samples also showed concentrations of COS in the range up to 220 ppb and CS_2 concentrations up to 300 ppb. SO_2 and H_2S were not detected in these soil gas samples (Hinkle and Harmes, 1978). The highest values occurred in the area east of the Opal Mound fault, near the Negro Mag Wash fault.

Anomalous flows of radon have been measured on both sides of the Opal Mound and Negro Mag Wash faults. Strong signatures are apparent for two branches of the latter. The Opal Mound fault showed a smaller anomaly than along some zones east of it and along the branching NW-trending fault underlying the cemented alluvium of the northeast part of section 4 (27S/9W). On a traverse across the southern part of the field, where the reservoir is much deeper, radon anomalies are apparently more subdued (Nielson, 1978).

PRESENT-DAY LIQUID DISCHARGE

The hot spring deposits and cemented alluvium clearly show that leakage of geothermal brines has occurred along various parts of the Opal Mound fault and other nearby faults, and along the Negro Mag Wash fault and Salt Cove faults, during at least the last few tens of thousands of years, and probably over a longer period of time.

Currently no leakage is observed south of the Negro Mag Wash fault, though along that fault there are signs of leakage in historic times in the northwest corner of section 3 of 27S/9W (Peterson, 1975).

The Roosevelt Hot Springs (Figure 24), formerly known as McKeans Hot Springs, were developed as a hot springs resort starting in 1902. The resort was still operating in the twenties. Lee (1908) recorded a group of springs, one of which was flowing 10 gpm at over 190^{o}F. In November 1950, the temperature had dropped to 185^{o}F, and the discharge was only 1 gpm. In September 1957, the temperature had dropped to 131^{o}F (Mundroff, 1970). In 1966 the area was dry, and showed indications that flow had probably stopped two years earlier. At present the site is dry, but fumaroles are still discharging water vapor and gases.

A quarter of a mile northwest of the former resort there is a small seep which is still leaking hot water. This is the "Roosevelt Seep" mentioned by several authors in the Roosevelt literature. The flow is small and the recorded temperatures are in the range 63^{o} to 83^{o}F.

SURFACE GEOCHEMICAL PROCESSES

Where the geothermal brines have approached or reached surface, a distinct pattern of surface and near-surface alteration has been noted (Parry et al., 1977, 1978; Bamford, 1978; Bamford et al., 1980). Acid sulfate waters appear to have developed by oxidation of H_2S, with the formation of alunite, and precipitation of opal as cooling temperature reduced the solubility of silica. Downward percolation of the acid sulfate waters next to the zone of continuing upflow of fresh geothermal fluid produces more alunite, along with kaolinite and montmorillonite, in the zone between the surface and the water table, which is generally deeper than one hundred feet. Below the water table pyrite is observed coated with marcasite (placing a temperature limit, since marcasite goes to pyrite irreversibly above about 160°C).

GEOCHEMISTRY OF THE SOILS

Capuano and Bamford (1978) and Bamford, Christensen and Capuano (1980) have studied geochemical anomalies in soils in a narrow zone along the Opal Mound fault, and in a broader zone to the north.

They found that anomalies occur in a broad area around the intersection of the Negro Mag Wash and the Opal Mound faults, and in a second area around the Opal Mound.

A portion of the data is shown as Figures 25 and 26. In the northern area, the arsenic anomalies are more or less balanced on either side of the northern extension of the Opal Mound fault. On the other hand, the mercury anomalies show asymmetry, with very minor development on the east side of the fault contrasted with very pronounced anomalies west of the Opal Mound fault.

In the southern area, around the Opal Dome, the arsenic results again show no particular asymmetry, but this time the mercury anomalies tend to be more marked on the east side of the Opal Mound fault, notably close to well 72-16.

It is interesting to note that along the Opal Mound fault there is a zone between the two areas of anomalies that shows only background values in both arsenic and mercury. The gap between the north and south mercury anomalies is smaller, by about 4,000', than the gap between the north and south arsenic anomalies.

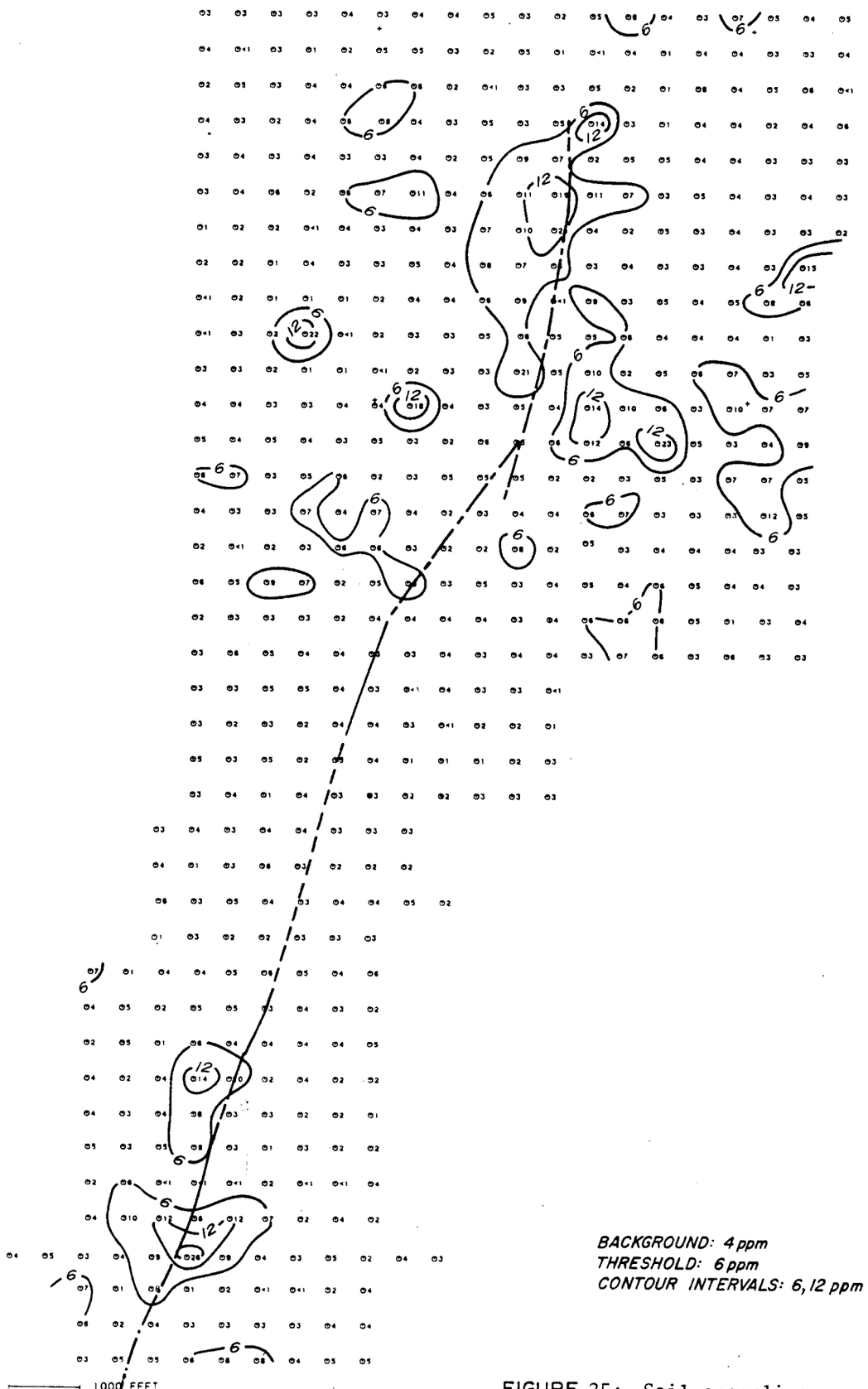

FIGURE 25: Soil anomalies: arsenic
ARSENIC PPM
SAMPLE TYPE: SOIL (-80 MESH)
ANALYTICAL METHOD: COLORIMETRIC

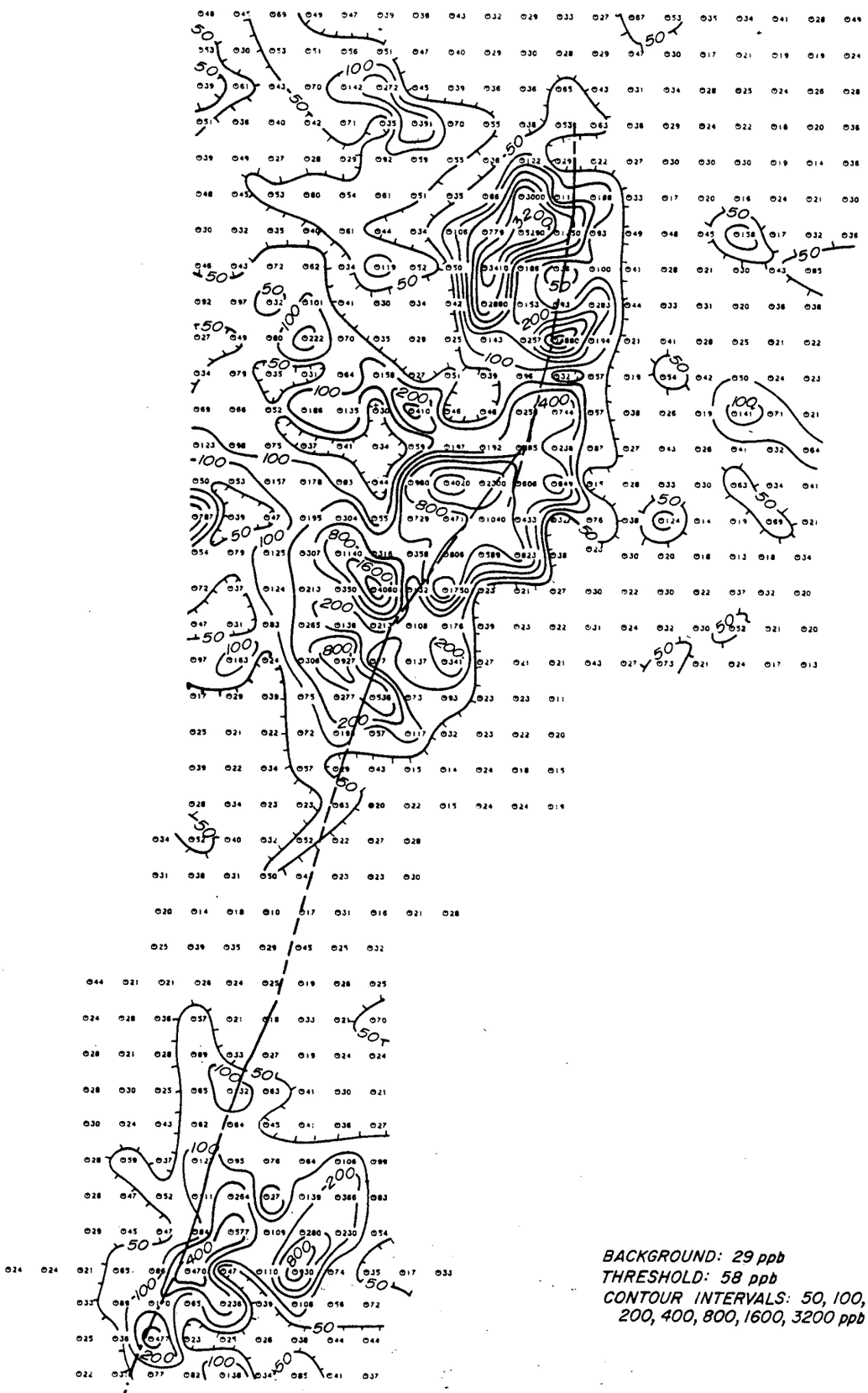

FIGURE 26: Soil anomalies: mercury

That barren gap in the mercury and arsenic anomalies led Bamford et al., to assume this section of the Opal Mound Fault was not presently a zone of upward leakage. The interpretation of the gap that emerges from the present study is discussed in a later section.

Bamford et al., (1980) also commented on the existence of anomalous concentrations of other elements in traverses crossing the Opal Mound fault near Opal Mound. Antimony is concentrated 1,500' west of the fault, and tungsten is concentrated at and near the fault, closely associated with the arsenic and mercury anomalies. They also tentatively identified anomalous concentrations of tin and thorium, and broad anomalies of lithium.

A detailed comparison of these soil data with the results of the present work on the surface microlayer will be made in a later section, but first the geochemistry of the shallow subsurface, and then of the caprock and the reservoir zone are discussed, in the next two sections.

GEOCHEMICAL PATTERNS BETWEEN SURFACE AND 300 FEET

Bamford et al., (1980) published data showing lateral variation in chemistry of samples from different drill holes in and around the field. Their published diagrams are for the depth interval between 100' and 200', for samples of whole rock and of fractions with specific gravity greater than 3.3 (magnetic materials removed). Similar data for the intervals from 0 to 100' and from 200 to 300' are open-filed.

There is an unfortunately large gap in the area of sampling west of the Opal Mound fault, due to the absence of available wells in that region.

The data on arsenic give a picture of maximum concentrations in the region of the field, with values falling off to NE and SE outside the field; there is possibly an extension of the anomaly in the WNW direction along the trend of the Negro Mag Wash and Salt Cove faults (Figure 27).

The mercury data give a sketchy picture of highest values close to the central part of the field and along the Opal Mound fault, with other high values to the northwest of the field.

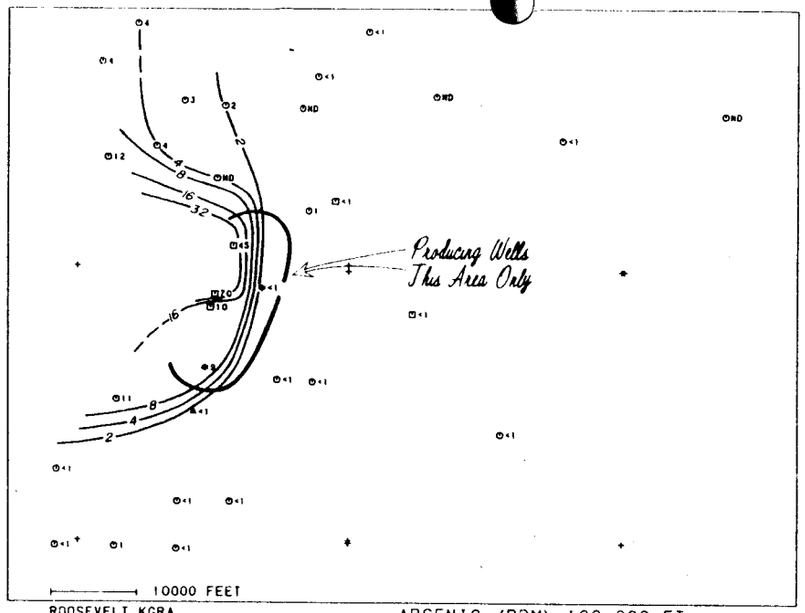

ROOSEVELT KGRA
BEAVER COUNTY, UTAH

ARSENIC (PPM) 100-200 FT.
SAMPLE TYPE: WHOLE ROCK
ANALYTICAL METHOD: COLOR

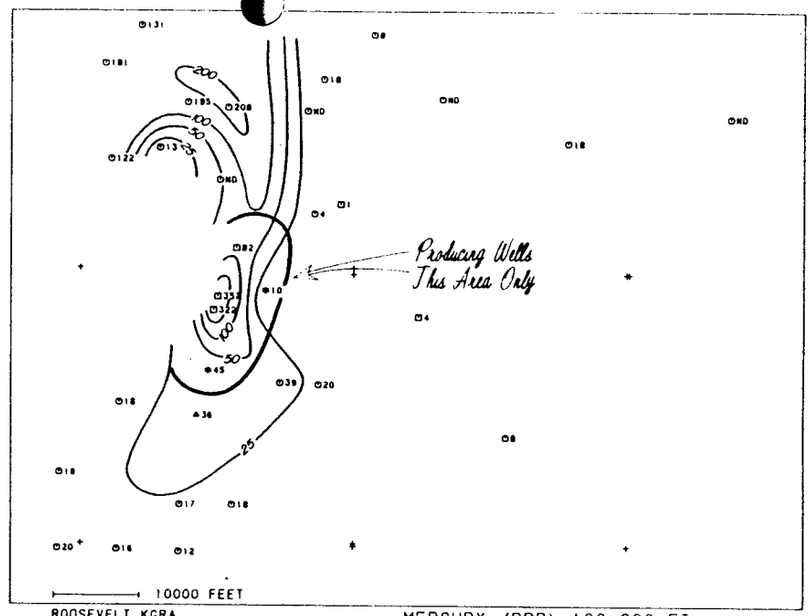

ROOSEVELT KGRA
BEAVER COUNTY, UTAH

MERCURY (PPB) 100-200 FT.
SAMPLE TYPE: WHOLE ROCK
ANALYTICAL METHOD: GOLD FILM

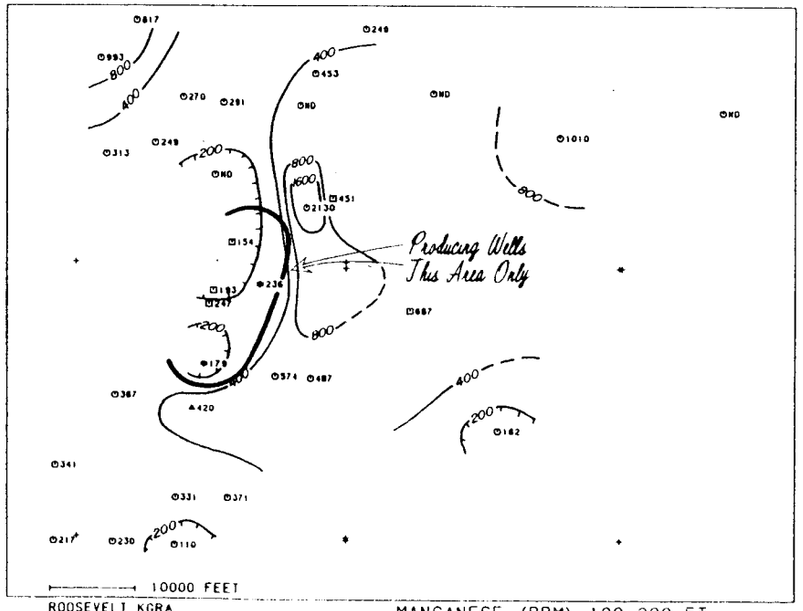

ROOSEVELT KGRA
BEAVER COUNTY, UTAH

MANGANESE (PPM) 100-200 FT.
SAMPLE TYPE: WHOLE ROCK
ANALYTICAL METHOD: ICPQ

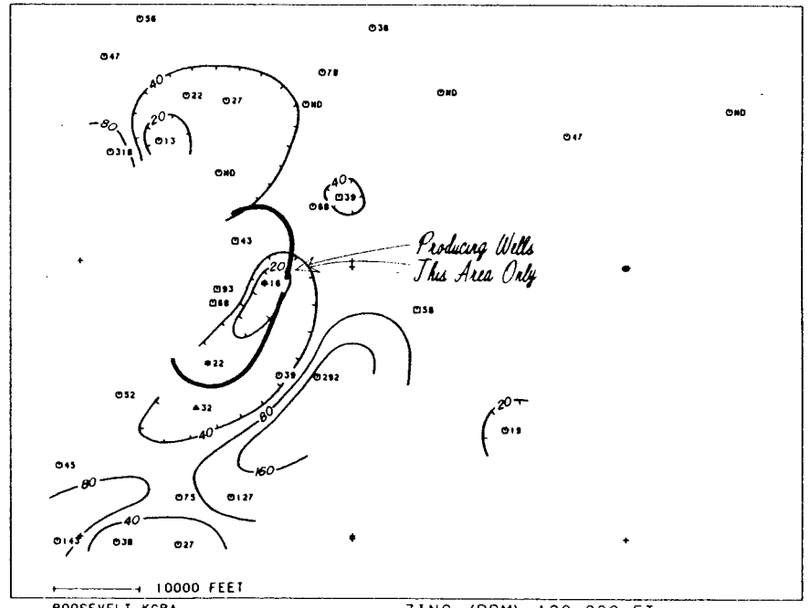

ROOSEVELT KGRA
BEAVER COUNTY, UTAH

ZINC (PPM) 100-200 FT.
SAMPLE TYPE: WHOLE ROCK
ANALYTICAL METHOD: AAS & ICPQ

Figure 27

Manganese shows lows in the west part of the field, and a peripheral high to the northwest, though this appears to be related to data at the single location, hole GPCR-8. However, despite the distortion that may be introduced by that single sampling location there still seems to be a peripheral anomaly to the north and to the southeast and southwest.

Zinc, like manganese, shows a similar low in the general area of the field, with a peripheral high to the southeast, plus a spot high to the northwest of the field at UU786-TG3.

Bamford et al., (1980) concluded that these peripheral zinc and managnese anomalies are not related to earlier episodes of mineralization, but are related to the present geothermal system.

Less clear anomalies were shown for lithium and iron, cerium and lanthanum. Weak lithium anomalies were described over the geothermal field and to the south of it. Iron is regarded as being strongly redistributed by geothermal processes especially in the area of the field, and immediately to the north, but apparently is not transported very far and is probably derived locally. This is consistent with the well known observation that a magnetic low characterizes the area of the field itself, which has been interpreted as showing the destruction of magnetite in the crystalline rocks by hydrothermal alteration. (see for example Bamford, 1978).

Cerium and lanthanum are shown as having almost identical patterns, with lows at two locations in the central part of the field and highs at a location just southeast of the field, at UU75-3CC. However, the data are so sparse that such contouring and interpretation is very difficult and uncertain.

Discussing molybdenum, tungsten, and tin, Bamford et al., suggested there may be anomalies, related to geothermal processes, arranged peripherally to the field.

GEOCHEMICAL PATTERNS IN AND ABOVE THE CAPROCK

In 1978 the hydrothermal alteration seen in well cuttings was described for well 14-2 by Ballantyne, for well 72-16 by Rohrs and Parry, and for well 52-21 by Ballantyne. Mineral assemblages in the altered zones include chlorite, sericite, and various clay minerals, K-spar, calcite, hematite, and epidote.

Bamford et al., (1980) suggested that some of the epidote, which is found at all depths, may be related to pre-geothermal events, while other epidote may have formed in an early stage of the geothermal development when the field was much larger and at present, a possibility discussed elsewhere in the present paper. Without detailed data on the variations in composition of the epidotes it is difficult to draw conclusions about the physico-chemical conditions and history.

Within these three wells a number of zones have been interpreted on good evidence as hot water zones, the centers of which represent points of influx or passage of geothermal fluids. The remainder of the zones represent diagnostic arrangements of characteristic minerals, seen in the well both above and below the entry point, with specific series of mineral assemblages at increasing distances from the center of the zone. These "hot water entries" correspond well with what one might interpret as major zones of fracturing from the geophysical and mud logs, from the drilling history, and the geologic data. (The term "hot water entry" is perhaps misleading in the sense that the phenomenon being described is a major channelway for geothermal fluids. It becomes an entry only when a well is drilled through the zone, and the fluids bypass their normal flow pattern, and instead enter the well).

In well 72-16, entries are considered to occur at 312' and 628' (the latter possibly contributing part of the well's production through imperfect cementing at 1,098') and at 1,245', which is probably the top of the main production interval between 1,245' and 1,245'.

In well 14-2, entries occur in the interval between 1,600' and 1,800', and between 2,850' and 2,890' with specific entries occurring at around 2,860' and 2,890'.

It was noted in an earlier section that no signs of hot water entry zones were detected in the cuttings from well 52-21, implying that chemical zoning related to entries may be ephemeral.

In the zones of hot water entry, arsenic and lithium give the clearest picture, with anomalous concentrations close to or at all of the inferred entries, often restricted to the zone 10' on either side of the entry points. Lithium in addition seems to show a widespread enrichment throughout well 72-16 and in parts of well 14-2.

Bamford et al., (1980) concluded that these arsenic and lithium anomalies that form around active hot water entry zones persist even after the entry is entirely self-sealed; but the evidence for this is not clear, since the fact that a hot water entry now appears to be sealed where it is intersected by the well does not preclude the possibility that the zone is still free a very short distance away from that point.

The issue is important because we are trying to distinguish between geochemical features that remain as fossil evidence of former geothermal conditions, and those which can be relied on to give details of current geothermal conditions and are rapidly lost when conditions change.

In this case it is important to know whether the mineral assemblages of an active hot water entry zone do or do not remain long after the channelway becomes inactive.

The mercury data give a less coherent picture. Mercury is present through-out the self-sealed rocks that characterize the entire depth of well 52-21. It is concentrated in 14-2 within the cap, and in well 72-16 it is specifically concentrated near obvious hot water entries within, or very close to, the base of the cap. Bamford et al., (1980) note that mercury concentrations are low around the deeper entry zones in 14-2, and it seems clear that mercury distribution is marginal in the reservoir, as one might expect.

High mercury values are found near surface in two of the shallow holes just west of the Opal Mound fault (UU75-1A and UU76-1).

It seems clear that much of the mercury data can best be explained by vapor transport.

Zinc and manganese anomalies are observed in the upper parts of the cap in well 14-2, and also in well 52-21. It appears that while zinc and manganese may both be enriched in the zone around the reservoir and particularly around hot water entries, zinc is slightly enriched within the reservoir rock itself.

Strontium, in contrast to the metals discussed above is noticeably depleted around the hot water entry at the 2,890' level in well 14-2 and probably also around the hot water entries of 72-16.

There seems to be some evidence of an association between antimony and arsenic and mercury, particularly the former, though antimony anomalies have not so far been defined as clearly in relation to hot water entries as those of arsenic and mercury. (This association is strongly apparent in the surface microlayer and is discussed in a later section of this report).

Beryllium tends to be slightly enriched within the cap, and at hot water entries, and in the zone very close to the surface. Beryllium is very strongly enriched in the siliceous sinter deposits along the Opal Mound fault and in alluvium that has been cemented with manganese oxides.

Tungsten is concentrated in some of the hot spring deposits and the soils over the Opal Mound fault, along with the mercury and arsenic anomalies there. Broad anomalies of tungsten may exist peripherally to the reservoir in the near surface.

Molybdenum seems to show a general association with zinc and manganese in the shallow rock above the cap in well 14-2, with marked enrichment in the hot water entry zone between 2,860' and 2,890'. In the near-surface, molybdenum appears to be anomalously present peripheral to the reservoir, and is also anomalously high in well 52-21.

Bamford et al., (1980) list a group of elements that show some signs of being mobilized and redeposited by the geothermal system, but about which data is very scanty at this time, including Mg, Fe, P, Ba, V, Cr, Co, Ni, Cu, Zr, La, and Ce.

Before comparing these geochemical data with those found in the surface microlayer work, the problem of inherited geochemical imprints from earlier episodes of mineralization and geothermal activity is discussed, in the next section.

INHERITED GEOCHEMICAL PATTERNS

GEOCHEMICAL PATTERNS FROM EARLIER STAGES OF GEOTHERMAL EVOLUTION

The area around the Roosevelt field has obviously been characterized by a flow of hot brines and gases to the surface or near-surface zone over a very long period of time. Some of the surface geochemistry may therefore be related to cumulative effects of these flows prior to the present day. Other aspects of the surface chemistry may reflect more ephemeral episodes presently occurring. It is desirable to separate the two. The older effects are of importance in unraveling the geothermal history of the reservoir. The present-day effects are much more important in terms of exploration, and for developing tools useful in elucidating details of presently active geothermal systems.

To do this, one would need to understand in detail the history of the geothermal system, but the available data are not yet sufficient to give a very certain picture of the evolution over time of the geothermal field at Roosevelt. We thus lack a good case-history background for separating the effects of the long-term cumulative geochemical processes from those that are actively occurring at the present time. In the main body of the field south of Negro Mag Wash, one may reasonably conclude that the reservoir may have contracted, with the southern part around well 52-21 having formerly been geothermally active but now being a zone in which self-sealing has pervaded the entire rock mass down to at least the bottom of that well. (It is interesting to note that Bamford et al., 1980, were able to detect no geochemical signals of hot water entries in that hole, whereas such diagnostic mineral assemblages were found in the actively producing 72-16 and 14-2. This may suggest that the characteristic mineral assemblages mapped around active hot water entries are later lost when a zone becomes sealed, as in 52-21).

Similarly, to the west there are signs of earlier leakage in a zone about a thousand feet west of the Opal Mound, and along the fault that branches northwest from the Opal Mound fault just south of Negro Mag Wash; yet at present, temperature gradients in 9-1 and in nearby stratigraphic tests are much lower than in the field itself, and it is usually considered that the Opal Mound fault now seals the reservoir fluids from passing west of it. This again suggests shrinkage of the field, in the west as well as the south.

To the north of Negro Mag Wash the picture is less clear, as there is far less available data related to that area. While a general picture of progressive reservoir shrinkage from heat loss and precipitation of silica can be argued, it is equally possible for new reservoir zones to develop as a result of breaching of the cap by active faulting, which obviously continues to occur.

In summary, little more can be said on earlier stages of evolution of the geothermal field at Roosevelt. The southern and western margins do show signs of being former reservoir zones that are now at least partly self-sealed.

EFFECTS OF PRE-GEOTHERMAL MINERALIZATION

There is a problem in separating the geochemical manifestations of present geothermal events and processes from those inherited from earlier hydrothermal episodes of mineralization during the Tertiary, related to the emplacement of the Mineral Mountains pluton.

That episode of mineralization probably occurred about ten million years ago and is best known in the Bradshaw mining district of the southern Mineral Mountains. Contact metamorphic deposits occur there, involving gold, silver, copper, lead, zinc, and tungsten mineralization. Throughout this whole region the Tertiary mineralization involves these elements, and manganese (Crawford and Buranek, 1957; Earll, 1957; Bullock, 1976).

The Mineral Mountains were in fact the site of the first production of lead-silver in Utah, during the middle part of the last century. Economically successful exploitation of base and precious metals appears to have been confined to the southeastern portion of the Mineral Mountains, in the Bradshaw district, the Granite and North Granite districts, and the Shag Hollow area.

In the area of the Roosevelt KGRA there are some test pits that were evidently dug following the observation of coatings of malachite. These copper occurrences in prospect pits are in altered mylonites (Sibbett and Nielson, 1980).

Just north of the mouth of Ranch Canyon there is a group of shafts in an area of pyrite-chalcopyrite mineralization along a fault zone; and between Ranch Canyon and Corral Canyon, near the Upper Ranch Canyon road, there are scarn deposits that have been worked for copper and perhaps precious metals.

It is interesting to note that on the eastern side of the Mineral Mountains, along the possible line of extension of the Negro Mag Wash fault, there is intense brecciation, with propylitic and argillic alteration, and with minor copper mineralization (Sibbett and Nielson, 1980). It thus appears that the WNW-trending set of faults may have a long history, and that the mylonite zones of the denudation faults are also old.

This Tertiary mineralization in the Roosevelt region predates the present geothermal system and adds some complexity to the interpretation of surface geochemistry, since some of the geochemical patterns may result from remobilization of the elements involved. There is also the ever-present possibility of the effect of detrital grains derived from erosion of the older mineralized material and transportation into the area of sampling in the valley.

In the next section, ideal geochemical tools for geothermal exploration are discussed, and the results of the microlayer work are analyzed.

GEOCHEMICAL INVESTIGATIONS AT ROOSEVELT SPRINGS

INTRODUCTION

Field programs at Roosevelt Springs were conducted in two phases, the first of these, (Phase II), being designed to establish the optimum sampling medium and to determine the most sensitive elements for detecting concealed geothermal activity. The second field survey, (Phase III), involved collecting a further 300 samples on a regular grid pattern over a broad region surrounding the geothermal area. Phase IV constituted analysis, mapping and interpretation of the surface microlayer geochemistry.

REVIEW OF GEOTHERMAL GEOCHEMISTRY OF SELECTED ELEMENTS

As a matter of routine the ion chromatography and induction coupled spectrometry used in the analysis of the samples for this program generates data for a total of some twenty-four species and elements. In addition, the non-routine atomic absorption and other analyses produce data for a further sixteen elements. Of these Hg, As, Se, Sb, Zn, Be, Mn, S (as sulphate), Rn, Si, B, Cs, Rb, Li, F, Pb, Mo, Cl and Br have been either used or proposed as potential pathfinder elements in geothermal exploration.

However, the review of elemental behaviour in geothermal solutions given below and the description of the data which follows, is confined to those elements and species which appear to have generated data which are relevant to the Roosevelt Springs area.

MERCURY

Mercury is commonly present in a mobile form, perhaps as sulphide, organic complexes or vapour, and in anomalous concentrations in geothermal waters (Barnes 1979). This was discussed by White (1967) and since then there have been a number of reports of the application of mercury in soil or soil gases, to geothermal exploration (Matlick and Buseck, 1976; Klusman et al 1977; Klusman and Landers, 1978; Capuano and Bamford, 1978; Parry et al 1977; Phelps and Buseck, 1978).

Mercury is probably released into the near surface environment in the elemental form either via a disproportionation reaction of Hg (I) ions within the geothermal solutions or by oxidation of mercury minerals in the upper levels of the geothermal system. Excessive concentrations of mercury generally indicate the presence of permeable fracture zones and the element can be an effective indicator of leakage from hot water or steam bearing aquifers. Gaseous dispersion, favored by the relatively high vapour pressure of this element, is enhanced by the elevated temperatures associated with geothermal activity. However, the concentrations in soil-gas and the mobility in the gaseous state are strongly affected by diurnal temperature and pressure variations, soil moisture, organic matter, overburden porosity and climate.

Sorption of mercury vapour onto clays, iron oxides or organic matter can lead to a surficial expression. Anomalous concentra-

tions of mercury in the surface microlayer have been reported to be associated with various types of sub-surface mineralization (Thompson and Read, 1978).

CESIUM

Cesium has received little attention as a pathfinder element for geothermal prospecting. However, as an element which is preferentially concentrated in late stage volatile-rich granitic rocks it may be expected to occur in geothermal solutions. Indeed cesium has such a marked tendency to accumulate in the volatile phase, that it may form its own mineral, pollucite, in some pegmatites. Furthermore the large difference between the ionic radii of cesium and potassium contributes to its preferential removal from feldspar, the principal host, during hydrothermal generation.

Furthermore, cesium is one of the very few elements whose concentrations in geothermal waters are not controlled by temperature and pressure dependent equilibria, the chemistry being principally governed by extraction and dilution processes.

Cesium concentrations in geothermal waters occur in the range 0.02-20 ppm (Ellis, 1979) with values generally in the ppm range. This is in marked contrast to non-geothermal water (Sreekumaran, et al 1979) where the values are generally of the order of a few hundreths of a part per billion. Cesium rich waters are particularly characteristic of an acidic rather than a basaltic heat source.

Cesium released into the surficial material is rapidly and strongly adsorbed by solid soil material (Davis, 1963) and perhaps, therefore, cesium anomalies are to be expected in geothermal areas.

ARSENIC

Arsenic, with mercury and antimony, is one of the metals most commonly precipitated at the surface, by geothermal activity. Concentrations of several hundreds of parts per million are common and they may reach several tens of percent (Weissberg et al 1979). Within metal-rich geothermal waters themselves, arsenic levels occur within the range 0.03-40 ppm. The mobile form is considered to be arsenite ion resulting from the hydrolysis of sulphide at lower temperatures.

It is not, therefore, surprising that arsenic is amongst the better established elements used in surficial geothermal exploration for geothermal activity (Ewers and Keays, 1977; Bamford et al (1980). This element would be expected to be of use in the Roosevelt Springs area as traces of realgar are found within the opaline sinter.

ANTIMONY

Antimony occurs in metal-rich geothermal waters with concentrations in the range 0.1-0.45 ppm (Wedepohl, 1972; Ritchie, 1961). Antimony rich precipitates at the surface are common and concentrations may be as high as 30% Sb. In contrast, the levels in non-geothermal waters are very low and are in the range 0.01-0.08 ppb (Landstrom and Wenner, 1965). In soils the levels are also low with background concentrations of the order of 2 ppm. Transport of antimony in the geothermal system is probably as sulphur or chloride ion complexes.

At Roosevelt Springs, Bamford et al (1980) were able to show that anomalous concentrations of antimony occur in the sinter forming the Opal Mound and in the overlying soils. Antimony anomalies were also found to be associated with fumarolic activity and with manganese cemented alluvium. However, in view of its common association with geothermal activity and the extreme contrast with the normal background, it is surprising that antimony has not found greater application in geothermal exploration in the past.

LITHIUM

Lithium exhibits behaviour that is transitional between that of the Group I alkaline metals and the Group II alkaline earths. It has a very small ionic radius, a high ionization potential and, consequently, an appreciable covalent character. Due to the small size of the lithium ion, compared with that of the next alkali metal, sodium, there is only limited substitution of Li^+ for Na^+ in feldspar and as a result, lithium tends to accumulate in late stage hydrothermal minerals. However, with appropriate charge adjustment, lithium can substitute in a silicate lattice, for Al^{3+}, Fe^{2+} and Mg^{2+}.

Lithium is present in sub-surface waters at low levels, generally less than 10 ppb (Livingstone, 1963). By contrast, levels in geothermal waters are much higher, normally over 100 ppb and fre-

quently of the order of 10,000 ppb (White, 1970). However, the concentration of lithium in geothermal waters normally reflects its abundance in the surrounding rocks with high values being associated with areas of granitic or andesitic rocks. Lithium tends to decrease in concentration in waters migrating to the surface due to the incorporation of the ions into low-grade hydrothermal alteration products such as clays and zeolites (Ellis, 1979). Lepidolite (lithium mica) has been reported from shallow, hydrothermally altered rocks (Bargar et al 1973). The median background concentrations of lithium in soils is 22 ppm (Connor and Shacklette, 1975).

Lithium has been proposed as a potential pathfinder element in geothermal exploration, Brondi et al (1973), Bamford et al (1980), and Cannon et al (1980), have proposed that the lithium content of accumulator plants can be used to locate lithium-rich brines.

SELENIUM

Selenium is a member of the Group 6A elements of the periodic table. In its geochemical behavior, therefore, it closely resembles sulphur. It is strongly chalcophile and its principal occurrence is in sulphide minerals associated with arsenic, antimony, copper, silver and gold. It may also be accumulated by secondary processes which result in the reduction of oxidizing waters, and it is therefore highly enriched in black shales and sedimentary uranium deposits.

Selenium may be expected to be enriched in metalliferous geothermal solutions, but little work has been reported. However, Ewers and Keays (1977), detected selenium concentrations up to 9800 ppm in drill-hole material from the Broadlands geothermal area in New Zealand, associated with epithermal type mineralization. There appears to be a strong depth/temperature control of the deposition of selenium which suggests that the stabilities of the mobile species decrease with falling temperature and that the selenium is co-precipitated with heavy metal sulphides.

The normal background concentration of selenium in soils is 0.3 ppm, and although this element has not been reported as a potential pathfinder in geothermal exploration, it is conceivable that the deposition of metal-rich sinter in the near surface environment may lead to a potentially useful selenium expression. Furthermore, selenium may form a variety of volatile species such as

H_2Se and dimethyselenide, $((CH_3)_2Se)$. This latter species is formed by bacterial action on inorganic, mineral precursors (Fleming and Alexander, 1972).

RUBIDIUM

Rubidium, the fourth member of the alkali metal family has a very similar ionic radius to the preceding element, potassium. As a result, rubidium does not form minerals of its own, but it is widely dispersed especially in the potassium minerals, feldspar and mica and it becomes enriched in the later crystallizates such as lepidolite, amazonite and microcline, where concentrations may reach several percent.

Rubidium is enriched in geothermal water with concentrations between 0.01-7.7 ppm and a mean of 0.82 ppm (Wedepohl, 1972). These values exclude the brines from the Salton Sea, where unusually high concentrations of 60-169 ppm are reported (Helgeson, 1968; White, 1965). The concentrations of rubidium in geothermal waters are a reflection of the surrounding rock types with levels that are low in basaltic areas and higher in granitic or andesitic environments (Golding and Speer, 1965). By contrast, the concentrations in non-geothermal groundwaters are much lower. Pentcheva (1965), reports rubidium values up to 0.8 ppb in groundwater.

As geothermal waters migrate towards the surface, the ions become incorporated into clays and zeolites, with a resulting drop in the concentration in solution.

The median concentration of rubidium in soils is 35 ppm. During weathering rubidium is strongly held in adsorption positions on clays (Goldschmidt, 1954).

BERYLLIUM

As a result of its low atomic number, beryllium has a high ionization potential and a very small ionic radius. It does not, therefore, behave as a normal Group II alkaline earth and it has a much more covalent character. It does not fit readily into the silicate lattice as a cation and is normally found in substitution for silicon. The difficulty with which beryllium is incorporated in silicate minerals results in its accumulation in late-stage crystallizates and beryllium bearing minerals commonly occur within pegmatitic or metasomatic lithologies.

Published data on beryllium dissolved in geothermal waters is not, apparently, available. However, Bamford et al (1980) report enhanced beryllium concentrations in the opaline sinter and the manganese cemented alluvium at Roosevelt Springs. These values were not reflected in the soils overlying the sinter.

ANION GEOCHEMISTRY

The total dissolved solids in geothermal waters may vary widely from as little as 3% to as much as 50% dissolved solids by weight. The concentration of solids depends upon the source of the water and history. In order of increasing salinity the four types of water are:

1. Surface water (river or groundwater).
2. Connate water derived from within sedimentary sequences.
3. Metamorphic water released during the metamorphism of water bearing minerals.
4. Magmatic water.

The predominant anion in these solutions is chloride with subsidiary and varying concentrations of bicarbonate, sulphate, sulphide (or hydrosulphide), bromide, iodide, and fluoride. The solutions may range from quite acid to mildly alkaline. The principal cations balancing the solutions are, of course, sodium, potassium, calcium and magnesium.

The discharge of geothermal waters onto the surface could conceivably lead to a build-up of these soluble species. However, the deposits would be easily removed by any surface water activity and would only be expected to accumulate in areas where there is a development of saline horizons within the soils. Even in these areas, the phenomena that would be most likely to control the position of these accumulations are likely to be the climate and the topography, rather than the point of supply.

RADON

Radon, a radioactive and inert gas, has three isotopes all unstable, of which the longest lived is Rn^{222} with a half-life of 3-8 days. The other isotopes have much shorter half-lives, which so severely limits their distribution as to preclude their use in geochemical exploration. Rn^{222} is generated during the radioactive decay series of uranium, but the immediate parent is radium

(Ra^{226}) which is highly mobile in some reducing brines (Rose et al 1979). Radium^{226} has a half-life of 1622 years and therefore its potential for movement through a geothermal system is considerable.

Radon has been detected in spring water from several geothermal areas (Cadigan and Felmlee, 1977) and soil gas radon anomalies may, therefore, be useful for detecting the presence of porous leakage zones beneath overburden cover. Anomalous radon in soil gas values have been reported from the Roosevelt Springs KGRA (Nielson, 1978).

Direct measurement of radon in soil gas is possible in the field but absolute radon values may be misleading due to variations brought about by climatic changes and varying soil composition.

SURFACE MICROLAYER GEOCHEMISTRY

The entire surface of the earth, both land and sea, is covered with a microlayer of surficial material that is in contact with the atmosphere and contains both organic and inorganic components. This surface microlayer is subjected to conditions not experienced by deeper material:

1. The surface is irradiated by the sun and the ultraviolet radiation can induce abnormal chemical conditions.

2. In arid areas the surface microlayer is often dry so that mineral surfaces are in direct contact with gas. Clays have a large absorption capacity in this state and microbial activity is reduced to a minimum.

3. Evaporation of solutions rising to the surface in arid areas can result in the accumulation of mobile ions as strongly held species within the surface material.

4. The elements that are present within the underlying soil profile are also found in the surface microlayer whether the surficial particulates are from organic, botanical or mineral sources. Strong evidence suggests that, if the appropriate size fraction is collected, then the geochemistry of the surface microlayer accurately reflects that of the underlying soils (Barringer, 1978).

5. In water covered areas there is a concentration of surface active material at the air/water interface.

COMPOSITION OF THE SURFACE MICROLAYER

The surface microlayer is composed of clay, silt, sand, and pebbles throughout most of the Roosevelt Hot Spring Area. At each sample site the fine fraction was treated with a few drops of dilute hydrochloric acid (Figure 28). Generally, very mild or no effervescence was seen on the east side and very strong reaction on the west. This gradation is probably due to the development of caliche toward the valley to the west. In the southern part of the sample area, lobate areas of mild effervescence correspond to areas of lag pebble pavement. In the northern portion of the area a linear NNE trending area of mild reaction probably corresponds with siliceous alteration localized along a fault trend.

The silt and fine sand fractions are depleted by wind erosion on the east side of the area. At least part of this material is redeposited on the west side of the area.

R 10 W

R 9 W

R 8 W

T 26 S

T 27 S

T 28 S

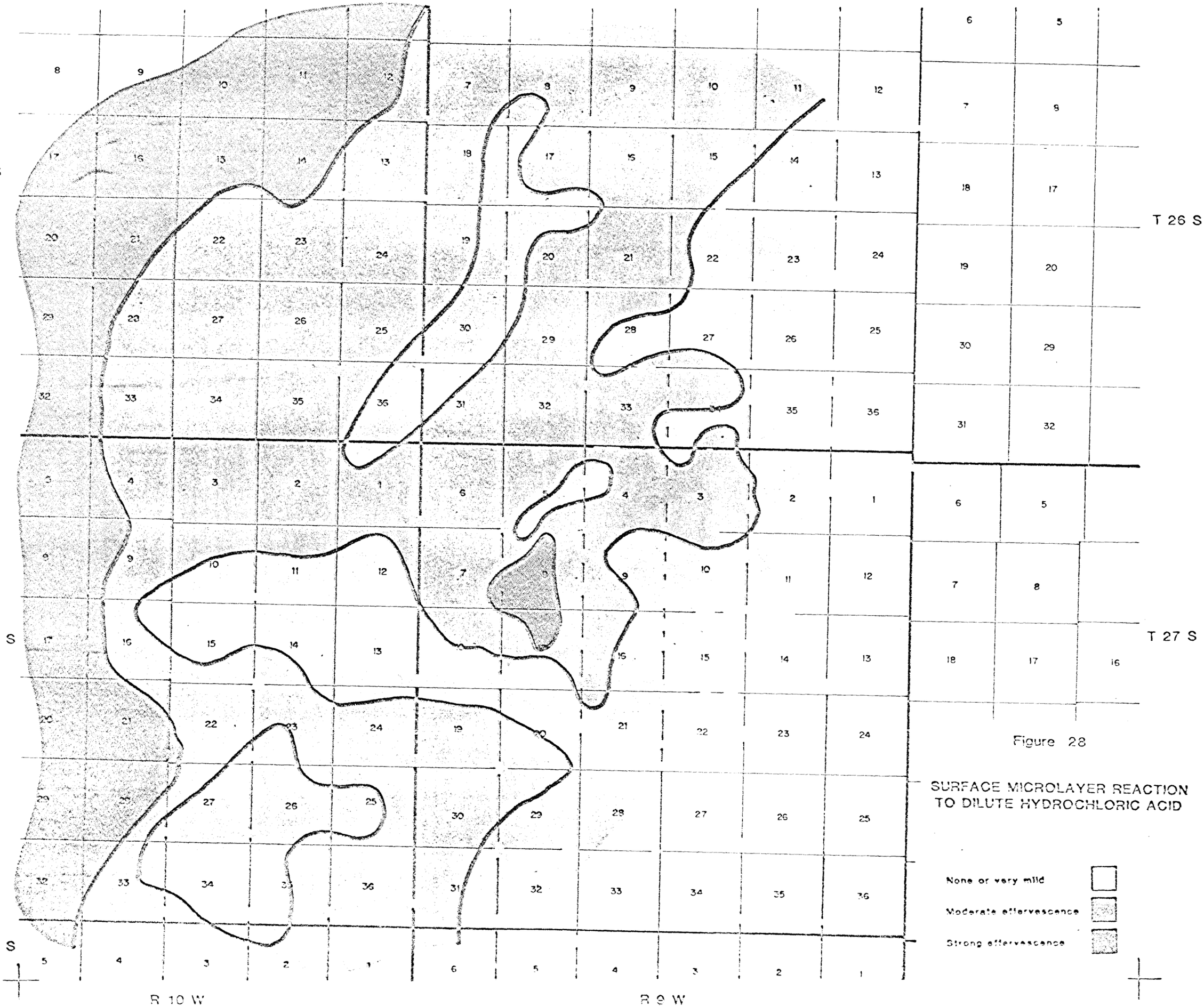

Figure 28

SURFACE MICROLAYER REACTION
TO DILUTE HYDROCHLORIC ACID

None or very mild

Moderate effervescence

Strong effervescence

The coarse fraction is composed of pebbles, cobbles, and small boulders derived from the Mineral Mountains. Granitic and volcanic fragments are most abundant. Limestone and quartzite fragments are common. The amount of obsidian flakes and the area covered by them is disproportionately large compared to the area of obsidian outcrop in the Mineral Range (Figure 29).

Vegetation in the sample area consists of sagebrush and sparse desert grasses. The sample area is periodicallly grazed by sheep, but is neither irrigated nor cultivated.

SURFACE MICROLAYER SAMPLING

Collection of the surface microlayer for geochemical exploration has a number of distinct advantages.

1. The material is readily available and can be collected very quickly without the need for augering, pitting or trenching.

2. The particulates are collected over a wide area at the sample site and are thus more representative of the area than a single spot sample.

3. Sampling along continuous traverses from moving aircraft, vehicles or on foot is possible, resulting in highly efficient programs capable of covering wide areas on a reconnaissance basis.

4. The surface particulates frequently have different properties than the soils and may give a better expression of underlying mineralization or other economic deposits.

5. The surface microlayer is universally present, even over rock outcrop or vegetation.

Barringer Research has developed SURTRACE, a specialized system for the collection of surface microlayer samples. The SURTRACE equipment is manufactured in both airborne and ground versions. The airborne equipment utilizes a helicopter with a specially designed sampling probe that is deployed beneath the aircraft.

A portable back-pack unit was used in this program. This version utilizes a light-weight chain-saw motor to create a vacuum which draws the surficial material through a pipe to a small cyclone which separates it from the air-stream and collects it in a test-tube. The unit requires only one operator and samples can be collected rapidly, giving high productivity.

R 10 W

R 9 W

R 8 W

T 26 S

T 27 S

T 28 S

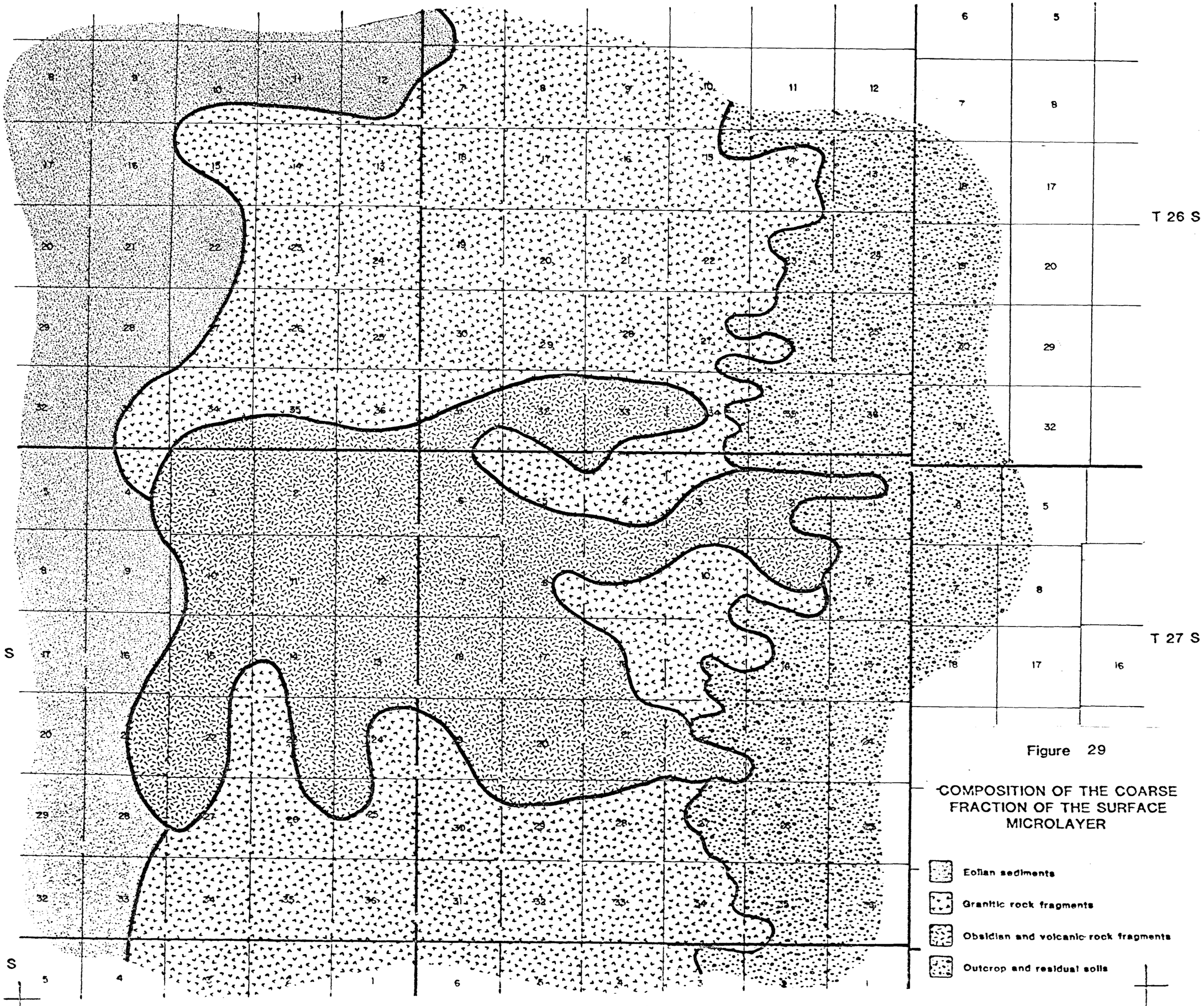

Figure 29

COMPOSITION OF THE COARSE FRACTION OF THE SURFACE MICROLAYER

- Eolian sediments
- Granitic rock fragments
- Obsidian and volcanic rock fragments
- Outcrop and residual soils

ANALYTICAL METHODS

The wide variety of elements and species determined during this program necessitated a number of different analytical and digestion techniques. These techniques are summarized in Table 3 and the analytical procedure is briefly described below.

Induction Coupled Plasma Emission Spectrometry (ICPS)

For analysis by induction coupled plasma spectrometry, the sample is introduced into a gas, in this case argon, which has been raised to a temperature high enough to develop a plasma state, by high frequency radio excitation. The elements in the sample are excited to strong spectral emission, and the output is analyzed by a direct reading spectrometer.

Samples are conventionally introduced by nebulization of a liquid, but during this program the Barringer LASERTRACE system was also used. In this method the sample is selectively vapourized into the argon stream, from a tape, by a pulse of laser light.

Atomic Absorption Spectrometry

The program entailed the use of conventional flame atomic absorption spectrometry (AAS) for Li, Rb and Cs, flameless, cold vapour AAS for Hg; and flameless AAS of the hydride for Sb, As and Se.

Ion Chromatography

Ion chromatography was used to determine anions after a weak extraction. In this technique the sample is carried through a column containing an ion exchange resin and each ionic species is detected discretely as it elutes from the column.

Emanometry

Radon was determined during Phase II only in soil-gas in the field by direct measurement of α-particle decay by scintillometry.

TABLE 3. Summary of Digestion Techniques and Analytical Methods.

Method	Digestion	Elements determined detection levels (ppm)
Cold vapour AAS	Conc. H_2SO_4/HNO_3	Hg(0.001)
Automatic hydride flameless AAS	$HClO_4/HNO_3$	As,Se;Sb(0.1)
ICPS	$LiBO_2$ fusion	Si (1.0); Ba (0.2)
ICPS	$HF/HClO_4/HNO_3$ dryness redissolved in HCl	Ca(1.0);Al(0.1);Mg(2.0); K(20.0);Na(40.0);Fe(2.0) Ti(0.1);Mn(2.0);Cr(2.0); Sr(0.2);V(0.1);P(10.0); Be(0.01);Ni(1.0);Co(1.0) Pb(4.0);Mo(4.0)
Flame AAS	$HF/HClO_4/HNO_3$	Li, Rb, Cs (0.2)
Ion Chromatography	12 hr. leach in 0.004M$NaHCO_3$/0.0034 Na_2CO_3	F^-(2);Cl^-(12);PO_4^{--}; NO_3^-(15);SO_4^-(8)
Emanometry	None (soil gas)	Rn
ICPS	Lasertrace	B (0.1)

PHASE II SAMPLING

Both surface microlayer and conventional soil samples were collected along four traverses designed to cover both background and geothermally active areas at Roosevelt Springs. Sample locations and numbers are indicated on a map at the scale of one inch to one mile (Plate 2). Traverses A, B and C were essentially east-west, while Traverse D followed a north-south line across the geothermal reservoir.

The sample interval was approximately one mile in the background areas, closing to quarter mile spacing in the geothermal areas, yielding a total of 89 sample pairs.

PRESENTATION OF RESULTS

For the purpose of making a direct comparison of the surface microlayer versus the conventional soil samples, the geochemical traverses have been plotted in the form of stacked profiles, with the surface microlayer result above the equivalent soil value. The profiles were prepared using the Barringer Research CANPLT Computer program with line printer output. This program reduces the analytical concentration of each element to standard deviation units which provides a uniform method of comparison of geochemical patterns. Obviously contaminated samples, such as those downslope from the Montreal Mine at the west end of Traverse A, were removed from all consideration in this study. In order to eliminate the effect of spurious high samples remaining within the data set, the initial mean and standard deviation are used to provide a threshold of mean plus three standard deviations. Samples with values exceeding this threshold are eliminated from the data set and the mean and standard deviation recalculated as the second pass statistics. The plotting program then provides a profile in which each symbol is equivalent to 0.5 standard deviations, starting at the minimum value or mean -3 standard deviation whichever is the larger value. High values are occasionally truncated, but the geochemical patterns for each sample type can be readily compared with one another using this method. Comparative first and second pass statistics for soil and surtrace samples are listed in Appendix A, and the profiles under discussion are contained in Appendix B. Table 4 lists the soil to surface microlayer correlation coefficients for the non ICP elements.

CORRELATION MATRIX
SAMPLE SIZE = 69

	AS X	AS X	LI X	RB X	CS X	SB X	HG X	AS Y	SE Y	LI Y	RB Y	CS Y	SB Y	HG Y
AS X	1.000													
SE X	.326	1.000												
LI X	.342	.411	1.000											
RB X	.129	-.008	.571	1.000										
CS X	.922	.133	.392	.242	1.000									
SB X	.881	.240	.204	.073	.835	1.000								
HG X	.010	.077	-.041	.139	-.031	-.065	1.000							
AS Y	.477	.525	.354	-.090	.336	.306	.047	1.000						
SE Y	.241	.440	.374	.032	.181	.117	-.027	.673	1.000					
LI Y	.096	.343	.848	.441	.155	-.027	-.155	.380	.541	1.000				
RB Y	-.154	-.002	.508	.792	-.056	-.203	.082	-.167	-.069	.596	1.000			
CS Y	.141	.278	.496	.071	.179	-.018	-.132	.434	.422	.661	.310	1.000		
SB Y	.111	.198	.034	-.203	-.028	.085	.042	.317	.087	-.010	-.202	-.015	1.000	
HG Y	.052	-.021	-.119	-.017	-.046	.026	.396	.270	.160	-.153	-.201	-.103	-.009	1.000

X = SURFACE MICROLAYER

Y = SOIL

TABLE 4: Correlation matrix for selected elements showing relationship between soil and surface microlayer results.

COMPARATIVE STATISTICS

A review of the tabulated statistics in Appendix A indicates a close relationship between the means of the second pass statistics for both soils and surface microlayer. Only six elements or ions show substantial deviations from a one to one soil to surface microlayer relationship in a plot of mean versus mean. These parameters are Co, Pb, Cl^-, $SO_4^=$ and NO_3^- which are enhanced in the surface microlayer, and Ca which is depleted in the microlayer. While the build-up of the anions Cl^-, $SO_4^=$ and NO_3^- can be readily explained by the concentration of salts at the surface due to the evaporation of groundwater, the enhancement of cobalt and lead are not that readily interpreted. Comparison of the correlation coefficients for cobalt in soil and surface microlayer (Meyer, 1980) indicates a strong positive correlation between Co, Ti, V and Fe in the surface microlayer which is not evident in the soil data. This combination may indicate enrichment of cobalt along with a resistate mineral or with Fe hydroxide accumulating at the surface. In contrast, Pb correlates well with Zn and Mn in the surface microlayer, possibly indicating a preference for Pb to be trapped in a Mn oxide-rich surface grain coating or desert varnish. The increase in calcium in conventional soils as compared to the surface microlayer can probably be attributed to the presence of caliche type soils, with calcium concentrated in the caliche layer which is located at a depth dependent on the amount of rainfall.

GEOCHEMICAL TRAVERSES

The soil and surface microlayer profiles of geochemical Traverses A, B, C and D can be compared by reviewing the computer profiles in Appendix B in relationship to the sample location map. A useful point of reference would be the Opal Mound Fault which intersects Traverses A, B and C at samples 119, 213 and 304 respectively, while a broad chemical response might be expected on Traverse D between samples 408 and 420. Significant positive and negative correlations with these zones have been noted by drawing a continuous outline of the profiles in the appropriate location.

Mercury:

Surface microlayer results for mercury show a broader indication of the region in the vicinity of the Opal Mound Fault on Traverse B, and a generalized high zone on Traverse D (Figure 30). By contrast, the soil values are sharply defined with a single strong response at 213 (368 ppb) with a number of individual erratic high values on Line D. In terms of establishing a rapid reconnaissance method using mercury for the detection of geothermal targets, the broader anomaly in the surface microlayer would appear to be more suitable.

Antimony:

Surface microlayer results for antimony indicate a broad anomalous region centered on the Opal Mound Fault at sample 213. This feature is not evident in the soil data, and both soils and surface microlayer results are not particularly definitive on the remaining lines. In its ability to detect the Opal Mound Fault on Traverse B, the surface microlayer is superior to soil as a sample for antimony (Figure 31).

Cesium:

The cesium data in this phase of the program is somewhat ambiguous. On Traverse B the surface microlayer samples give a strong positive anomaly at the Opal Mound Fault compared to a low in the soil data (Figure 32). Conversely on Traverses A and D, the geothermal area was apparently marked by strongly positive values for both soils and surface microlayer.

Lithium:

Lithium exhibits a low in both the soil and surface microlayer samples collected at 213 on the Opal Mound Fault. Traverse C shows high values for both sample types, and anomalous values are also present at the western end of Traverse B. The presence of a low flanked by relatively high values at the Opal Mound Fault may be useful in exploration, but no significant difference exists between the soil and surface microlayer profiles (correlation coefficient 0.848 (Table 4).

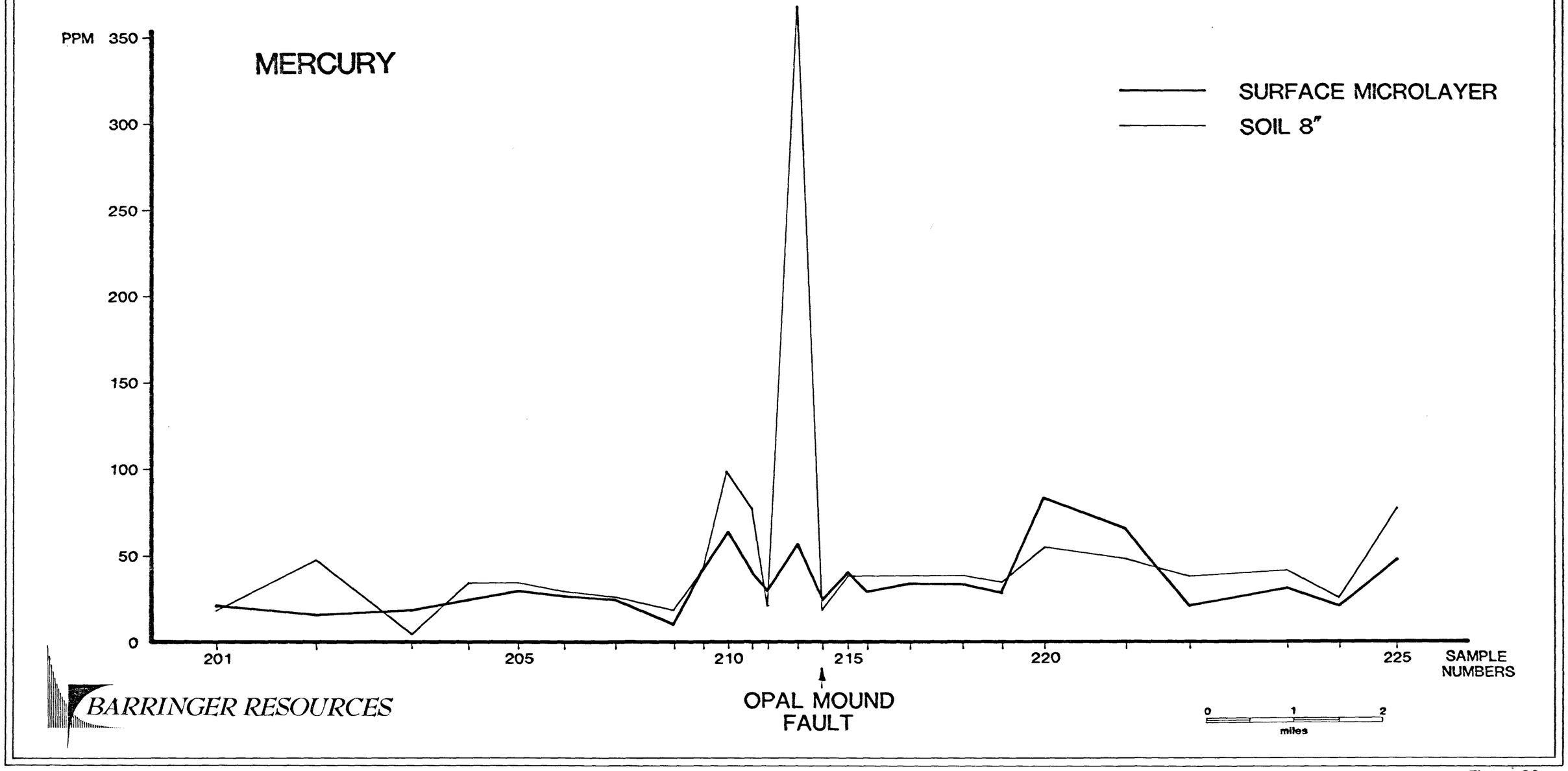
MERCURY
PPM
350
300
250
200
150
100
50
0
SURFACE MICROLAYER
SOIL 8"
201
205
210
215
220
225
SAMPLE NUMBERS
OPAL MOUND FAULT
BARRINGER RESOURCES
0
1
2
miles

Figure 30

ANTIMONY

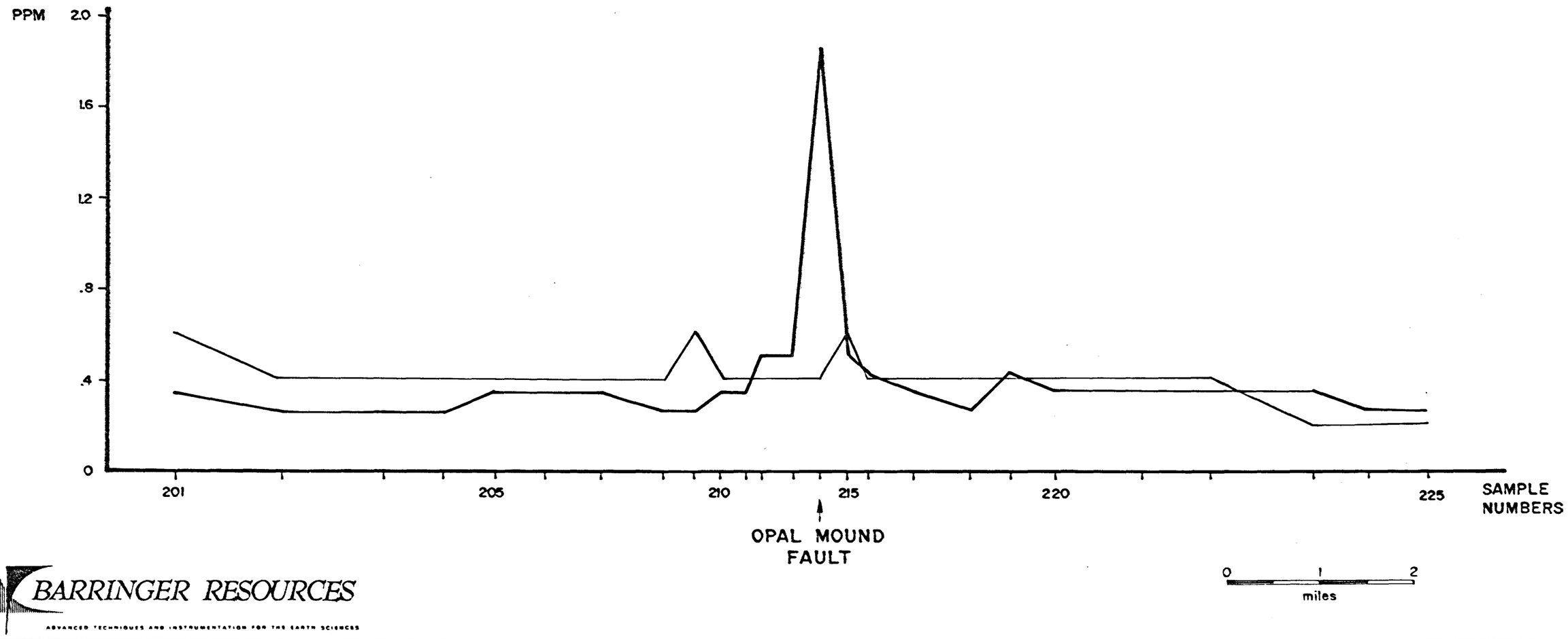

BARRINGER RESOURCES

ADVANCED TECHNIQUES AND INSTRUMENTATION FOR THE EARTH SCIENCES

Figure 31

CESIUM

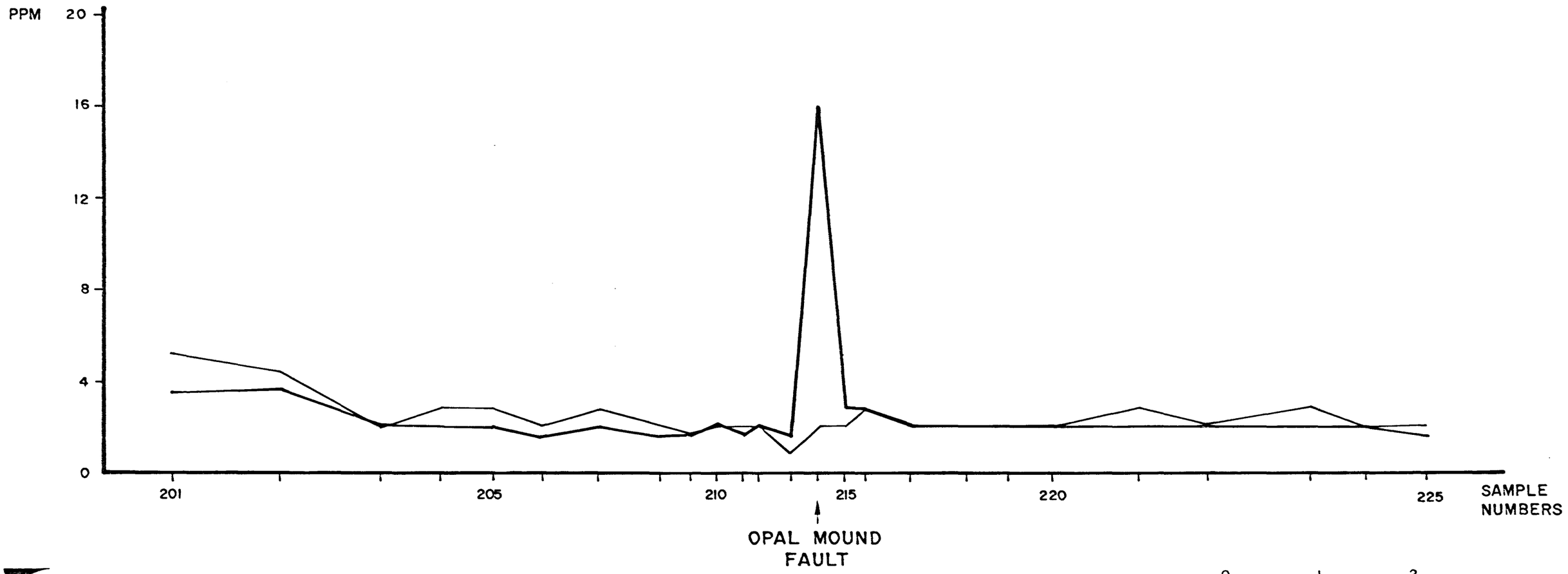

BARRINGER RESOURCES

ADVANCED TECHNIQUES AND INSTRUMENTATION FOR THE EARTH SCIENCES

Figure 32

Selenium:

A close relationship between soil and surface microlayer results is again found in the case of selenium, with the single exception of a positive soil anomaly centered on Traverse C that is not evident in the surface microlayer. The relatively noisy pattern on line D complicates the interpretation to the point that based on Phase II data, selenium would have to be considered of marginal use in exploration at Roosevelt Springs.

Arsenic:

The arsenic pattern is strongly similar to that of selenium, except that the arsenic anomaly in both soils and surface microlayer is better defined in the vicinity of the Opal Mound Fault of Traverse B (Figure 33) than on the equivalent selenium profile. Arsenic values are less erratic in the center of Traverse D making this element marginally of greater potential usefulness than selenium.

Rubidium:

The rubidium patterns are somewhat similar to the lithium profiles (Rb-Li correlation coefficients of 0.596 for soils, 0.571 for surface microlayer). No significant difference can be seen between the soils and surface microlayer response.

Beryllium:

There are very low contrast anomalies on either side of the Opal Mound Fault shown on one traverse in both the soils and the surface microlayer samples. These anomalous values are, however, lower than those recorded in samples collected from the Mineral Mountains.

Anions:

Of the anions, sulfate and fluoride show a positive response in both soils and surface microlayer in the vicinity of the Opal Mound Fault on Traverse B, while a broad chloride high on line D may be related to the subsurface geothermal reservoir. In the case of chloride, the surface microlayer results provide a superior geochemical pattern.

ARSENIC

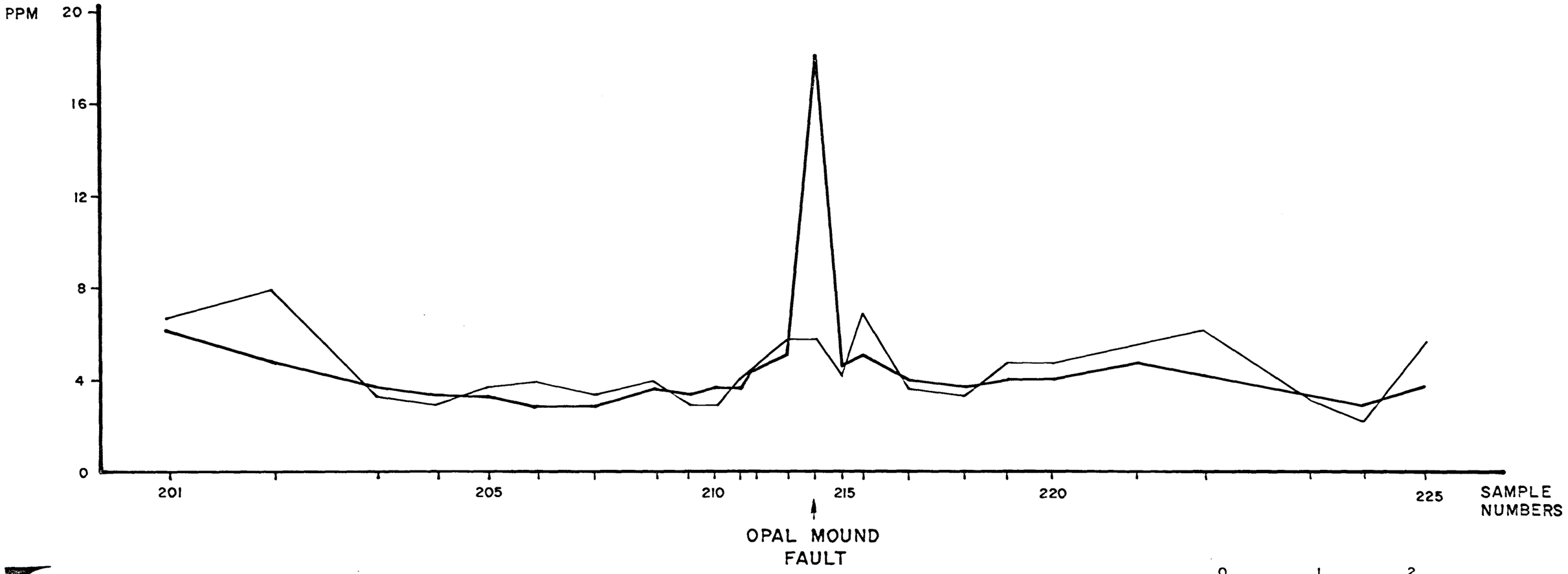

BARRINGER RESOURCES

ADVANCED TECHNIQUES AND INSTRUMENTATION FOR THE EARTH SCIENCES

Figure 33

Multi-element ICP Results:

A review of the ICP element profiles indicates potentially significant patterns for Zn in both soils and surface microlayer over a broad area. Ni and Co show marked anomalies in the surface microlayer samples from the vicinity of the Opal Mound Fault on Traverse B, while Pb gave a positive response from this area in both soils and surface microlayer. On the traverses sampled in the preliminary study, none of the other major or minor elements appeared to be helpful in defining the area of geothermal activity.

Radon and Temperature:

Radon gas analysis failed to detect the Opal Mound Fault on either the A, B or C traverse. Relatively high values were associated with granitic rocks and some areas of mineralization. Temperature profiles were noisy and inconclusive, probably due to the absence of a continuous recording control station.

PHASE II CONCLUSIONS

The geochemical response of selected elements and ions to the geothermal test area is summarized in Table 5. On the whole, the surface microlayer samples proved advantageous in the case of Hg, Sb, As, Zn, Ni and Co and were generally less erratic, providing a smoother profile. This broadening of the anomaly is a distinct advantage in reconnaissance for geothermal areas in that a wider sample spacing can be used. As a consequence, surface microlayer sampling was used exclusively in the Phase III regional sampling program.

TABLE 5: Comparison of soil and surface microlayer geochemical response to geothermal activity at Roosevelt Springs.

Element/Ion	Surface Microlayer	Soils
Hg	Strong, broad	Strong, narrow
Sb	Strong, OM fault	None
Cs	Low on fault	Low on fault
Li	Low on fault, possible halo	Low on fault, possible halo
Se	Erratic, noisy	Erratic, noisy
As	Strong, OM fault	Moderate, OM fault
Rb	Possible broad halo	Low on fault, possible halo
Cl^-	Possible broad zone	None
$SO_4^=$	High on fault, erratic	High on fault, erratic
F^-	High on fault	High on fault
NO_3^-	Broad zone Traverse D	Erratic
Zn	Broad anomalous zone	Low on fault, broad halo
Ni	Strong, OM fault	None
Pb	Broad zone, OM fault	Broad zone, OM fault
Co	Strong, OM fault	None
Be	Marginal anomaly, OM fault	Marginal anomaly, OM fault

PHASE III FIELD RECONNAISSANCE

In this phase of the field program all samples were taken from the surface microlayer using the Barringer SURTRACE backpack sampler. The samples were collected over an area within a 25 ft. radius of each site, thus providing an integrated sample more representative of the site than a spot sample.

In this second field program, samples were collected in three distinct schemes (Figure 34).

A. Background samples

Beyond the boundaries of the Roosevelt Springs KGRA, in the background areas of the Escalante Desert and the Mineral Mountains, samples were collected at section corners and, to the north and west, at section centers. This gave an overall sample density of 2-2½ samples per square mile and yielded a total of 107 samples.

B. Detailed samples

Within the KGRA the sample spacing was reduced, where possible, to quarter mile centers on lines spaced at half mile intervals. The total area sampled at this density was 31 square miles with 4.1 samples per square mile. This yielded a total of some 127 samples.

C. Close spaced samples

Two lines of close spaced sampling were completed across the Opal Mound Fault. Each line was somewhat over one mile in length and the sample interval was 200 ft., yielding a total of some 64 samples.

325000 R 10 W 330000 R 9 W 340000 R 8 W 347000

4271500 — 4271500

4260000 — 4260000

4252000 — 4252000

T 26 S — T 26 S

T 27 S — T 27 S

T 28 S

Figure 34

SAMPLE LOCATION MAP

DISCUSSION OF THE GEOCHEMICAL DATA FROM THE PHASE III SAMPLING PROGRAM

MERCURY

Surface Microlayer Soil Grid Data

The most prominent features of the mercury data are two strong contrast anomalies with maxima over 100 ppb (Figure 35). One of these lies on Negro Mag Wash Fault, a little to the west of the intersection with the Opal Mound Fault. The anomaly cannot be related to the presence of any of the surficial geothermal deposits of silica and is not near any of the producing geothermal wells. The anomaly is due to a single, highly anomalous sample with a value of 321 ppb Hg. This anomaly is not reflected in the nearest samples to the north, south, east or west.

The main geothermal area, the silica deposits and the Opal Mound Fault do not have a recognizable expression in this mercury data. There is a zone of low contrast mercury anomalies extending westwards along the line of the Salt Cove Fault, but the contrast is not great enough to be of use in an exploration context.

The second major feature is again due to a single high sample, in this case with a value of 110 ppb. The sample was collected from the flanks of a small hill of Tertiary syenite which lies to the north of Big Cedar Cove. The anomaly is not reflected in the samples immediately to the east or west, but there are two elevated samples to the south which were collected from the alluvial fill of the cove. There is no clear reason for this area of high values, but the calculation of a trerd surface for the whole survey area, reveals this to be part of a regional high in the mercury data. The implications of this are discussed later.

A value of 90 ppb on the contoured data on Bailey Mountain Ridge derives from the sampling carried out under Phase II. This sample also exhibits an anomalous concentration of zinc and, to a lesser extent lead, and probably, therefore reflects the presence of nearby mineralization.

An area of somewhat elevated values in the southern section of the survey area, to the west of Ranch Canyon does not correspond with any known geothermal activity, but it is an area of more frequent faulting.

325000 R 10 W 330000 335000 R 9 W 340000 345000 R 8 W 347033

4271638 4270000 4265000 4260000 4255000 4252000

T 26 S T 27 S T 28 S

Figure 35

MERCURY

Contour Interval 5 ppb

In comparing the mercury data with Figure 29 which shows the composition of the coarse fraction of the surface microlayer, there is a clear correlation between the higher values and the presence of granitic rock fragments in the alluvial areas. In the areas where obsidian and volcanic rock fragments predominate, the mercury values are low.

Detailed Surface Microlayer Traverses

There is an expression of the Opal Mound Fault in the mercury data from both of the closely spaced soil traverses (Figures 36 and 37). The mean mercury concentration for these sample sets was 28 ppb and the standard deviation is 7.7 ppb. On both traverses, therefore, there is a single sample which may be considered to be truly anomalous (+ 2 standard deviations) although on Traverse 1 the anomaly is only marginal (Figure 36). Even when sampled at this scale, there is no dispersion of mercury beyond the fault.

Conclusions

The mercury data may be considered to be somewhat discouraging as the main geothermal areas have not been delineated on the soil grid by this element. However, the principal anomaly on Negro Mag Wash lies within the area of strongest heat flow and the fact that it does not also correspond to macroscopic deposits of geothermal origin may suggest that mercury has a role in detecting more subtle expressions of geothermal activity. The limited dispersion shown by the detailed sampling across the Opal Mound Fault and the fact that the main anomaly derives from a single sample suggests that this element may be most useful on a detailed rather than a regional scale.

These data do not compare well with the results of Bamford et al., (1980). The background values from both sets of data are very similar but these authors were able to demonstrate the existence of somewhat more extensive and more intense areas of anomalous mercury values. However, the sampling was carried out on 500 ft. centers and the discrepancy between the two sets of data can probably be ascribed to the different sample patterns.

The 4th order trend surface for the mercury data has been calculated and is shown in Figure 38. This reveals a major regional high approximately centered under Bearskin Flat, and elongated north-south. It is possible that this regional anomaly is a

Figure 36

Traverse 1

Mercury

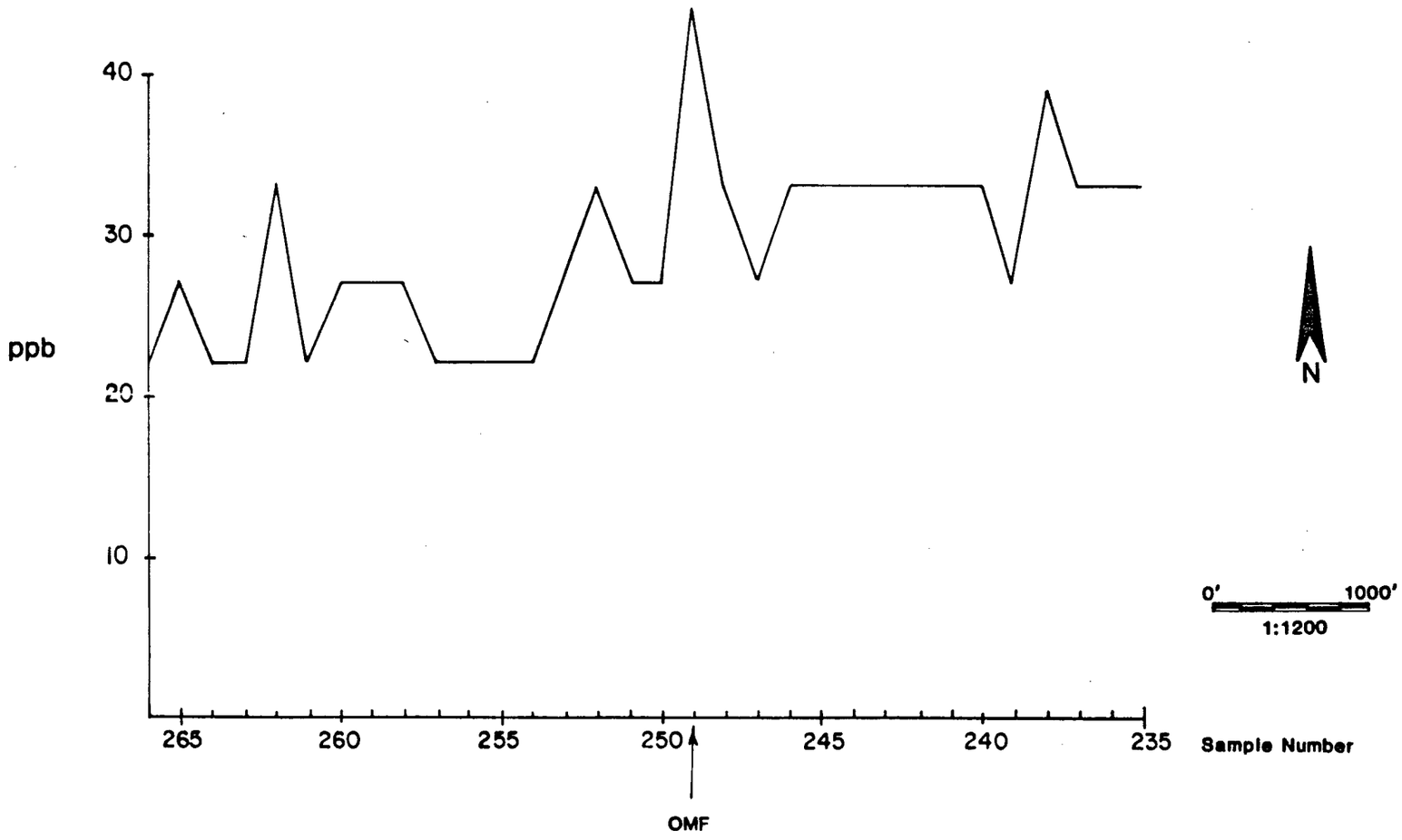

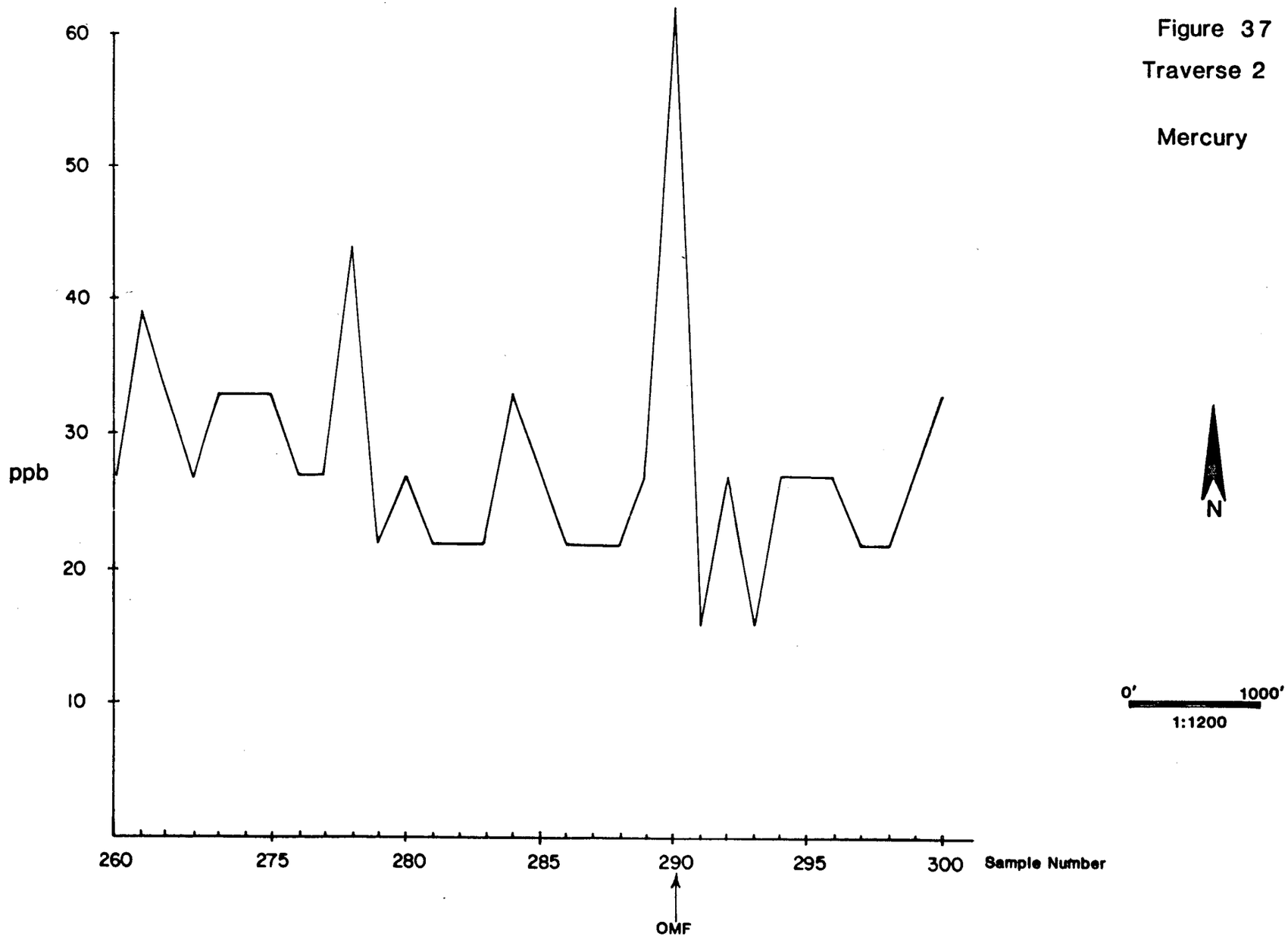

Figure 37

Traverse 2

Mercury

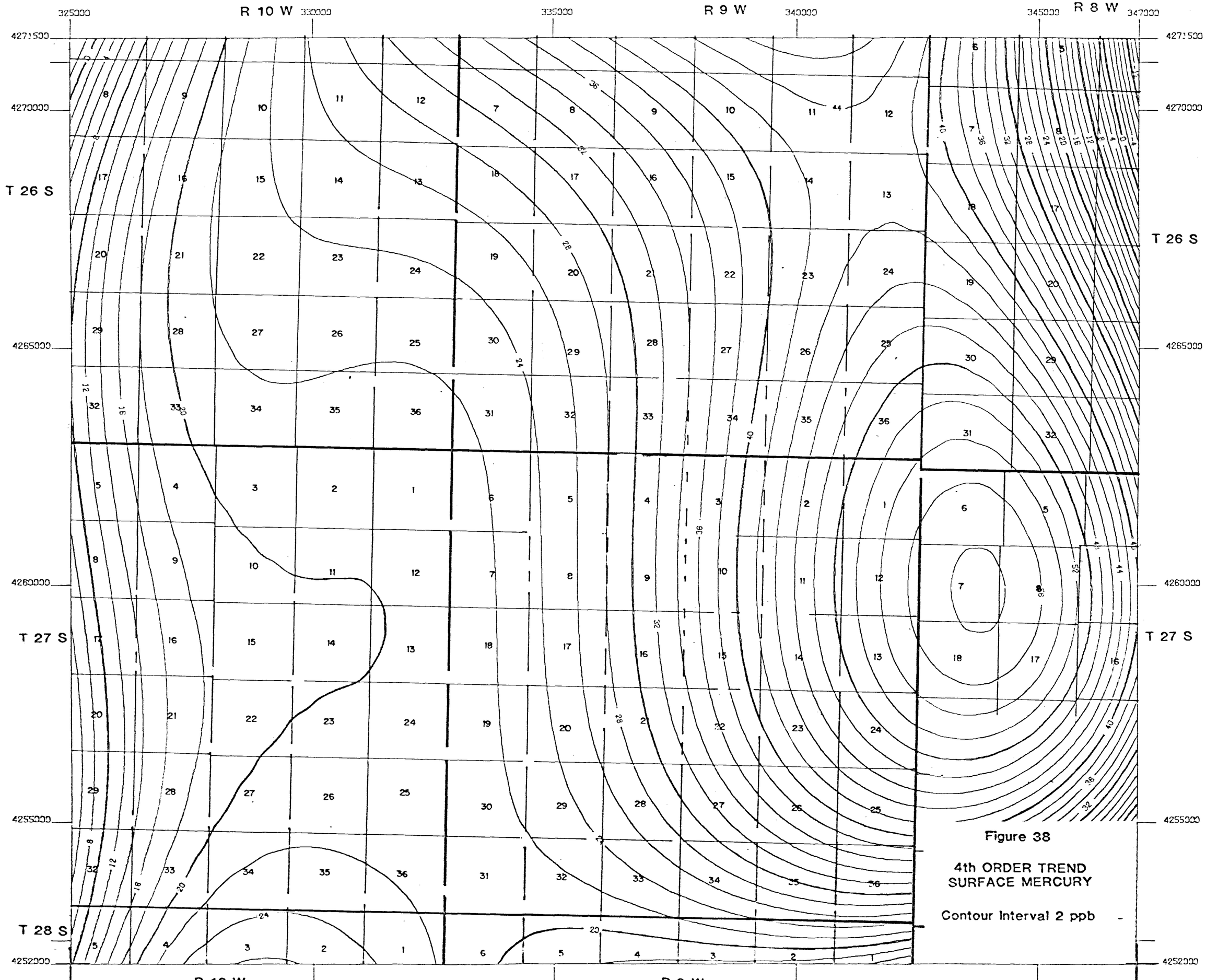

Figure 38

4th ORDER TREND
SURFACE MERCURY

Contour Interval 2 ppb

reflection of a major heat source at depth and its position approximately corresponds the site of the intrusive igneous heat source postulated by Ward et al., (1978). However, whether this is coincidental or not must, at this stage, remain speculative.

ARSENIC

Surface Microlayer Grid Data

The mean concentration of arsenic in the soils of the survey area is 3.7 ppm, the standard deviation is 1.4 ppm and values above 6.5 ppm may, therefore, be considered to be anomalous (Table 7). This corresponds well with the background of 4 ppm and the threshold of 6 ppm reported by Bamford et al., (1980).

The major feature of the contoured arsenic data (Figure 39) is a series of strongly anomalous values that follow the line of the Salt Cove Fault (WNW 3, Fig 9). The anomalous samples form a quite coherent pattern running west northwesterly across the northern part of the survey area, with a maximum value of 12.6 ppm As. The anomalous values become more intense and more closely grouped in the northwest corner of the survey where the Salt Cove Fault converges with Negro Mag Wash Fault (WNW 4). A strong north-south lineament (N3), which may be projected to extend across the whole area, also intersects these two faults at this point.

The remaining prominent feature of these data is a moderately strong anomaly derived from a single sample collected from near the intersection of Opal Mound Fault and Negro Mag Wash Fault. This anomaly is clearly related to, and is an expression of, the geothermal activity.

The remaining section of the geothermal area including the areas of opaline sinter and silica cemented alluvium, do not have an expression with the arsenic data.

Arsenic is not strongly correlated with any single element determined in this survey, but there are moderate correlations with selenium, cesium, calcium, strontium and the anions chloride and nitrate. There is also a moderate negative correlation with silica. However, the anomalous values are not, apparently, related to the areas showing a strong carbonate reaction that were mapped during the survey (Figure 28).

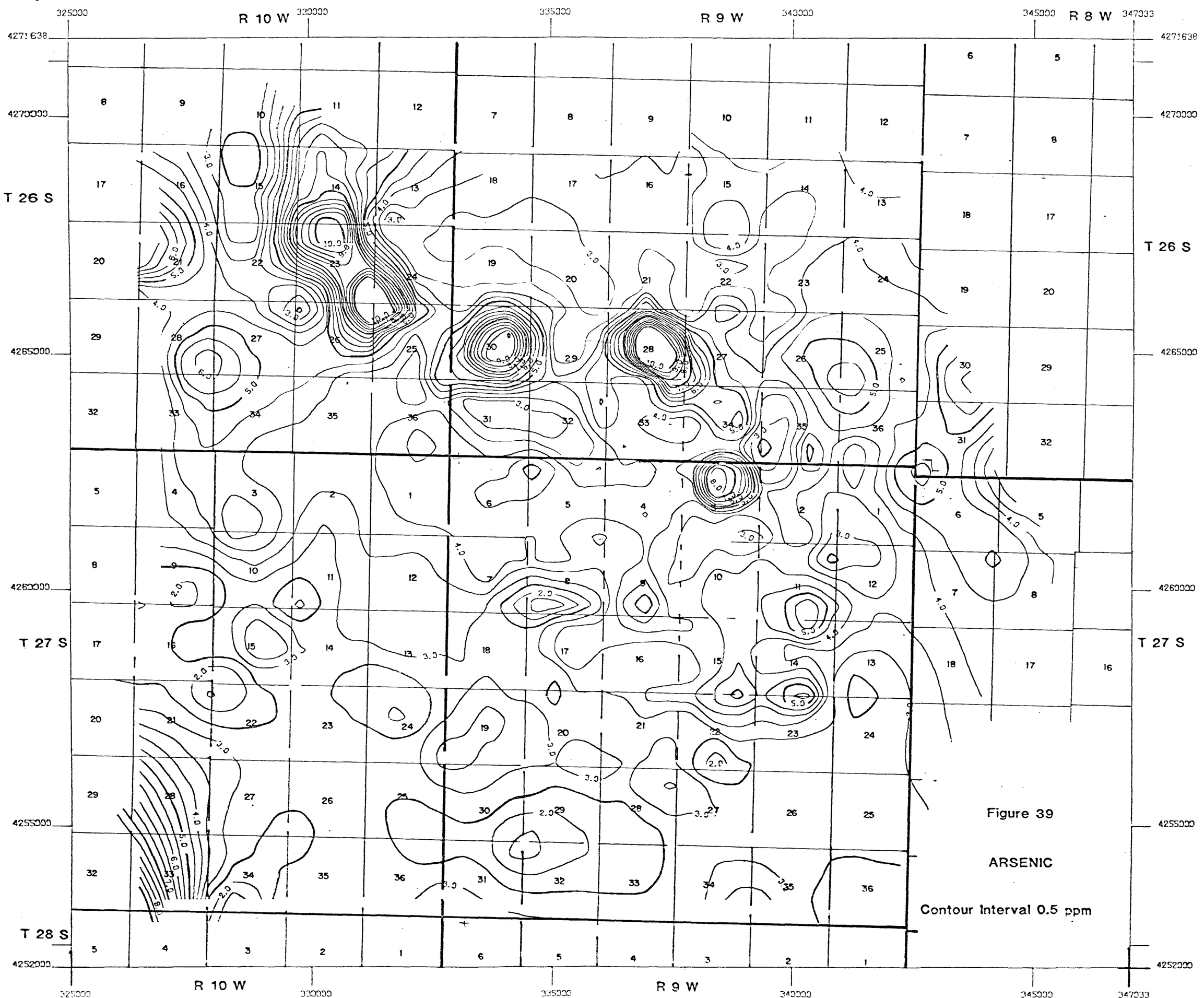
325000
R 10 W
330000
335000
R 9 W
340000
345000
R 8 W
347033
4271638
4270000
4265000
4260000
4255000
4252000
T 26 S
T 27 S
T 28 S
Figure 39
ARSENIC
Contour Interval 0.5 ppm

The remainder of the area was, on the whole, geochemically quiet in the arsenic data. An anomalous feature in the extreme southwest of the survey may be ascribed to a single sample.

Detailed Surface Microlayer Traverses

The level of the arsenic data from these traverses is, overall, lower than that in the area as a whole, with a mean of 3.4 ppm and a threshold of 4.8 ppm As. There is not, therefore, any indication of the geothermal activity on regional scale. Furthermore, the position of the Opal Mound Fault is only evident on Traverse 1, where there is a maximum in the data of 5.2 ppm to the east of the fault and there are two elevated values of 4.4 ppm which do not, however, exceed the threshold (Figure 40). Traverse 2 does not have any expression of the fault at all, despite the fact that it crossed an area of opaline sinter (Figure 41).

Conclusions

It may be surmised that the line of arsenic anomalies along the Salt Cove Fault outline an area of geothermal activity and that the intersection of the three faults in the northwest corner of the survey is highly prospective, but in the absence of drilling in this area, this must remain speculative. However, if drilling were to confirm the presence of a geothermal resource in this area, then it would provide strong encouragement for the use of arsenic in the surface microlayer as a reconnaissance exploration tool.

It is unfortunate that the main geothermal area and the surficial siliceous deposits do not have a recognizable expression in the arsenic data. Bamford et al., (1980) report strong arsenic in soil anomalies associated with this area and it is therefore probable that the wider sampling interval ·s the reason for the absence of an anomaly. It is to be noted that, even in the survey by Bamford et al., the central section of the Opal Mound Fault is overlain by soils with only background concentrations of arsenic.

CESIUM

Surface Microlayer Data

The mean concentration of cesium in the soils of the survey area is 7 ppm and the standard deviation is 7.4 ppm Cs (Table 7),

Figure 40

Traverse 1

Arsenic

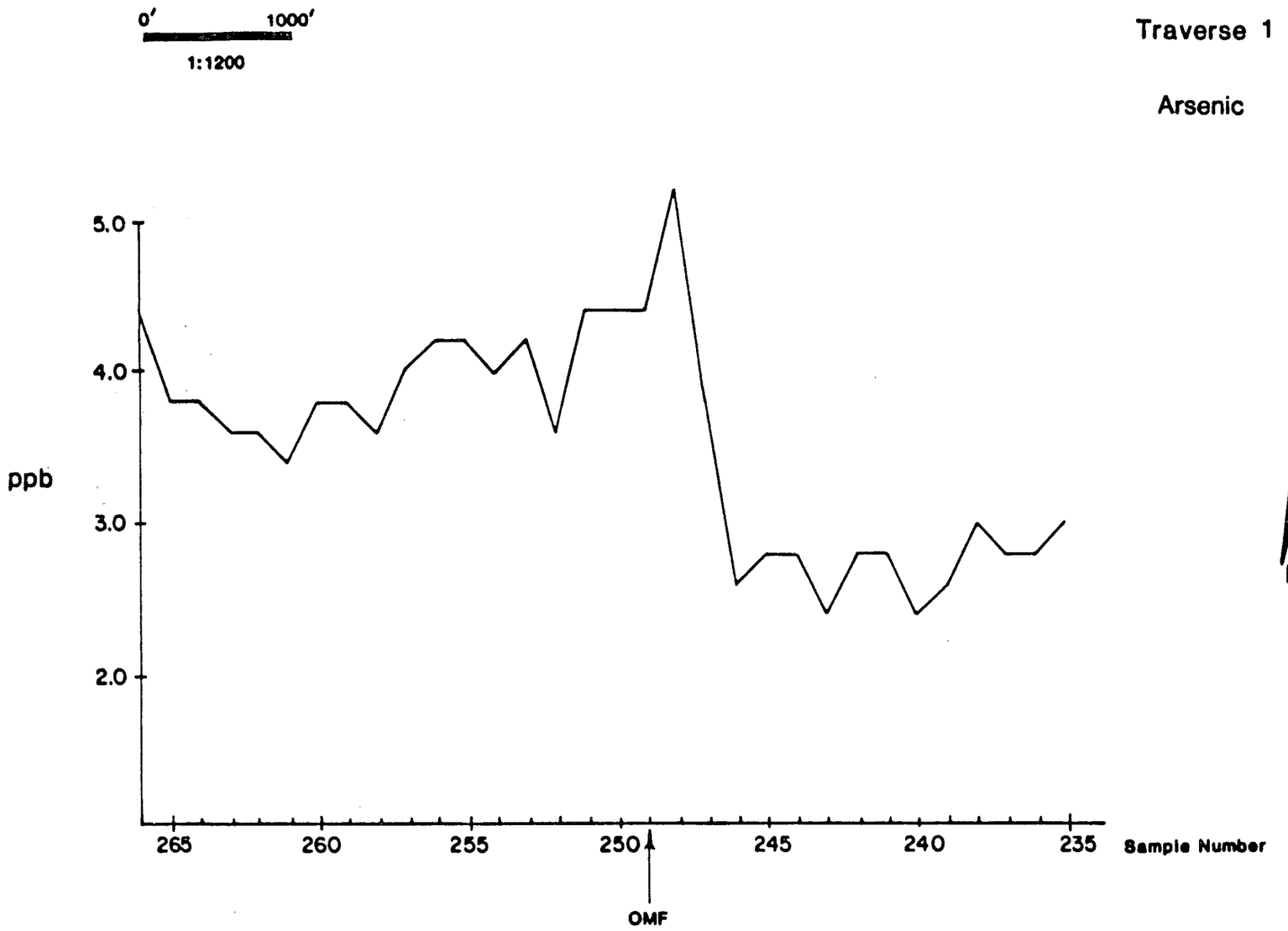

Figure 4 1

Traverse 2

Arsenic

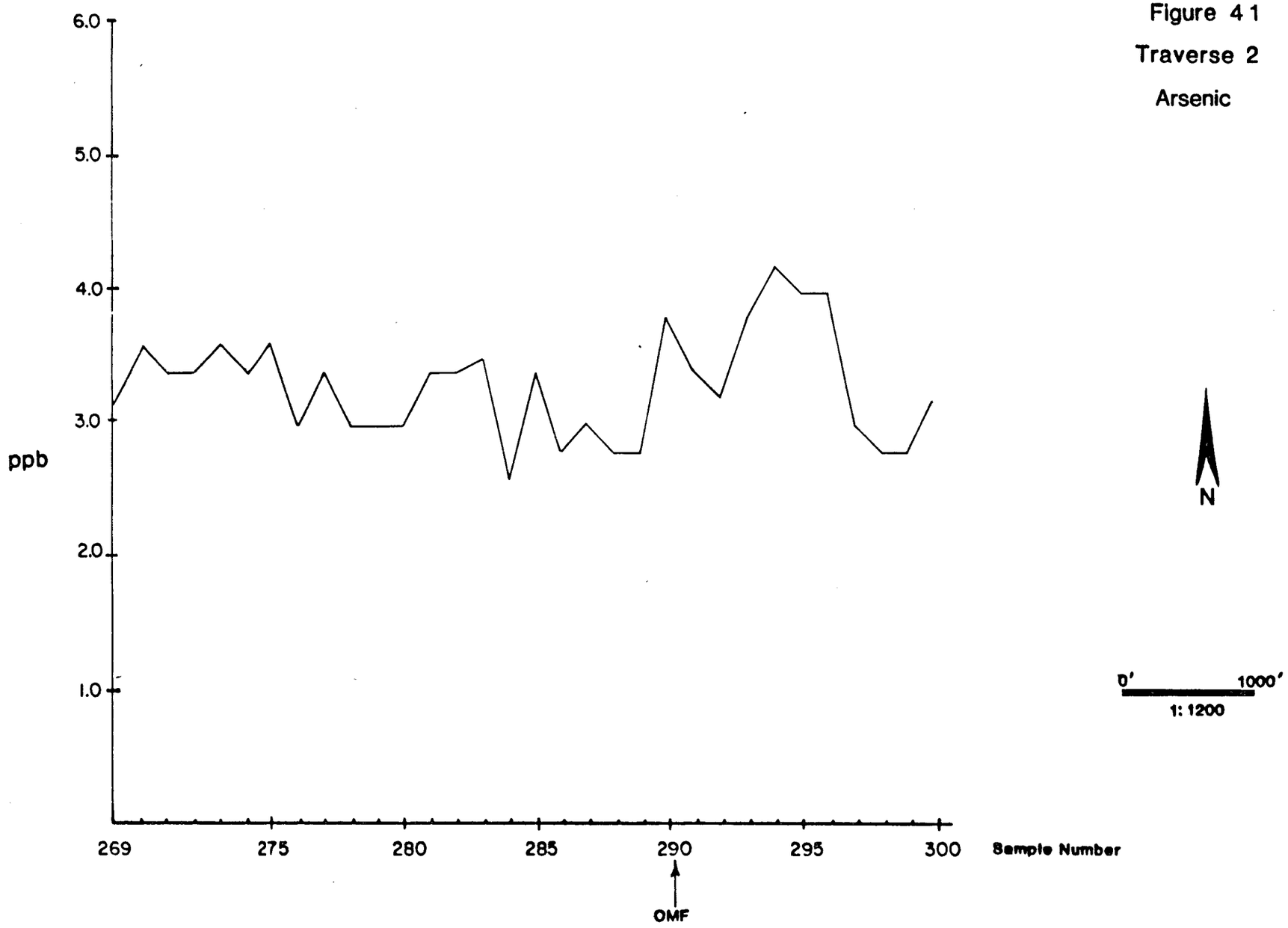

giving a threshold of 21.8 ppm Cs. However, these data include a group of highly anomalous samples collected in the selective sampling on closely spaced lines and these strongly and incorrectly contribute to the high value of the standard deviation in proportion to the mean. If the data from the traverses are removed from the remainder of the results, then the mean drops to 6 ppm Cs, the standard deviation to 4.5 ppm Cs and the threshold to 15 ppm Cs.

The cesium data shows a good correlation with antimony and a moderate correlation with arsenic, both of which may be considered to be geothermal indicators. There is also a moderate correlation with the alkaline metals lithium and calcium.

The principal feature of the cesium data (Figure 42) has been generated by a group of anomalous samples in the northwest corner of the survey area. The anomaly is derived from a contiguous group of four samples with a maximum value of 86 ppm. The anomaly may, therefore, be accepted with considerable confidence as genuine. The anomaly lies at the intersection of the Salt Cove Fault with the strong north-south fault N3 (Figure 10). The second strongest anomaly in the area is to be found some 3½ miles to the southeast, also overlying the Salt Cove Fault.

The geothermal area has a good expression in these data. There is a low contrast anomaly at the intersection of the Negro Mag Wash Fault and the Opal Mound Fault. This is close to Phillips well 54-3 rated "best well" and at the center of the heat-flow anomaly. The sample came from the Negro Mag Wash, and there is no evidence of macroscopic geothermal alteration or deposition in this area. There is a second, more intense, single sample anomaly, centered approximately 3/4 mile to the west of Opal Mound. This is close to the area that was shown to be hot but with a small flow and low permeability by Phillips well 9-1. Beyond these anomalous areas the cesium data is extremely quiet.

Detailed Surface Microlayer Traverses

Soil traverse #2 includes a large proportion of samples that contain highly anomalous concentrations of cesium. Therefore, for the purpose of calculating the background and threshold values, the two traverses have been treated independently. Viewed in this manner, traverse #1 has two low contrast anomalies on either side of the Opal Mound fault (Figure 43). A single, extremely low

325000 330000 335000 340000 345000 347033

R 10 W R 9 W R 8 W

4271638 4270000 4265000 4260000 4255000 4252000

T 26 S T 27 S T 28 S

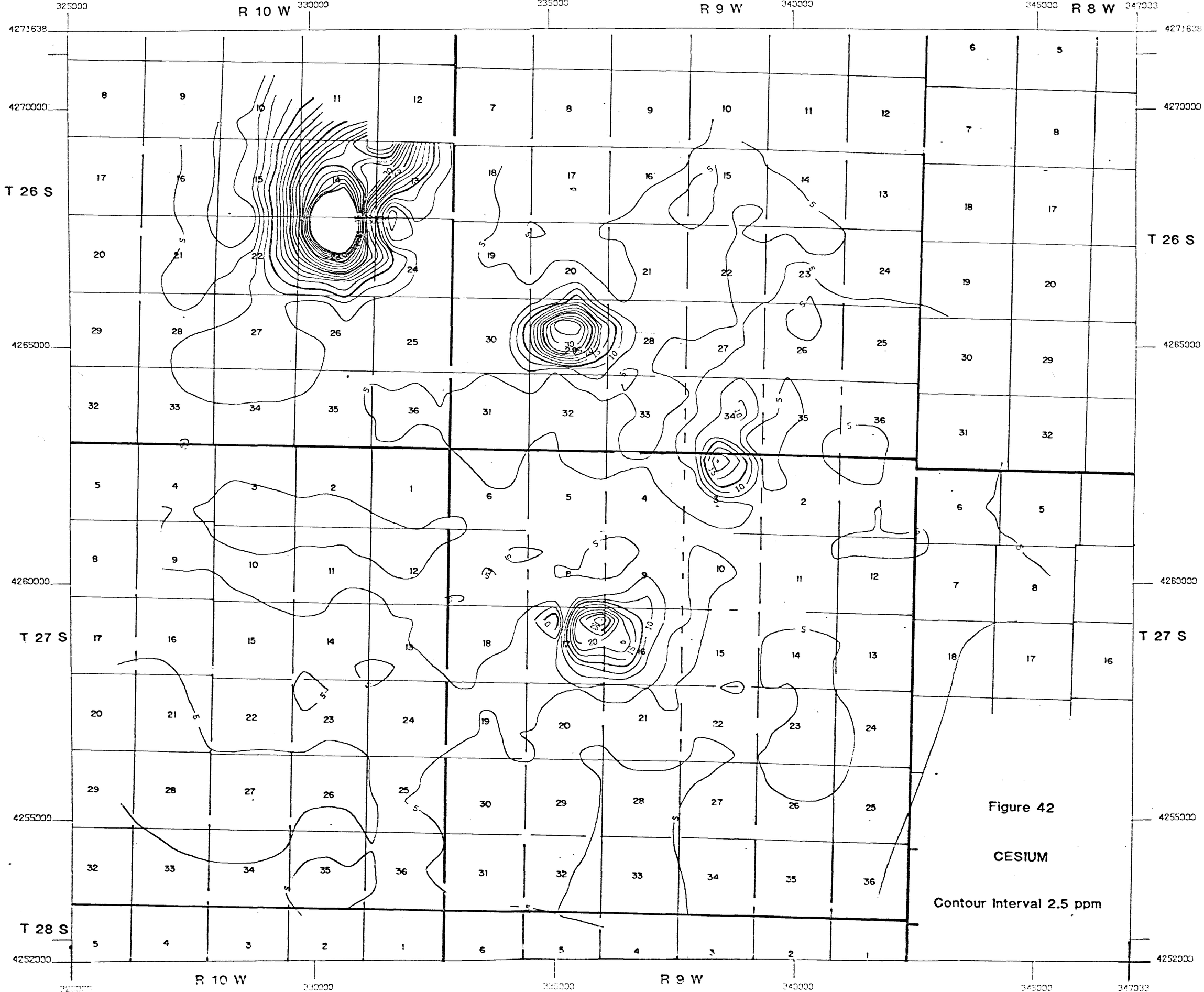

Figure 42

CESIUM

Contour Interval 2.5 ppm

Figure 43

Traverse 1

Cesium

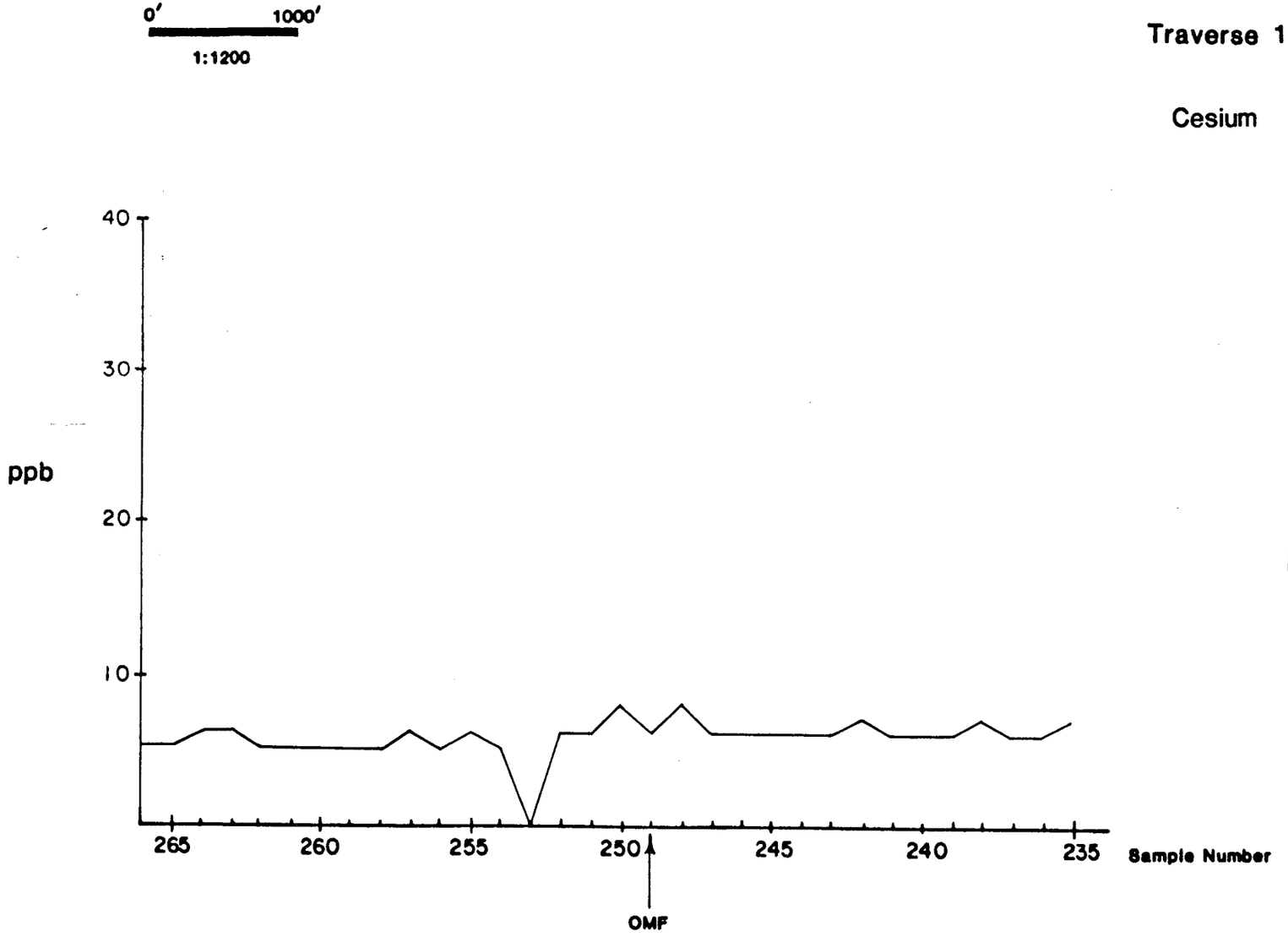

value in a sample collected some 600 ft. to the west of the fault can probably be ascribed to analytical error, as this result is outstandingly different from the remainder of the entire sample set.

The second traverse (Figure 44) shows a very highly anomalous set of samples extending 300 ft. to the west and at least 1300 ft. to the east of the Opal Mound Fault. The maximum value is 48 ppm Cs, giving a very high contrast on both a local and a regional scale. This traverse extends across the southern extension of the Opal Mound, but the anomaly extends well beyond the area of visible opaline cement or opal fragments.

Conclusions

Cesium appears to offer promise as one of the most useful elements for geochemical, geothermal exploration. This is strongly supported by the extremely quiet background and the high contrast which in effect gives two very distinct populations.

However, the usefulness of this element could only be confirmed or denied by exploration along the Salt Cove Fault. If a geothermal resource were proven in this area, then it would strongly support the widespread determination of this element in the surface microlayer as a regional exploration tool.

ANTIMONY

Surface Microlayer Grid Data

The antimony data for this area are, generally, extremely quiet and apart from 6 samples the concentration of antimony in all the soils are uniformly 0.2 ppm or less. This concentration is low for an average soil (Rose et al., 1979), but can probably be ascribed to the poorly developed nature of the soils in the Escalante Desert. The six samples showing higher concentrations have produced four geochemical anomalies within the contoured data (Figure 45). A small apparent anomaly in the west-southwest of the survey area is an artifact of the computer contouring. Antimony shows little correlation with the other elements determined during this program, with the single exception of cesium with which the correlation is moderately strong. There is a weak to moderate negative correlation with sodium and aluminum.

Figure 44

Traverse 2

Cesium

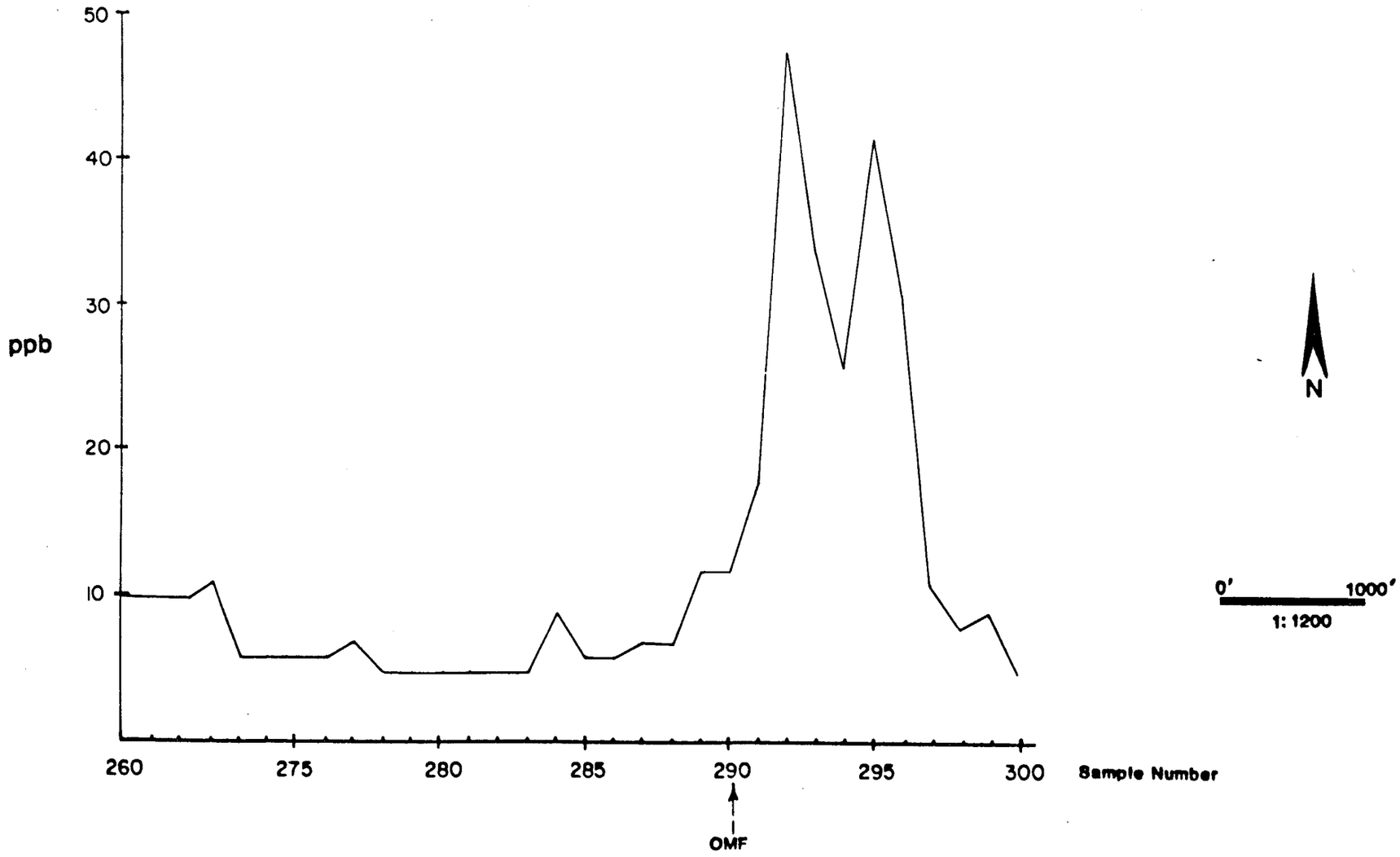

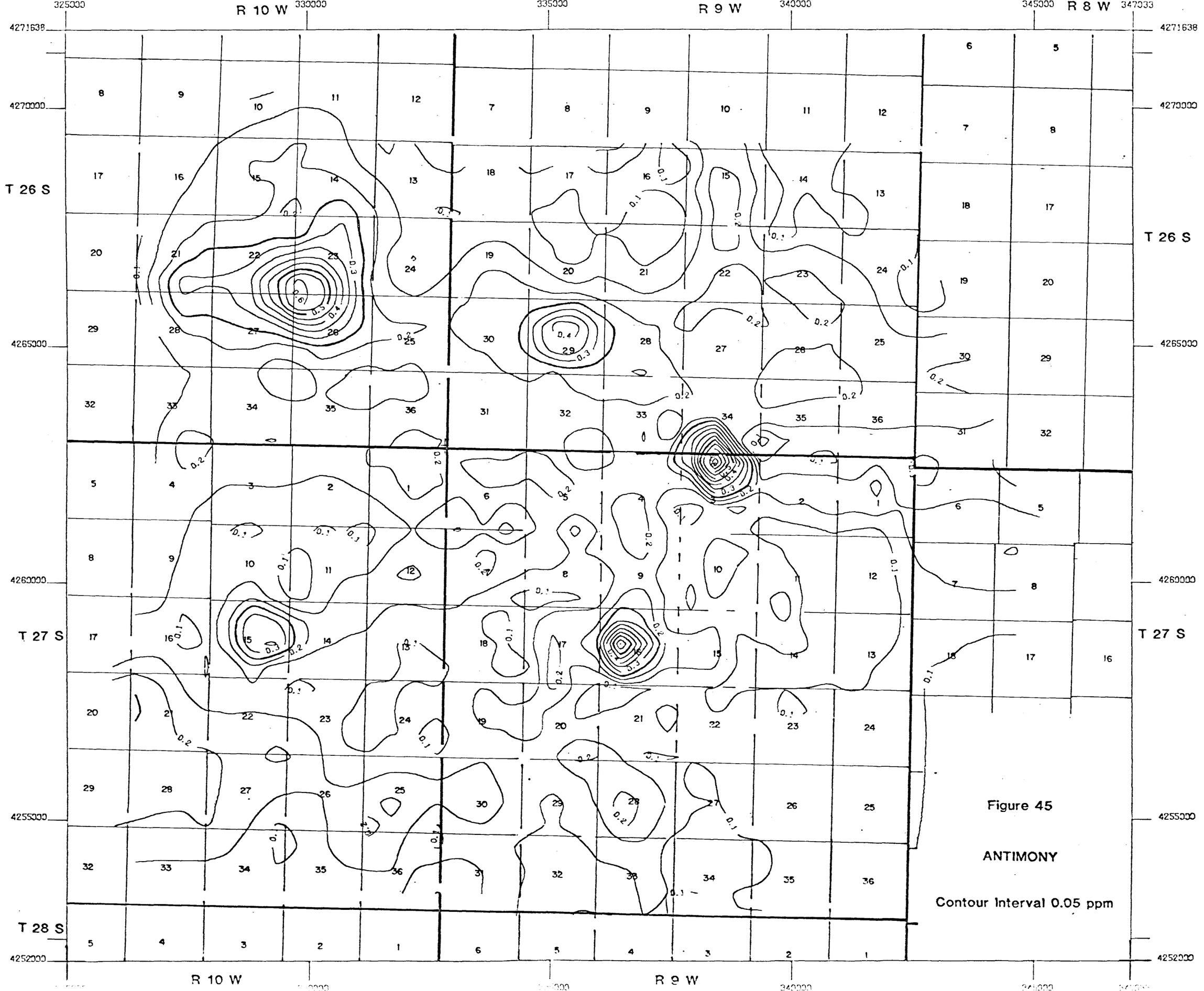
325000
R 10 W
330000
335000
R 9 W
340000
345000
R 8 W
347033
4271638
4270000
4265000
4260000
4255000
4252000
T 26 S
T 27 S
T 28 S
Figure 45
ANTIMONY
Contour Interval 0.05 ppm

Of the four genuine antimony soil anomalies on the contoured data, the largest lies in the northwest corner of the survey. This is due to a single sample, but it lies within an area that has been shown to be geochemically active in a number of elements. The anomaly lies at the intersection of the extension of Negro Mag Wash Fault, and the north-south fault N-3. A second anomaly lies some 3½ miles to the east-southeast and is again due to a single sample. This anomaly occurs on the westward projection of the Salt Cove Fault in an area where it intersects a number of east-west en echelon fractures.

A strong, two sample anomaly is to be found at the intersection of Negro Mag Wash Fault and Opal Mound Fault. The samples were collected from the bottom of Negro Mag Wash and no visible evidence of geothermal deposition was seen during the sampling. This is the area of maximum heat flow and high hot water production.

The final contoured anomaly lies at the southern end of the Opal Mound and has been generated by the high values in the center of the detailed soil traverse #2.

Detailed Surface Microlayer Traverses

The position of the Opal Mound Fault has been only indicated by the antimony data on traverse #2 (Figure 46). On this traverse, there is an anomaly 1000 ft. long extending mainly to the west of the fault trace. The anomaly begins on, but is not confined to, the Opal Mound. The anomalous samples are not restricted to those with visible siliceous deposition or opal fragments.

Conclusions

It would appear that antimony may offer some promise as a useful element in geothermal exploration. This is made particularly true of an environment such as this, where the background values are both low and quiet.

Bamford et al., (1980) report very strong enrichments of antimony in the opaline sinter and the overlying soils, and in the manganese cemented alluvium. There is not a close correlation between the antimony concentrations recorded by the two surveys. This may be ascribed to either the different sampling media or to different analytical laboratories.

Figure 46

Traverse 2

Antimony

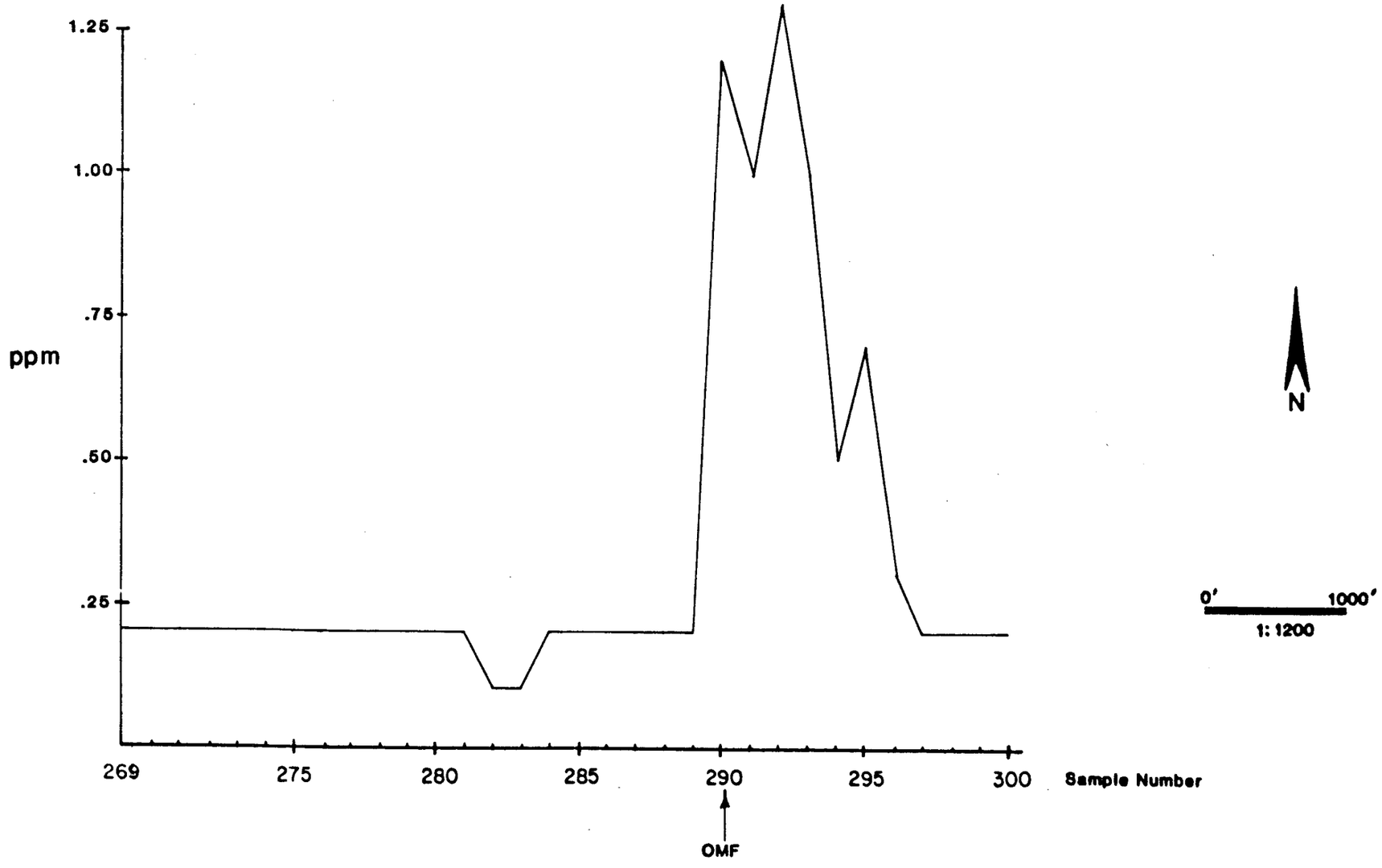

As with many other elements, however, the real evaluation of this metal in geothermal exploration depends very much on an investigation of the geothermal activity along the Salt Cove Fault and the region in the northwest corner of the survey area.

LITHIUM

Surface Microlayer Grid Data

The most prominent feature of the contoured lithium data (Figure 47) is a 60 ppm anomaly which forms the southern end of a southwest-northeast trending anomalous zone across the northwestern corner of the survey area. This anomalous zone and its trend do not conform to any known structures or geothermal activity, but the anomalous area includes 5 samples with values greater than the threshold value of 40 ppm Li.

Lithium has a strong correlation with rubidium and a moderate correlation with cesium, copper, beryllium, calcium, magnesium, lead and manganese. There is a moderately strong negative correlation with silica. This suggests that the anomaly is probably due to the alkaline conditions created by the drainage in this area.

The remainder of the area is geochemically quiet in lithium and there is no indication of the geothermal area.

Detailed Surface Microlayer Traverses

The position of the Opal Mound fault has not been indicated by the lithium data. Although the values on Traverse 1 tend to be higher near the fault, the concentrations are not greater than the local threshold of 35 ppm Li (Figure 48).

Conclusions

Considering the acidic nature of the country rocks at Roosevelt Springs and the high concentrations of lithium in the geothermal waters, it is surprising that lithium in surface soils does not provide a better guide to the position of the geothermal area.

However, Bamford et al., (1980) note that lithium tends to be concentrated in the rocks and soils of the hydrothermally altered areas and in the self-sealed zones. Furthermore, although they

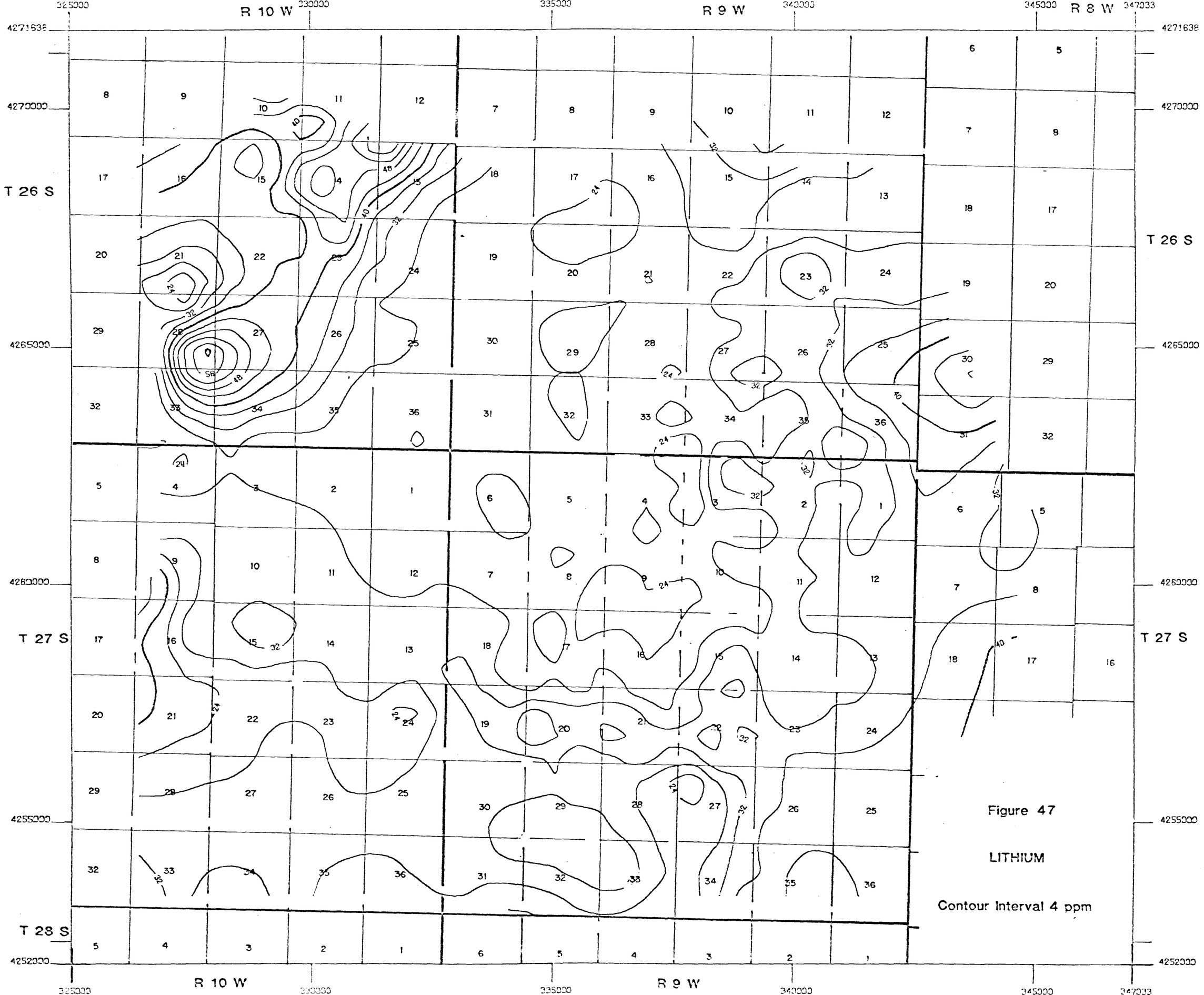

Figure 47

LITHIUM

Contour Interval 4 ppm

Figure 48

Traverse 1

Lithium

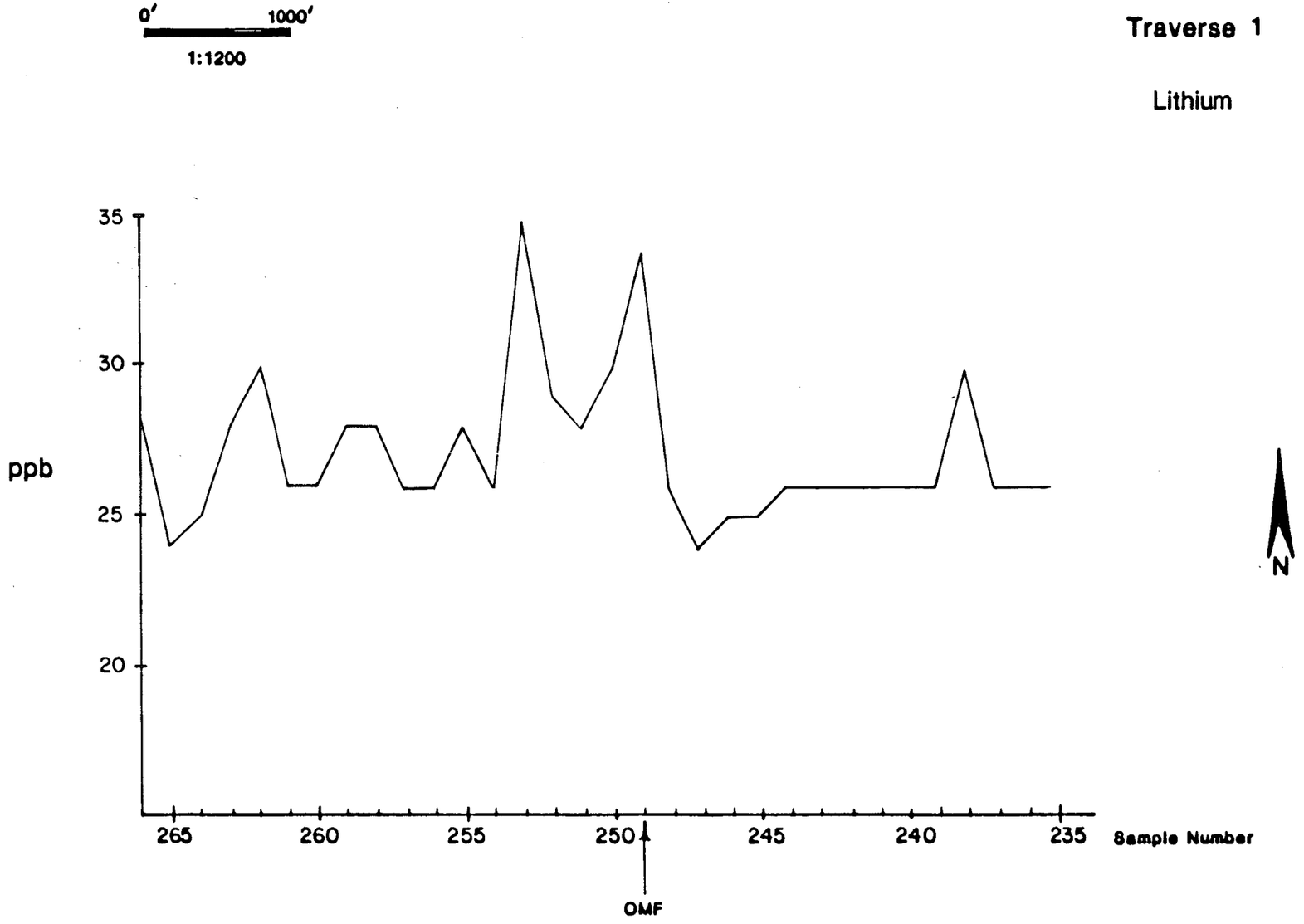

were able to demonstrate that lithium was strongly enriched in the sinter of the Opal Mound, the concentrations in the overlying soils were strictly background.

Lithium would not, therefore, appear to be useful in this area in geothermal exploration.

SELENIUM

Surface Microlayer Grid Data

The general tenor of the selenium values in this area is low with a background concentration of 0.07 ppm Se (Table 7). This reflects the poorly developed, inorganic nature of the soils. In this area values above 0.13 ppm Se may be regarded as anomalous.

The only feature in these data which, therefore stands out above the background is a very well marked series of anomalies running ESE-WNW across the northern section of the survey area (Figure 49). This line of anomalous values can be traced from the extreme east of the area, where the samples were collected within the Mineral Mountains, into the extreme northwest corner. This trend coincides with and overlies the trace of the Salt Cove fault and the more consistent, higher values in the area where this fault interects the north-south fault N3.

Within the Mineral Mountains anomalous values appear to be associated with areas of Tertiary intrusives, but are not related to any particular rock type. The Roosevelt Springs KGRA has not been delineated by the selenium data.

Detailed Surface Microlayer Traverses

The position of the Opal Mound fault has no expression in the selenium data.

Conclusions

The absence of any indication of the position of the known area of geothermal activity in the selenium data is disappointing. However, a true evaluation of the usefulness of this element must await the exploration of the Salt Cove fault area.

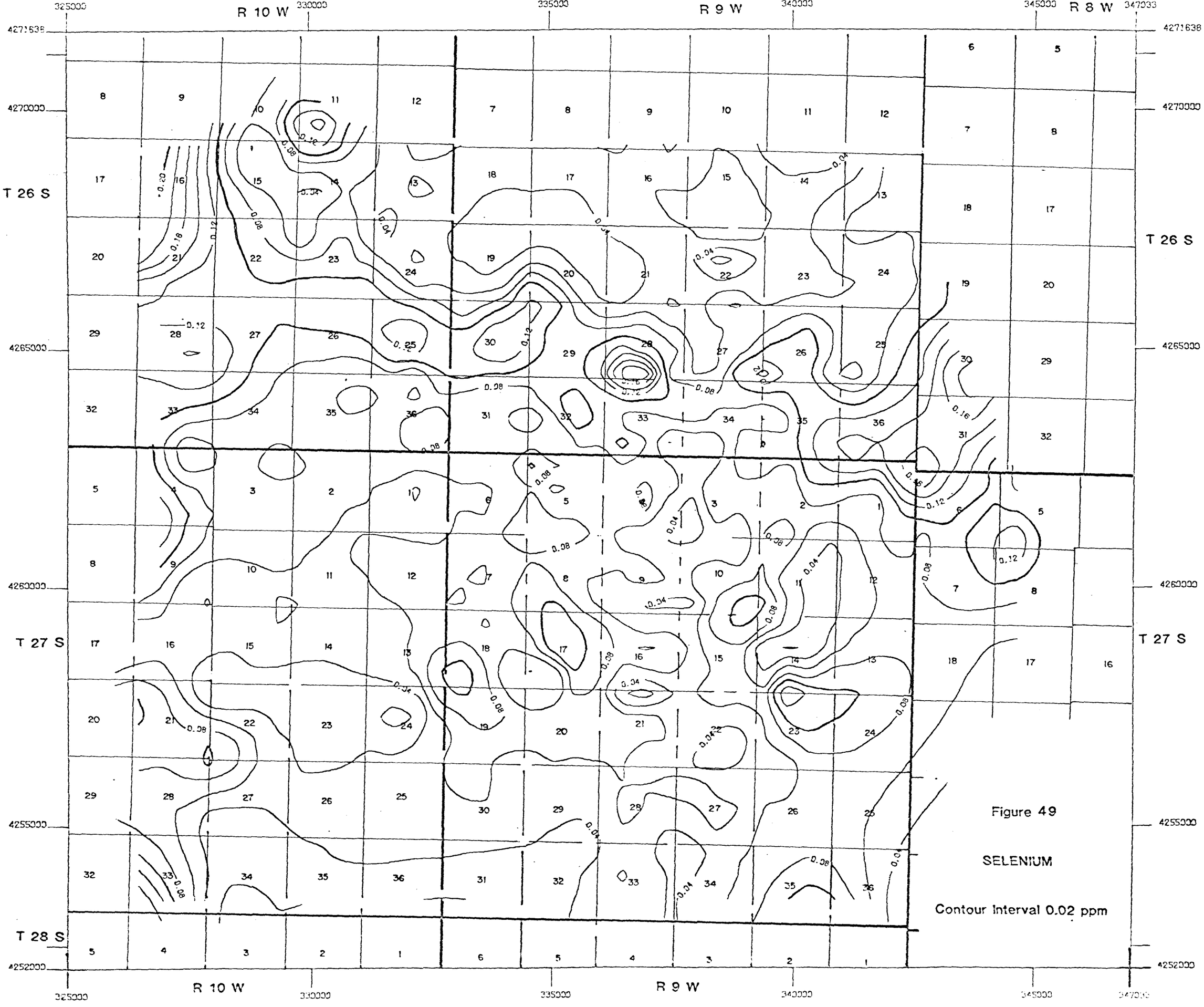
R 10 W
R 9 W
R 8 W
T 26 S
T 27 S
T 28 S
325000
330000
335000
340000
345000
347033
4271638
4270000
4265000
4260000
4255000
4252000
Figure 49
SELENIUM
Contour Interval 0.02 ppm

RUBIDIUM

Surface Microlayer Grid Data

The rubidium soil data (Figure 50) contains no expression of the geothermal area. In fact the area of greatest geothermal activity is shown to be low in rubidium. Anomalous areas in the Mineral Mountains appear to be associated with acidic Tertiary intrusive rocks.

To the west of the geothermal area there are anomalies lying to the north of the line of the Salt Cove fault but their significance is not clear. Within the Escalante Desert, there is no obvious association between areas that are anomalously high in rubidium and areas that contain a large proportion of granitic material in the surface microlayer.

Detailed Surface Microlayer Traverses

The rubidium data from the samples collected along the closely spaced sample lines do not indicate the position of the geothermal area.

Conclusions

Rubidium in the surface microlayer would not appear to have materially assisted in exploration. However, rubidium is a contributor to Factor 3 in the data processing which, in combination with the lithium and beryllium data, indicates that a geochemical low in these three elements occurs in the geothermal area.

BERYLLIUM

Surface Microlayer Grid Data

With a threshold concentration of 3.5 ppm Be, the only areas within the contoured data (Figure 51) that may be considered to be truly anomalous lie along the eastern edge of the survey area, within the Mineral Mountains, and along the southern margin. However, in comparison with the local, very quiet background which applies to the remainder of the area, there appears to be a localized anomaly centered over the intersection of the Opal Mound and Negro Mag Wash faults. This anomaly is lobate in shape and the contouring clearly indicates that it can be traced back along the trace of the Negro Mag Wash fault.

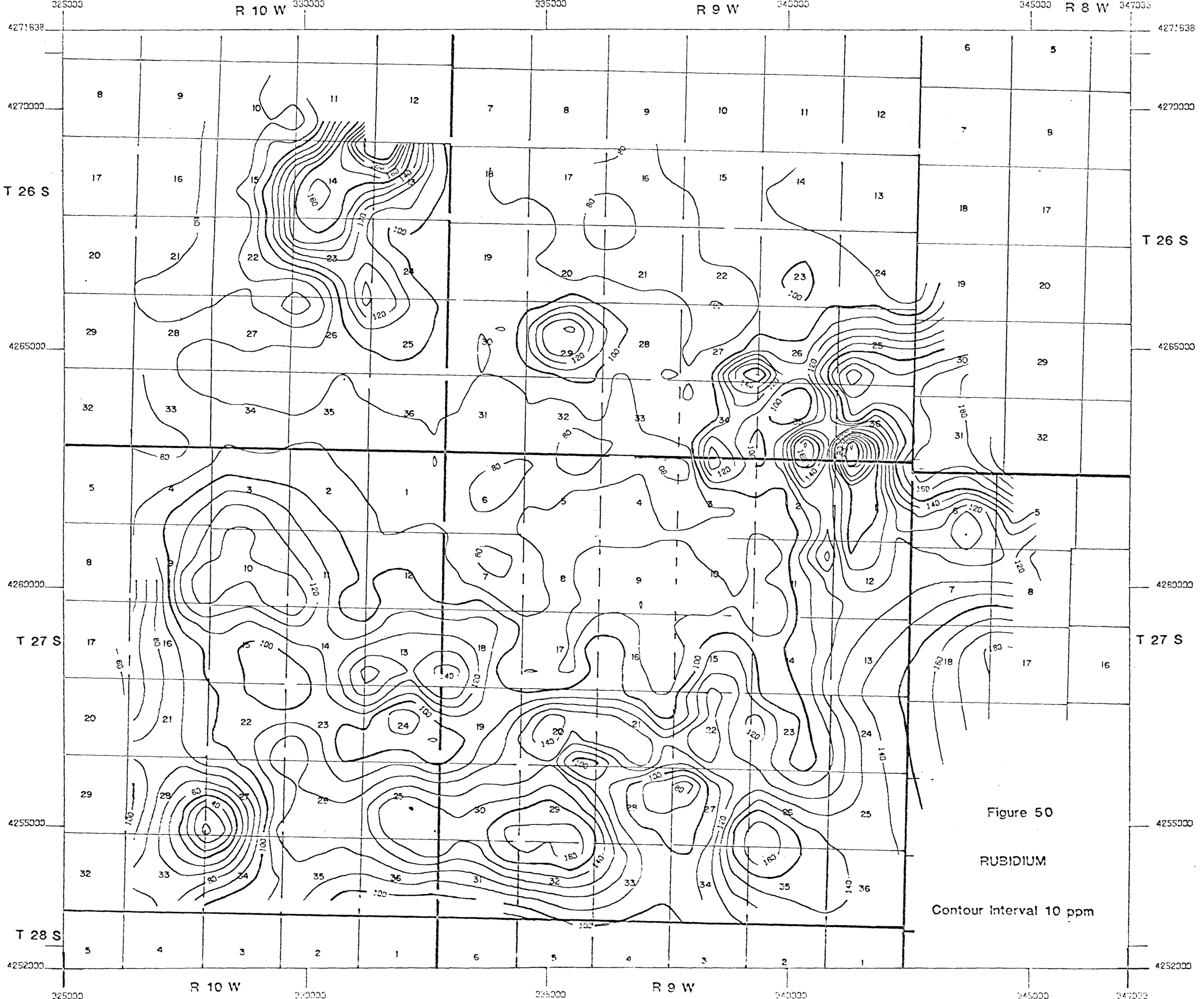

Figure 50

RUBIDIUM

Contour Interval 10 ppm

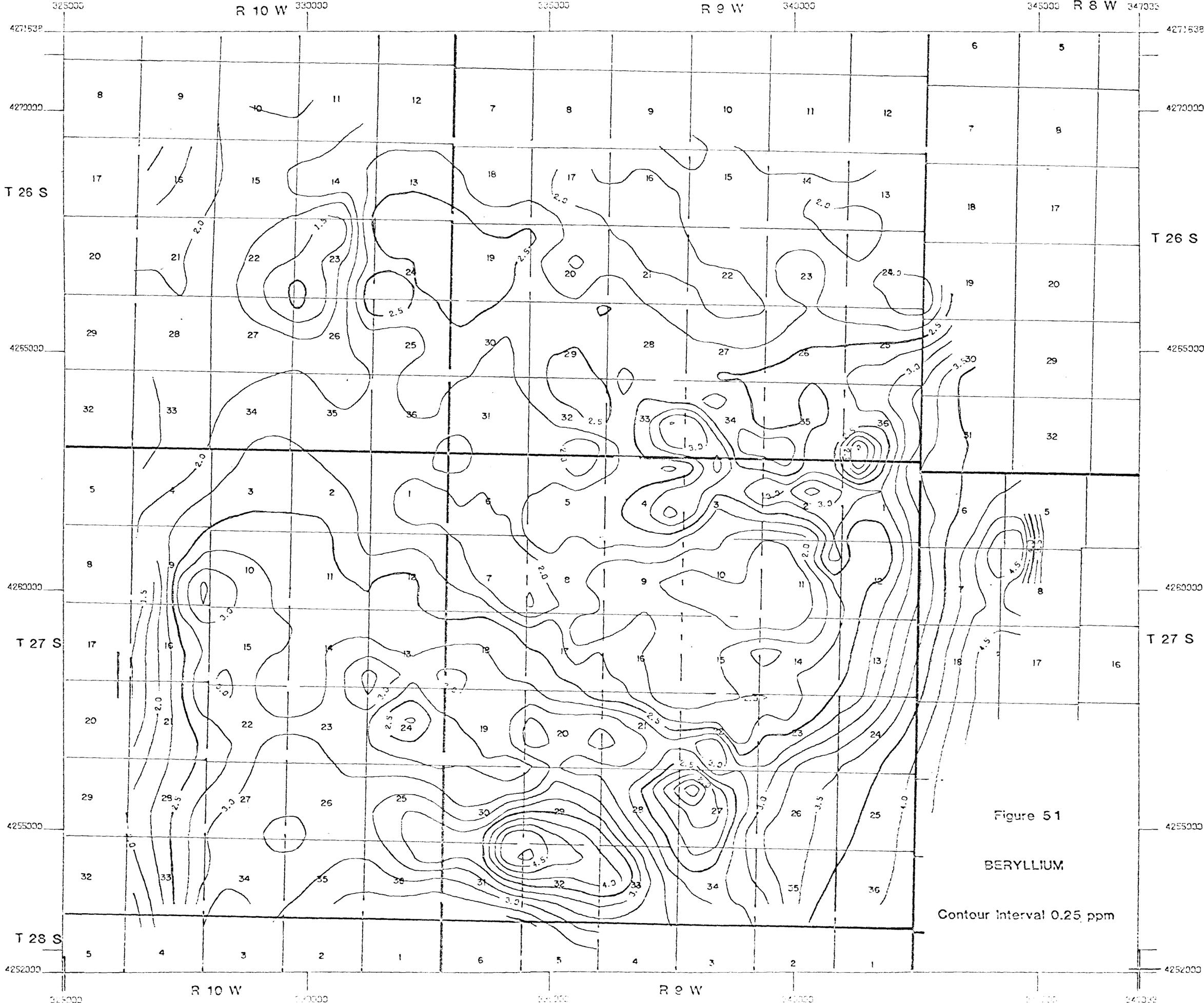
R 10 W
R 9 W
R 8 W
T 26 S
T 27 S
T 28 S
Figure 51
BERYLLIUM
Contour Interval 0.25 ppm

However, the fault also underlies the Negro Mag Wash itself, and the most probable explanation for this anomaly is that it is due to detrital minerals carried down the wash and dumped in the flat area at its mouth. The areas that are anomalous in beryllium within the Mineral Mountains appear to be closely associated with the rhyolite domes which, presumably, are the source of the beryllium rich detrital minerals.

Detailed Surface Microlayer Traverses

The detailed soil sampling has provided no indication of the geothermal area or the Opal Mound fault within the beryllium data.

Conclusions

Beryllium would not appear to have been a useful indicator of the geothermal activity in this area. Bamford et al., (1980) were able to detect highly anomalous concentrations of beryllium in the sinter of the Opal Dome, but this was not reflected in the overlying soils. Enhanced beryllium concentrations were also associated with an area of manganese cemented alluvium.

It seems probable that the extreme immobility of beryllium in the surface environment, limits its distribution within the soils.

OTHER ELEMENTS

The remaining non-anion parameters determined during this program do not, when considered individually, contribute meaningful information to the geothermal study area. However, the computer contoured maps for these elements are included as Figures 52-73.

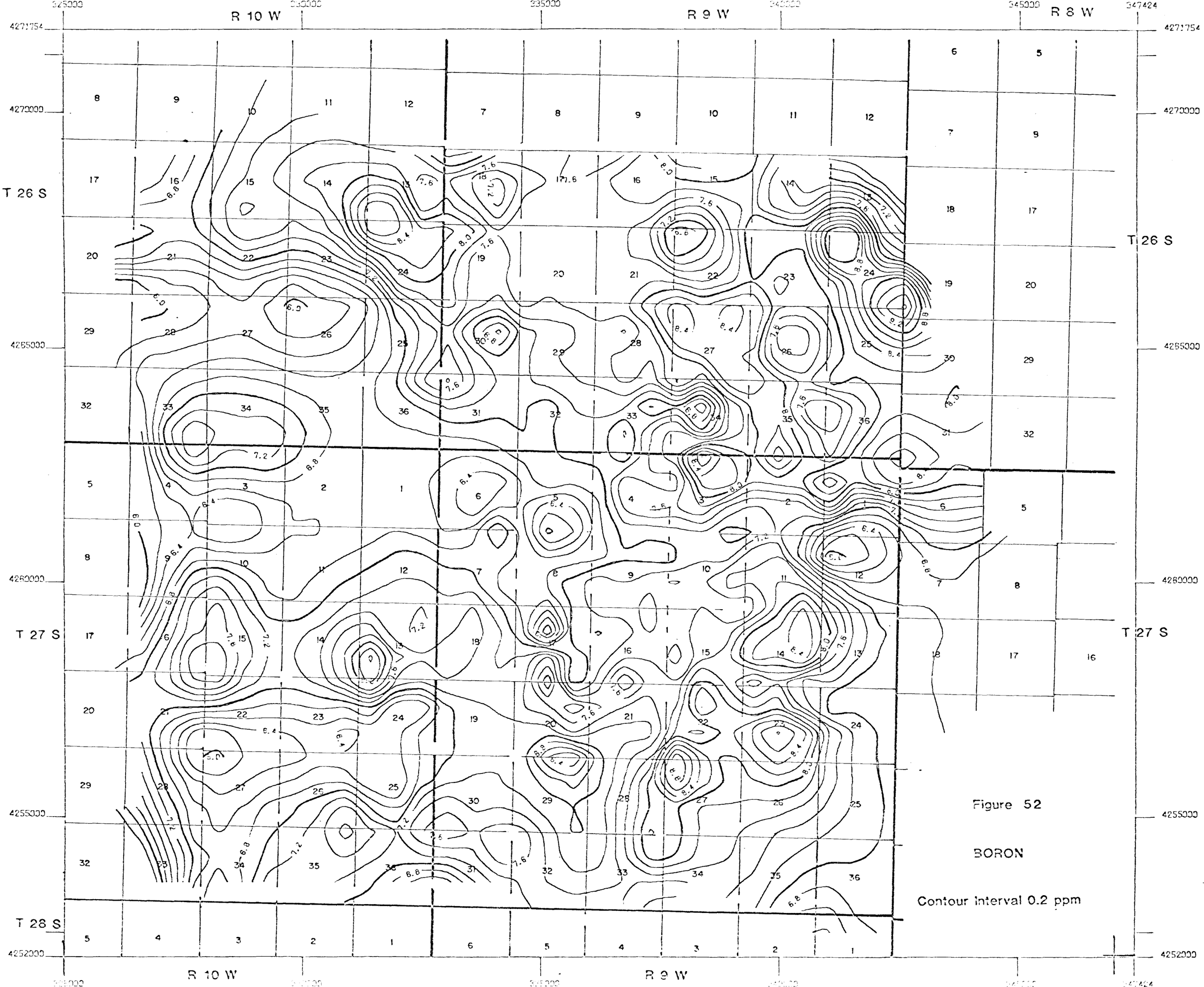

Figure 52

BORON

Contour interval 0.2 ppm

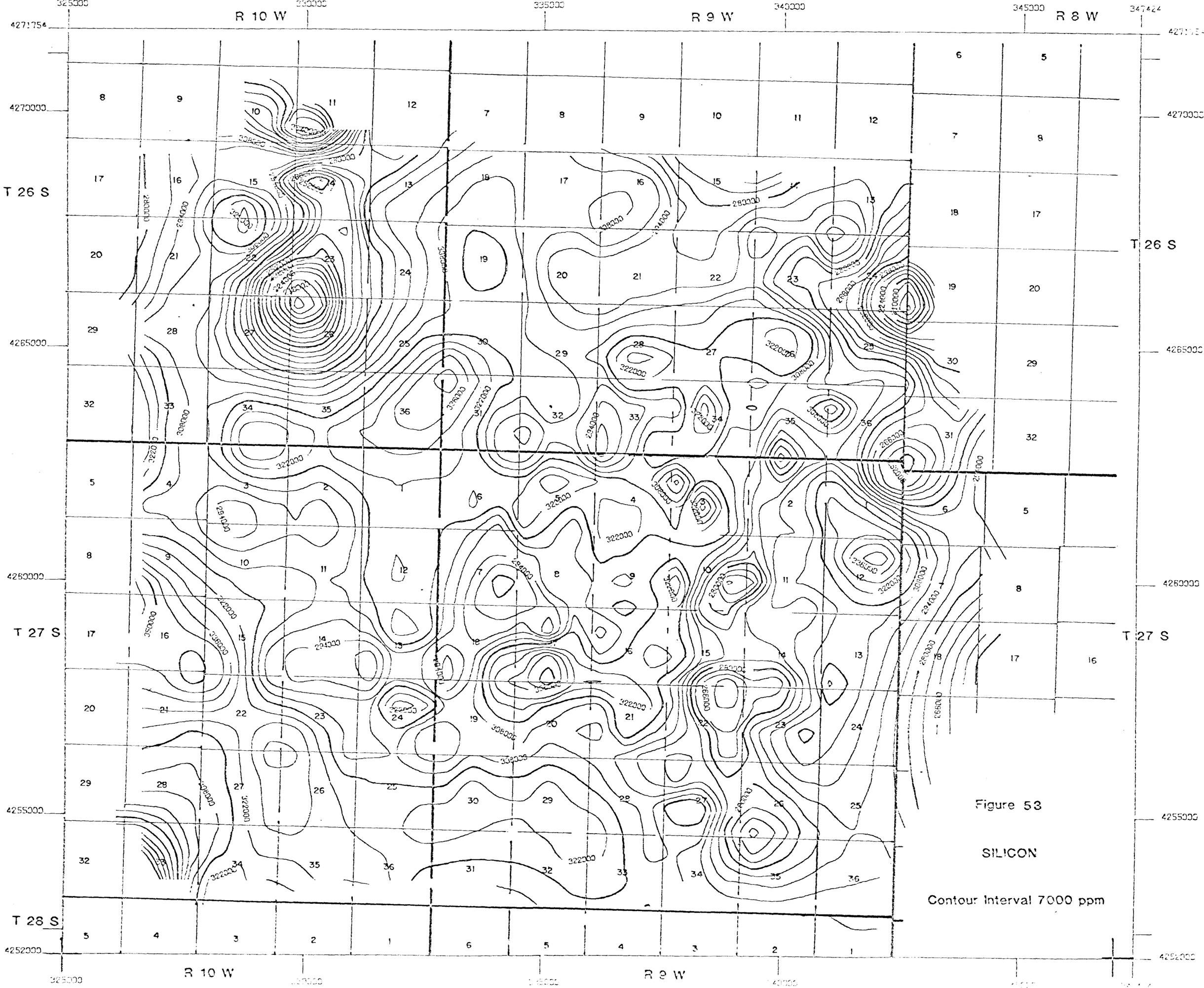

Figure 53

SILICON

Contour Interval 7000 ppm

R 10 W

R 9 W

R 8 W

T 26 S

T 27 S

T 28 S

Figure 54

ALUMINUM

Contour Interval 2500 ppm

R 10 W

R 9 W

R 8 W

T 26 S

T 27 S

T 28 S

Figure 55

POTASSIUM

Contour Interval 750 ppm

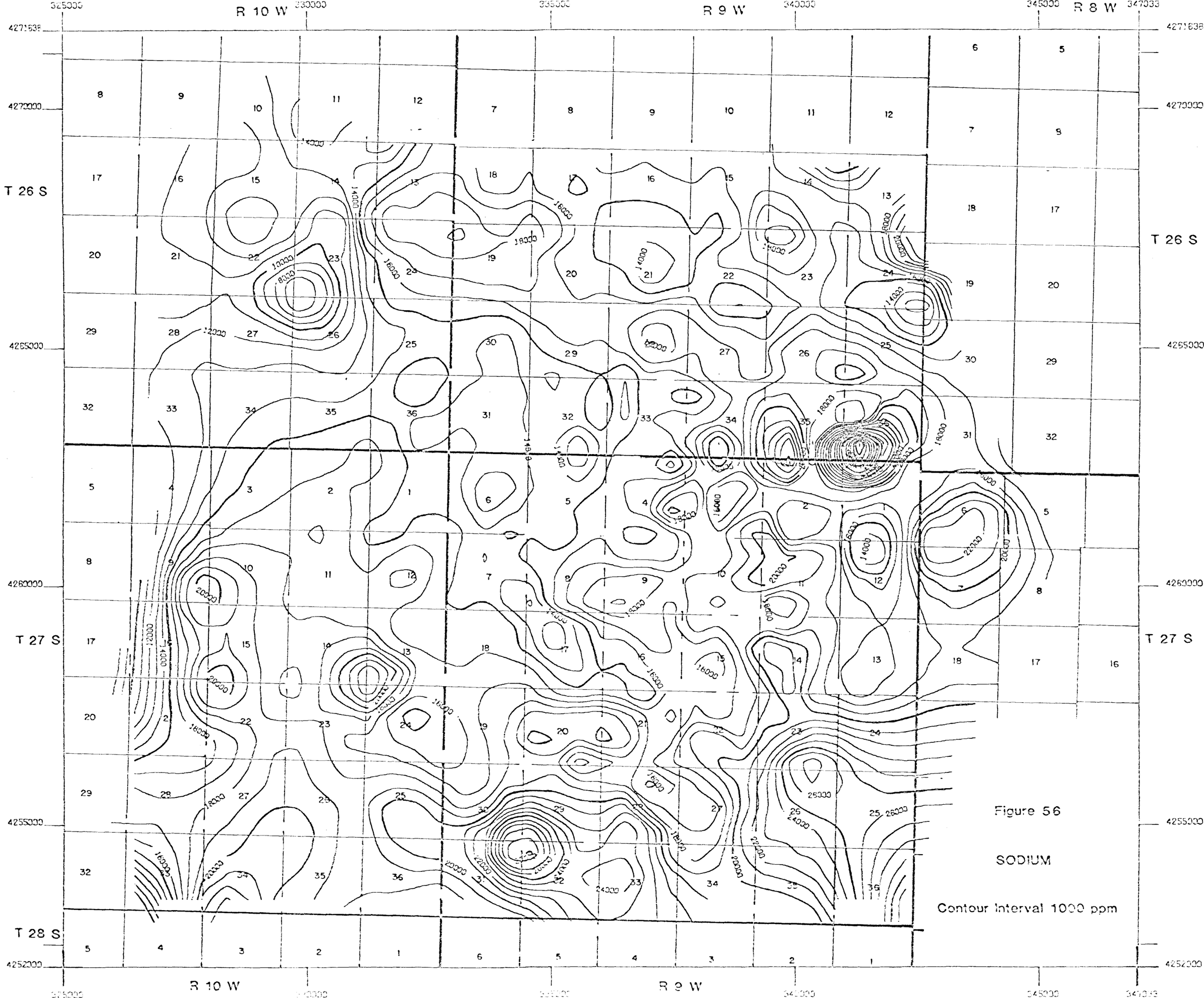

Figure 56

SODIUM

Contour Interval 1000 ppm

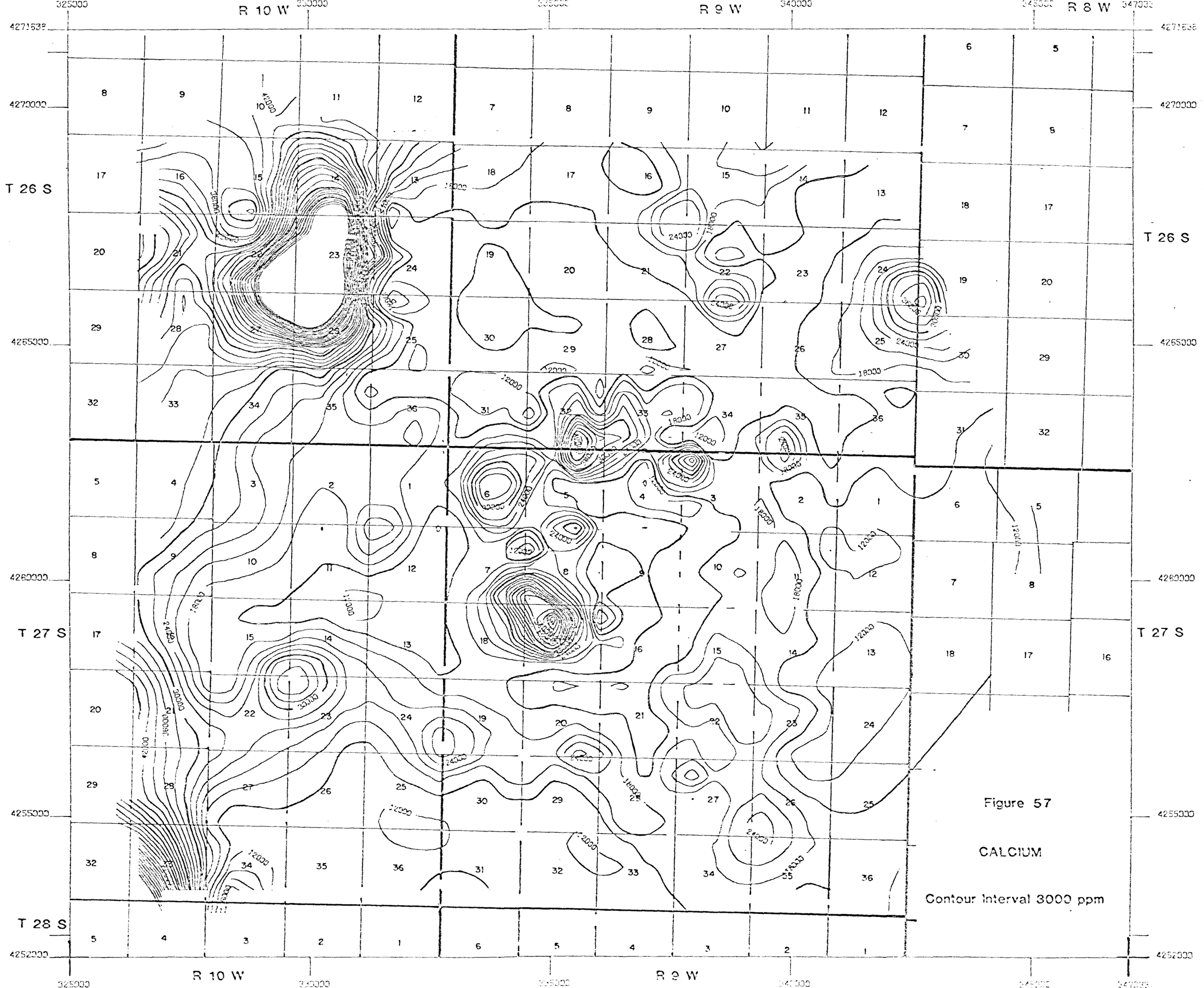

Figure 57

CALCIUM

Contour Interval 3000 ppm

R 10 W

R 9 W

R 8 W

T 26 S

T 27 S

T 28 S

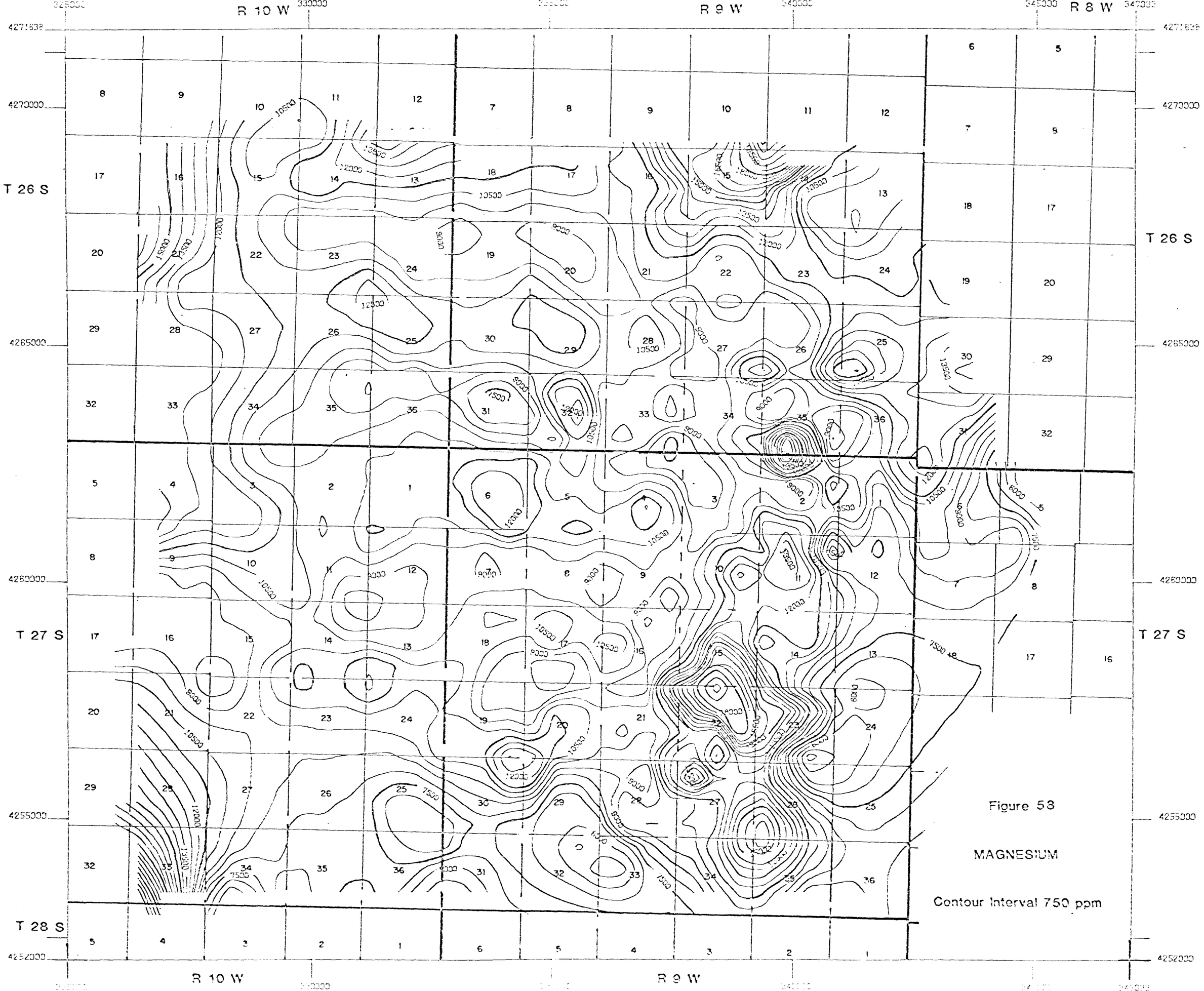

Figure 58

MAGNESIUM

Contour Interval 750 ppm

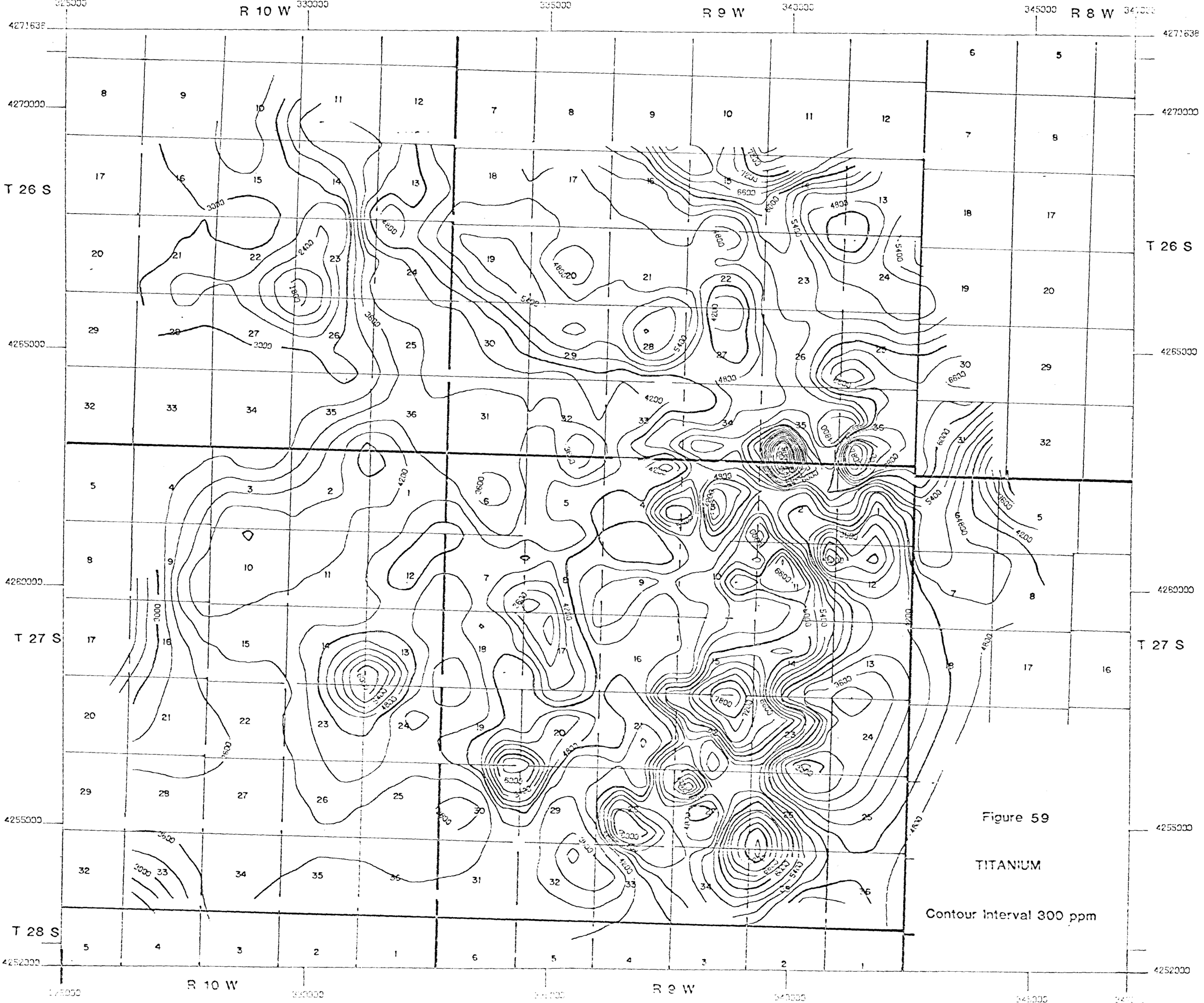
R 10 W
R 9 W
R 8 W
T 26 S
T 27 S
T 28 S
4271638
4270000
4265000
4260000
4255000
4252000
325000
330000
335000
340000
345000
Figure 59
TITANIUM
Contour Interval 300 ppm

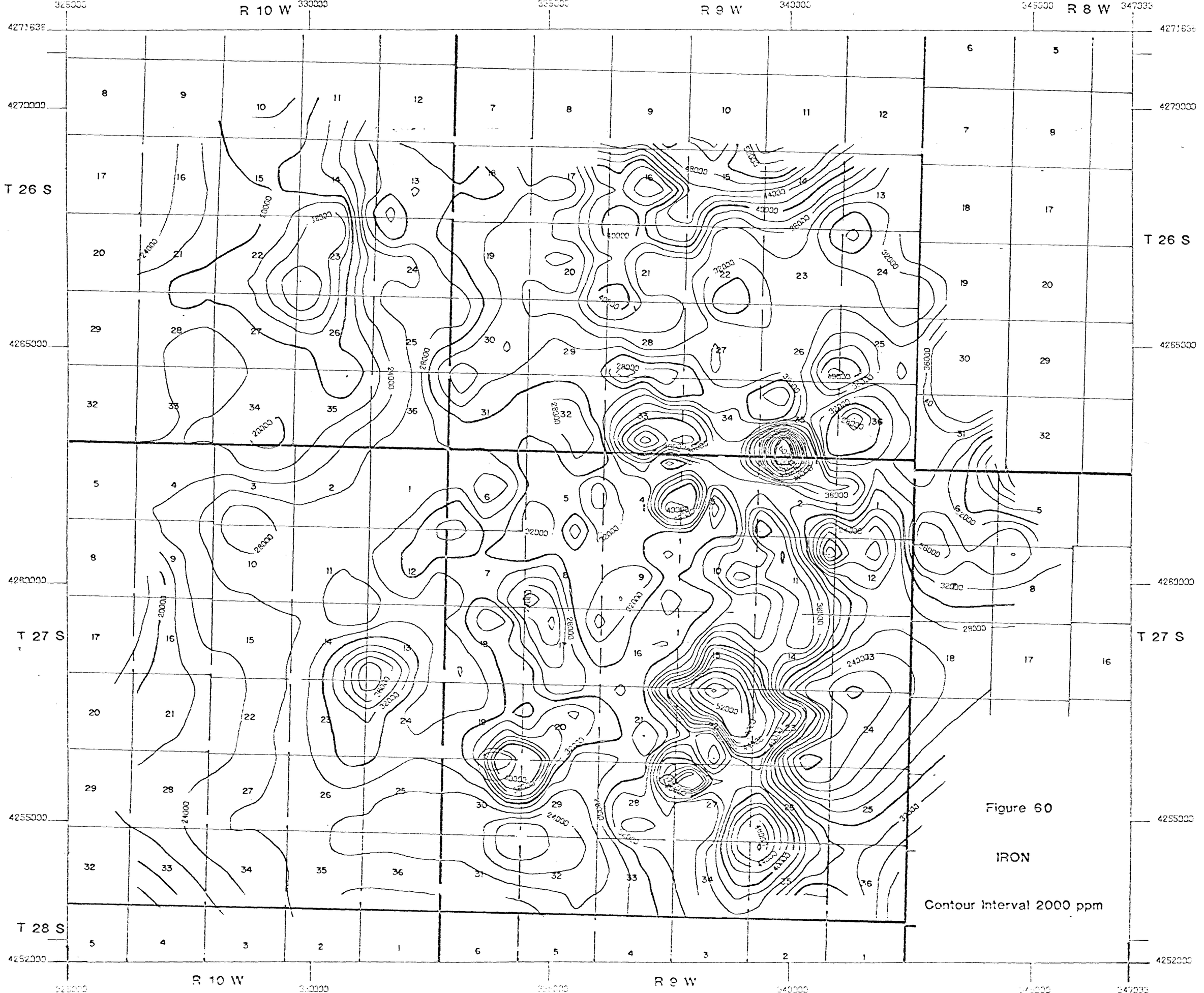

Figure 60

IRON

Contour Interval 2000 ppm

325000 R 10 W 330000 335000 R 9 W 340000 345000 R 8 W 347033

4271638 4270000 4265000 4260000 4255000 4252000

T 26 S T 27 S T 28 S

Figure 61

PHOSPHORUS

Contour Interval 100 ppm

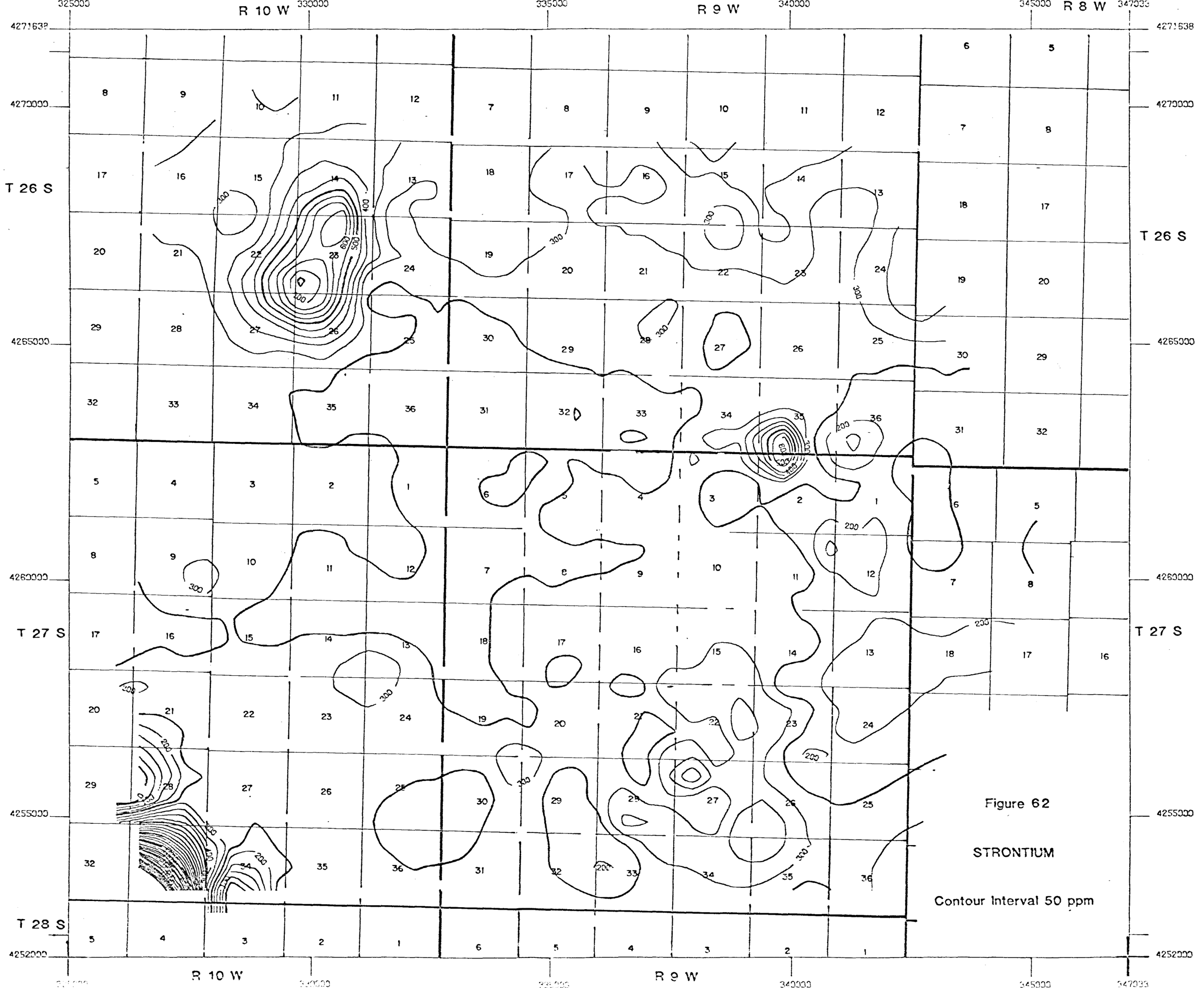
325000
R 10 W
330000
335000
R 9 W
340000
345000
R 8 W
347033
4271638
4271538
4270000
4265000
4260000
4255000
4252000
T 26 S
T 27 S
T 28 S
Figure 62
STRONTIUM
Contour Interval 50 ppm

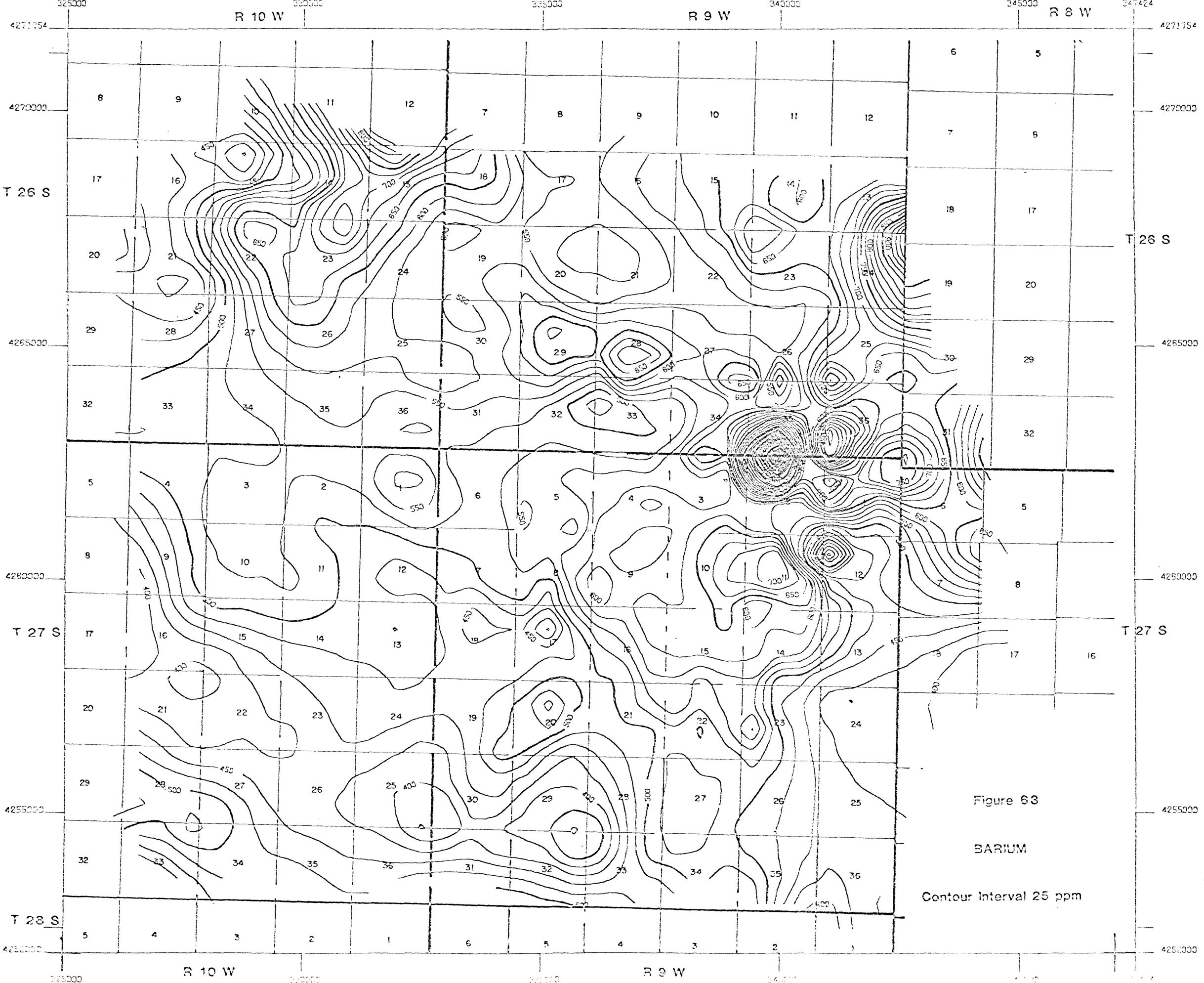

Figure 63

BARIUM

Contour Interval 25 ppm

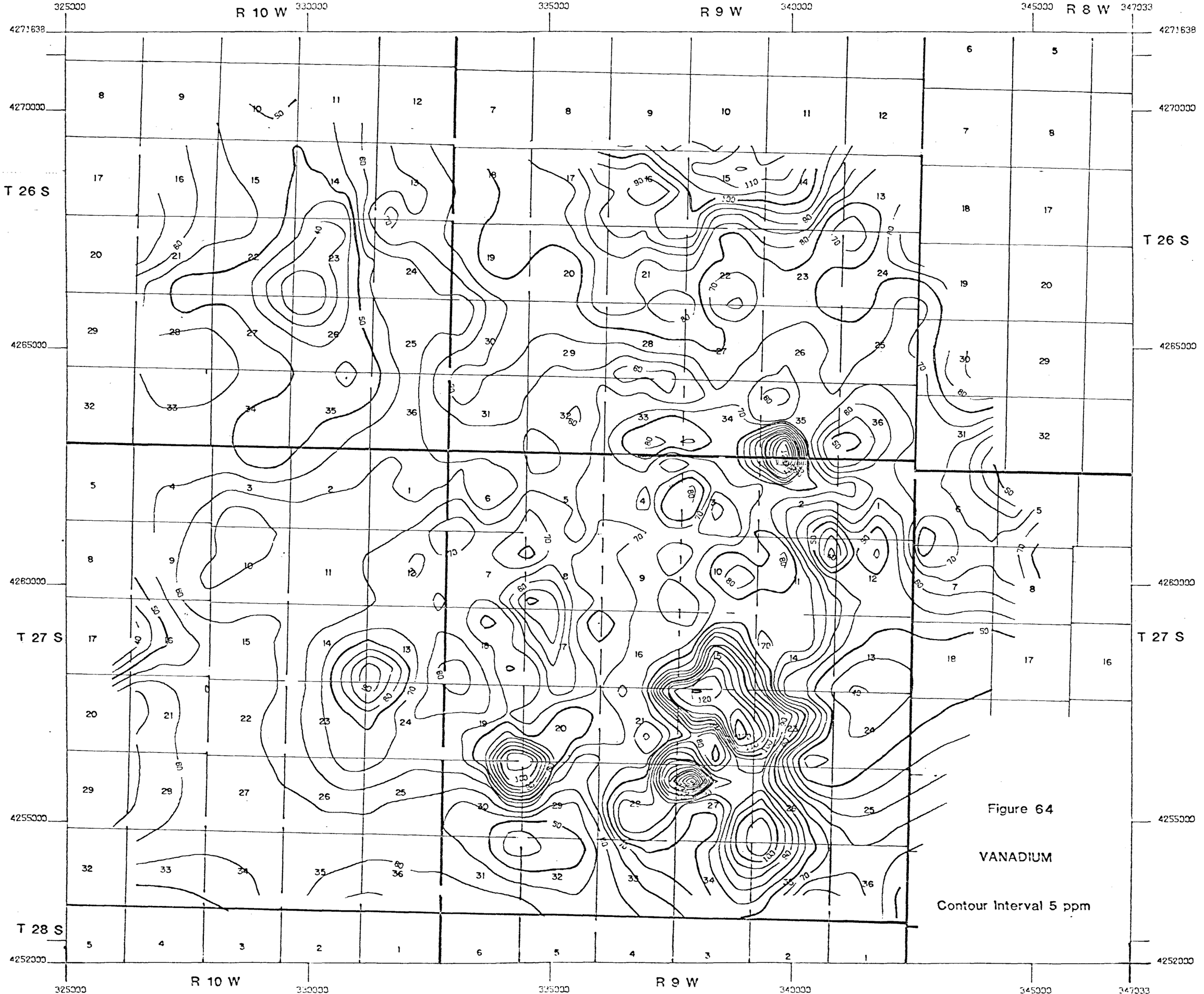

Figure 64

VANADIUM

Contour Interval 5 ppm

325000 R 10 W 330000 335000 R 9 W 340000 345000 R 8 W 347033

4271638 4270000 4265000 4260000 4255000 4252000

T 26 S T 27 S T 28 S

Figure 65

MANGANESE

Contour Interval 75 ppm

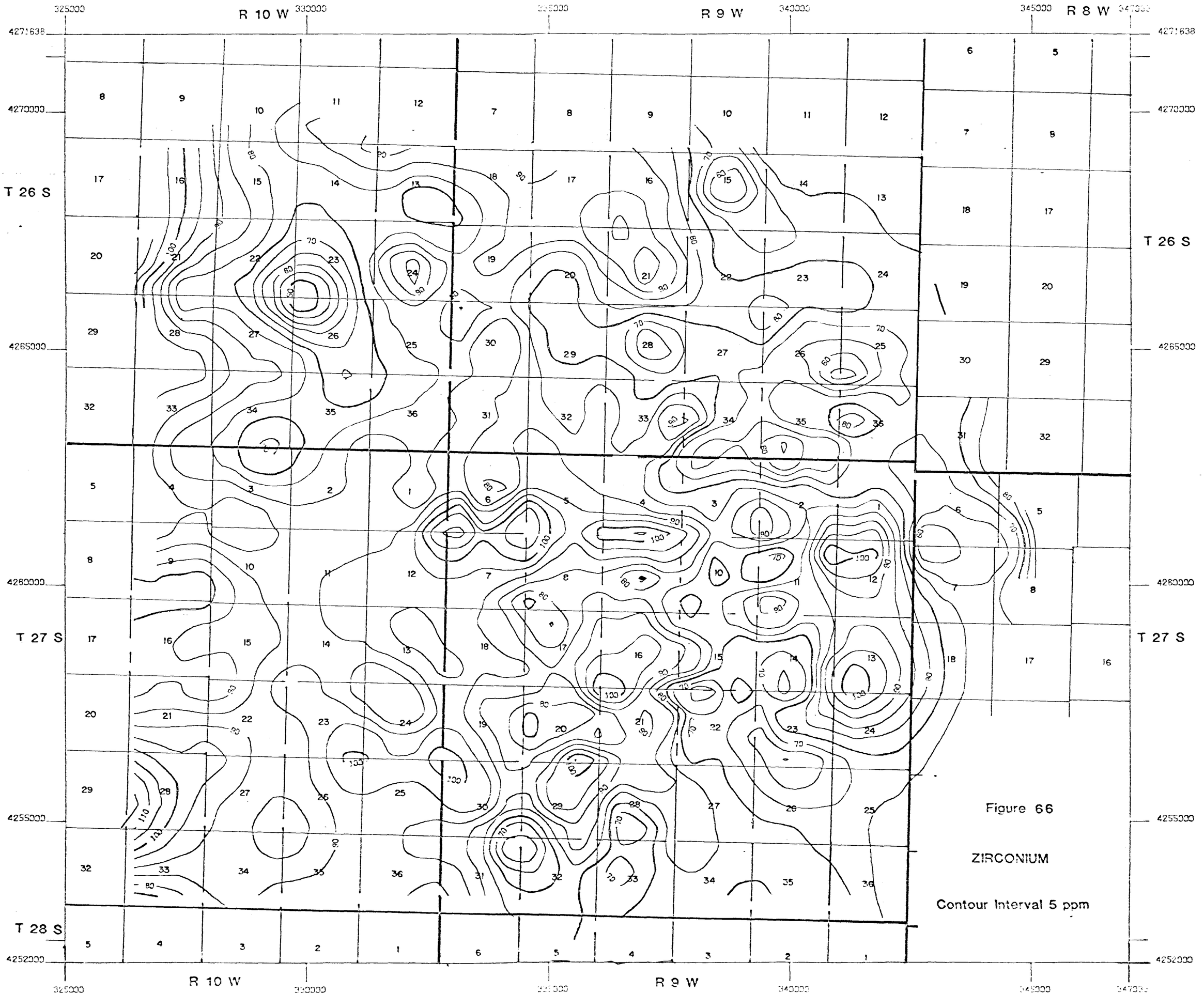

Figure 66

ZIRCONIUM

Contour Interval 5 ppm

325000 R 10 W 330000 335000 R 9 W 340000 345000 R 8 W 347033

4271638 4270000 4265000 4260000 4255000 4252000

T 26 S T 27 S T 28 S

Figure 67

CHROMIUM

Contour interval 10 ppm

325000 R 10 W 330000 335000 R 9 W 340000 345000 R 8 W 347000

4271636 4270000 4265000 4260000 4255000 4252000

T 26 S T 27 S T 28 S

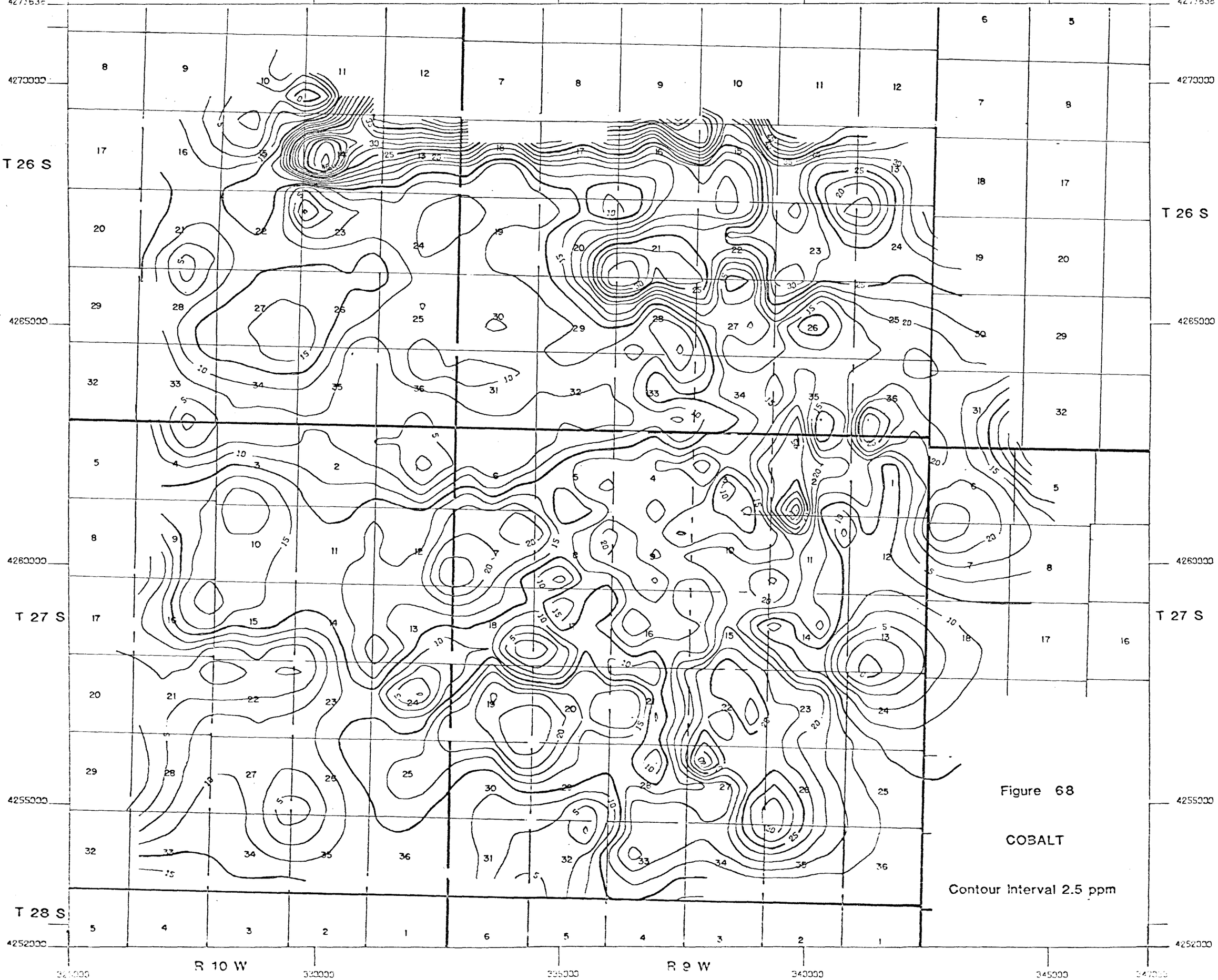

325000 R 10 W 330000 335000 R 9 W 340000 345000 R 8 W 347033

4271538 4270000 4265000 4260000 4255000 4252000

T 26 S T 27 S T 28 S

Figure 69

NICKEL

Contour Interval 10 ppm

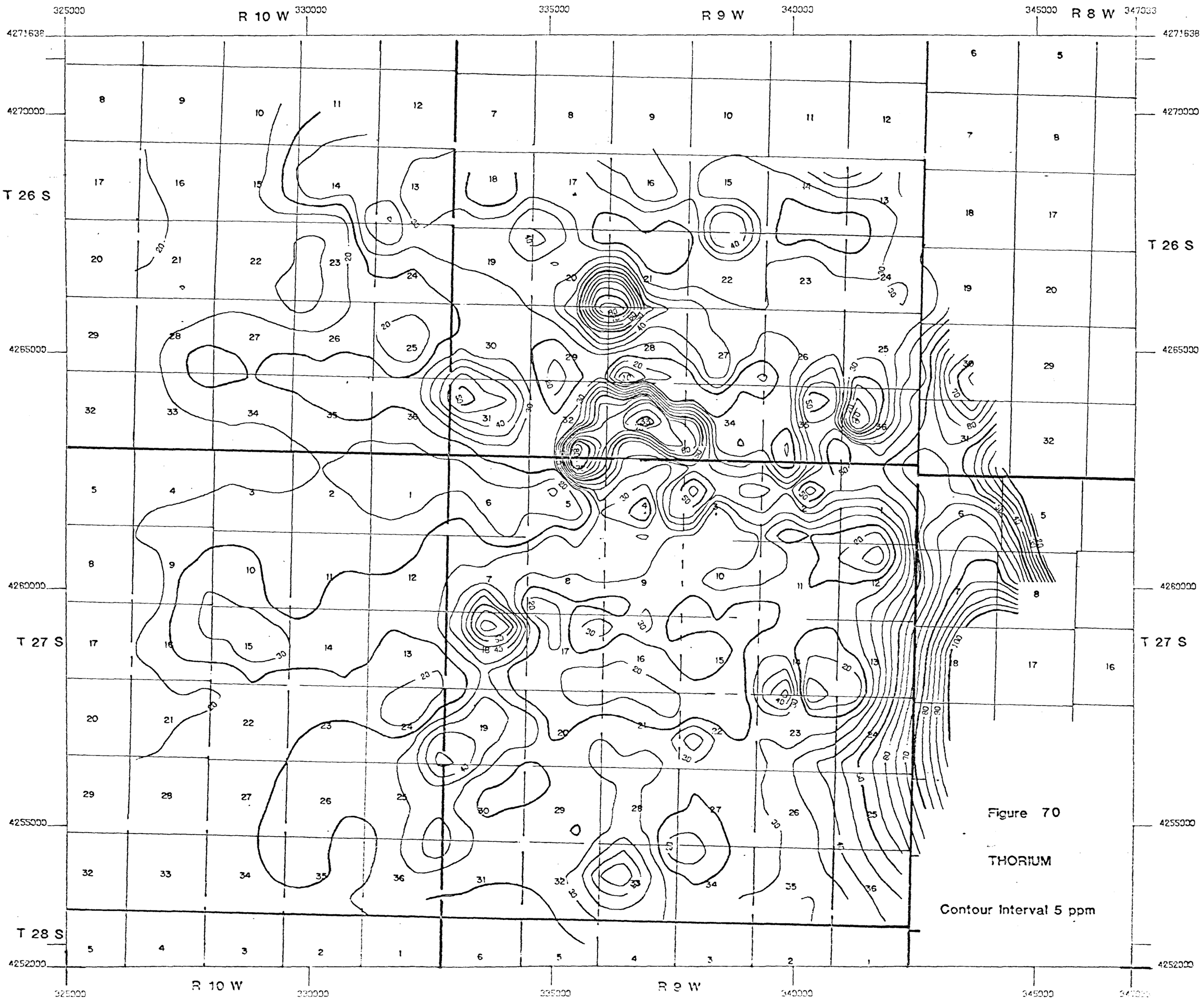

Figure 70

THORIUM

Contour Interval 5 ppm

R 10 W
R 9 W
R 8 W
T 26 S
T 27 S
T 28 S
325000
330000
335000
340000
345000
347033
4271638
4270000
4265000
4260000
4255000
4252000

Figure 71

LEAD

Contour Interval 3 ppm

325000 R 10 W 330000 335000 R 9 W 340000 345000 R 8 W 347033

4271638 4270000 4265000 4260000 4255000 4252000

T 26 S T 27 S T 28 S

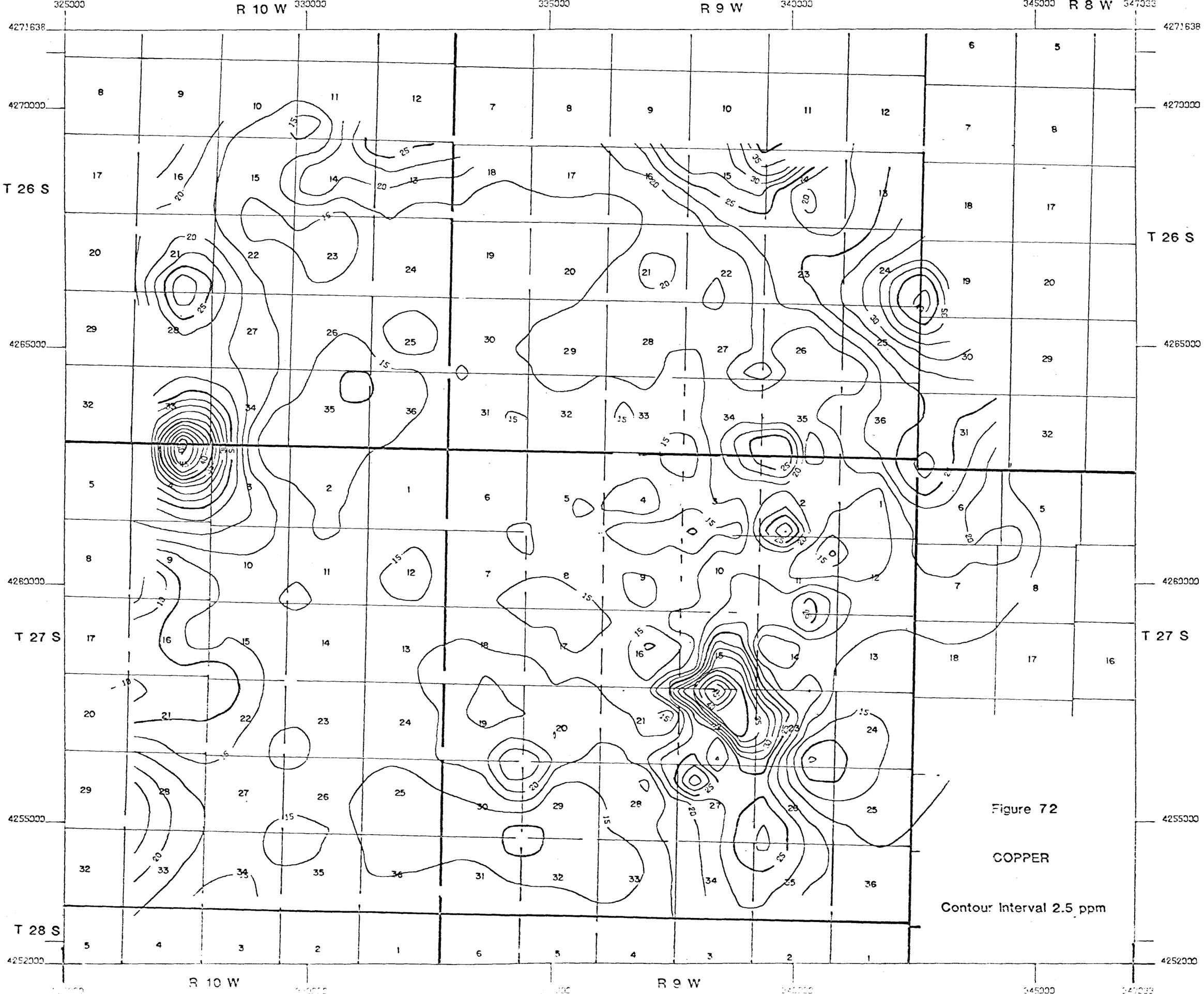

Figure 72

COPPER

Contour Interval 2.5 ppm

325000 R 10 W 330000 335000 R 9 W 340000 345000 R 8 W 347033

4271638 4270000 4265000 4260000 4255000 4252000

T 26 S T 27 S T 28 S

Figure 73

ZINC

Contour Interval 15 ppm

ANIONS

SURFACE MICROLAYER GRID DATA

Chloride

The contoured map of the chloride ion data shows that the area can, essentially, be divided into two parts. The eastern part of the survey is essentially featureless, and, as this includes the geothermal zone, there is no expression of the Roosevelt Springs KGRA (Figure 74).

There are a series of elevated samples running along the western edge of the survey area. The result of this is that there are, in effect, two populations of data, and this is the reason for the very high standard deviation for this anion (Table 7).

The chloride data shows little or no correlation with the other elements determined in this program, with the exception of nitrate, calcium and magnesium where there is moderate positive correlation and with silica, where there is a moderately weak negative anomaly.

Nitrate

The only feature in the nitrate data in the eastern section of the survey area was collected from a small unnamed cove at the edge of the Mineral Mountains (Figure 75). The sample was collected from an area of grazing land on which the vegetation had been recently burned. This would undoubtedly result in the formation of a great deal of nitrate, and is the most probable source of the anomaly.

To the west there is a single sample, high contrast anomaly. Nitrate is well correlated with chloride and with calcium and magnesium.

Fluoride

The fluoride data (Figure 76) is more complex than that for chloride and nitrate. All of the anomalous values are in the Escalante Desert and the majority are associated with an area in which obsidian and volcanic rock fragments predominate (Figure 29). Fluoride shows only poor correlation with any of the other

R 10 W

R 9 W

R 8 W

T 26 S

T 27 S

T 28 S

4271754

4270000

4265000

4260000

4255000

4252000

Figure 74

CHLORIDE

Contour Interval 10 ppm

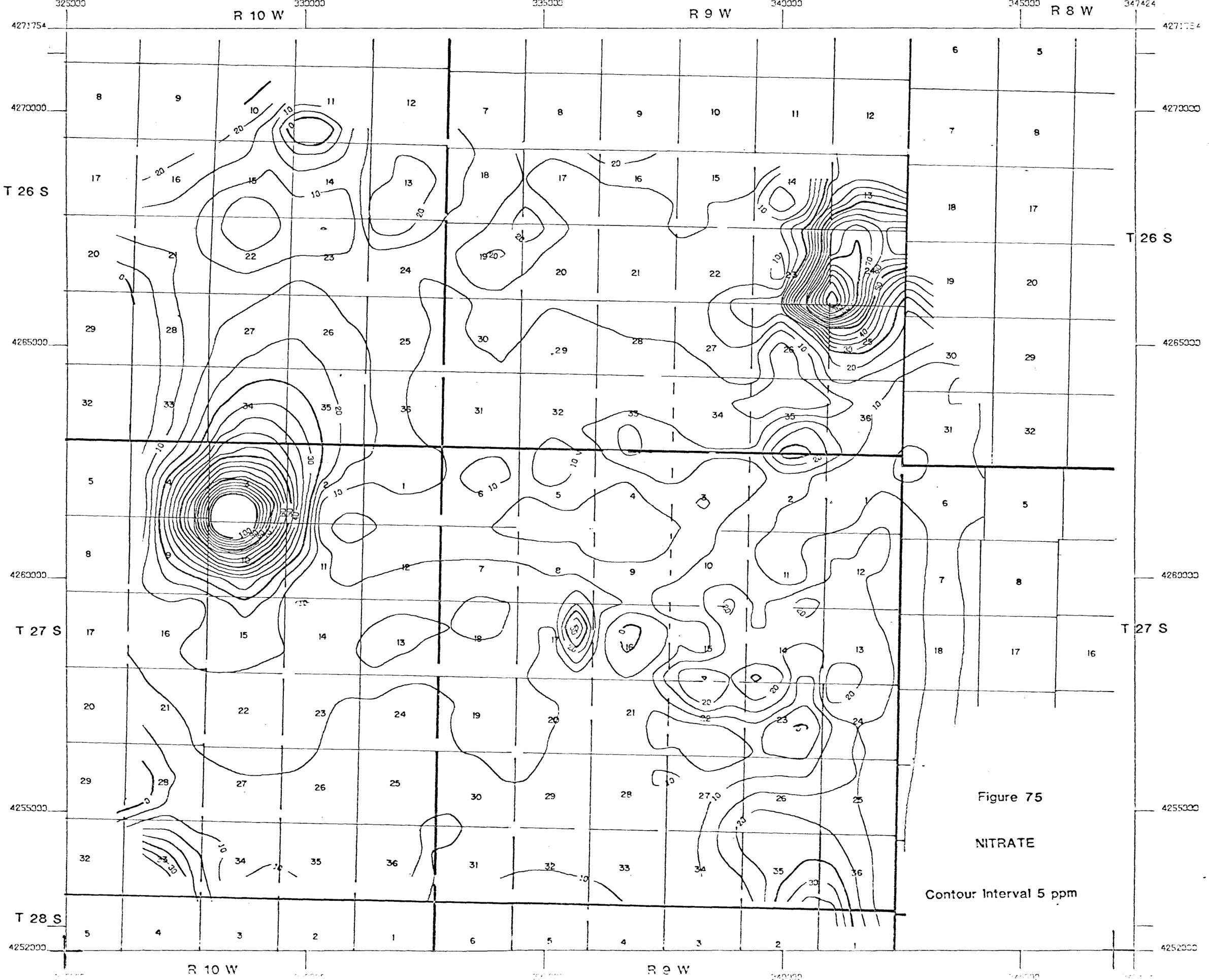

Figure 75

NITRATE

Contour Interval 5 ppm

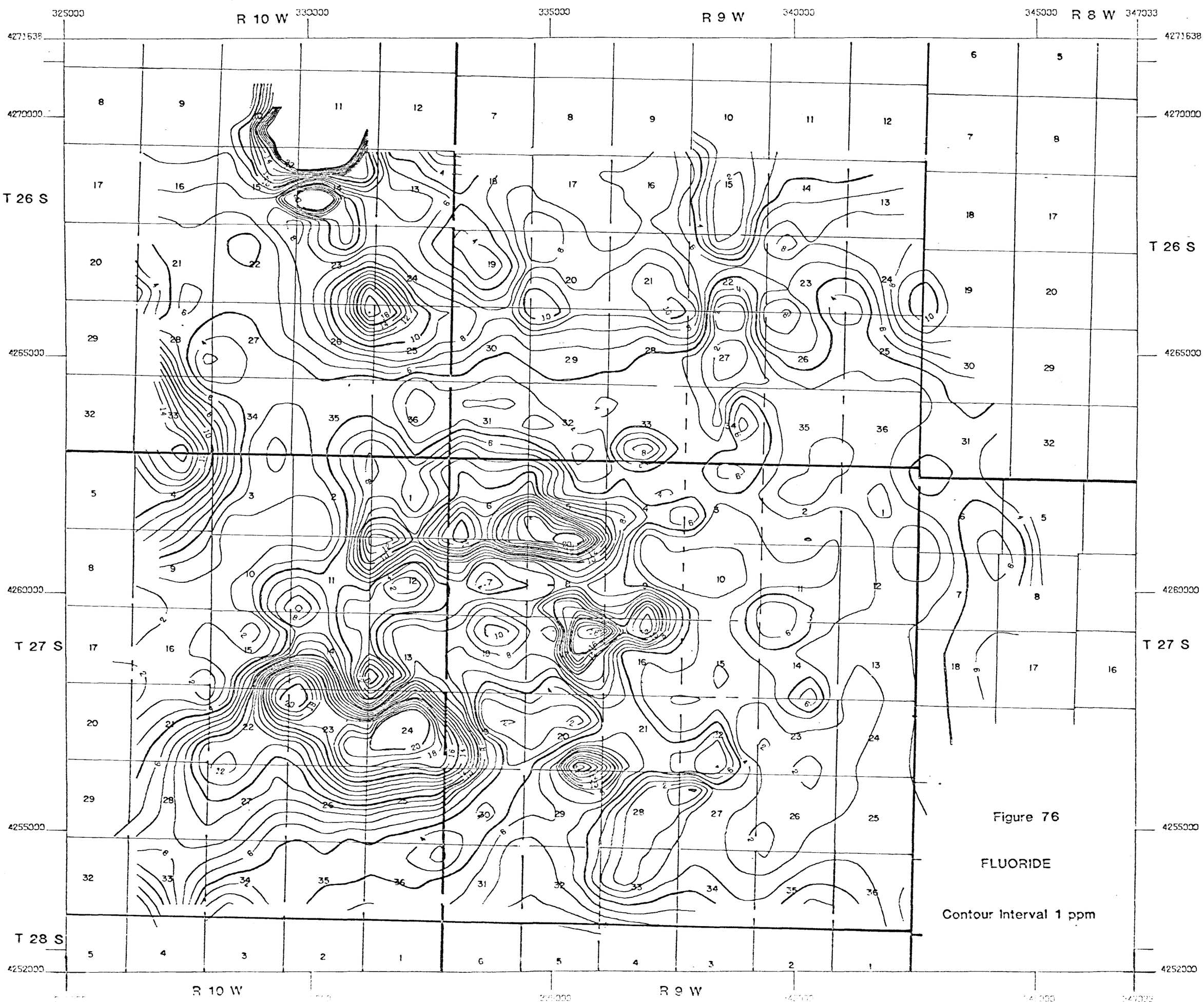

Figure 76

FLUORIDE

Contour Interval 1 ppm

elements determined during this project (Table 7), suggesting that the principal control of its distribution is lithological rather than being related to a particular mineral species.

Although the anomalous areas of fluoride encroach onto a section of the geothermal field, this data would have been of no use in indicating its position.

Sulphate

The majority of the sulphate activity in this area is concentrated to the west (Figure 77). Minor anomalies in the east are, in each case due to single samples. One of these lies within the Mineral Mountains and shows anomalous values of arsenic and mercury in the same sample with a slightly elevated concentration of copper. It seems probable, therefore that the sulphate is an indication of nearby oxidizing sulphide mineralization.

The anomalous areas to the east are probably a reflection of salt accumulation in the soils.

DETAILED SURFACE MICROLAYER TRAVERSES

There is no indication of the position of the Opal Mound Fault in any of the anion geochemistry data.

Conclusions

Anion geochemistry in the surface microlayer does not appear to offer any encouragement for its use as a method of exploration for geothermal areas. It is probable that these species are too mobile in the surficial environment to accumulate preferentially at the point of discharge onto the surface, and are also subject to changes in concentration as a result of weather conditions.

R 10 W

R 9 W

R 8 W

T 26 S

T 27 S

T 28 S

Figure 77

SULFATE

Contour interval 7.5 ppm

FACTOR ANALYSIS

The handling and interpretation of a large number of geochemical variables can be a time consuming task if all the elements are to be considered separately. This problem is met in the case of the 34 chemical parameters measured in the Roosevelt Springs surface microlayer survey. Statistical methods, such as factor analysis, can be used to reduce the data handling problem. Factor analysis is an approach whereby a large number of geochemical variables may be simplified into substantially fewer factors (combination and weighting of geochemical results) that contain essentially the same information as the entire data set.

Two types of factor analysis are commonly used. The first, R-mode, determines the inter-relationships between the variables while the second, Q-mode, classifies each sample in terms of end-member samples of distinctive composition. R-mode analysis is most useful for isolating the effect of chemical and physical processes within the environment, and it was anticipated that this form of analysis would separate identifiable element associations in the surface microlayer at Roosevelt Springs.

In R-mode analysis, a factor refers to the product derived from the combination of a number of weighted variables, in this case derived from the correlation matrix of the analytical results. The computer sequentially determines the factor that accounts for the largest proportion of the total variance within the data set, and factor loadings, the weighting of the variables in that factor, are determined for each geochemical variable. These factor loadings are numbers from -1.0 to +1.0, with +1.0 representing a perfect correlation between that variable and the factor, and -1.0 being a perfect inverse correlation. Factor loadings near 0.0 indicate that the variable concerned has no influence on the factor.

Factor scores may be computed for each sample once all the factors and factor loadings have been determined. These factor scores indicate the normalized correlation of each sample with the factor, and the spatial distribution of the factor scores can provide a useful medium for the identification and interpretation of the geochemical associations. Further discussion of this statistical method may be found in Cooley and Lohnes (1962), McCammon (1975) and Joreskog, et al., (1976).

METHOD

The computer program used for the factor analysis was made available as part of the Statistical Package for the Social Sciences (SPSS) described by Nie et al., (1975). As well as performing the factor analysis, statistics provided by the program included means and standard deviations (Table 6) and a matrix of correlation coefficients (Appendix C). The factoring method used was that of principal factoring with iteration followed by oblique rotation. Output from the factor analysis is included as Appendix D, while the oblique factor structure matrix indicating the loadings for each element in the nine factor model is also included as Table 7. Factor scores were determined for the regional data and have been plotted as a series of contour maps showing the spatial variation of the nine factors. The significance and meaning of the factor model is discussed in the following section.

RESULTS

The nine factor models provided a simplification of the multivariate data set into a meaningful grouping of chemical parameters. These factors have been mapped over the Roosevelt Springs survey area (Figures 78 to 86) and are described in the following sections.

Factor One: This factor exhibits a strong loading in elements which are characteristic of a mafic-metamorphic mineral assemblage (V. 929, Fe .914 and Ti .856). The factor score distribution confirms this association, with strong positive scores coincident with older metamorphic rocks on the western flanks of the Mineral Mountains (Figure 78). Evidence of detrital dispersion of minerals derived from weathering of the more mafic rocks can also be seen in the Quaternary alluvium located down slope from the area of metamorphic rocks.

Factor Two: Strong positive loadings for elements and anions forming seepage related surface precipitates characterize the chemical grouping in Factor Two (Sr 0.952, Cl^- 0.942, NO_3^- 0.526, and Ca 0.521). The factor score distribution map (Figure 79) shows a zone of high values parallel to the trend of the valley floor and somewhat coincident with the map of strong effervescence in the surface microlayer (Figure 28) indicative of caliche development.

R 10 W

R 9 W

R 8 W

T 26 S

T 27 S

T 28 S

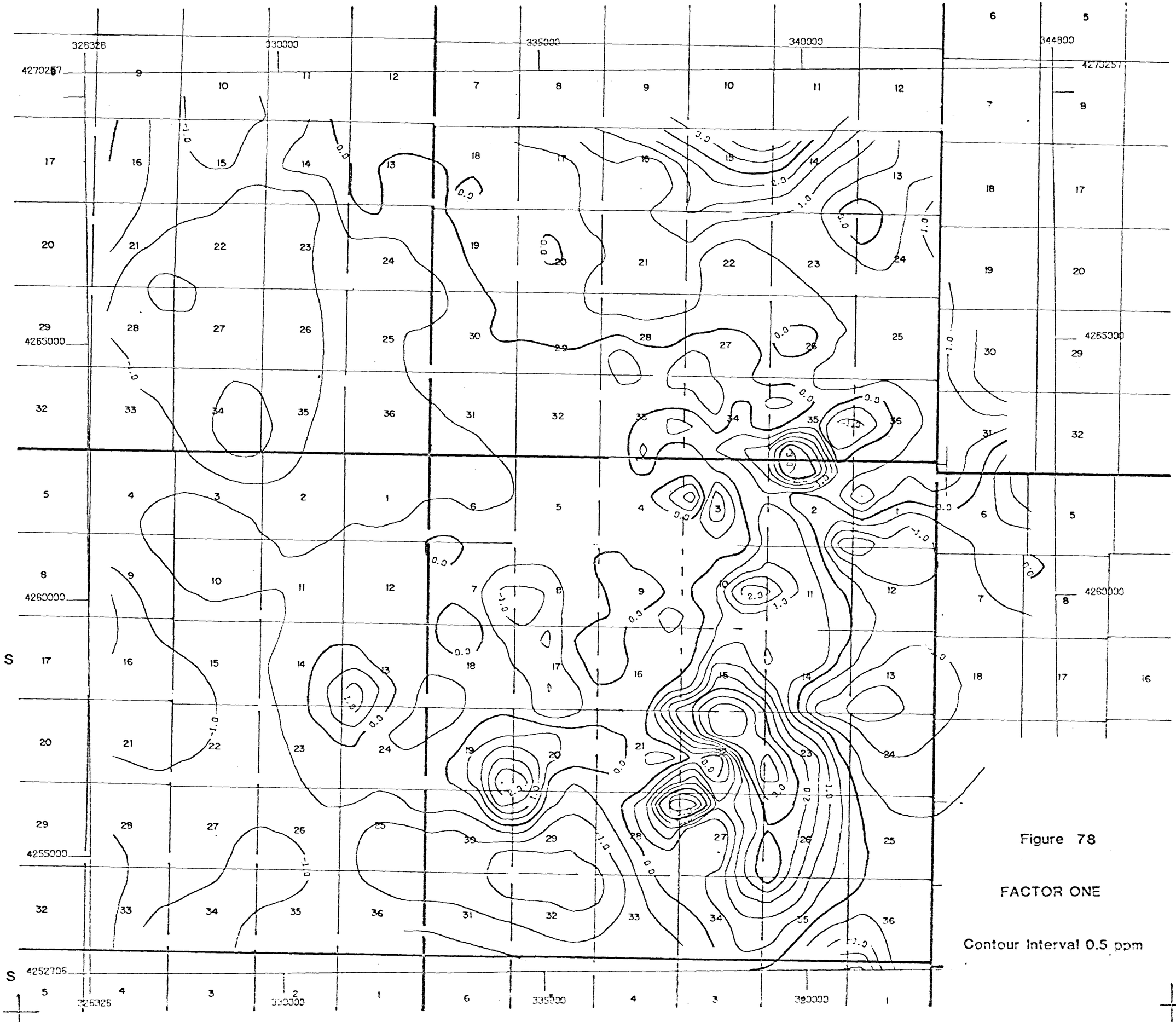

Figure 78

FACTOR ONE

Contour Interval 0.5 ppm

R 10 W

R 9 W

R 8 W

T 26 S

T 27 S

T 28 S

326326

330000

335000

340000

344800

4270250

4265000

4260000

4255000

4252705

Figure 79

FACTOR TWO

Contour Interval 0.5 ppm

TABLE 6. Means and Standard Deviations for Surface Geochemical Data

VARIABLE	MEAN	STANDARD DEV	CASES
AS	3.7330	1.4308	300
SE	.0674	.0336	300
LI	28.3167	5.3559	300
RB	101.7533	24.2932	300
SB	.1713	.1385	300
HG	30.9967	21.1495	300
SR	287.7940	166.0906	300
TH	28.7730	13.1366	300
CS	7.0200	7.4236	300
F	6.2167	4.4490	300
NO3	22.7687	76.6533	300
SO4	10.7120	12.3082	300
CL	60.2643	669.3298	300
CR	45.1730	57.6451	300
CO	15.2997	8.0486	300
CU	18.0217	5.6930	300
PB	22.8833	6.8989	300
NI	22.6823	57.2965	300
ZN	96.1393	29.7663	300
BE	2.3563	.5437	300
ZR	84.7960	11.9426	300
V	69.3611	15.1697	300
BA	560.9333	101.8406	300
B	7.3120	.6679	300
AL	64889.4667	5971.0667	300
FE	31329.0667	7451.9918	300
CA	20008.2767	15683.3077	300
MG	10607.5800	2607.6658	300
TI	4728.2667	1093.2078	300
MN	966.7067	278.4347	300
NA	16727.4233	3088.3128	300
K	23548.2333	2294.9985	300
P	1019.7533	436.6337	300
SI	306321.0000	24076.7848	300

Factor Three: Lithium, rubidium and beryllium form strong positive loadings on Factor Three (Table 7), and appear to reflect the contrast between elements associated with clay-rich soils as opposed to sandy alluvium. Positive factor scores coincide with the clay-rich residual soils of the Mineral Mountains, while negative scores are associated with coarse grained sandy alluvium deposited along the western edge of the mountains (Figure 80). Deposition of clay-rich sediments in low energy areas of the valley floor may explain the positive factor score anomaly in the northeast corner of Township 26S, Range 10W.

Factor Four: This factor is characterized by strong positive loadings for Cr (.988) and Ni (.984), with minor support from Cu (.328) and Co (.300). A metal association of this kind may well be indicative of previously unreported mineralization or a unique rock type in the vicinity of Little Cedar Cove (Figure 81). As expected, Factor Four is most strongly correlated with Factor One, representing the mafic association.

Factor Five: This negative factor with strong loadings for Cs (-.757) and Sb (-.549) is of particular interest due to its potential hydrothermal association. Examination of the distribution of factor scores (Figure 82) shows a negative factor score pattern to be coincident with the surface trace of the Opal Mound fault, with a high near the intersection of the Opal Mound and Negro Mag faults. The negative factor pattern extends to the northwest along a zone which may be related to down-gradient movement of cesium and antimony-rich waters. The strong Factor Five anomaly occurring on the floor of the valley at the break of slope may represent a seepage zone for these same cesium and antimony-rich waters, or could be directly related to a separate subsurface source of geothermal waters.

Factor Six: Rhyolite domes, and alluvium derived from the weathering of these rhyolites, are outlined by the positive factor score distribution (Figure 83), with high loadings of Zr (0.715) and Si (.471). Negative loadings of Mn (-.705), Zn (-.698) and P (-.675) provide a pattern which is most closely associated with Tertiary granites and quartz monzonites and may well represent a late-stage mineralizing phase related to these intrusives. Down slope dispersion can also be traced from the area of quartz monzonite north of Negro Mag Wash, to the seepage zone in the northwest corner of the survey area.

R 10 W

R 9 W

R 8 W

T 26 S

T 27 S

T 28 S

326326

330000

335000

340000

344800

4270257

4265000

4260000

4255000

4252706

Figure 80

FACTOR THREE

Contour Interval 0.5 ppm

R 10 W

R 9 W

R 8 W

T 26 S

T 27 S

T 28 S

326326

330000

335000

340000

344800

4270287

4270257

4265000

4260000

4255000

4252706

0.0

1.0

Figure 81

FACTOR FOUR

Contour Interval 0.5 ppm

R 10 W

R 9 W

R 8 W

T 26 S

T 27 S

T 28 S

326326

330000

335000

340000

344800

4270257

4265000

4260000

4255000

4252706

Figure 82

FACTOR FIVE

Contour Interval 0.5 ppm

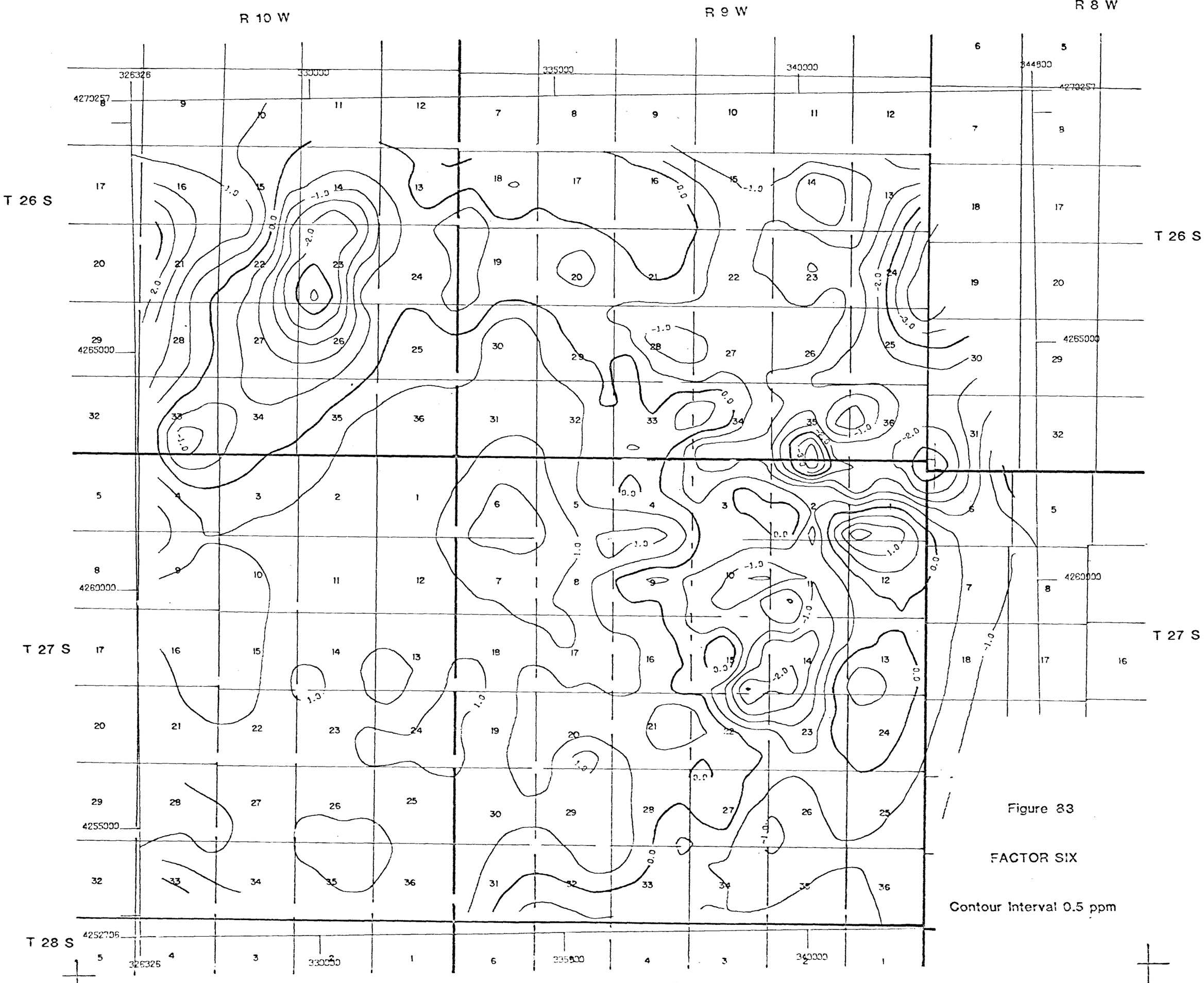
R 10 W
R 9 W
R 8 W
T 26 S
T 27 S
T 28 S
326326
330000
335000
340000
344800
4270257
4265000
4260000
4255000
4252706
Figure 83
FACTOR SIX
Contour Interval 0.5 ppm

TABLE 7. Oblique Factor Structure Matrix for Nine Factor Model

	FACTOR 1	FACTOR 2	FACTOR 3	FACTOR 4	FACTOR 5	FACTOR 6	FACTOR 7	FACTOR 8	FACTOR 9
AS	.05570	.35559	.08098	.06180	-.32598	-.20221	-.00799	-.19468	.50753
SE	-.05099	.20699	.13892	.09179	-.12330	-.02002	.01007	-.12335	.50727
LI	.10662	.20014	.80547	.06778	-.02397	-.14682	.09117	-.04843	.35643
RB	.04530	-.05085	.80592	.03741	.02619	-.14898	-.21761	.28591	.05878
SB	-.11894	-.03209	-.11427	-.06215	-.54919	.08643	.01916	-.09418	.08113
HG	.15293	-.04766	-.09102	.01464	-.04379	-.39900	-.32240	.08938	.20494
SR	.13193	.95218	.07984	.01370	-.07629	-.20678	.19734	-.24442	.13028
TH	.14102	-.07244	.12093	.00807	.07078	-.22737	-.68093	.11919	.10298
CS	-.05369	.05828	.26504	.00369	-.75783	-.02807	.15720	-.18662	.13147
F	-.14215	.11010	.04861	-.01920	-.06838	.19382	.10412	-.30226	.11291
NO3	-.04098	.52684	.08857	-.00682	.01374	.05775	.15903	-.11157	.21500
SO4	.14783	.32719	.11910	.08253	.18719	-.29726	.06128	-.02391	.21153
CL	-.01613	.94257	.01421	.00376	.03312	-.05599	.05317	-.17838	.16850
CR	.15816	-.01395	.01504	.98874	.05408	-.01943	.01224	.01733	.06479
CO	.60358	.03944	.10737	.30084	.02253	-.24578	.02404	.09747	.10386
CU	.63398	.10860	.30334	.32800	.25845	-.38349	.15019	.02033	.39769
PB	.11406	-.05330	.36455	.09596	.29499	-.40541	-.38794	.27538	.35854
NI	.13256	.00550	.02225	.98465	.02492	-.00868	.03361	-.02360	.06027
ZN	.57769	-.00054	.26502	.15324	.34550	-.69791	-.16523	.42358	.46710
BE	-.14069	-.11537	.58142	.00926	.30792	.04270	-.63369	.27984	-.16834
ZR	-.23576	-.09045	-.15148	-.05186	-.09644	.71578	.17578	-.07843	-.08429
V	.92963	-.05830	-.06332	.11473	.15854	-.21178	-.00744	.19746	-.11051
BA	.44566	-.06004	-.04297	.04296	-.15375	-.52353	.13538	.41366	.19278
B	.41309	.17696	.11612	.09714	.05591	-.51904	-.03846	.30280	-.00453
AL	.41620	-.24793	.34182	.14806	.48573	-.25133	-.34920	.76035	-.13475
FE	.91480	-.11178	-.02092	.17678	.16293	-.36248	-.25193	.32961	-.02742
CA	-.09007	.52132	.18077	-.00180	-.32563	-.07613	.38180	-.65835	.28755
MG	.68055	.46437	.22675	.11281	.09392	-.12777	.41440	-.09803	.46689
TI	.85656	-.12859	-.01168	.11130	.19664	-.53733	-.12084	.53228	-.08558
MN	.41130	.01815	.34147	.10253	.19574	-.70535	-.10800	.57171	.40330
NA	.21173	-.17962	.24242	.03689	.41563	-.35459	-.32326	.65589	-.40889
K	.15193	-.08533	.37530	.01807	.18856	-.10520	-.05869	.76744	.05841
P	.76239	.11789	.20016	.10984	.20382	-.67523	.03681	.43143	.28380
SI	-.43841	-.42442	-.38022	-.16154	.00008	.47195	-.01642	.22802	-.43400

Factor Seven: This negative factor with high loadings for Th (-.680) and Be (-.634) shows a distribution pattern which is probably related to the concentration of heavy detrital minerals with alluvial deposits at the mouths of canyons draining areas where rhyolites are being eroded. This is particularly evident in the case of Negro Mag Wash and Lower Ranch Canyon (Figure 84).

Factor Eight: High positive loadings for potassium (0.767), aluminum (0.760) and sodium (0.656) give factor scores with an anomalous distribution immediately to the north of Negro Mag Wash (Figure 85), perhaps related to a zone of hydrothermal alteration. Sibbett and Nielson (1980) noted areas of albitization in the eastern part of Negro Mag Wash.

Factor Nine: This factor may well be related to sulfide mineralization, with high factor loadings for As (.507), Se (.507), Zn (.467) and Mg (.466). The strongest factor scores are found within an area of Tertiary quartz monzonite to the north of the Negro Mag Fault (Figure 86). Salt Cove fault is also anomalous, but it is not clear whether this pattern represents downstream drainage from the quartz monzonite source, or leakage of mineral-rich fluids along the fault zone.

R 10 W

R 9 W

R 8 W

T 26 S

T 27 S

T 28 S

326326

330000

335000

340000

344800

4270257

4265000

4260000

4255000

4252705

Figure 84

FACTOR SEVEN

Contour Interval 0.5 ppm

R 10 W

R 9 W

R 8 W

T 26 S

T 27 S

T 28 S

326326

330000

335000

340000

344800

4270257

4265000

4260000

4255000

4252705

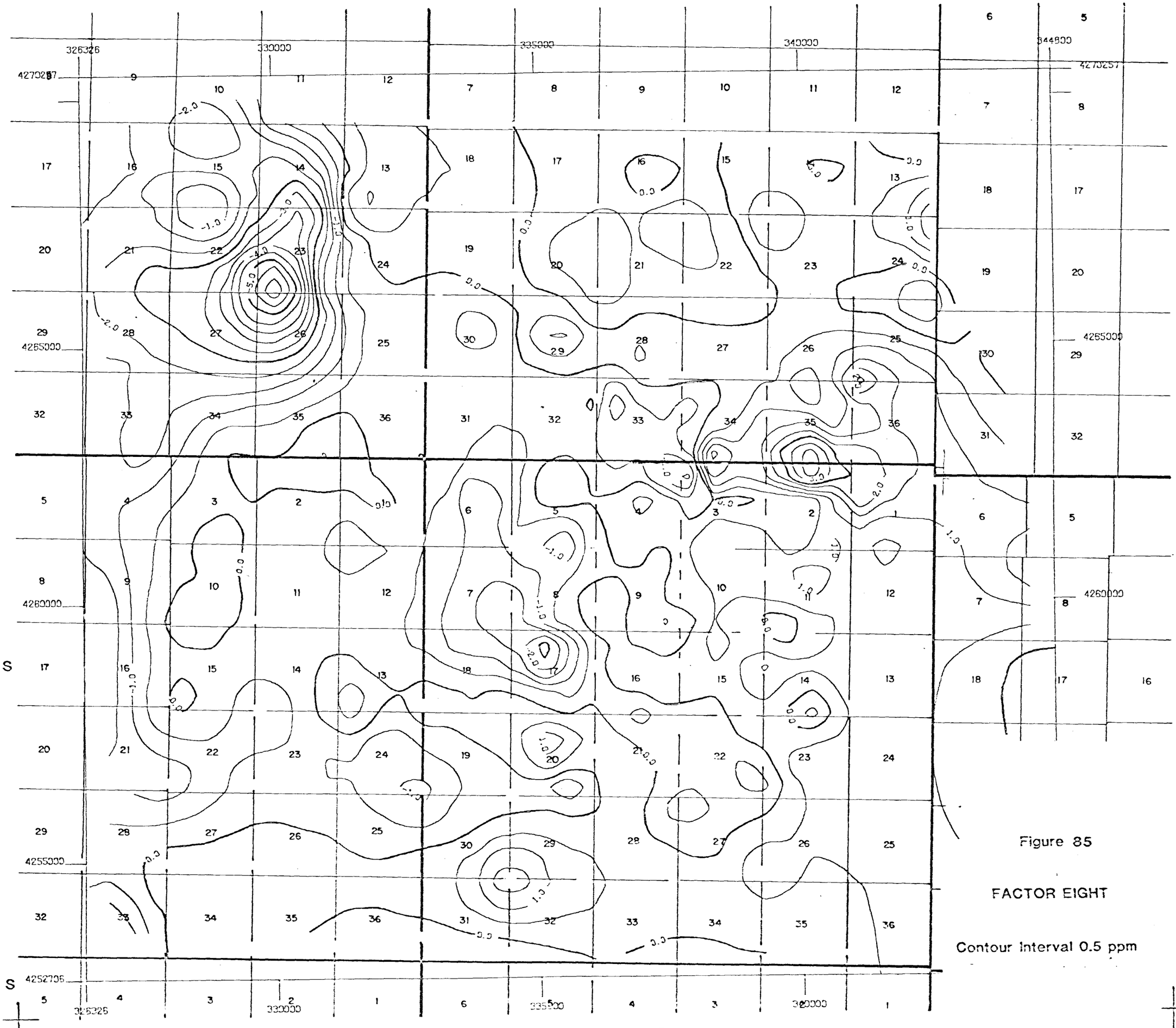

Figure 85

FACTOR EIGHT

Contour Interval 0.5 ppm

R 10 W

R 9 W

R 8 W

T 26 S

T 27 S

T 28 S

326326

330000

335000

340000

344800

4270257

4265000

4260000

4255000

4252706

Figure 86

FACTOR NINE

Contour Interval 0.5 ppm

CONCLUSIONS

1. Phase II sampling showed that the surface microlayer was the optimum sampling medium for geothermal exploration in the environment existing in the Roosevelt Springs area. This approach has clear cut advantages in terms of sampling speed, with potential for helicopter reconnaissance of large areas. Furthermore, some elements, notably As, Sb and Cs showed strong expression of the Opal Mound Fault in the surface microlayer, which was absent in the underlying soils.

2. If a limited number of elements are to be used to explore for Roosevelt Springs-type geothermal activity, the results of this survey suggest that the preferred elements are Hg, As, Sb and Cs. However, Bamford et al., (1980) also suggest that Mn, W, Li, Be, Zn, Th and Sn may be of use. It is probable that, in a different soil and fluid flow regime, these elements may become more prominent. For example, in the data from this survey the geothermal area is occupied by an area in which the surface microlayer is low in lithium and beryllium although both of these elements have been deposited in anomalous concentrations within the opaline sinter. It is probable that the low values are in fact due to the masking effect of highly siliceous detritus derived from the Mineral Mountains, a process clearly unrelated to geothermal activity.

3. Multi-element ICP analysis proved useful as an interpretation aid when combined with R-mode factor analysis to develop a model of the geochemical processes controlling the distribution of elements in the surface microlayer. Aqueous geothermal components are typified by the Factor Five distribution based on Cs, Sb and As in the surface microlayer (Figure 87). This factor has a surface distribution which closely reflects the heat flow pattern in the vicinity of the Opal Mound and Negro Mag faults, indicates leakage of geothermal-related fluids along the Salt Cove fault zone, and is enhanced at the intersection of the Salt Cove and N-3 faults. This latter area may well be related to a separate source of heat at depth or to leakage of geothermal fluids moving westwards along the Salt Cove Fault Zone.

4. The smoothed mercury data (Figure 38) has indicated the presence of a regional high, situated over the possible

location of the dry heat source (Figure 87). Mercury could have been driven to the surface by vapour phase transport following a thermal gradient and have become separated from other components traveling in aqueous solution.

5. While relatively detailed sampling is required to identify leakage of geothermal fluids in the vicinity of the Opal Mound Fault using the single element approach, the use of R-mode factor analysis of multi-element data identified a broad response at the surface. This was achieved because a single factor related to the geothermal solutions could be identified, and this association was more readily extracted from background than were the single element anomalies. Using this approach, regional sampling on half-mile centers provides a suitable grid for regional geothermal exploration.

6. This program has demonstrated the importance of mapping the surficial float material and of determining the sediments reaction to hydrochloric acid as a measure of the carbonate concentration. These data have materially assisted in interpreting the multi-element geochemistry and must be considered to be an essential component of future surveys of this type.

7. Analysis of groundwaters from wells (Figure 20) and surface geochemistry (Figure 82) both suggest that there may be a WNW leakage of geothermal fluids along the Salt Cove Fault zone and an upwelling of brines at the intersection of north-south fault N3. There is some support for this conclusion in that the heat flow pattern (Figure 87) shows a well defined WNW trending lobe. In view of these data and with the lack of conflicting evidence, geochemistry points to a potential hot-water source in this area.

8. The most relevant data from this program have been synthesized in Figure 87. This figure combines the major faulting, Factor 2 (Figure 79) which outlines the accumulation of salts in the center of the Escalante valley, the heat-flow pattern after Ward et al., (1978), the potential dry heat source indicated by the mercury trend surface and Factor 5 (Figure 82) which is considered to be the best geothermal indicator. It is considered that these data present a coherent picture of the main geothermal activity in this area and their relationship to the surface geochemistry.

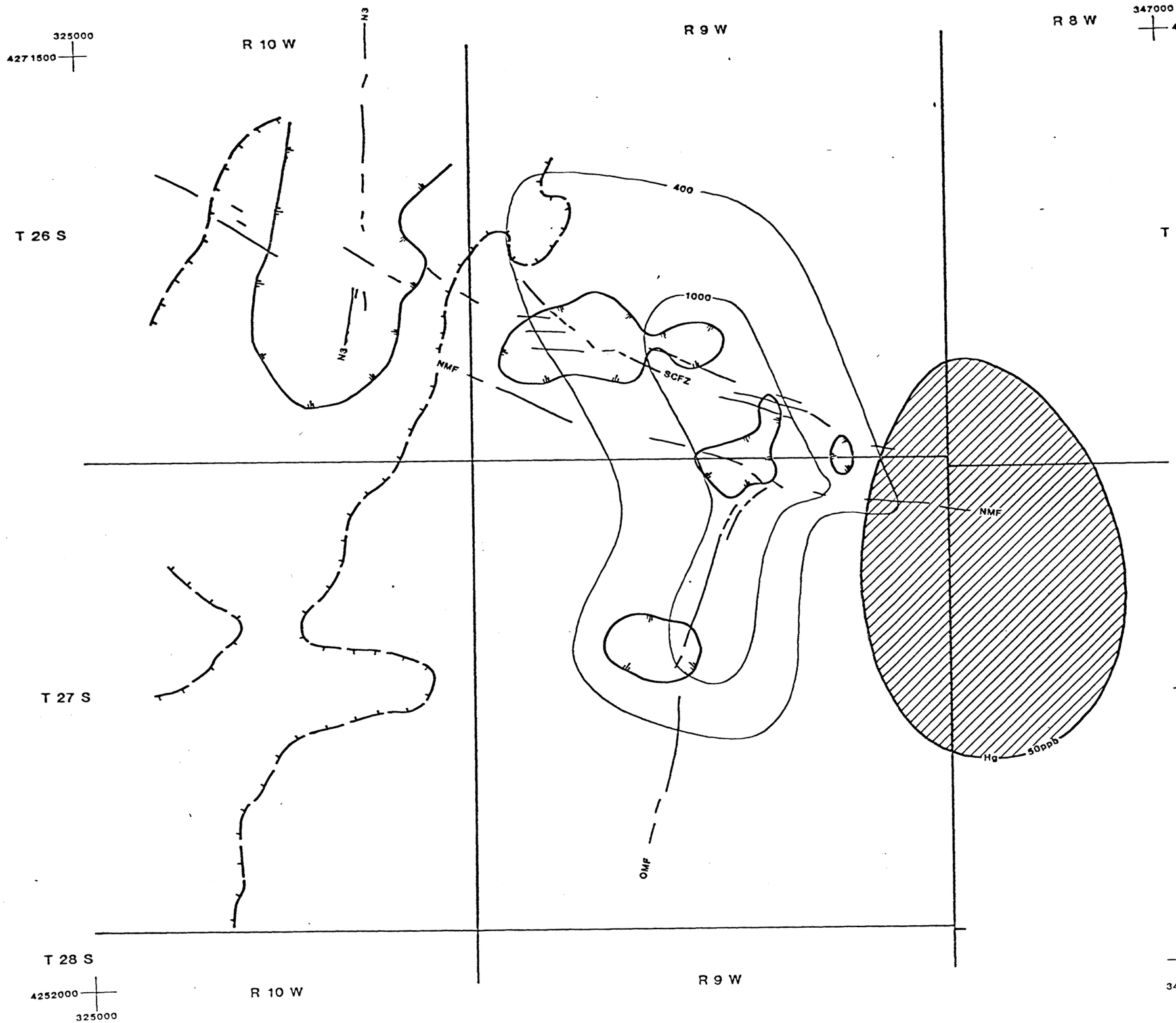

LEGEND

- Zone of surface microlayer precipitates
- Evidence of geothermal fluid chemistry detected in surface microlayer
- Regional mercury anomaly overlying possible buried heat source
- Heat flow contours in mWm^{-2} (after Ward et al, 1978)

OMF	Opal Mound Fault
NMF	Negro Mound Fault
SCFZ	Salt Cove Fault Zone
N3	Fault N3

Figure 87

SUMMARY OF SURFACE MICROLAYER GEOCHEMISTRY
ROOSEVELT SPRINGS SURVEY AREA

REFERENCES

Abou-Zied, S., 1973. Geology of the Milford Flat Quadrangle, Star District, Beaver County, Utah: Utah Geol. Assn. Pub. 3, 43-48.

Anderson, J.J., and Rowley, P.D., 1975. Cenozoic stratigraphy of southwestern high plateaus of Utah, in Anderson, J.J., Rowley, P.D., Fleck, R.J. and Nairn, A.E.M., Cenozoic geology of southwestern high plateaus of Utah: Geol. Soc. Amer. Spec. Paper 160, p. 1-52.

Archambeau, C.F., E.A. Flinn, and D.G. Lambert, 1969. Fine structure of the upper mantle: Jour. Geophys. Research, v. 74, p. 5825-5865.

Armstrong, R.L., 1968. Sevier orogenic belt in Nevada and Utah: Geol. Soc. Amer. Bull., v. 79, p. 429-458.

Armstrong, R.L., 1970. Geochronology of Tertiary igneous rocks, eastern Basin and Range Province, western Utah, eastern Nevada, and vicinity, U.S.A.: Geochimica et Cosmochimica Acta, v. 34, p. 203-232.

Atkinson, D.J., and W.T. Meyer, 1980. Low cost airborne geochemical detection and evaluation of "blind" geothermal reservoirs. URC Trans., v. 4, p. 141-143.

Baer, J., 1973. Summary of stratigraphy and structure of the Star Range, Beaver County, Utah: Utah Geol. Assn. Pub. 3, p. 33-38.

Bamford, R.W., 1978. Geochemistry of solid materials from two U.S. geothermal systems and its application to exploration. UURI.

Bamford, R.W., O.D. Christensen, R.M. Capuano, 1980. Multi-element geochemistry of solid materials in geothermal systems and its applications; Part 1: The hot-water system at the Roosevelt Hot Springs KGRA, Urah: DOE/ET/27002-7, ESL-30, 168p.

Bargar, K.E., Beeson, M.H., Fournier, R.D. and Muffler, L.J.P., 1973. Present day deposition of lepidolite from thermal waters in Yellowstone National Park: Am. Mineral., 58, 901-904.

Barnes, H.L., 1979. Geochemistry of Hydrothermal Ore Deposits, 2nd Ed., Barnes H.L., ed. Wiley and Sons, 1979.

Barosh, P.J., 1960. Beaver Lake Mountains, Beaver County, Utah: Utah Geol. Min. Survey Bull. 68.

Barringer, A.R., et al., 1978. Surtrace™, An Airborne Geochemical System, presented at 12th International Symposium on Remote Sensing of the Environment, Manila, Phillipines, April, 1978.

Blackwell, D.D., 1969. Heat flow determinations in the northwestern United States: Jour. Geophys. Research, v. 74, p. 992-1007.

Bowers, D., 1978. Potassium - argon age dating and petrology of the Mineral Mountains pluton, Utah: Univ. of Utah, Dept. of Geol. and Geophysics, Unpubl. M.S. Thesis.

Braile, L., Smith, R.B., Keller, R., Welch, R. and Meyer, R.P., 1974. Crustal structure across the Wasatch Front from detailed seismic refraction surveys: Jour. Geophys. Research.

Brondini, M., Dall'Aglio, M. and Vitrani, F., 1973. Lithium as a pathfinder element in the large scale hydrogeochemical exploration for hydrothermal systems: Geothermics vol. 2, nos. 3-4, p. 142.

Brown, F.H., 1977. Attempt at paleomagnetic dating of opal, Roosevelt Hot Springs KGRA: Quarterly Progress Report to ERDA, contract EY-76-S-07-1601, p. 11.

Bryant, N.L., and Parry, W.T., 1977. "Hydrothermal alteration at Roosevelt Hot Springs KGRA - DDH 1976-1," UURI Tech. Vol. 77-5, p. 87.

Bullock, K.C., 1976. Fluorite occurrences in Utah: Utah Geol. and Mineral Survey Bull. 110, p. 89.

Butler, B.S., 1913. Geology and ore deposits of the San Francisco and adjacent districts, Utah: U.S. Geol. Survey Prof. Paper 80, p. 212.

Butler, B.S., 1913. Geology and ore deposits of the San Francisco and adjacent districts, Utah: U.S. Geol. Survey Prof. Paper 111, p. 672.

Cadigan, R.A. and Felmlee, J.K., 1977. Radioactive springs geochemical data related to uranium exploration. J. Geochem Expl. 8, 381-395.

Cannon, H.E., Harms, T.F. and Hamilton, J.C., 1975. Lithium in unconsolidated sediments and plants of the Basin and Range Province, southern California and Nevada. U.S. Geol. Surv. Prof. Pap. 918, 23 p.

Capuano, R.M., and Bamford, R.W., Initial investigation of soil mercury geochemistry as an aid to drill site selection in geothermal systems: IDO/78-120/.6.3.3, ESL-13, p. 32.

Carter, J.A. and Cook, K.L., 1978. Regional gravity and aeromagnetic surveys of the Mineral Mountains and vicinity, Millard and Beaver Counties, Utah: UURI Final Vol. 77-11, p. 178.

Christensen, F.W., 1951. A summary of the structure and stratigraphy of the Canyon Range: Int. Assn. of Pet. Geol., Guidebook 6, p. 5-18.

Cohenour, R.E., 1963. The beryllium of western Utah, in "Beryllium and uranium mineralization in western Juab County, Utah": Utah Geol. Soc. Guidebook to the Geology of Utah, no. 17, p. 4-7.

Connor, J.J. and Shacklette, H.T., 1975. Background concentrations of some soils, plants and vegetables in the conterminous United States. U.S. Geol. Survey Prof. Pap. 574-F, 164 p.

Cooley, W.W. and Lohner, P.R. (1962); Multivariate procedures for the Behavioral Sciences: John Willy and Sons, New York, 211p.

Crawford, A.L. and Buranek, A.M., 1957. Tungsten deposits of the Mineral Range, Beaver County, Utah: Utah Geol. and Mineral Survey Rep. no. 56, p. 48.

Crebs, T.J., and Cook, K.L., 1976. Gravity and ground magnetic surveys of the Central Mineral Mountains, Utah: NSF Final Report, Grant GI 43741, v. 6, 129 p.

Davis, J.J., 1963. Cesium and its relationship to potassium in ecology: Radioecology (Schultz and Kelment, eds.) New York: Reinholt Publ. Corp. 1963.

Eardley, A.J., 1968. Major structures of the Rocky Mountains of Colorado and Utah: Missouri Univ. of Rolla, Jour. no. 1, p. 79-99.

Eardley, A.J., 1969. Charting the Laramide structures of western Utah in "Guidebook of northern Utah": Utah Geol. and Min. Survey Bull. 82, p. 51-70.

Earll, F.N., 1957. Geology of the Central Mineral Range, Beaver County, Utah: Univ. Utah, unpub. Ph.D. thesis, 112 p.

East, E.H., 1966. Structure and stratigraphy of San Francisco Mountains, western Utah: AAPG Bull. v. 50, p. 901-920.

Ellis, A.J., and Mahon, W.A.J., 1964. Natural hydrothermal systems and experimental hot-water/rock interactions: Geochim. Cosmochim. Acta, 28, 1323-1358.

Ellis, A.J., 1979. Explored geothermal systems: in Geochemistry of Hydrothermal Ore Deposits. Barnes, H.L., ed. John Wiley and Sons., New York.

Erickson, M.P., 1973. Volcanic rocks of the Milford area, Beaver County, Utah: Utah Geological Association Publ. 3, p. 901-920.

Evans, S.H. Jr., and Nash, W.P., 1978. Quaternary rhyolite from the Mineral Mountains, Utah, U.S.A.: UURI Final Vol. 77-10, 59 p.

Ewers, G.R. and Keays, R.R., 1977. Volatile and precious metal zoning in the Broadlands Geothermal Field, New Zealand: Econ. Geol., v. 72, p. 1337-1354.

Fleming, R.W. and Alexander, M., 1972. Appl. Microbiol. 24: 424-429.

105

Foster, N.D., 1960. Interpretation of the composition of Li-micas: U.S. Geol. Survey Prof. Pap. 354E, 115-147.

Gertson, R.C. and Smith, R.B., 1979. Interpretation of a seismic refraction profile across the Roosevelt Hot Springs, Utah and vicinity. IDO/78-1701 a. 3, 109 p. of Geol. and Geophys., IDO 78-1701.

Glenn, W.E. and Julen, J.B., 1979. Interpretation of well log data from four drill holes at Roosevelt Hot Springs KGRA: (DOE/ET/28392-27, ESL-28), 74 p.

Golding, R.M. and Speer, M.G., 1965. Alkali ion analysis of thermal waters in New Zealand. N.Z. Jour. of Sci., 4, 203-213.

Goldschmidt, V.M., 1954. Geochemistry. Oxford University Press, 1954.

Helgeson, H.C., 1968. Geologic and thermodynamic characteristics of the Salton Sea geothermal system. Am. J. Sci. 266, 129-166.

Hilpert, L.S. and Roberts, R.J., 1964. Geology - Economic Geology, in U.S. Geologic Survey, Mineral and Water Resources of Utah: U.S. 88th Cong., 2nd Sess., p. 28-38.

Hinkle, M.E. and Harms, T.F., 1978. CS_2 and COS in soil gases of the Roosevelt Hot Springs Known Geothermal Resource Area, Beaver County, Utah: Jour. Research U.S. Geol. Survey, v. 6, no. 5, p. 571-578.

Hintze, L.F., 1973. Geologic history of Utah: Brigham Young Univ. Geology Studies, v. 20, pt. 3, p. 181.

Hulen, J.B., 1978. Stratigraphy and alteration, 15 shallow thermal gradient holes, Roosevelt Hot Springs KRGA and Vicinity: IDO 178-1701.6.b.1.1.1, 14 p.

Joreskog, K.G., Klovan, J.E., and Teyment, R.A., (1976); Geological Factor Analysis: Elsevier Publishing Company, New York, 178 p.

Julian, B., 1970. Variations in upper mantle structures beneath North America (Ph.D. thesis): Pasadena, California Institute of Technology, 208 p.

Keller, G.R., Smith, R.B., and Braile, L.W., 1975. Crustal structure along the Great Basin - Colorado Plateau transition from seismic refraction studies: Jour. Geophys. Res., v. 80, no. 8, p. 1093-1098.

Klusman, R.W., Cowling, S., Culvey, B., Roberts, C., and Schwab, A.P., 1977. Preliminary evaluation of secondary controls on mercury in soils of geothermal districts: Geothermics, v. 6, no. 1/2, p. 1-8.

Klusman, R.W., and Landress, R.A., 1979. Mercury in soils of the Long Valley, California, geothermal system: J. Volc. Geotherm. Res., v. 5, p. 49-65.

Landstrom, O., Wenner, C.G., 1965. Neutron activation analysis of natural water applied to hydrogeology. Aktiebolaget Atomenergi, AE-204.

Lee, W.T., 1908. Water resources of Beaver Valley, Utah: U.S. Geol. Survey, Water-Supply Paper 217, p. 56.

Lenzer, R.C., A.W. Crosky and C.W. Berge, 1977. Recent developments at the Roosevelt Hot Springs KGRA: ANS Topical Meeting, April 1977: US DOE Tech. Info. Cen. Conf. 770440.

Liese, H.C., 1957. Geology of the northern Mineral Range, Millard and Beaver Counties, Utah: Univ. of Utah, unpub. M.S. thesis, 88 p.

Lindsey, D.A., Ganow, H., and Mountjoy, W., 1973. Hydrothermal alteration associated with beryllium deposits at Spor Mountain, Utah: U.S. Geol. Survey Prof. Paper 818-A, p. 20.

Lindsey, D.A., Naeser, C.W., and Shawe, D.R., 1975. Age of volcanism, intrusion, and mineralization in the Thomas Range, Keg Mountain, and Desert Mountain, western Utah: U.S. Geol. Survey Jour. Research, v. 3, no. 5, p. 597-604.

Lipman, P.W., Rowley, P.D., Mehnert, H.H., Evans, S.H., Nash, W.P. and Brown, F.H., 1978. Pleistocene rhyolite of the Mineral Mountains, Utah-geothermal and archeological significance: Jour. Research U.S. Geol. Survey, v. 6, no. 1, p. 133-147.

Livingstone, D.A., 1963. Chemical composition of rivers and lakes. U.S.G.S. Prof. Pap. 440-9, 1-64.

Mattick, J.S. III, Buseck, P.R., 1976. Exploration for geothermal areas using mercury: a new geochemical technique, in Proceedings Second U.N. Symposium on Development and Use of Geothermal Resources: Lawrence Berkeley Laboratory.

McCammon, R.B., ed., (1975); Concepts in Geostatistics: Springer-Verlag, New York, 168 p.

Mower, R.W. and R.M. Cordova, 1973. Ground-water in the Milford area, Utah: Utah Geol. Assn. Pub. 3, p. 63-71.

Mower, R.W. and R.M. Cordova, 1974. Water resources of the Milford area, Utah, with emphasis on ground water: Utah Dept. Nat. Res. Tech. Pub. 43, 106 p.

Mundorff, J.C., 1970. Major thermal springs of Utah: Utah Geol. and Min. Survey, Water Resources Bull. 13, 60 p.

Nie, N.H., Hull, C.H., Jenkins, J.G., Steinbrenaer, K., Bent, D.H. (1975). SPSS Statistical Package for the Social Sciences, 2nd edition: McGraw Hill, N.Y., 675 p.

Nielson, D.L., Radon emanometry as a geothermal exploration technique; theory and an example from Roosevelt Hot Springs KGRA, Utah. IDO/78-1701.6.1.12, ESC-14, 31 p.

Nielson, D.L., Sibbett, B.S., McKinney, D.B., Hulen, J.B., Moore, J.N. and Samberg, S.M., 1978. Geology of Roosevelt Hot Springs KGRA, Earth Science Laboratory, Univ. of Utah Research Institute, Salt Lake City, Utah.

Nolan, T.B., 1943. The Basin and Range province in Utah, Nevada and California: U.S. Geol. Survey Prof. Paper 197-D, p. 141-196.

Parry, W.T., Ward, S.H., Nash, W.P. and others, 1977. Part I - Geology and geochemistry of the Roosevelt Hot Springs - A Summary: UURI Final vol. 77-2, 19 p.

Parry, W.T., Bryant N.L., Dedolph, R.E., Ballantyne, J.M., Ballantyne, G.H., Rohrs, D.T. and Mason, J.L., 1978. Hydrothermal alteration at the Roosevelt Hot Springs thermal area, Utah. IDO 78-1701.a.11, p. 29.

Pentcheva, E., 1965. The distribution of rare and disposed elements in Bulgarian saline underground waters. Compt. Rend. Acad. Bulgare Sci. 18 (2), 149-151.

Petersen, C.A., 1974. Geology of the Roosevelt Hot Springs Area, Beaver County, Utah: Utah Geology, v. 2, no. 2, 9. 109-116.

Phelps, P.W., and Buseck, P.R., 1978. Mercury in soils as an indicator of geothermal activity. 71st Int. Expl.'Geochem. Symposium. 1978, 153-160.

Prodehl, C., 1970. Seismic refraction study of crustal structure in the western United States: Geol. Soc. Amer. Bull., v. 81, p. 2629-2646.

Ritchie, J.A., 1961. Arsenic and Antimony in some New Zealand thermal waters. New Zealand J. Sci. 4, 218.

Rowley, P.D., Lipman, P.W., Mehnert, H.H., Lindsey, D.A. and Anderson, J.J., 1978. Blue Ribbon lineament, an east-trending structural zone within the Pioche mineral belt of southwestern Utah and eastern Nevada: Jour. Research U.S. Geol. Survey, v. 6, no. 2, p. 175-192.

Rowley, P.D., Anderson, J.J., Williams, P.L., and Fleck, R.J., 1977. Age of structural differentiation between the Colorado Plateaus and Basin and Range provinces in southwestern Utah: Geology.

Roberts, R.J., 1964. Economic geology, in "Mineral and water resources of Nevada": U.S. 88th Congress, 2nd session, Senate Doc. 87, p. 73-74.

Rohrs, D.T. and J.R. Bowman, 1980. A light stable isotope study of the Roosevelt Hot Springs thermal area, southwest of Utah: IDO/DOE/ET/28392-46 78-1701.a.1.5, 89 p.

Rose, A.W., Hawkes, H.E. and Webb, J.S., 1979. Geochemistry in mineral exploration. Academic Press. London, 657 p.

Roy, R.F., Decker, E.R., Blackwell, D.D. and Birch, R. Heat flow in the United States: Jour. Geophys. Res., v. 73, p. 5207-5221.

Roy, R.F., Blackwell, D.D. and Decker, E.R., 1971. Continental heat flow, in "Symposium on the nature of the solid earth, McGraw Hill.

Ryall, A. and Stuart, D.J., 1963. Travel times and amplitudes from nuclear explosions, Nevada test site to Ordway, Colorado: Jour. Geophys. Res., v. 68, p. 5821-5835.

Sbar, M.L., Barazangi, M., Dorman, J., Scholz, C.H. and Smith, R.B., 1972. Tectonics of the Intermountain Seismic Belt, Western United States: Microearthquake seismicity and composite fault plane solutions. Geol. Soc. of Amer. Bull., v. 83, p. 13-28.

Shawe, D.R. and Stewart, J.H. 1976. Ore deposits as related to tectonics and magmatism, Nevada and Utah: Am. Inst. Min., Met. and Petr. Engl. Trans., v. 260, p. 225-232.

Sibbett, B.S. and Nielson, D.L., 1980. Geology of the Central Mineral Mountains, Beaver County, Utah, Univ. of Utah Research Institute Rept.: DOE/ET/28392-40, ESL-33, 42 p.

Sill, W.R. and Bodell, J., 1977. Thermal Gradients and Heat Flow at Roosevelt Hot Springs: UURI Test. Rep. vol. 77-3, 46 p.

Smith, S., 1980. A model study of the regional hydrologeologic regime, Roosevelt Hot Springs, Utah: IDO/DOE/ET/28392-44.

Smith, R.B. and Sbar, M., 1974. Contemporary tectonics and seismicity of the Western United States with emphasis on the Intermountain Seismic Belt: Geol. Soc. Amer. Bull. v. 85, p. 1205-1218.

Sreekumaran, C., Pillai, K.C. and Folsom, T.R., 1968. The concentrations of lithium, potassium, rubidium and cesium in some western American rivers and marine sediments: Geochim. Cosmochim. Acta, 26, 685-722.

Stewart, J.H., Moore, W.J. and Zeitz, I., 1977. East-west patterns of Cenozoic igneous rocks, aeromagnetic anomalies, and mineral deposits, Nevada and Utah: Geol. Soc. Amer. Bull. v. 88, no. 1, p. 67-77.

Stokes, W.L., 1973. Stratigraphic problems of the Triassic and Jurassic sedimentary rocks of Central Utah: Utah Geol. Assn. Pub. 3, p. 21-38.

Shuey, R.T., Schellinger, D.K., Johnson, E.G. and Alley, L.B., 1973. Aeromagnetics and the transition between the Colorado Plateau and Basin and Range provinces: Geology, v. 1, p. 107-110.

Thompson, I. and Read, D., 1978.

Tripp, A.C., Ward, S.H., Sill, W.R., Swift, C.M., Jr. and Petrick, W.R., 1978. Electromagnetic and Schlumberger resistivity sounding in the Roosevelt Hot Springs KGRA: Geophysics, v. 43, no. 7, p. 1515-1542.

U.S.G.S. Utah Geological Mining Survey, 1964.

Van Alstine, R.E., 1976. Continental rifts and lineaments associated with major fluorspar districts: Econ. Geol., v. 71, no. 6, p. 977-987,

Walker, G.W., and Osterwald, F.W., 1963. Introduction to the geology of uranium-bearing veins in the conterminous United States, incluyding sections on geographic distribution and classification of veins: U.S. Geol. Survey Prof. Paper 455-A, p. A1-A28.

Ward, S.H., Parry, W.T., Nash, W.P., Sill, W.R., Cook, K.L., Smith, R.B., Chapman, D.S., Brown, F.H., Whelan, J.A. and Bowman, J.R., 1978. A summary of the geology, geochemistry and geophysics of the Roosevelt Hot Springs thermal area, Utah: Geophysics v. 43, no. 7, p. 1515-1542.

Ward, S.H., and Sill, W.R., November, 1976. Dipole-dipole resistivity surveys, Roosevelt Hot Springs KGRA: UURI Final vol. 2, 29 p.

Wedepohl, K.H., 1972. Handbook of Geochemistry. Springer-Verlag, Berlin.

Weissberg, B.G., Browne, P.R.L., and Seward, T.M., 1979. Ore metals in active geothermal systems: in Geochemistry of Hydrothermal Ore Deposits. Barnes, H.L., ed. John Wiley and Sons, New York.

Welsh, J.E., 1973. Geology of the Beaver Lake Mountains, Beaver County, Utah. Utah Geol. Assn. Pub. 3, p. 49-53.

Welsh, J.E., 1973. Paleozoic and Mesozoic stratigraphy of the Milford area, Beaver County, Utah. Utah Geol. Assn. pub. 3, p. 12.

Whelan, J.A., 1973. Geology of the Rocky Range., Beaver County, Utah. Utah Geol. Assn. pub. 3, p. 55-56.

White, D.E., 1965. Saline waters of sedimentary rocks. Am. Assoc. Pet. Geol., Mem 4. (Young and Galley, eds.)

White, D.E., 1967. Mercury and base-metal deposits with associated thermal and mineral waters: in Geochemistry of Hydrothermal Ore Deposits, H.L. Barnes, ed., 1st Ed., New York, Holt, Rhinehart and Winston, p. 575-631.

White, D.E., 1970. Geochemistry applied to the discovery, evaluation and exploitation of geothermal energy resources. Geothermics: Special Issue No. 2. U.N. Symposium on the Development and Utilization of Geothermal Resources, v. sec. 5.

Wilson, W.R. and Chapman, D.S., 1980. Thermal Studies at Roosevelt Hot Springs, Utah: DOE/ID/12079-19, 102 p.

Woodward, L.A., 1973. Upper Precambrian stratigraphy of Central Utah: Utah Geol. Assn. pub. 3.

Woodward, L.A., July, 1968. Lower Cambrian and Upper Precambrian strata of Beaver Mountains, Utah. AAPG Bull., v. 52, no. 7, p. 1279-1290.

Woodward, L.A., 1970. Tectonic implications of structures of Beaver and northern San Francisco Mountains, Utah: Geol. Soc. Amer. Bull., v. 81, p. 1577-1584.

Zietz, I., Shuey, R.T. and Kirby, J.R., Jr., 1976. Aeromagnetic maps of Utah: U.S. Geol. Surv. Geophys. Invest. Map GP-907.

EXPLANATION

QUATERNARY

- Qls — Landslide
- Qs — Opaline and chalcedonic sinter
- Qcal — Silica-cemented alluvium
- Qh — Hematite-cemented alluvium
- Qm — Magnanese oxide-cemented alluvium
- Qal — Alluvium
- Qbc — Basalt
  Lava flows and spatter cones.
- Qrd — Rhyolite Domes
  Glassy, 1-6% phenocrysts, perlite and pumice mantles.
- Qra — Pyroclastics
  Air fall and non-welded ashflow tuff. White to light tan. Weakly consolidated.
- Qrf — Rhyolite Flow
  Non-porphyritic glassy, gray, flow-banded lava and obsidian. Perlitic rubble on flow tops.

TERTIARY

- Tlf — Lava Flows
  Pink to tan, sparsely porphyritic felsite with flow structure.
- Tpr — Porphyritic Rhyolite Dikes
  Resistant, brown to pink dikes containing 20% 2 mm phenocryst in a granophyric matrix.
- Trd — Rhyolite Dikes
  Aphanitic, gray rhyolite dikes with approximately 5% k-feldspar phenocrysts and minor biotite. Often silicified and typically strongly jointed.
- Tds — Diabase Dikes
  Aphanitic, light brown or light gray green, with 3% plagioclase phenocrysts. Typically strongly jointed.
- Tmd — Microdiorite Dikes
  Dark green, dark gray, or black fine-grained dikes, plagioclase phenocrysts often present.
- Tgr — Granite Dikes
  Fine-grained phaneritic, resistant, dark brown, closely joined outcrops, forming blocky to rounded talus. Joints are typically limonite-stained. Unlabeled dikes are Tgr.
- Tg — Granite
  Coarse- to medium-grained, leucocratic with large quartz grains. Forms massive rounded outcrops, weathers to grus.
- Ts — Syenite
  Medium-grained, xenomorphic, with 1 to 3% sphene. Forms white or very light brown stained, massive, rounded outcrops, weathers to grus.
- Tbg — Biotite Granite
  Coarse- to medium-grained, forms massive, rounded outcrops and weathers to grus. Porphyritic in NW contact zone.
- Tfi — Porphyritic Quartz Monzonite
  Medium-grained, biotite-rich with 1 cm feldspar phenocrysts. Forms resistant, massive outcrops.
- Tqm — Quartz Monzonite
  Coarse-grained, massive, rounded, light brown outcrops. Flow foliation and mafic xenoliths typical in the contact zone. Forms some talus in the contact zone, but weathers to grus in the interior of the pluton.
- Tdb — Diorite Breccia
  Fine- to medium-grained intrusive breccia with abundant biotite and hornblende. Forms dark colored outcrops or weathers to fine, brown soil.
- Td — Diorite
  Fine- to medium-grained biotite and hornblende diorite. Forms dark gray outcrops.
- Tv — Porphyritic Adesite Flow
  Greenish gray to brown; propylitized; 2 mm plagioclase laths.

AGE UNCERTAIN

- hd — Hornblende Granodiorite
  Medium-grained, weakly foliated in some outcrops. Forms grus-covered slopes.
- gd — Biotite Granodiorite
  Highly variable biotite and biotite-hornblende granodiorite. Typically massive to weakly foliated, dark colored, sphene-rich and fine-to medium-grained. Non-resistant, forming dark micaceous soil.
- hgn — Hornblende Gneiss
  Medium-grained gneissic hornblende quartz monzonite. Forms resistant outcrops.
- qtzt — Quartzite
  White, yellow to red, massive, medium- to fine-grained quartzite. Small scale cross bedding in some outcrops.
- phl — Phyllite
  Dark brown to red, thinly bedded argillite.
- dol/ls — Dolomite and Limestone
  Light to dark gray, massive to thick bedded.
- dm — Dolomitic Marble
  White or yellow to medium gray, friable.
- mbl — Marble
  Light- to medium-gray, generally massive.

MISS.

- Mrd / Mrls — Redwall Limestone
  Light- to medium-gray dolomite (Mrd) and limestone (Mrls), massive to thick bedded with a few pink to tan argillaceous zones.

CAMBR.

- Cmb — Marble
  Light- to medium-gray marble, undifferentiated Cambrian carbonate rocks.

PRECAMBRIAN

- pEs — Sillimanite Schist
  Dark gray to green, fine-grained, finely laminated schist containing abundant biotite, fibrolitic sillimanite, and minor garnet porphyroblasts.
- pEq — Quartzite
  White, bedded metaquartzite containing minor biotite and feldspar.
- pEbg — Banded Gneiss
  Gray to white, conspicuously layered biotite gneiss, schist and migmatite. Highly variable in composition. Well developed isoclinal and ptygmatic folding.

- Contact, dashed where approximate.
- Fault, intruded by microdiorite dike.
- Fault, dashed where inferred, dotted where covered. Breccia zones shown where mappable.
- Fault, mapped from linears on aerial photos, may have some topographic relief.

PLATE 1 GEOLOGY OF ROOSEVELT SPRINGS AREA

Plate 2

PHASE II SOIL & SURFACE
MICROLAYER SAMPLE SITES

APPENDIX A

COMPARATIVE STATISTICS, SOIL AND SURTRACE RESULTS - PHASE II SAMPLING

FIRST PASS STATISTICS

	VARIABLE	MEAN	SD	MIN	MAX	RANGE
SURTRACE	AL	.114E+02	.112E+01	.801E+01	.142E+02	.630E+01
	FE	.438E+01	.797E+00	.251E+01	.669E+01	.418E+01
	CA	.247E+01	.109E+01	.153E+01	.650E+01	.497E+01
	MG	.166E+01	.422E+00	.864E+00	.325E+01	.239E+01
	TI	.727E+00	.144E+00	.373E+00	.111E+01	.737E+00
	MN	.111E+00	.210E-01	.484E-01	.156E+00	.110E+00
	NA	.221E+01	.411E+00	.121E+01	.360E+01	.239E+01
	K	.274E+01	.240E+00	.202E+01	.343E+01	.145E+01
	P	.258E+00	.836E-01	.110E+00	.580E+00	.470E+00

	VARIABLE	MEAN	SD	MIN	MAX	RANGE
SOILS	AL	.114E+02	.140E+01	.724E+01	.149E+02	.793E+01
	FE	.449E+01	.972E+00	.222E+01	.734E+01	.512E+01
	CA	.318E+01	.276E+01	.114E+01	.146E+02	.135E+02
	MG	.168E+01	.474E+00	.668E+00	.371E+01	.304E+01
	TI	.720E+00	.172E+00	.388E+00	.136E+01	.972E+00
	MN	.995E-01	.233E-01	.386E-01	.144E+00	.105E+00
	NA	.199E+01	.455E+00	.106E+01	.345E+01	.239E+01
	K	.266E+01	.318E+00	.173E+01	.315E+01	.142E+01
	P	.229E+00	.865E-01	.900E-01	.580E+00	.490E+00

SECOND PASS STATISTICS

	VARIABLE	MEAN	SD	MIN	MAX	RANGE
SURTRACE	AL	.114E+02	.112E+01	.801E+01	.142E+02	.630E+01
	FE	.438E+01	.797E+00	.251E+01	.669E+01	.418E+01
	CA	.245E+01	.101E+01	.153E+01	.573E+01	.420E+01
	MG	.166E+01	.405E+00	.864E+00	.293E+01	.207E+01
	TI	.727E+00	.144E+00	.373E+00	.111E+01	.737E+00
	MN	.111E+00	.210E-01	.484E-01	.156E+00	.110E+00
	NA	.221E+01	.404E+00	.121E+01	.344E+01	.223E+01
	K	.274E+01	.240E+00	.202E+01	.343E+01	.145E+01
	P	.257E+00	.799E-01	.110E+00	.509E+00	.399E+00

	VARIABLE	MEAN	SD	MIN	MAX	RANGE
SOILS	AL	.114E+02	.140E+01	.724E+01	.149E+02	.793E+01
	FE	.449E+01	.972E+00	.222E+01	.734E+01	.512E+01
	CA	.314E+01	.258E+01	.114E+01	.115E+02	.103E+02
	MG	.167E+01	.441E+00	.668E+00	.311E+01	.244E+01
	TI	.718E+00	.165E+00	.388E+00	.124E+01	.847E+00
	MN	.995E-01	.233E-01	.386E-01	.144E+00	.105E+00
	NA	.199E+01	.450E+00	.106E+01	.335E+01	.229E+01
	K	.266E+01	.318E+00	.173E+01	.315E+01	.142E+01
	P	.227E+00	.816E-01	.900E-01	.488E+00	.398E+00

FIRST PASS STATISTICS

SURTRACE

VARIABLE	MEAN	SD	MIN	MAX	RANGE
AS	.415E+01	.194E+01	.220E+01	.182E+02	.160E+02
SE	.717E-01	.174E-01	.400E-01	.140E+00	.100E+00
LI	.296E+02	.581E+01	.190E+02	.580E+02	.390E+02
RB	.947E+02	.159E+02	.600E+02	.136E+03	.760E+02
CS	.552E+01	.439E+01	.400E+01	.400E+02	.360E+02
SB	.185E+00	.104E+00	.100E+00	.920E+00	.820E+00
HG	.306E+02	.119E+02	.700E+01	.710E+02	.640E+02
V	.710E+02	.142E+02	.359E+02	.121E+03	.851E+02
ZN	.855E+02	.174E+02	.420E+02	.120E+03	.780E+02

SOILS

VARIABLE	MEAN	SD	MIN	MAX	RANGE
AS	.386E+01	.112E+01	.220E+01	.780E+01	.560E+01
SE	.980E-01	.386E-01	.500E-01	.330E+00	.280E+00
LI	.306E+02	.853E+01	.150E+02	.670E+02	.520E+02
RB	.945E+02	.190E+02	.510E+02	.138E+03	.870E+02
CS	.506E+01	.173E+01	.200E+01	.130E+02	.110E+02
SB	.240E+00	.914E-01	.100E+00	.600E+00	.500E+00
HG	.352E+02	.465E+02	.400E+01	.368E+03	.364E+03
V	.738E+02	.160E+02	.479E+02	.139E+03	.911E+02
ZN	.851E+02	.198E+02	.350E+02	.141E+03	.106E+03

SECOND PASS STATISTICS

SURTRACE

VARIABLE	MEAN	SD	MIN	MAX	RANGE
AS	.403E+01	.114E+01	.220E+01	.996E+01	.776E+01
SE	.713E-01	.156E-01	.400E-01	.124E+00	.838E-01
LI	.295E+02	.512E+01	.190E+02	.471E+02	.281E+02
RB	.947E+02	.159E+02	.600E+02	.136E+03	.760E+02
CS	.521E+01	.200E+01	.400E+01	.187E+02	.147E+02
SB	.179E+00	.652E-01	.100E+00	.498E+00	.398E+00
HG	.306E+02	.117E+02	.700E+01	.664E+02	.594E+02
V	.708E+02	.139E+02	.359E+02	.114E+03	.777E+02
ZN	.855E+02	.174E+02	.420E+02	.120E+03	.780E+02

SOILS

VARIABLE	MEAN	SD	MIN	MAX	RANGE
AS	.385E+01	.109E+01	.220E+01	.722E+01	.502E+01
SE	.963E-01	.299E-01	.500E-01	.214E+00	.164E+00
LI	.303E+02	.729E+01	.150E+02	.562E+02	.412E+02
RB	.945E+02	.190E+02	.510E+02	.138E+03	.870E+02
CS	.501E+01	.153E+01	.200E+01	.102E+02	.825E+01
SB	.239E+00	.869E-01	.100E+00	.514E+00	.414E+00
HG	.324E+02	.285E+02	.400E+01	.175E+03	.171E+03
V	.736E+02	.151E+02	.479E+02	.122E+03	.740E+02
ZN	.851E+02	.198E+02	.350E+02	.141E+03	.106E+03

FIRST PASS STATISTICS

	VARIABLE	MEAN	SD	MIN	MAX	RANGE
SURTRACE	BE	.228E+01	.562E+00	.140E+01	.400E+01	.260E+01
	CR	.260E+02	.524E+01	.117E+02	.464E+02	.347E+02
	CO	.164E+02	.535E+01	.500E+01	.270E+02	.220E+02
	CU	.186E+02	.434E+01	.123E+02	.384E+02	.261E+02
	PB	.246E+02	.607E+01	.100E+02	.550E+02	.450E+02
	NI	.204E+02	.426E+01	.120E+02	.360E+02	.240E+02
	SR	.246E+03	.341E+02	.207E+03	.356E+03	.149E+03
	TH	.338E+02	.106E+02	.180E+02	.770E+02	.590E+02
	ZR	.774E+02	.933E+01	.494E+02	.960E+02	.470E+02

	VARIABLE	MEAN	SD	MIN	MAX	RANGE
SOILS	BE	.231E+01	.603E+00	.120E+01	.400E+01	.280E+01
	CR	.289E+02	.587E+01	.113E+02	.474E+02	.382E+02
	CO	.676E+01	.347E+01	.300E+01	.190E+02	.160E+02
	CU	.184E+02	.451E+01	.890E+01	.338E+02	.249E+02
	PB	.151E+02	.569E+01	.500E+01	.350E+02	.300E+02
	NI	.208E+02	.611E+01	.110E+02	.460E+02	.350E+02
	SR	.241E+03	.401E+02	.185E+03	.387E+03	.202E+03
	TH	.356E+02	.190E+02	.160E+02	.138E+03	.122E+03
	ZR	.708E+02	.101E+02	.420E+02	.950E+02	.530E+02

SECOND PASS STATISTICS

	VARIABLE	MEAN	SD	MIN	MAX	RANGE
SURTRACE	BE	.228E+01	.560E+00	.140E+01	.396E+01	.256E+01
	CR	.260E+02	.499E+01	.117E+02	.418E+02	.301E+02
	CO	.164E+02	.535E+01	.500E+01	.270E+02	.220E+02
	CU	.185E+02	.394E+01	.123E+02	.316E+02	.193E+02
	PB	.245E+02	.529E+01	.100E+02	.428E+02	.328E+02
	NI	.204E+02	.408E+01	.120E+02	.332E+02	.212E+02
	SR	.246E+03	.336E+02	.207E+03	.349E+03	.142E+03
	TH	.336E+02	.987E+01	.180E+02	.658E+02	.478E+02
	ZR	.774E+02	.933E+01	.494E+02	.960E+02	.470E+02

	VARIABLE	MEAN	SD	MIN	MAX	RANGE
SOILS	BE	.231E+01	.603E+00	.120E+01	.400E+01	.280E+01
	CR	.289E+02	.583E+01	.114E+02	.465E+02	.373E+02
	CO	.673E+01	.339E+01	.300E+01	.172E+02	.142E+02
	CU	.184E+02	.442E+01	.890E+01	.319E+02	.230E+02
	PB	.151E+02	.555E+01	.500E+01	.322E+02	.272E+02
	NI	.207E+02	.574E+01	.110E+02	.391E+02	.281E+02
	SR	.241E+03	.388E+02	.185E+03	.362E+03	.177E+03
	TH	.349E+02	.160E+02	.160E+02	.926E+02	.766E+02
	ZR	.708E+02	.101E+02	.420E+02	.950E+02	.530E+02

FIRST PASS STATISTICS

	VARIABLE	MEAN	SD	MIN	MAX	RANGE
SURTRACE	F-	.287E+01	.115E+01	.120E+01	.760E+01	.640E+01
	NO3-	.443E+02	.454E+02	.550E+01	.204E+03	.198E+03
	SO4=	.462E+02	.779E+02	.102E+02	.668E+03	.658E+03
	CL-	.386E+02	.145E+02	.106E+02	.805E+02	.699E+02

	VARIABLE	MEAN	SD	MIN	MAX	RANGE
SOILS	F-	.290E+01	.183E+01	.700E+00	.103E+02	.960E+01
	NO3-	.198E+02	.542E+02	.500E+00	.449E+03	.448E+03
	SO4=	.394E+01	.319E+01	.200E+00	.147E+02	.145E+02
	CL-	.806E+01	.374E+02	.200E+00	.313E+03	.313E+03

SECOND PASS STATISTICS

	VARIABLE	MEAN	SD	MIN	MAX	RANGE
SURTRACE	F-	.285E+01	.108E+01	.120E+01	.632E+01	.512E+01
	NO3-	.440E+02	.443E+02	.550E+01	.181E+03	.175E+03
	SO4=	.406E+02	.328E+02	.102E+02	.280E+03	.270E+03
	CL-	.386E+02	.145E+02	.106E+02	.805E+02	.699E+02

	VARIABLE	MEAN	SD	MIN	MAX	RANGE
SOILS	F-	.287E+01	.173E+01	.700E+00	.838E+01	.768E+01
	NO3-	.160E+02	.247E+02	.500E+00	.182E+03	.182E+03
	SO4=	.390E+01	.306E+01	.200E+00	.135E+02	.133E+02
	CL-	.530E+01	.145E+02	.200E+00	.120E+03	.120E+03

APPENDIX B

TRAVERSE PROFILES -

PHASE II SAMPLING

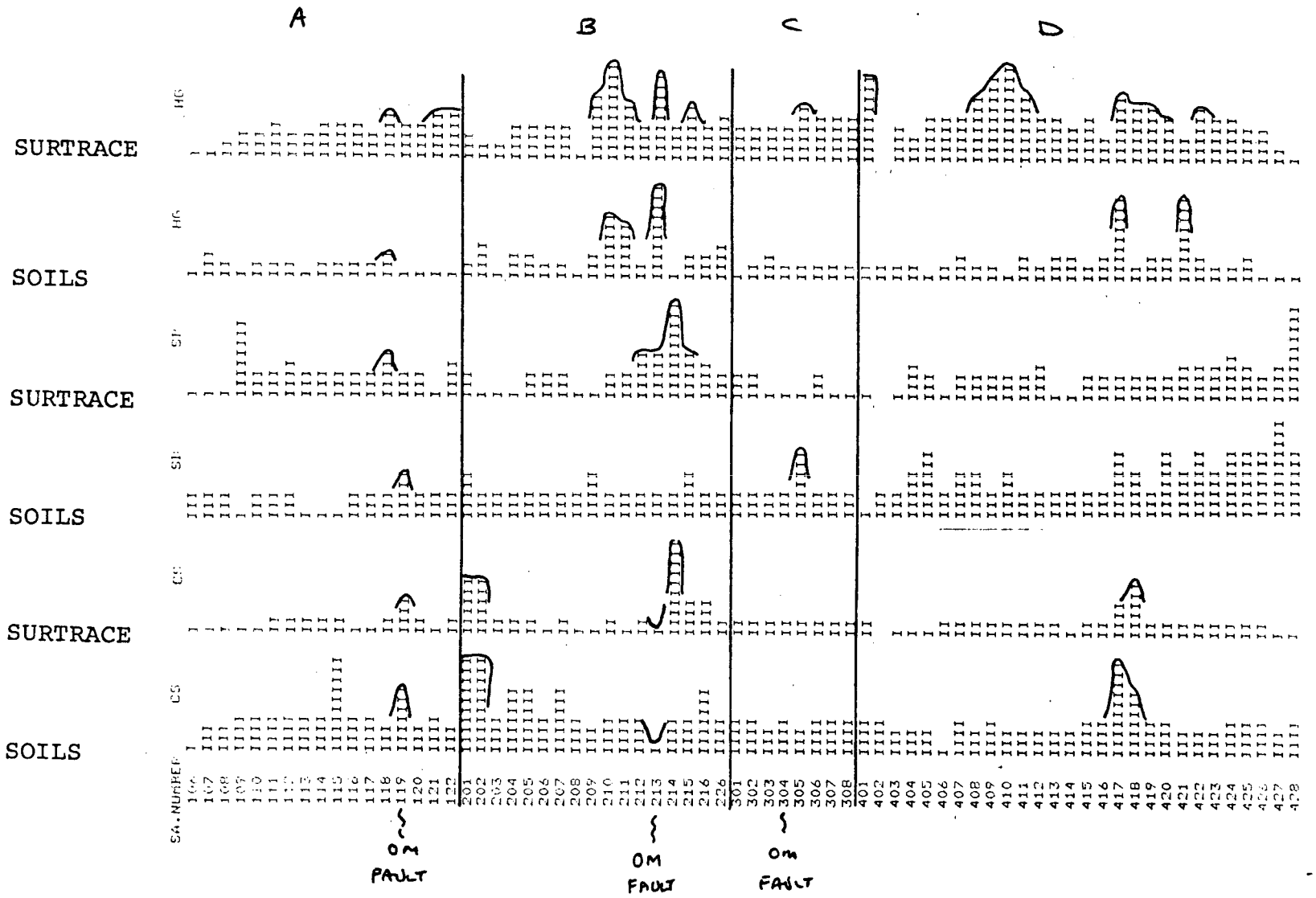
A
B
C
D
SURTRACE
SOILS
SURTRACE
SOILS
SURTRACE
SOILS
SA. NUMBER
OM
FAULT
OM
FAULT
OM
FAULT

A
B
C
D
SURTRACE
SOILS
SURTRACE
SOILS
SURTRACE
SOILS
SA. NUMBER
OM
FAULT
OM
FAULT
OM
FAULT

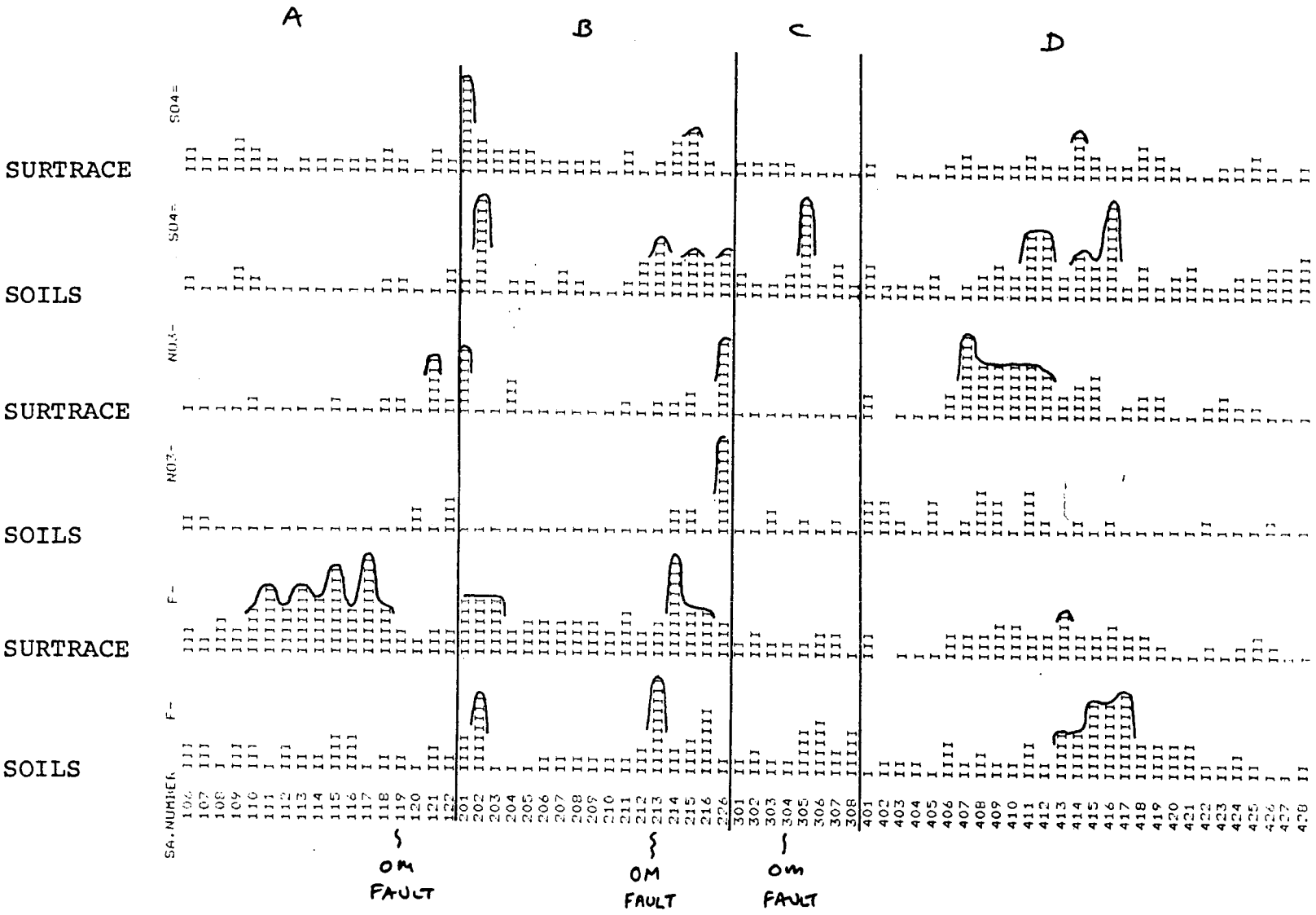
A
B
C
D
SURTRACE
SOILS
SURTRACE
SOILS
SURTRACE
SOILS
SO4=
SO4=
NO3-
NO3-
F-
F-
SA. NUMBER
OM
FAULT
OM
FAULT
OM
FAULT

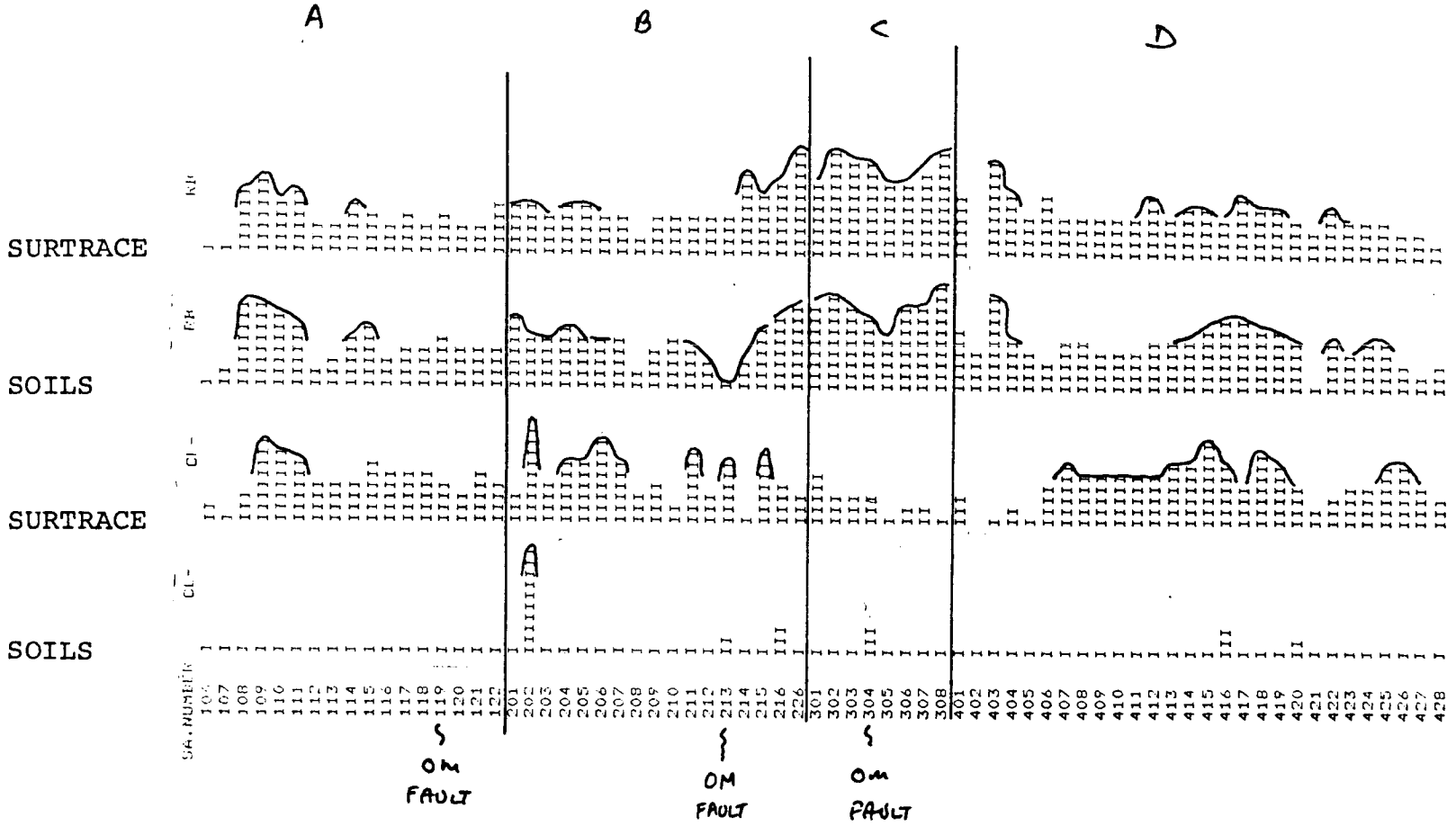
A
B
C
D
SURTRACE
SOILS
SURTRACE
SOILS
OM FAULT
OM FAULT
OM FAULT

A
B
C
D
SURTRACE
SOILS
SURTRACE
SOILS
SURTRACE
SOILS
SA. NUMBER
AL
FE
CA
OM
FAULT
OM
FAULT
OM
FAULT

A
B
C
D
SURTRACE
SOILS
SURTRACE
SOILS
SURTRACE
SOILS
OM
FAULT
OM
FAULT
OM
FAULT

A
B
C
D
SURTRACE
SOILS
SURTRACE
SOILS
SURTRACE
SOILS
OM
FAULT
OM
FAULT
OM
FAULT

A
B
C
D
SURTRACE
SOILS
SURTRACE
SOILS
SURTRACE
SOILS
SA. NUMBER
OM
FAULT
OM
FAULT
OM
FAULT

A
B
C
D
SURTRACE
SOILS
SURTRACE
SOILS
SURTRACE
SOILS
SA.NUMBER
ZK
TH
SK
OM
FAULT
OM
FAULT
OM
FAULT

A
B
C
D
SURTRACE
SOILS
SURTRACE
SOILS
SURTRACE
SOILS
SA.NUMBER
CU
FB
NI
OM
FAULT
OM
FAULT
OM
FAULT

A
B
C
D
SURTRACE
SOILS
SURTRACE
SOILS
SA.NUMBER
OM
FAULT
OM
FAULT
OM
FAULT

VARIABLE	MEAN	SD	MIN	MAX	RANGE
RAD	.701E+01	.207E+02	-.793E+02	.717E+02	.151E+03
TEMP	.356E+02	.314E+01	.300E+02	.480E+02	.180E+02

VARIABLE	MEAN	SD	MIN	MAX	RANGE
RAD	.697E+01	.206E+02	-.549E+02	.692E+02	.149E+03
TEMP	.356E+02	.297E+01	.300E+02	.451E+02	.151E+02

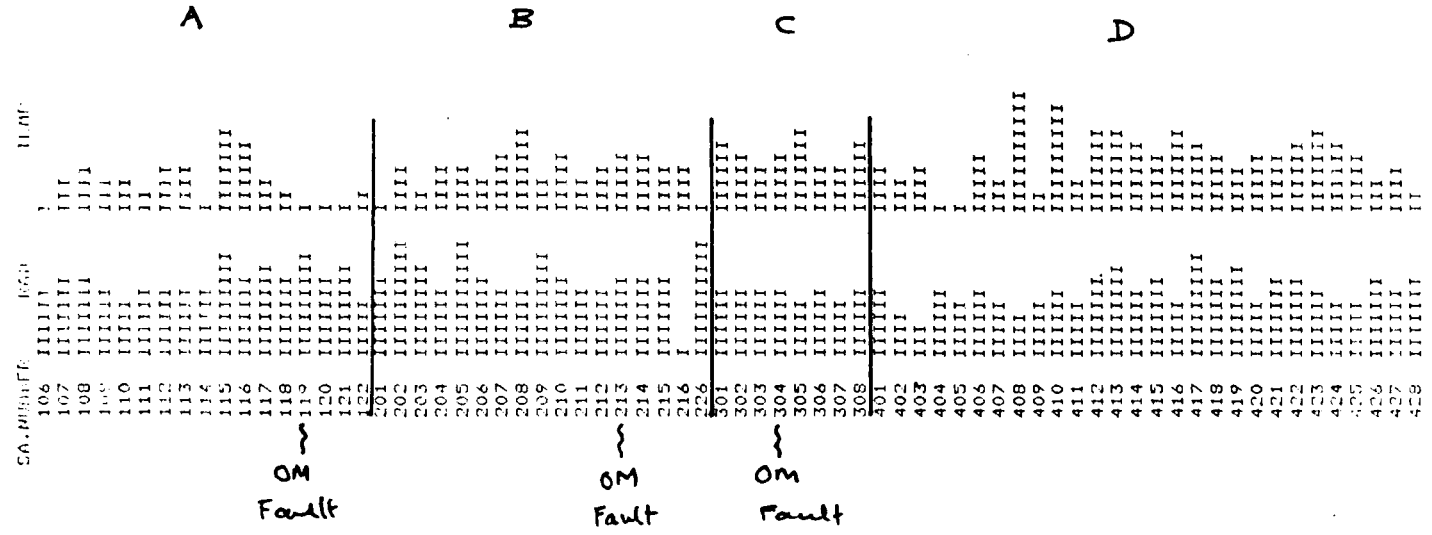

APPENDIX C

CORRELATION MATRIX

1FACTOR ANALYSIS OF DOE SURTRACE DATA 09/03/80. ,PAGE 4

FILE ROOSEVEL (CREATION DATE = 09/03/80.) SPRINGS GEOTHERMAL AREA,UTAH

CORRELATION COEFFICIENTS..

	AS	SE	LI	RB	SB	HG	SR	TH	CS	F
AS	1.00000	.35450	.21825	.03641	.12295	.18993	.30643	.08911	.31585	.11669
SE	.35450	1.00000	.18404	.07367	.13852	.07741	.13436	.03025	.09905	.11062
LI	.21825	.18404	1.00000	.62579	-.11894	-.04903	.16919	.07123	.31141	.07529
RB	.03641	.07367	.62579	1.00000	-.08751	.02556	-.07972	.16706	.25519	-.06845
SB	.12295	.13852	-.11894	-.08751	1.00000	.05501	-.01575	-.07647	.47361	-.00422
HG	.18993	.07741	-.04903	.02556	.05501	1.00000	-.03103	.26713	-.03057	-.11838
SR	.30643	.13436	.16919	-.07972	-.01575	-.03103	1.00000	-.07879	.10311	.09166
TH	.08911	.03025	.07123	.16706	-.07647	.26713	-.07879	1.00000	-.08202	-.07739
CS	.31585	.09905	.31141	.25519	.47361	-.03057	.10311	-.08202	1.00000	.12734
F	.11669	.11062	.07529	-.06845	-.00422	-.11838	.09166	-.07739	.12734	1.00000
NO3	.27953	.12262	.12208	-.01559	-.02135	-.04172	.41764	-.05329	.01094	.05433
SO4	.11827	.09293	.13157	.02255	-.13543	.09382	.29154	-.01059	-.03798	-.01215
CL	.28857	.16578	.07868	-.09013	-.03041	-.02449	.93377	-.02623	-.02326	.09093
CR	.04746	.08189	.01092	-.00442	-.06082	-.00074	-.02179	-.00931	-.02381	-.01801
CO	.00913	-.03085	.17837	.04427	-.05840	.06163	.11228	.16228	.05521	-.10924
CU	.14081	.16135	.31199	.18475	-.14388	.13572	.12013	-.05168	-.03173	.01036
PB	.07690	.07379	.29110	.31816	-.14950	.23100	-.06672	.38764	-.10333	-.07632
NI	.04893	.08093	.02013	-.01208	-.04508	-.00820	-.00398	-.02045	.00732	-.01630
ZN	.14004	.12693	.24393	.23807	-.16666	.29075	.01730	.25997	-.13996	-.16819
BE	-.14862	-.01072	.28835	.60897	-.10020	.00269	-.15389	.41332	-.14380	-.03086
ZR	-.15363	-.07478	-.10250	-.18813	.08125	-.35716	-.17402	-.16026	.02137	.13368
V	-.08477	-.16868	-.06727	-.02616	-.12398	.09734	.04464	.11532	-.13111	-.15042
BA	.13791	-.00535	.04363	-.00513	.02434	.21442	.04871	.02236	.09951	-.14829
B	.10303	-.10684	.10402	.17223	-.08739	.18460	.24024	.10386	.00960	-.19554
AL	-.20757	-.10163	.11799	.38956	-.26931	.11922	-.24087	.23180	-.28683	-.23675
FE	-.00847	-.10689	-.03833	.05714	-.13196	.22371	-.02053	.31849	-.15280	-.19451
CA	.33449	.24006	.34556	-.07964	.12016	-.12390	.54405	-.15900	.35726	.22577
MG	.27393	.23578	.35036	.02369	-.08907	-.02312	.44402	-.14230	.02228	.06299
TI	-.05164	-.16344	-.04324	.08523	-.15408	.22282	-.03880	.21824	-.16437	-.26031
MN	.14980	.13999	.34672	.36722	-.15337	.22547	.02814	.23850	-.06317	-.21981
NA	-.29336	-.25961	-.01767	.29982	-.24746	.04555	-.14111	.21101	-.22868	-.21640
K	-.14649	.04022	.21860	.43353	-.08096	.00623	-.13670	.07809	-.08858	-.19470
P	.13679	.02567	.22394	.18592	-.15804	.22160	.16774	.15013	-.09914	-.19874
SI	-.31372	-.21153	-.42981	-.18358	.03028	-.16002	-.44766	-.17820	-.17387	-.04184

FILE ROOSEVEL (CREATION DATE = 09/03/80.) SPRINGS GEOTHERMAL AREA,UTAH

	NO3	SO4	CL	CR	CO	CU	PB	NI	ZN	BE
AS	.27953	.11827	.28857	.04746	.00913	.14081	.07690	.04893	.14004	-.14862
SE	.12262	.09293	.16578	.08189	-.03085	.16135	.07379	.08093	.12693	-.01072
LI	.12208	.13157	.07868	.01092	.17837	.31199	.29110	.02013	.24393	.28835
RB	-.01559	.02255	-.09013	-.00442	.04427	.18475	.31816	-.01208	.23807	.60897
SB	-.02135	-.13543	-.03041	-.06082	-.05840	-.14388	-.14950	-.04508	-.16666	-.10020
HG	-.04172	.09382	-.02449	-.00074	.06163	.13572	.23100	-.00820	.29075	.00269
SR	.41764	.29154	.93377	-.02179	.11228	.12013	-.06672	-.00398	.01730	-.15389
TH	-.05329	-.01059	-.02623	-.00931	.16228	-.05168	.38764	-.02045	.25997	.41332
CS	.01094	-.03798	-.02326	-.02381	.05521	-.03173	-.10333	.00732	-.13996	-.14380
F	.05433	-.01215	.09093	-.01801	-.10924	.01036	-.07632	-.01630	-.16819	-.03086
NO3	1.00000	.31499	.45113	-.02374	-.06715	.07684	-.05421	-.00512	-.04955	-.06615
SO4	.31499	1.00000	.27434	.04938	.13342	.27854	.15781	.04110	.27564	-.05111
CL	.45113	.27434	1.00000	-.02087	.01311	.01043	-.02256	-.00820	-.01364	-.07152
CR	-.02374	.04938	-.02087	1.00000	.27181	.28558	.04843	.98314	.10641	-.00634
CO	-.06715	.13342	.01311	.27181	1.00000	.45252	.12729	.27233	.34208	-.11797
CU	.07684	.27854	.01043	.28558	.45252	1.00000	.32292	.25774	.63248	-.06151
PB	-.05421	.15781	-.02256	.04843	.12729	.32292	1.00000	.04162	.60427	.36539
NI	-.00512	.04110	-.00820	.98314	.27233	.25774	.04162	1.00000	.07756	-.02688
ZN	-.04955	.27564	-.01364	.10641	.34208	.63248	.60427	.07756	1.00000	.08430
BE	-.06615	-.05111	-.07152	-.00634	-.11797	-.06151	.36539	-.02688	.08430	1.00000
ZR	.10543	-.25701	-.05619	-.01904	-.05609	-.33116	-.23775	.00170	-.42702	-.11302
V	-.08584	.08644	-.08806	.10562	.54506	.53265	.00227	.07204	.38197	-.10651
BA	-.07632	.06730	-.14335	.03615	.30120	.24124	.17850	.01621	.44654	-.25518
B	.07789	.16037	.16638	.07595	.28557	.33781	.15940	.04253	.41614	.00476
AL	-.17296	.06747	-.21009	.13053	.23547	.28818	.39932	.08915	.53824	.51716
FE	-.14765	.08177	-.11397	.17197	.51305	.49288	.13442	.12890	.52983	.03613
CA	.30082	.13422	.35755	-.03749	-.03222	.06480	-.16127	.02121	-.18252	-.27595
MG	.28271	.20118	.33554	.08344	.38187	.63247	-.00549	.08023	.40399	-.26281
TI	-.14957	.08291	-.13674	.09593	.48540	.43171	.15160	.07078	.64988	-.02358
MN	-.04867	.26679	-.00576	.06812	.29679	.40199	.52530	.03249	.80681	.12404
NA	-.10753	.04459	-.14898	.01584	.09022	.03428	.28615	.00579	.38419	.46493
K	.05099	.01878	-.10601	.01300	.07497	.11674	.30485	-.01258	.33249	.33680
P	-.00391	.23382	.05538	.07726	.43085	.54076	.32817	.06182	.80460	-.04751
SI	-.19362	-.33569	-.30996	-.08900	-.38041	-.49972	-.28631	-.11179	-.45137	.02958

	ZR	V	BA	B	AL	FE	CA	MG	TI	MN
AS	-.15363	-.08477	.13791	.10303	-.20757	-.00847	.33449	.27393	-.05164	.14980
SE	-.07478	-.16868	-.00535	-.10684	-.10163	-.10689	.24006	.23578	-.16344	.13999
LI	-.10250	-.06727	.04363	.10402	.11799	-.03833	.34556	.35036	-.04324	.34672
RB	-.18813	-.02616	-.00513	.17223	.38956	.05714	-.07964	.02369	.08523	.36722
SB	.08125	-.12398	.02434	-.08739	-.26931	-.13196	.12016	-.08907	-.15408	-.15337
HG	-.35716	.09734	.21442	.18460	.11922	.22371	-.12390	-.02312	.22282	.22547
SR	-.17402	.04464	.04871	.24024	-.24087	-.02053	.54405	.44402	-.03880	.02814
TH	-.16026	.11532	.02236	.10386	.23180	.31849	-.15900	-.14230	.21824	.23850
CS	.02137	-.13111	.09951	.00960	-.28683	-.15280	.35726	.02228	-.16437	-.06317
F	.13368	-.15042	-.14829	-.19554	-.23675	-.19451	.22577	.06299	-.26031	-.21981

FILE ROOSEVEL (CREATION DATE = 09/03/80.) SPRINGS GEOTHERMAL AREA,UTAH

	ZR	V	BA	B	AL	FE	CA	MG	TI	MN
NO3	.10543	-.08584	-.07632	.07789	-.17296	-.14765	.30082	.28271	-.14957	-.04867
SO4	-.25701	.08644	.06730	.16037	.06747	.08177	.13422	.20118	.08291	.26679
CL	-.05619	-.08806	-.14335	.16638	-.21009	-.11397	.35755	.33554	-.13674	-.00576
CR	-.01904	.10562	.03615	.07595	.13053	.17197	-.03749	.08344	.09593	.06812
CO	-.05609	.54506	.30120	.28557	.23547	.51305	-.03222	.38187	.48540	.29679
CU	-.33116	.53265	.24124	.33781	.28818	.49288	.06480	.63247	.43171	.40199
PB	-.23775	.00227	.17850	.15940	.39932	.13442	-.16127	-.00549	.15160	.52530
NI	.00170	.07204	.01621	.04253	.08915	.12890	.02121	.08023	.07078	.03249
ZN	-.42702	.38197	.44654	.41614	.53824	.52983	-.18252	.40399	.64988	.80681
BE	-.11302	-.10651	-.25518	.00476	.51716	.03613	-.27595	-.26281	-.02358	.12404
ZR	1.00000	-.13515	-.28703	-.39799	-.17439	-.26376	-.12047	-.09157	-.32028	-.44085
V	-.13515	1.00000	.34688	.34552	.39031	.91026	-.21439	.53539	.78880	.21603
BA	-.28703	.34688	1.00000	.33975	.26055	.41035	-.03524	.21496	.52356	.56072
B	-.39799	.34552	.33975	1.00000	.25580	.37177	-.09845	.20635	.47787	.45671
AL	-.17439	.39031	.26055	.25580	1.00000	.53980	-.60320	.06343	.61606	.50494
FE	-.26376	.91026	.41035	.37177	.53980	1.00000	-.29047	.44619	.86767	.38292
CA	-.12047	-.21439	-.03524	-.09845	-.60320	-.29047	1.00000	.34771	-.34035	-.18289
MG	-.09157	.53539	.21496	.20635	.06343	.44619	.34771	1.00000	.38350	.25262
TI	-.32028	.78880	.52356	.47787	.61606	.86767	-.34035	.38350	1.00000	.55278
MN	-.44085	.21603	.56072	.45671	.50494	.38292	-.18289	.25262	.55278	1.00000
NA	-.30448	.21227	.17325	.29768	.78546	.33592	-.44854	-.18217	.53690	.38348
K	-.03067	.09741	.33405	.21574	.63229	.18821	-.38961	.07503	.30387	.49423
P	-.43047	.58760	.57599	.48505	.46440	.67527	-.06204	.59138	.82017	.74254
SI	.32701	-.24649	-.17980	-.24269	-.02743	-.27192	-.49820	-.53425	-.25529	-.34503

	NA	K	P	SI
AS	-.29336	-.14649	.13679	-.31372
SE	-.25961	.04022	.02567	-.21153
LI	-.01767	.21860	.22394	-.42981
RB	.29982	.43353	.18592	-.18358
SB	-.24746	-.08096	-.15804	.03028
HG	.04555	.00623	.22160	-.16002
SR	-.14111	-.13670	.16774	-.44766
TH	.21101	.07809	.15013	-.17820
CS	-.22868	-.08858	-.09914	-.17387
F	-.21640	-.19470	-.19874	-.04184
NO3	-.10753	.05099	-.00391	-.19362
SO4	.04459	.01878	.23382	-.33569
CL	-.14898	-.10601	.05538	-.30996
CR	.01584	.01300	.07726	-.08900
CO	.09022	.07497	.43085	-.38041
CU	.03428	.11674	.54076	-.49972
PB	.28615	.30485	.32817	-.28631
NI	.00579	-.01258	.06182	-.11199
ZN	.38419	.33249	.80460	-.45137
BE	.46493	.33680	-.04751	.02958

FILE ROOSEVEL (CREATION DATE = 09/03/80.) SPRINGS GEOTHERMAL AREA,UTAH

	NA	K	P	SI
ZR	-.30448	-.03067	-.43047	.32701
V	.21227	.09741	.58760	-.24649
BA	.17325	.33405	.57599	-.17980
B	.29768	.21574	.48505	-.24269
AL	.78546	.63229	.46440	-.02743
FE	.33592	.18821	.67527	-.27192
CA	-.44854	-.38961	-.06204	-.49820
MG	-.18217	.07503	.59138	-.53425
TI	.53690	.30387	.82017	-.25529
MN	.38348	.49423	.74254	-.34503
NA	1.00000	.48117	.36323	.03945
K	.48117	1.00000	.35425	.05587
P	.36323	.35425	1.00000	-.48058
SI	.03945	.05587	-.48058	1.00000

DETERMINANT = .0000000 (.19357204E-14)

APPENDIX D

FACTOR ANALYSIS OUTPUT

FILE ROOSEVEL (CREATION DATE = 09/03/80.) SPRINGS GEOTHERMAL AREA,UTAH

VARIABLE	EST COMMUNALITY	FACTOR	EIGENVALUE	PCT OF VAR	CUM PCT
AS	.46261	1	7.86382	23.1	23.1
SE	.35959	2	4.62445	13.6	36.7
LI	.73340	3	2.99158	8.8	45.5
RB	.74363	4	2.13313	6.3	51.8
SB	.43934	5	1.96423	5.8	57.6
HG	.33931	6	1.68352	5.0	62.5
SR	.98955	7	1.41285	4.2	66.7
TH	.60407	8	1.33371	3.9	70.6
CS	.64937	9	1.15708	3.4	74.0
F	.21003	10	.90004	2.6	76.7
NO3	.53124	11	.88694	2.6	79.3
SO4	.36660	12	.83880	2.5	81.7
CL	.98782	13	.78857	2.3	84.1
CR	.97758	14	.69449	2.0	86.1
CO	.52128	15	.61760	1.8	87.9
CU	.81726	16	.61045	1.8	89.7
PB	.68370	17	.53625	1.6	91.3
NI	.97725	18	.43653	1.3	92.6
ZN	.89602	19	.41389	1.2	93.8
BE	.81044	20	.35075	1.0	94.8
ZR	.64710	21	.31321	.9	95.7
V	.95701	22	.27641	.8	96.6
BA	.82843	23	.25770	.8	97.3
B	.47334	24	.20501	.6	97.9
AL	.92254	25	.15590	.5	98.4
FE	.95133	26	.13570	.4	98.8
CA	.91742	27	.11294	.3	99.1
MG	.88937	28	.09586	.3	99.4
TI	.94506	29	.07131	.2	99.6
MN	.84926	30	.05642	.2	99.8
NA	.87945	31	.03558	.1	99.9
K	.67350	32	.02860	.1	100.0
P	.92140	33	.01181	.0	100.0
SI	.69178	34	.00486	.0	100.0

1FACTOR ANALYSIS OF DOE SURFACE DATA 09/03/80. PAGE 14

FILE ROOSEVEL (CREATION DATE = 09/03/80.) SPRINGS GEOTHERMAL AREA,UTAH

FACTOR MATRIX USING PRINCIPAL FACTOR WITH ITERATIONS

	FACTOR 1	FACTOR 2	FACTOR 3	FACTOR 4	FACTOR 5	FACTOR 6	FACTOR 7	FACTOR 8	FACTOR 9
AS	.06737	.50661	.15795	.01963	-.18079	-.19331	-.05760	.05682	.24461
SE	.01007	.32407	.21284	.12986	-.12784	-.09355	.02018	-.16201	.27144
LI	.26894	.31633	.57431	.17832	-.20194	.36929	.01068	-.04981	-.11359
RB	.33113	-.12084	.64956	.15902	-.13668	.32625	-.02032	.16447	-.07614
SB	-.22003	.11025	-.03225	-.00808	-.34142	-.06643	.01671	.30117	.20908
HG	.26965	.00300	.02783	-.08068	-.13194	-.38090	-.20149	.02689	.09887
SR	.06904	.76776	.09482	-.20717	.47772	-.02217	.04202	.27384	-.02031
TH	.28673	-.16799	.22503	-.01245	.02482	-.18807	-.50071	.08672	.24029
CS	-.13757	.32270	.17429	.09971	-.54250	.12893	.03736	.48163	.02002
F	-.23197	.19657	.05358	.06529	-.02639	.10514	-.07973	-.11350	.00974
NO3	-.04811	.41261	.14167	-.06197	.27294	.05229	.12797	-.01607	.14234
SO4	.24500	.29553	.10400	-.03654	.17455	-.11946	.03650	-.11290	-.09753
CL	-.02472	.64633	.16393	-.18297	.61501	-.08227	.03295	.17459	.17335
CR	.19503	.07587	-.22284	.90523	.17180	-.16610	.07151	.09697	.00192
CO	.50621	.16391	-.25158	.15995	-.05426	.14127	-.09190	.07931	.01574
CU	.63833	.32354	-.09115	.20283	-.08007	.13392	-.03745	-.28310	-.09614
PB	.46280	-.09714	.43023	.08105	-.02756	-.21207	-.11726	-.21758	.07731
NI	.15931	.10617	-.21347	.90958	.16312	-.15984	.06838	.11176	-.01922
ZN	.85320	.05738	.12595	-.03006	-.09586	-.21593	.03359	-.25908	.03260
BE	.16867	-.42515	.62829	.14107	.23584	.18797	-.32125	.09682	.04866
ZR	-.45570	-.12426	-.15960	.11430	.05158	.36571	.13258	-.08455	.34520
V	.66408	.01629	-.56526	-.09863	.02113	.33497	-.21726	.07453	.03819
BA	.52976	.05767	-.15967	-.14126	-.29741	-.19484	.30228	.14415	.02563
B	.53016	.10480	-.00919	-.11472	.07228	-.11818	.07967	.23298	-.12662
AL	.69887	-.51800	.15548	.06118	.20236	.14514	.08262	.01408	.07562
FE	.78540	-.07708	-.42787	-.05042	-.00088	.14860	-.29034	.11999	.13240
CA	-.23765	.76928	.12645	.01173	-.12389	.05085	-.07525	.02377	-.24695
MG	.47889	.63563	-.19590	-.03090	.01805	.39247	.08840	-.22451	.12601
TI	.85357	-.14784	-.36153	-.15892	-.01350	.03882	-.01890	.15621	-.01578
MN	.78131	.00776	.28371	-.05916	-.14048	-.24102	.24762	-.07232	.02413
NA	.51563	-.52136	.17985	-.08073	.28645	-.00834	.08058	.21075	-.21549
K	.45482	-.32784	.31598	-.00236	.05292	.16421	.45151	.07014	.23229
P	.88092	.16764	-.08672	-.14602	-.06859	-.03698	.12419	-.02943	-.03018
SI	-.45874	-.59704	-.16240	-.04045	.06129	-.01529	.22885	.03907	.11135

0MORE THAN 5 ITERATIONS REQUIRED.

FILE ROOSEVEL (CREATION DATE = 09/03/80.) SPRINGS GEOTHERMAL AREA,UTAH

VARIABLE	COMMUNALITY
AS	.42296
SE	.29271
LI	.72667
RB	.72985
SB	.31736
HG	.29359
SR	.95200
TH	.51319
CS	.70807
F	.13067
NO3	.31059
SO4	.22784
CL	.92533
CR	.98451
CO	.40989
CU	.67672
PB	.52810
NI	.97742
ZN	.87314
BE	.82976
ZR	.54194
V	.93739
BA	.56865
B	.40120
AL	.85942
FE	.94671
CA	.74955
MG	.90115
TI	.93310
MN	.83945
NA	.75602
K	.70669
P	.85624
SI	.66519

FACTOR	EIGENVALUE	PCT OF VAR	CUM PCT
1	7.62783	33.9	33.9
2	4.35220	19.3	53.3
3	2.74647	12.2	65.5
4	2.03745	9.1	74.5
5	1.64719	7.3	81.9
6	1.32959	5.9	87.8
7	1.06880	4.8	92.5
8	.98813	4.4	96.9
9	.69541	3.1	100.0

FILE ROOSEVEL (CREATION DATE = 09/03/80.) SPRINGS GEOTHERMAL AREA,UTAH

ROTATION FOR DIRECT OBLIMIN LOADINGS DELTA = 0

ITERATION	CRITERION
0	20.088249
1	18.983285
2	17.694840
3	16.687297
4	15.905373
5	15.219771
6	14.422698
7	13.501728
8	12.744773
9	12.296009
10	12.034998
11	11.841065
12	11.675741
13	11.534845
14	11.411252
15	11.292127
16	11.166192
17	11.028274
18	10.881225
19	10.734910
20	10.601832
21	10.491947
22	10.409561
23	10.353115
24	10.317296
25	10.295856

FILE ROOSEVEL (CREATION DATE = 09/03/80.) SPRINGS GEOTHERMAL AREA,UTAH

OBLIQUE FACTOR PATTERN MATRIX
AFTER ROTATION WITH KAISER NORMALIZATION

DELTA = 0

	FACTOR 1	FACTOR 2	FACTOR 3	FACTOR 4	FACTOR 5	FACTOR 6	FACTOR 7	FACTOR 8	FACTOR 9
AS	.01069	.24736	-.00392	.03015	-.29365	-.11284	-.10908	-.07488	.39183
SE	-.08475	.09785	.05397	.06598	-.07693	.06605	-.04944	-.00786	.48485
LI	.04760	.01464	.78888	-.01822	-.06341	-.03984	.10668	-.09566	.17608
RB	-.02908	-.07181	.80787	-.00989	-.11266	-.03142	-.12851	.17579	-.05357
SB	-.03558	-.02477	-.06558	-.01999	-.54114	.05899	-.04955	.04053	.07485
HG	.04038	-.05268	-.17067	-.01339	-.06981	-.33381	-.29457	-.00205	.18802
SR	.07870	.95229	-.01095	-.00877	-.07479	-.14010	.02220	-.06736	-.15097
TH	.14548	.00829	.05170	-.03108	-.02089	-.05447	-.69027	-.03325	.10009
CS	.00618	-.03185	.35695	.01992	-.77729	-.06785	.08933	-.07500	-.02596
F	-.04939	.03043	.07741	-.01479	.00374	.14658	.03569	-.24305	.09670
NO3	-.04822	.51268	.01657	-.01506	.04032	.12280	.05578	.06101	.12670
SO4	.00398	.25682	.02564	.03627	.19544	-.25144	.06165	-.04100	.09972
CL	-.04749	1.00552	-.11100	.00527	.03941	.03777	-.13170	.05270	-.02628
CR	-.00847	-.01562	-.05793	.99819	-.00222	.04379	.00567	.02825	-.00046
CO	.57133	-.00482	.06147	.19455	-.06187	-.01504	-.00226	-.02515	.00298
CU	.50330	-.08458	.20158	.17205	.23072	-.15098	.16821	-.14908	.27530
PB	-.08868	-.09965	.23030	.03200	.23277	-.26485	-.28122	.13158	.34724
NI	-.02761	-.00472	-.04213	.99851	-.02393	.03622	.02028	-.00424	-.01667
ZN	.28549	-.10017	.07816	.01216	.25941	-.43429	-.04037	.22241	.41101
BE	-.13305	.01824	.57041	.00666	.16412	.14977	-.56740	.12989	-.16987
ZR	.02421	-.01838	-.08066	-.00344	-.05324	.74337	.07474	.12027	.08722
V	1.01565	-.03554	-.08187	-.04086	.03649	.13188	-.05246	-.02863	-.16339
BA	.23467	-.08679	-.12243	-.01807	-.23222	-.39290	.22360	.37403	.14515
B	.22015	.20503	.03779	.03844	-.05350	-.39726	.01352	.20641	-.14881
AL	.26159	-.09590	.24771	.07377	.27693	.02699	-.19295	.55893	-.08230
FE	.92677	-.05513	-.08669	.02448	.00247	.01917	-.26522	.07382	-.07276
CA	-.06347	.28695	.21425	-.01805	-.19744	-.21136	.24941	-.55675	.04636
MG	.70321	.28527	.13215	-.05443	.09555	.19003	.29508	-.08376	.32362
TI	.73151	-.06126	-.09021	-.01972	.02361	-.23084	-.04537	.28896	-.13813
MN	.06404	-.03595	.16750	.00555	.08127	-.49896	.05114	.45327	.33357
NA	.01505	.00737	.20215	.02303	.22595	-.27296	-.14324	.44876	-.42301
K	-.01148	.03766	.28130	-.01075	.02370	.11827	.07155	.79680	.11895
P	.52756	.05291	.05689	-.04074	.08708	-.38517	.11564	.26059	.16338
SI	-.33690	-.23042	-.29091	-.03638	.00931	.31402	.04529	.33178	-.18457

FILE ROOSEVEL (CREATION DATE = 09/03/80.) SPRINGS GEOTHERMAL AREA,UTAH

FACTOR PATTERN CORRELATIONS

	FACTOR 1	FACTOR 2	FACTOR 3	FACTOR 4	FACTOR 5	FACTOR 6	FACTOR 7	FACTOR 8	FACTOR 9
FACTOR 1	1.00000	.04321	.06621	.18225	.12337	-.38291	.03541	.21606	.10758
FACTOR 2	.04321	1.00000	.11875	.01878	-.01608	-.09616	.18866	-.23384	.24286
FACTOR 3	.06621	.11875	1.00000	.07837	.10288	-.11915	-.06120	.10760	.18020
FACTOR 4	.18225	.01878	.07837	1.00000	.06065	-.06979	.00462	.00461	.09225
FACTOR 5	.12337	-.01608	.10288	.06065	1.00000	-.06187	-.12033	.20752	-.09102
FACTOR 6	-.38291	-.09616	-.11915	-.06979	-.06187	1.00000	.14628	-.22164	-.20076
FACTOR 7	.03541	.18866	-.06120	.00462	-.12033	.14628	1.00000	-.17656	.05517
FACTOR 8	.21606	-.23384	.10760	.00461	.20752	-.22164	-.17656	1.00000	-.12073
FACTOR 9	.10758	.24286	.18020	.09225	-.09102	-.20076	.05517	-.12073	1.00000

FILE ROOSEVEL (CREATION DATE = 09/03/80.) SPRINGS GEOTHERMAL AREA,UTAH

OBLIQUE FACTOR STRUCTURE MATRIX
AFTER ROTATION WITH KAISER NORMALIZATION

DELTA = 0

	FACTOR 1	FACTOR 2	FACTOR 3	FACTOR 4	FACTOR 5	FACTOR 6	FACTOR 7	FACTOR 8	FACTOR 9
AS	.05570	.35559	.08098	.06180	-.32598	-.20221	-.00799	-.19468	.50753
SE	-.05099	.20699	.13892	.09179	-.12330	-.02002	.01007	-.12335	.50727
LI	.10662	.20014	.80547	.06778	-.02397	-.14682	.09117	-.04843	.35643
RB	.04530	-.05085	.80592	.03741	.02619	-.14898	-.21761	.28591	.05878
SB	-.11894	-.03209	-.11427	-.06215	-.54919	.08643	.01916	-.09418	.08113
HG	.15293	-.04766	-.09102	.01464	-.04379	-.39900	-.32240	.08938	.20494
SR	.13193	.95218	.07984	.01370	-.07629	-.20678	.19734	-.24442	.13028
TH	.14102	-.07244	.12093	.00807	.07078	-.22737	-.68093	.11919	.10298
CS	-.05369	.05828	.26504	.00369	-.75783	-.02807	.15720	-.18662	.13147
F	-.14215	.11010	.04861	-.01920	-.06838	.19382	.10412	-.30226	.11291
NO3	-.04098	.52684	.08857	-.00682	.01374	.05775	.15903	-.11157	.21500
SO4	.14783	.32719	.11910	.08253	.18719	-.29726	.06128	-.02391	.21153
CL	-.01613	.94257	.01421	.00376	.03312	-.05599	.05317	-.17838	.16850
CR	.15816	-.01395	.01504	.98874	.05408	-.01943	.01224	.01733	.06479
CO	.60358	.03944	.10737	.30084	.02253	-.24578	.02404	.09747	.10386
CU	.63398	.10860	.30334	.32800	.25845	-.38349	.15019	.02033	.39769
PB	.11406	-.05330	.36455	.09596	.29499	-.40541	-.38794	.27538	.35854
NI	.13256	.00550	.02225	.98465	.02492	-.00868	.03361	.02360	.06027
ZN	.57769	-.00054	.26502	.15324	.34550	-.69791	-.16523	.42358	.46710
BE	-.14069	-.11537	.58142	.00926	.30792	.04270	-.63369	.27984	-.16834
ZR	-.23576	-.09045	-.15148	-.05186	-.09644	.71578	.17578	-.07843	-.08429
V	.92963	-.05830	-.06332	.11473	.15854	-.21178	-.00744	.19746	-.11051
BA	.44566	-.06004	-.04297	.04296	-.15375	-.52353	.13538	.41366	.19278
B	.41309	.17696	.11612	.09714	.05591	-.51904	-.03846	.30280	-.00453
AL	.41620	-.24793	.34182	.14806	.48573	-.25133	-.34920	.76035	-.13475
FE	.91480	-.11178	-.02092	.17678	.16293	-.36248	-.25193	.32961	-.02742
CA	-.09007	.52132	.18077	-.00180	-.32563	-.07613	.38180	-.65835	.28755
MG	.68055	.46437	.22675	.11281	.09392	-.12777	.41440	-.09803	.46689
TI	.85656	-.12859	-.01168	.11130	.19664	-.53733	-.12084	.53228	-.08558
MN	.41130	.01815	.34147	.10253	.19574	-.70535	-.10800	.57171	.40330
NA	.21173	-.17962	.24242	.03689	.41563	-.35459	-.32326	.65589	-.40889
K	.15193	-.08533	.37530	.01807	.18856	-.10520	-.05869	.76744	.05841
P	.76239	.11789	.20016	.10984	.20382	-.67523	.03681	.43143	.28380
SI	-.43841	-.42442	-.38022	-.16154	.00008	.47195	-.01642	.22802	-.43400

FILE ROOSEVEL (CREATION DATE = 09/03/80.) SPRINGS GEOTHERMAL AREA,UTAH

FACTOR SCORE COEFFICIENTS

	FACTOR 1	FACTOR 2	FACTOR 3	FACTOR 4	FACTOR 5	FACTOR 6	FACTOR 7	FACTOR 8	FACTOR 9
AS	-.00591	.05218	-.00891	-.00418	-.09586	-.03809	-.03890	-.01766	.11231
SE	.00892	.00520	-.01655	-.00151	-.08736	-.02120	-.02926	-.01266	.05372
LI	.04079	-.02207	.25064	.02685	.08428	.11258	-.05014	-.07511	.04801
RB	-.00192	.00914	.31870	.01375	-.05926	-.07813	.14135	.01687	-.13288
SB	.00991	-.00071	-.01458	.01058	-.14684	-.03974	.05817	.03630	-.02003
HG	-.00806	.01175	-.03027	.00109	-.03646	-.06674	-.09033	-.01603	.07212
SR	.43003	.67924	.52399	.05743	-1.44191	-2.70043	2.06215	-.29487	-2.19588
TH	-.02177	.04524	.01991	.01487	.01823	-.01477	-.10175	-.01632	.07170
CS	.01047	-.03401	.09165	.00535	-.47966	.10996	-.13369	.07556	.13479
F	.01219	-.01433	.01601	.00495	.00792	-.02237	.03406	-.01984	-.00482
NO3	.01915	.04375	-.00308	.00639	-.05589	-.14287	.04572	.04518	-.04153
SO4	.00262	.05585	.01802	.00310	.04598	-.00271	.04782	-.03756	.00108
CL	-.41024	.18378	-.56373	-.03298	1.33002	2.38793	-2.02555	.36650	1.87179
CR	-.06305	-.02094	-.16239	.58889	.22826	.24334	.03697	.17888	.12905
CO	.02941	-.03094	.01745	-.00338	-.02000	-.01376	-.03673	-.01379	.02172
CU	-.04784	.06094	.05764	-.00487	.14000	.00132	-.00495	-.05821	.10172
PB	.06306	-.01032	.01532	.00402	-.09056	-.14142	.00354	-.01215	-.06763
NI	.09070	.02859	.15618	.40379	-.23074	-.20384	.04359	-.18346	-.14948
ZN	.07382	-.10561	.00272	.06078	.27521	-.24420	-.18752	-.06248	.45132
BE	-.04722	.01606	.25638	-.01934	.06362	.23809	-.58035	-.04862	.06697
ZR	.00595	.06118	.04944	-.02299	-.06804	.16992	.09710	.03145	-.01837
V	.27074	-.15983	-.04931	.09018	.70811	.81337	-.16819	.06102	.23513
BA	-.07984	-.03106	-.12163	-.01272	.12086	.42804	-.30124	.09736	.43359
B	.00843	-.00192	.01062	.00254	-.00592	-.03580	-.00881	.01806	-.02443
AL	-.01718	-.09545	.13529	.05622	.31714	-.01773	.13293	.44936	-.05331
FE	.30142	.00474	-.12129	-.08651	-.57639	-.44360	-.56290	-.24088	-.12163
CA	-.09526	-.05265	-.00421	-.01143	.36616	.45797	-.36679	-.03637	.46097
MG	.22399	.21081	.23704	-.01811	-.01868	.33589	.55702	-.15741	.30141
TI	.32741	-.00119	-.19263	-.00720	-.40084	-.26269	.09230	.27768	-.54351
MN	.01540	.04404	.10255	.00604	-.10061	.32127	.18849	.21071	.10368
NA	-.08425	.09019	.09313	-.01388	.27428	.19414	-.07954	-.04623	-.10662
K	.00296	.04403	.03492	-.01079	-.09674	.09126	.05257	.30894	.06714
P	-.07812	-.01256	.00263	-.04374	.14109	.21462	.09833	.15483	.02674
SI	-.04911	-.03169	-.07323	-.03353	.01287	-.04074	.13086	.17871	-.11485